UNIVERSITÀ
DEGLI STUDI
DI PADOVA

Sede Amministrativa: Università degli Studi di Padova

Dipartimento di Geoscienze

DOCTORAL COURSE IN EARTH SCIENCES
SERIES: XXXIV

SEDIMENTARY FACIES VARIABILITY ALONG FLUVIAL AND TIDAL MEANDERS: EXAMPLES FROM THE HOLOCENE VENETIAN PLAIN

Coordinator: Prof. Claudia Agnini
Supervisor: Prof. Massimiliano Ghinassi
Co-Supervisor: Prof. Andrea D'Alpaos

PhD Candidate: Elena Bellizia

Università degli Studi di Padova

Department of Geosciences

Doctoral Course in Earth Sciences

Sedimentary facies variability along fluvial and tidal meanders: examples from the Holocene Venetian Plain

Ph.D. Candidate: Elena Bellizia
Matricola: 1203258
XXXIV series

Thesis supervisor: Prof. Massimiliano Ghinassi
Thesis co-supervisor: Prof. Andrea D'Alpaos

This dissertation is submitted for the degree of *Doctor of Philosophy*

May 2022

'It always seems
impossible
until it's done'

Nelson Mandela

To my *Family*,
To my *Everything.*

ABSTRACT

Along the coastal plains, point-bar deposits originating from tidal and fluvial meandering channels host most of the surficial aquifers, which are the major source of groundwater for the socio-economic development of these areas. However, overexploitation of these aquifers has favoured seawater intrusion, and urbanisation has led to pollution of the aquifers. Detailed knowledge of point-bar deposits hosting these aquifers is crucial to gaining a better understanding of subsurface pathways for groundwater flows and providing insights into aquifer management.

Through a multidisciplinary approach, which combines remote-sensing analysis, sedimentary-core data, geophysical surveys, literature review, and statistical analyses, the present work analyses Holocene deposits from fluvial and tidal meandering channels of the Venetian Plain (Italy). The Venetian Plain provides a unique setting to study fluvial and tidal meandering channel deposits since commonly allows combining planform evidence with subsurface data. The results allow the characterisation of fluvial and tidal meandering channels from the bar the channel-belt scale and provide qualitative and quantitative data that can fruitfully contribute to model groundwater flows. Specifically, results: i) contribute to enriching current knowledge by providing insights to challenge the paradigms related to the internal lithological heterogeneity of point-bar deposits, along with the development of meander bends from straight channels; ii) allow to set up a new quantitative approach to efficiently study sediment-property variability within point-bar bodies; iii) highlight the impact of floodplain morphologies and substrate heterogeneities on the morphodynamic evolution of meandering rivers.

SOMMARIO

Nelle piane costiere, i depositi di point-bar originati dai canali meandriformi fluviali e tidali ospitano la maggior parte degli acquiferi superficiali, il cui sfruttamento ha contribuito allo sviluppo socioeconomico di queste zone. Tuttavia, lo sfruttamento eccessivo di questi acquiferi insieme all'intensa urbanizzazione ha favorito l'intrusione di acqua marina e la contaminazione degli acquiferi stessi da parte di sostanze inquinanti. Una conoscenza dettagliata dei depositi di point-bar è essenziale per comprendere al meglio il flusso negli acquiferi e per una loro migliore gestione.

Attraverso un approccio multidisciplinare che combina analisi statistiche e l'analisi di immagini satellitari, dati sedimentologici e indagini geofisiche, il presente lavoro analizza i depositi olocenici derivanti dall'evoluzione di canali meandriformi fluviali e tidali della Pianura Veneta (Italia). La Pianura Veneta è l'ambiente ideale per studiare questi depositi in quanto consente di combinare lo studio dell'evoluzione in pianta dei meandri con dati di sottosuolo. Le analisi hanno permesso di caratterizzare i depositi di canali meandriformi fluviali e tidali dalla scala della point-bar a quella dell'intero canale e forniscono dati qualitativi e quantitativi per la modellazione del flusso negli acquiferi. In particolare, i risultati: i) hanno contribuito ad arricchire le conoscenze attuali fornendo spunti di riflessione rispetto a quanto descritto finora sull'eterogeneità litologica interna dei depositi di point-bar e sullo sviluppo di meandri a partire da canali rettilinei; ii) hanno permesso di sviluppare un nuovo approccio quantitativo per studiare la variabilità delle proprietà dei sedimenti all'interno dei corpi di point-bar; iii) hanno evidenziato l'impatto che le morfologie della piana alluvionale e le eterogeneità del substrato hanno sull'evoluzione morfodinamica dei fiumi meandriformi.

ACKNOWLEDGEMENTS

I am grateful to my supervisors, Prof. Massimiliano Ghinassi and Prof. Andrea D'Alpaos, for giving me the opportunity to undertake this challenging and educational journey, and for being an example of what it means to love what you do.
My gratitude also goes to all my co-authors, whose scientific knowledge has always fascinated me and pushed me to give more.
I would also like to thank the reviewers of this thesis, Dr. Ivan Martini and Dr. Miquel Poyatos Morè, for their constructive comments that contributed to improving the quality of this work.
I extend my thanks to all the owners and professionals who have made data-collection possible over the years, without whom this work would not have been possible. The willingness of some of them will never be sufficiently paid off. A special thanks goes to B.L. for the valuable lessons he gave me.

My sincere thanks go to my fellow adventurers, without whom this experience would have been much more empty (and boring): Marta and Alice, my office mates, who advised and supported me, even going along with my bizarre ideas; Ally, for always being by my side and sharing every moment of this trip, which together we have made constructive; and all my colleagues, for their practical and/or moral support over the years.
I wish to thank my 'geologist friends' and 'non-geologist friends', who have been there for me over the years even though our commitments have kept us apart.
A sweet thought goes to my grandparents, who have never failed to support me.
A heartfelt thank you goes to those who have always been there, to those who have always understood and loved me: Mum and Dad, whose advice has never been in vain, and Nico, for always giving me new points of view and food for thought.
Last but not least, I would like to deeply thank my better half for patiently putting up with my mood swings, and for supporting me, accepting me, and loving me every day.

LIST OF CONTENTS

1

INTRODUCTION

1.1 Coastal plains and surficial aquifers

All over the world, the most densely populated areas are placed along sea coasts (Martínez et al., 2007), as they provide fruitful conditions for quality of life and economic development (Dillon, 2005) since the morphological setting of coastal plain largely promotes mobility and guarantees large availability of water (Boyer et al., 2006; Delagnes et al., 2012). Water is essential in almost all human activities, from drinking to food production, from industrial processes to energy production, as well as for sustainable management and conservation of the environment (UNEP, 2005). Freshwater is largely stored in surficial aquifers as groundwater. In coastal areas, human activity is increasingly causing groundwater depletion by triggering seawater intrusion and polluting aquifers with contaminants. Although coastal plains can suffer from seawater intrusion for natural reasons (i.e., sea-level rise, land subsidence and storm surge), the over-pumping of groundwater without adequate knowledge of the hydrogeological setting has increased this process, causing large scale seawater intrusion onto freshwater aquifers (Van Dam and Meulenkamp, 1967; Fennema and Newton, 1982; Frohlich et al., 1994; Tularam and Krishna, 2009; Klassen and Allen, 2017; Hussain et al., 2019). Seawater intrusion jeopardises the soil productivity affecting agricultural activity, as clearly documented on coastal plains all over the world, from European coasts (Van Dam and Meulenkamp, 1967; De breuck and De moor, 1969; De Franco et al., 2009; Da Lio et al., 2015) to Asian ones (Abdul Nassir et al., 2000; Choudhury and Saha, 2004; Qahman and Larabi, 2006; Abidin et al., 2011; Qi and Qiu, 2011), as well as for America's (Zohdy, 1969; Nowroozi et al., 1999; Barlow, 2003; Garcés-Vargas et al., 2020),

Africa's (Ebraheem et al., 1997; Paniconi et al., 2001; Pousa et al., 2007; Nofal et al., 2015; Agoubi, 2021) and Australian (Narayan et al., 1993; Mulrennan and Woodroffe, 1998; Werner, 2010) coastal plains (Fig. 1.1). Groundwater is also vulnerable to surface-derived, human-induced pollution: wastes from old landfills, hydrocarbon spills, industries may all contribute to groundwater degradation (Christensen and Hatfield, 1994; Zeidan, 2017). Worldwide, studies documented contaminations related to nitrate and chemical compounds (Cartwright and McComas, 1968; Tappe et al., 2002; Voudouris et al., 2004), also from industrial wastes (Ibrahim et al., 2011; Yang and Lee, 2012), as well as, arsenic pollution (Ravenscroft et al., 2005; Harvey et al., 2006; Ahuja, 2008; Carraro et al., 2013; Desbarats et al., 2014), which is globally considered as a serious human health threat (Berg et al., 2001; Polya et al., 2005; Deng et al., 2009).

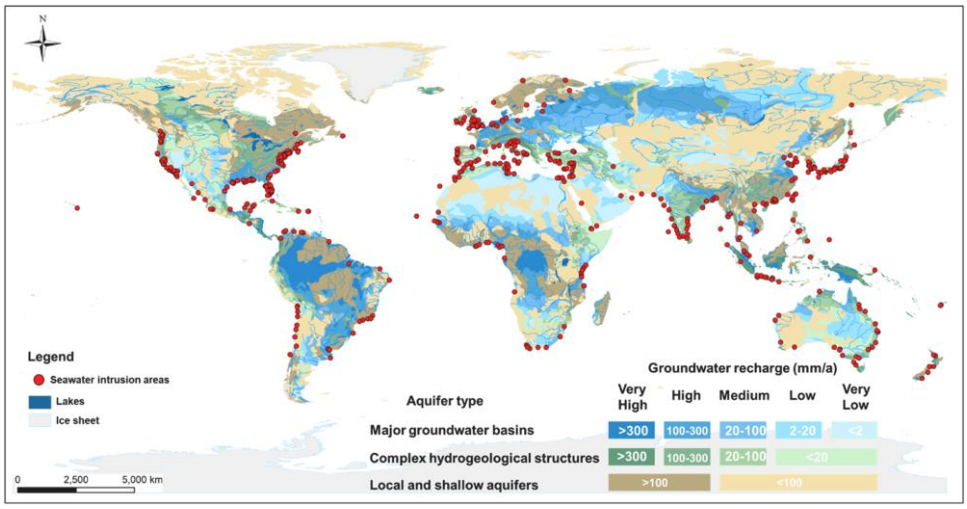

Fig. 1.1. Global geographic distribution of coastal areas that suffer from salt-water intrusion (from Cao et al., 2021).

To mitigate the effects of contaminants in the groundwater, a detailed investigation of the subsurface is needed. Accordingly, it is not possible to predict pollutant propagation or saltwater-intrusion processes without knowing the "preferential pipelines", which form the skeleton of coastal sedimentary succession. Subsurface integrated investigations, supported by geophysical approaches (i.e., electrical conductivity/resistivity investigations), allow to map the spatial distribution of the major sedimentary bodies and related aquifers (Van Dam and Meulenkamp, 1967; Cartwright and McComas, 1968; Zohdy et al., 1974; Goodell, 1986; Abdul Nassir et al., 2000; Awad et al., 2014; Amaya et al.,

2016), and reveal that the main pathways for groundwater flow are driven by primary sediment permeability: the groundwater flows through the most permeable sedimentary bodies that accumulate in the plain, taking advantage of the interconnectivity within them to propagate in different directions. These permeable bodies host both surficial and deep aquifers. Surficial aquifers, commonly hosted within the first few tens of meters below the ground, are those commonly more exploited for human activities, but they are also the most polluted, due to contaminant percolation from the ground surface and the conveyance of wastewater. Although hydrogeological and geophysical studies often consider surficial aquifers as isotropic and homogenous bodies, which include a limited spatial variability of hydraulic or electric properties (Christensen and Hatfield, 1994; Yang et al., 2001; Harvey et al., 2006), their internal characteristics and extensions can largely vary according to the depositional history of the plain.

1.2 Fluvial and tidal meandering channels (FTMC)

In coastal plains, meandering channels are widespread and are among the major morphological elements that act to shape the landscape and accumulate deposits. Meandering channels consist of a single channel thread that develops bends with a sinuosity greater than 1.25 (Brice, 1975; Kellerhals et al., 1976; Schumm, 1985; Friend and Sinha, 1993); the sinuosity is described as the ratio of the watercourse length to the valley length, thus representing how far a course deviates from the shortest possible straight path (Leopold and Wolman, 1957). In coastal areas, meandering channels can be both tidal or fluvial in origin (Fluvial and Tidal Meandering Channels, FTMC). Independently of their fluvial or tidal nature, meander bends evolve by eroding the outer bank and depositing sediment on the inner bank (Dietrich and Smith, 1984; Seminara, 2010). There are two main theories explaining how meander bends develop and evolve: the Bar Theory (Ikeda et al., 1981) and the Bend Theory (Gorycki, 1973). According to the Bend Theory, meander bends develop following natural variations in the turbulence of the flow, whereas Bar Theory states that bars start forming from obstacles of the inner bank, which force the flow to deviate laterally.

Once they are formed, FTMC evolve across the plain accumulating sediments and building up the internal structure of coastal plains (see an example of it in Fig. 1.2). During Holocene time, the evolution of the FTMC modelled modern coastal plains, where they still evolve shaping the landscape. Worldwide

examples of FTMC are in the Aegean coast of Turkey (Kayan, 1999) and in the coastal plains of Texas (Blum and Valastro, 1994). Traces of FTMC evolution have been identified and studied through remote-sensing analysis coupled with sedimentary cores also in Australian plains, for instance in the New South Wales (Wray, 2009), in the Amazonian lowland in Brazil (Rossetti and Valeriano, 2007; Rossetti, 2010), in Indus plains (e.g., Mehdi et al., 2016) and Italian ones (Piovan et al., 2010; Giacomelli et al., 2018). During their evolution, FTMC accumulate different depositional bodies (Allen, 1965; Daniel, 1971; Smith, 1987; Van de Lageweg et al., 2013) that define the internal architecture of a coastal plain succession (Fig. 1.3).

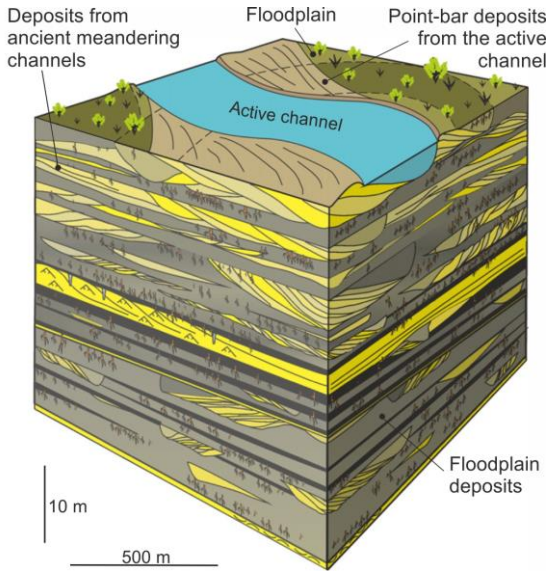

Fig. 1.2. Example of the internal structure of a coastal plain where meandering channels developed through time (modified from Shiers et al., 2014).

These bodies can be subdivided into two main groups, with levees, crevasse-splays, channel-fill and floodplain deposits being characterised by a mainly vertical accretion, and channel bars by a lateral one (Leopold and Wolman, 1957; Allen, 1965) (Fig. 1.3).

Dealing with channel bars, in FTMC, the sediment accumulation at the inner bank of each meander bend gives rise to point-bar bodies, which are the main depositional product of the evolution of FTMC. All the depositional elements from FTMC evolution develop following different depositional processes, therefore being characterised by different amounts of energy (Allen, 1965; Miall, 1985). This has implications on the sedimentological characteristics of

related deposits (i.e., grain size) and, therefore, on their permeability and porosity. Point bars are generally linked with sand deposition, whereas floodplains promote deposition of mud-prone successions. Identifying mud- and sand-prone deposits in coastal plain is relevant to the oil and gas industry since sand-prone deposits can form excellent reservoirs (Fielding and Crane, 1987; Miall, 1988; Martinius et al., 2017).

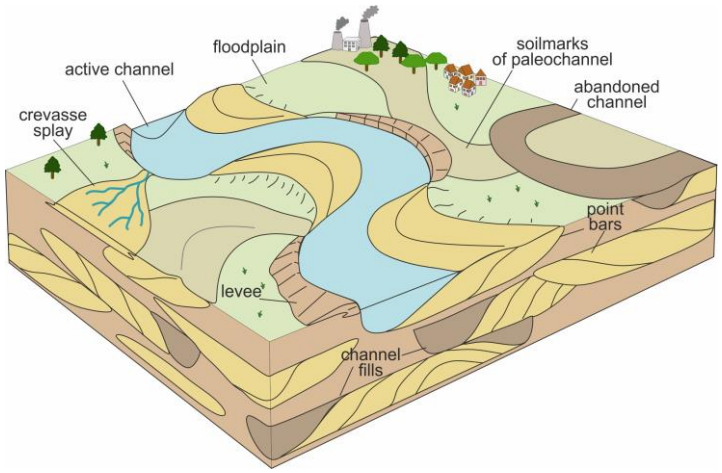

Fig. 1.3. Graphic representation of the structure of a coastal plain, where the evolution of ancient and modern meandering channels develops different depositional bodies thus shaping the plain (modified from Cabello et al., 2018).

Between the range of depositional bodies deriving from FTMC evolution, point-bars are those characterised by the highest permeability, potentially being good hydrocarbon reservoirs (Jordan and Pryor, 1992). Consecutive point-bar deposits form FTMC belts, which, in coastal plains, can develop in three major depositional settings: purely fluvial, purely tidal, and where both fluvial and tidal forces are acting together (i.e., fluvio-tidal transition zone) (Fig. 1.4).

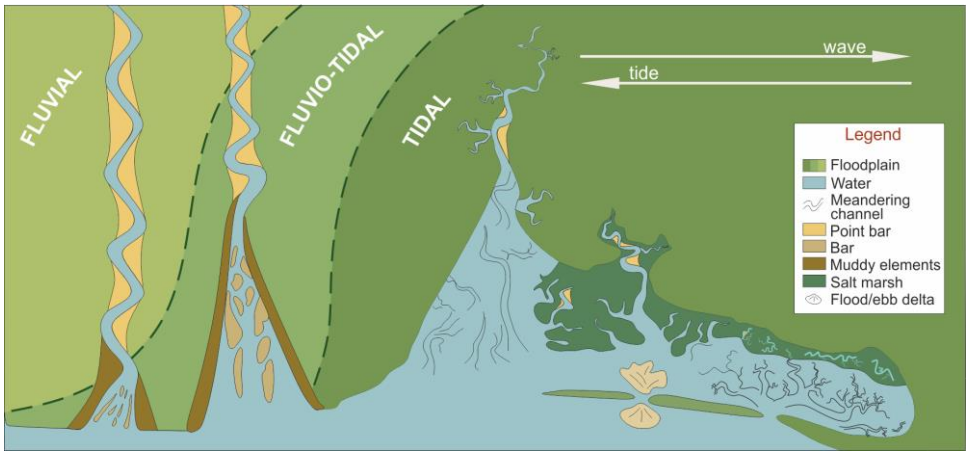

Fig. 1.4. Graphic representation of the different morphologies that meandering channels acquire in (from left to right) i) purely fluvial settings, ii) fluvio-tidal transition zones, and iii) purely tidal environments.

1.2.1 Fluvial channel belts and point bars

Among the three realms, point bars and channels belts from fluvial environments are those mostly studied around the world. Fluvial meandering channel belts are scale-invariant at both meander and network scales (Fig. 1.5), as observation and processes can be applied to both small and large channels (Leopold and Wolman, 1960; Rodriguez-Iturbe and Rinaldo, 1997).

Fig. 1.5. Example of a fluvial meandering channel: the Mississippi River, Louisiana (USA).

As in all fluvial systems, the sedimentation in point bars is related to flood events, when high water and sediment discharges are kept for a long time (i.e., weeks to months). Along their longitudinal profiles, fluvial meandering channels experience a progressive decrease in the stream gradient from up-valley to down-valley, stabilising between 0.01 and 0.5 ‰ (Gibling et al., 1998; Dunne and Aalto, 2013), and this decrease, in turn, induces a decrease in bed shear stress. Consequently, the progressive diffusion of fine and coarse sediments occurs, as the stream flux reduces its ability to transport sediment (Knighton, 1999; Rice and Church, 2001; Frings, 2008). Meander bends can evolve following three basic transformation stiles that are expansion, translation and rotation, or through a combination of them (Daniel, 1971; Brice, 1974; Jackson, 1976) (Fig. 1.6). Expansion and translation lead the channel to migrate laterally almost orthogonal and parallel to the main channel-belt orientation, respectively,

whereas rotation implies a downstream skewness of the bend, with the bend apex moving toward the belt (Ghinassi et al., 2014). Planform evolution of fluvial meandering channels leads to the accumulation and preservation of sedimentary bodies characterised by internal differences (i.e., heterogeneities), which influence the interconnectivity between point-bar bodies (Miall, 1988; Bridge, 2003; Willis and Tang, 2010; Hagstrom et al., 2019). Evolution patterns are commonly visible from satellite images or aerial photos [i.e., Mississippi River, USA (Strick et al., 2018)] and planform exposures [i.e., Scalby Formation, UK (Ghinassi and Ielpi, 2015)], as they portray the scroll-bar pattern, which is an essential tool to reconstruct channel-belt dynamic (Hickin, 1974; Hickin and Nanson, 1975; Strick et al., 2018).

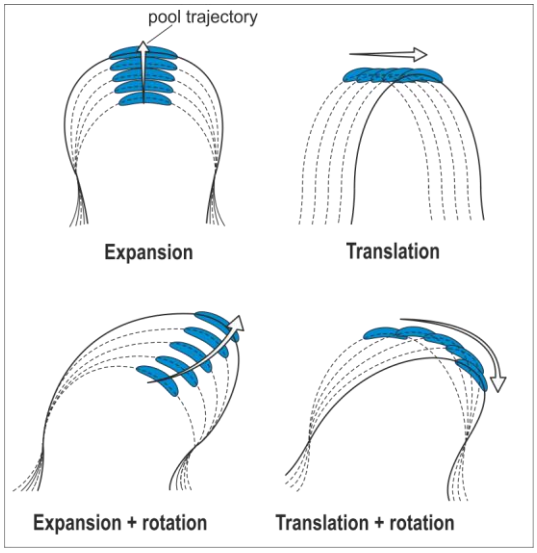

Fig. 1.6. The main transformation styles of migrating meander bends, modified from Ielpi and Ghinassi (2014).

Fluvial meandering channels can range in length from a few hundred kilometres, as in the case of the Beatton River (Canada), the North Thompson River (Canada) and the Powder River (USA), to a few thousand kilometres (i.e. around 6000 km) as in the case of the Nile (Egypt and Sudan, Africa), the Amazon (Brazil) and the Yangze Rivers (China) (Gupta, 2008). Their channel width can be a few tens of metres, e.g., the Brenta River (Italy), up to more than 1 km, like the Mississippi River (USA).

Planform evolution of meandering channels leads to the accumulation of point bar bodies (Nanson, 1980). A point bar develops after the lateral migration of a meander bend (Bagnold, 1960; Leopold and Wolman, 1960; Bhattacharyya et al., 2015) that increases its sinuosity starting from an almost straight channel (Brice, 1974; Lewin, 1976). Entering a bend, the water flow acquires a helical

behaviour (Dietrich, 1982; Seminara, 2006), being largely responsible for the classical fining-upward grain size trend that characterises point-bar deposits (Allen, 1970; Jackson, 1976; Nanson and Page, 1983; Durkin et al., 2018) (Fig. 1.7).

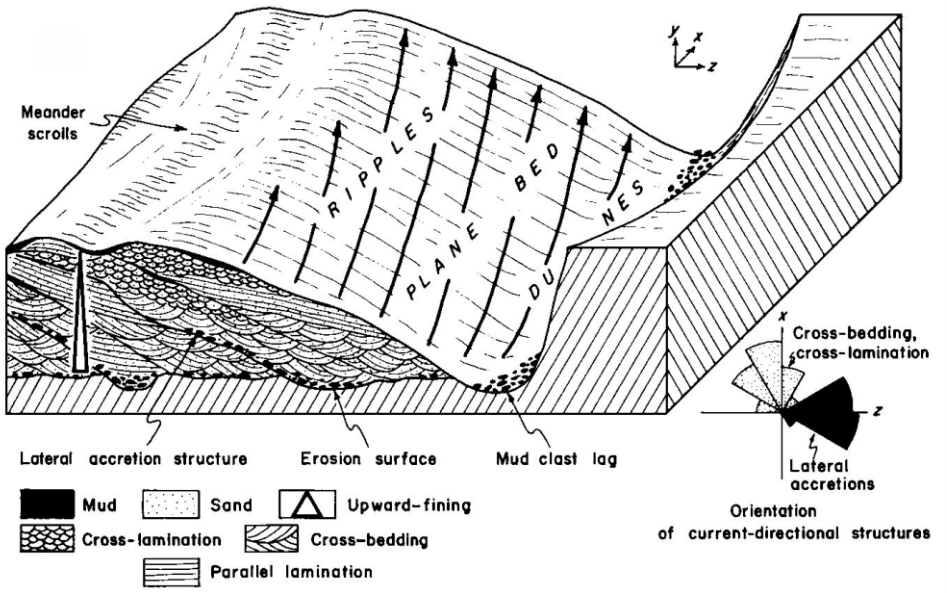

Fig. 1.7. Facies model of sedimentary structures, lithologies, and grain-size trends of a fluvial point bar (from Allen, 1982).

Flow configuration along a bend is also responsible for a progressive downstream decrease in grain size (Bluck, 1971; Bridge et al., 1995; Ielpi and Ghinassi, 2014). However, upstream portions of point bar deposits often show a different vertical grain-size distribution respect to the fining upward one, being characterised by a coarsening to "blocky" (sensu Willis, 1989) grain-size trend (Dietrich and Smith, 1983; Frothingham and Rhoads, 2003), since that part of the bar is not generally affected by the secondary helical circulation (Ghinassi et al., 2016). Point-bar deposits are composed of a wide range of grain sizes, from mud to gravel, although more commonly they are sandy. Point-bar deposits are characterised by erosive basal surfaces, with channel-lag deposits that are commonly sandy to gravelly and rich in mud clasts. Coastal point bars, especially where tidal influence occurs, are generally characterised by inclined heterolithic stratification (IHS) (Thomas et al., 1987), consisting of cross-stratified sand with muddy interbeds, with a greater proportion of mud in the upper portions since the flow ability to suspension decreases toward the top (Nanson, 1980; Strobl et al., 1997; Durkin et al., 2017). In addition to unidirectional cross-stratification,

the most commonly observed sedimentary structures in sands are parallel stratification, and ripple cross-lamination especially in the upper portions (Labrecque et al., 2011; Ielpi and Ghinassi, 2014; Bhattacharyya et al., 2015) (Fig. 1.8).

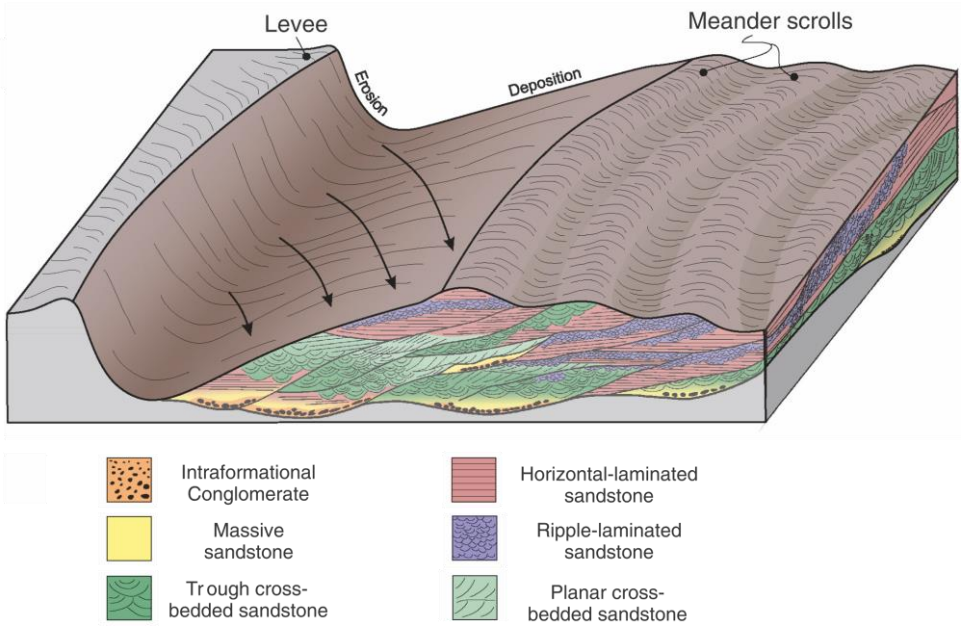

Fig. 1.8. Example of the 3D depositional model of facies and architecture of a sandstone-dominated point-bar element (from Shiers et al., 2018).

Meander bends evolving through expansion (i.e. laterally-migrating meanders) show a progressive increase of the channel sinuosity (Daniel, 1971; Brice, 1974; Jackson, 1976) and commonly accumulate point-bar deposits characterised by sand sedimentation concentrated at the bend apex (Hagstrom et al., 2019). Moreover, the expansion of the bend allows the deposits on the upstream and downstream sides of the bar to be preserved (Jackson, 1976; Ghinassi et al., 2014). In the case of a meander bend translation (i.e., downstream-migrating meanders), where the meander bend grows keeping almost constant its sinuosity (Daniel, 1971; Brice, 1974; Jackson, 1976), deposits are preserved downstream of the bend apex, whereas the upstream deposits are mainly removed during bend evolution (Willis, 1993; Nicoll and Hickin, 2010; Ghinassi and Ielpi, 2015). When a rotation component is associated with expansion or translation, the meander-bend sinuosity varies during the evolution and the preservation of deposits located upstream or downstream to the bend apex depends on whether the rotation is up-valley or down-valley, respectively (Jackson, 1976; Ghinassi et al., 2014). In the case of downstream-migrating

meandering channels (i.e., channels migrating under translation), counter-point bars and eddy-accretion deposits can develop (Nanson and Page, 1983; Vietz et al., 2006; Smith et al., 2009, 2011) (Fig. 1.9). Counter-point bars form where the flow impinges at low angles (i.e., 40° or less) against erosion resistant outer banks (Makaske and Weerts, 2005; Smith et al., 2011). They develop attached to the downstream portion of point bars, showing peculiar concave-shaped scroll patterns, and are characterised by thinner and finer deposits compared to classical point-bar ones (Nanson and Page, 1983; Hickin, 1986; Smith et al., 2009, 2011). If the flow impinges against the outer bank at great angles (i.e., 40° or more), it splits into two sub-flows, including one characterised by reverse eddy currents (Smith et al., 2011). By modifying counter-point bar deposits, eddy currents produce eddy-accretion bodies characterised by thicker and coarser deposits than classical point-bar ones (Burge and Smith, 1999).

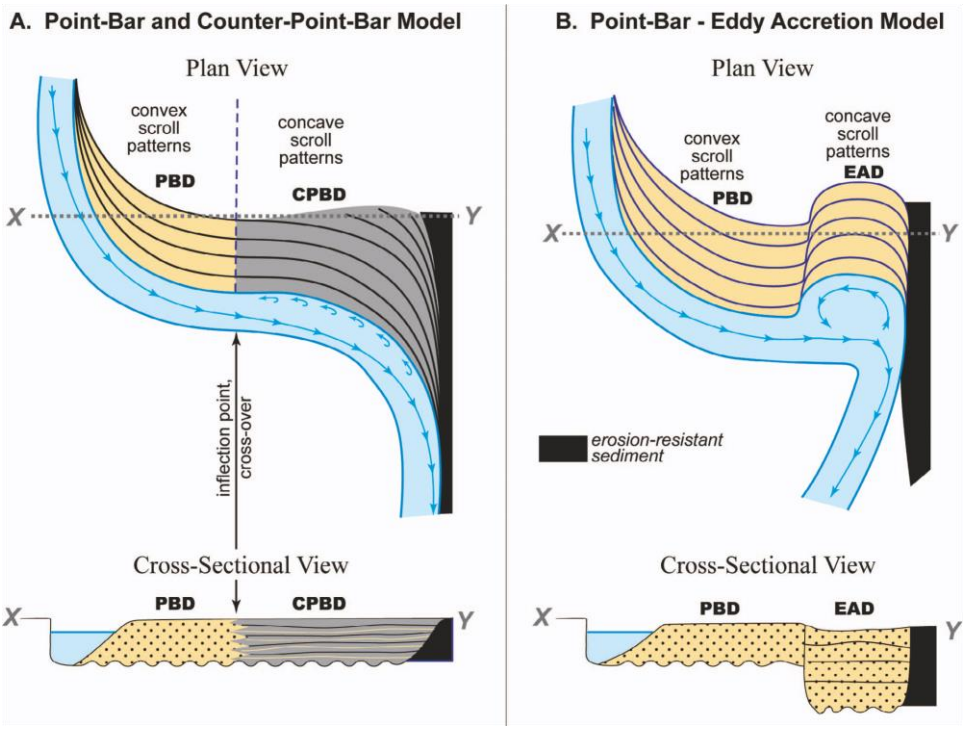

Fig. 1.9. Schematic representation of the planform view and cross-sectional deposits of (A) a point bar with counter-point bar deposit, and (B) a point bar with an Eddy accretion deposit (from Smith et al., 2011).

These different styles of planform evolution cause channel belts to be characterised by adjacent point-bar bodies with different architecture and grain-size distribution (Hagstrom et al., 2019), thus having implications on inter-

bar connectivity (Willis and Tang, 2010). Inter-bar connectivity at the channel-belt scale is also strongly influenced by channel-fill deposits accumulated during abandonment phases (Fisk, 1947; Constantine et al., 2010; Toonen et al., 2012) (Fig. 1.10). Channel-fill deposits are generally mud-rich, but their internal stratigraphy can vary depending on the abandonment mechanism. Muddy deposits are found when a neck cut-off occurs (Fisk, 1947; Allen, 1965), whereas a greater amount of sand occurs in the case of chute cut-offs (Fisk, 1947; Fustic et al., 2018). A variable amount of sand also occurs in the abandoned channel as a function of different types of avulsion mechanisms, which cause entire channel-belt segments to be abandoned (Mackey and Bridge, 1995; Toonen et al., 2012).

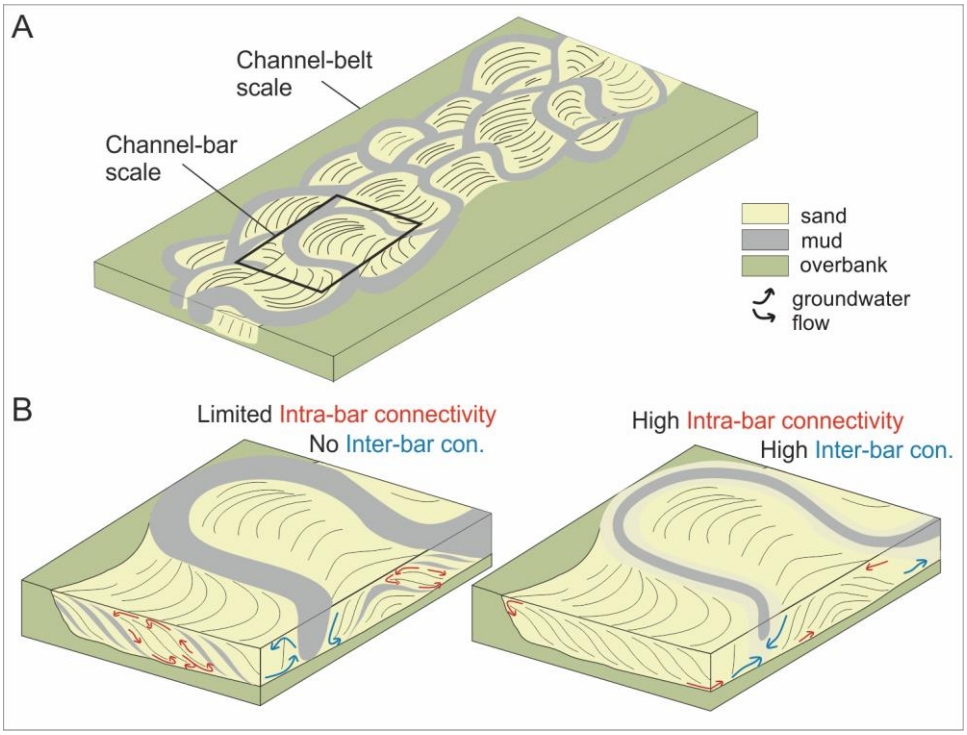

Fig. 1.10. (A) The channel-belt and the channel-bar scales in a cartoon of a floodplain characterised by many traces of paleo-meandering channels. (B) Inter-bar and intra-bar connectivity examples: the occurrence of mud deposits (i.e., mud layers within point-bar bodies and muddy channel-fill deposits) can affect flow propagation, and therefore inter- and intra-bar connectivity.

1.2.2 Tidal channel belts and point bars

Studies on purely tidal meandering channels mainly developed over the recent years, as they were for a long time approached based on sedimentological principles developed for fluvial meandering systems. However, meandering channels play a key role in tidal environments, by allowing water, sediment, and nutrient mobility (Barbier et al., 2011; Kearney and Fagherazzi, 2016). They can develop in microtidal (< 2 m), mesotidal (2 - 4 m) and macrotidal (> 4 m) regimes (Davies, 1964) (Fig. 1.11), with macrotidal ones being commonly characterised by tidal ranges greater than 6 m (e.g., Cook Inlet in Alaska, Bay of Fundy in Canada, Straits of Magellan in Chile, Gulf of St. Malo in Normandy, France) (Archer, 2013).

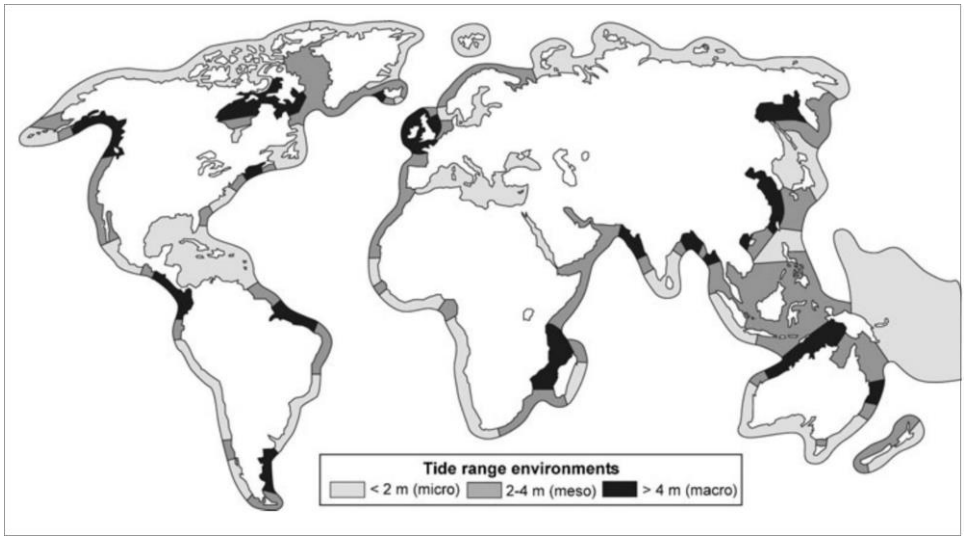

Fig. 1.11. Variation of the tidal ranges along the coasts of the whole world (after Davies, 1980).

Tidal meanders have been largely described from macrotidal settings, where they are described along with morpho-depositional elements, such as tidal flats and salt marshes (Choi et al., 2004, 2013; Choi and Jo, 2015). Smith (1987) documented mesotidal creeks in The Willapa River, USA, and they can be found also in Europe [e.g., Solway Firth, Scotland (Bridges and Leeder, 1976; de Mowbray, 1983), Haringvliet, Netherlands (Oomkems and Terwindt, 1960)]. Microtidal meandering channels are less studied worldwide, and available information is mainly provided by the studies on the Venice Lagoon, Italy (Brivio et al., 2016; Ghinassi et al., 2018b, 2018a; Cosma et al., 2020; Finotello et al., 2020b). Overall, tidal meandering channels differ from fluvial counterparts because of the effects of tidal prism and the occurrence of bidirectionality of the

flow (i.e., flood and ebb currents). The tidal prism is responsible for the characteristic funnel shape of tidal channels, which typically narrow landward (Lanzoni and D'Alpaos, 2015). Tidal channels mainly develop as dense channel networks, with a dendritic shape, including numerous minor tributaries (Finotello, 2017) (Fig. 1.12). Tidal systems are not scale-invariant, since observation and processes of small channels cannot often be applied to larger channels in a system (Hughes, 2012).

Fig. 1.12. Example of tidal meandering channels of the Georgia's coast (USA).

The bidirectionality of the flow is responsible for the planform evolution and sedimentation of tidal channels (Fenies and Faugères, 1998; Fagherazzi et al., 2004; Dalrymple and Choi, 2007) in terms of several processes, including: i) due to the tidal cycle, tidal channels experience daily variations in channel discharge and flow velocity, with high velocity flows lasting only hours and alternating with low phases; ii) the asymmetry of the local tidal flow causes intensity and dominance inequalities between flood and ebb periods, with asymmetric distribution of grain size along the landward and seaward sides of the bend; iii) flood and ebb flows follow different paths within a channel, influencing sedimentation (Fagherazzi et al., 2004; Hughes, 2012). This bidirectionality can also lead to peculiar meander-bend morphologies, like cuspate and "box-shaped" bends.

Tidal meandering channels can be characterised by a wide range of planform morphologies (Rinaldo et al., 1999; Kearney and Fagherazzi, 2016), experiencing different transformation styles, only differing from fluvial counterparts because point-bar evolution in the tidal realm is influenced by the progressive increase

of the tidal prism, which causes the channel to widens instead of increasing its depth (Finotello, 2017). Lateral migration of tidal meandering channels originates point-bar bodies defined by sub-horizontal erosional basal surface and internally characterised by an upward-fining grain size sequence (Figs. 1.13, 1.14).

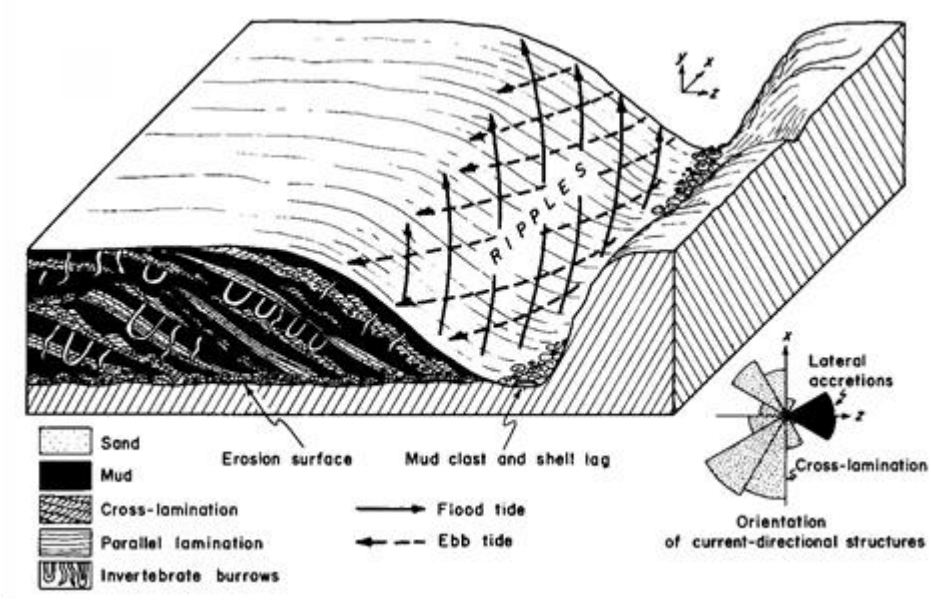

Fig. 1.13. Facies model of sedimentary structures, lithologies, and grain-size trends of a tidal point bar (from Allen, 1982).

Point-bar deposits are described as interbedded sigmoidal layers of mud and sand [i.e., Inclined Heterolithic Stratification (Thomas et al., 1987)], with sandy layers becoming more common and thicker toward the base (de Mowbray, 1983; Fruergaard et al., 2011; Choi and Jo, 2015). Point-bar deposits can be abundantly bioturbated, especially toward the top, and they are characterised by sedimentary structures bearing tidal signatures (Choi et al., 2004; Pearson and Gingras, 2006; Johnson and Dashtgard, 2014; Gugliotta et al., 2016) including reactivation surfaces, bidirectional flow indicators, rhythmites, mud-drapes in cross-sets, tidal bundles, and herringbone cross-stratification (Barwis, 1977; Tessier, 1993; Choi and Park, 2000; Choi and Dalrymple, 2004; Choi, 2011).

The higher the tidal range, the better the sedimentary features representing tidal signature are expressed, and consequently, the wider is the available range of grain sizes to be transported [e.g., west coast of Korea (Choi and Dalrymple, 2004; Choi et al., 2013), Venice Lagoon (Brivio et al., 2016)]. Tidal meandering

channels may undergo abandonment (Tirsgaard, 1993; Gray et al., 2016; Cosma et al., 2020) through cut-off events, with neck cut-off being more documented than chute ones (Choi et al., 2013; Brivio et al., 2016; D'Alpaos et al., 2017), and even less common channel avulsion events. After the abandonment of a tidal channel, the high channel density of tidal networks leads to the re-distribution of the local tidal prism, favouring connection between adjacent channels and piracy events rather than the incision of a new watercourse (Fagherazzi, 2008; Cosma et al., 2020).

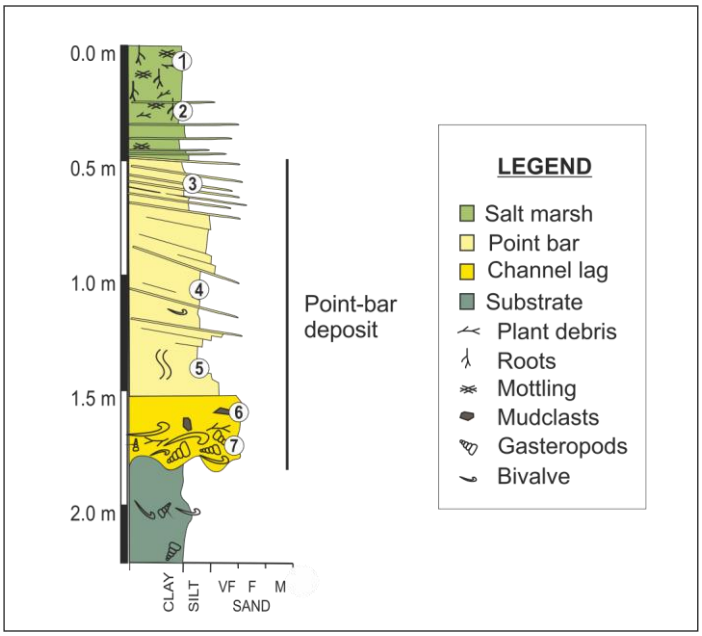

Fig. 1.14. Example of the internal stratigraphy of a tidal point bar from the microtidal Venice Lagoon, Italy (modified from Cosma et al., 2019).

1.2.3 Fluvio-tidal channel belts and point bars

Approaching the coastline, fluvial meandering channels may be influenced by tidal currents as they enter the so-called "fluvio-tidal transition zone" (Dalrymple and Choi, 2007; Dashtgard and La Croix, 2015; Gugliotta, 2016) (Fig. 1.15). This zone lies between the landward limit of detectable tidal currents and the seaward occurrence of fluvial textural features (Van den Berg et al., 2007; Martinius and Gowland, 2011), and it may ranges in length from a few to hundreds of kilometres depending on several features, including the relationship between fluvial discharge and tidal range, along with the gradient

of coastal areas (Dalrymple and Choi, 2007; Martinius and Gowland, 2011). Moving seaward in the fluvio-tidal transition zone, the cross-sectional area of fluvial meandering channels widens (Myrick and Leopold, 1963), acquiring the funnel shape that characterises tide-dominated systems (e.g., the Fly River delta, the Ganges–Brahmaputra River delta, the Thames estuary) (Fig. 1.15).

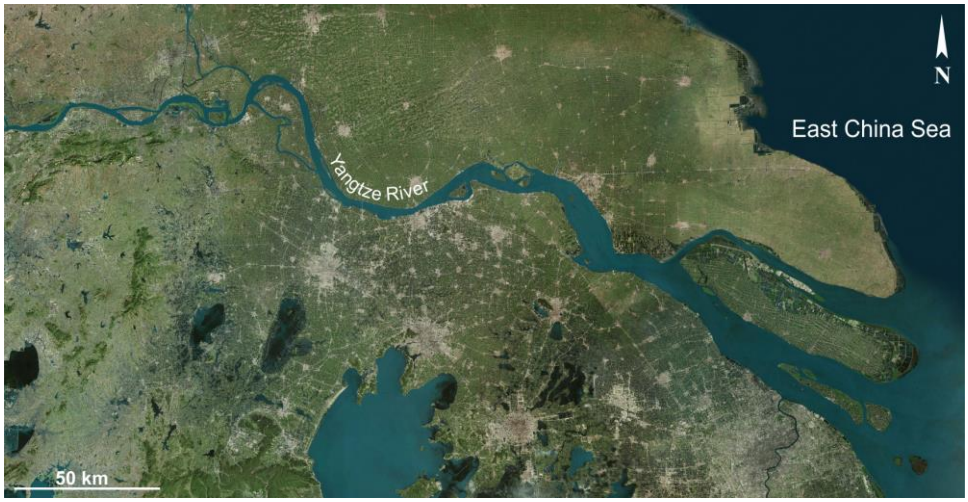

Fig. 1.15. Example of a meandering channel in the fluvio-tidal transition zone: the Yangtze River, Jiangsu (China).

The fluvio-tidal transition zone hosts a turbidity maximum, which develops in response to the turbulent resuspension of sediment and flocculation of fine grains, leading to the accumulation of thick mud drapes (Dalrymple and Choi, 2007). In the whole transition zone, unidirectional river currents generally prevail and the flow experiences variations in speed due to tidal modulation. Therefore, the cyclicity characterising deposits accumulated by tidal flows are commonly detected, but they do not imply the dominance of tidal processes on the morphodynamic of the system (Dalrymple and Choi, 2007; Dalrymple et al., 2015) (Fig. 1.16). Consequently, point-bar bodies from the fluvio-tidal transition zone show classical sedimentary features and grain-size trends of fluvial deposits, with rhythmites and mud deposits testifying to the tidal influence (Fig. 1.17). The only exception is made for point bars located in the turbidity maximum zone where mud drapes are more abundant (Martinius et al., 2015; Jablonski and Dalrymple, 2016).

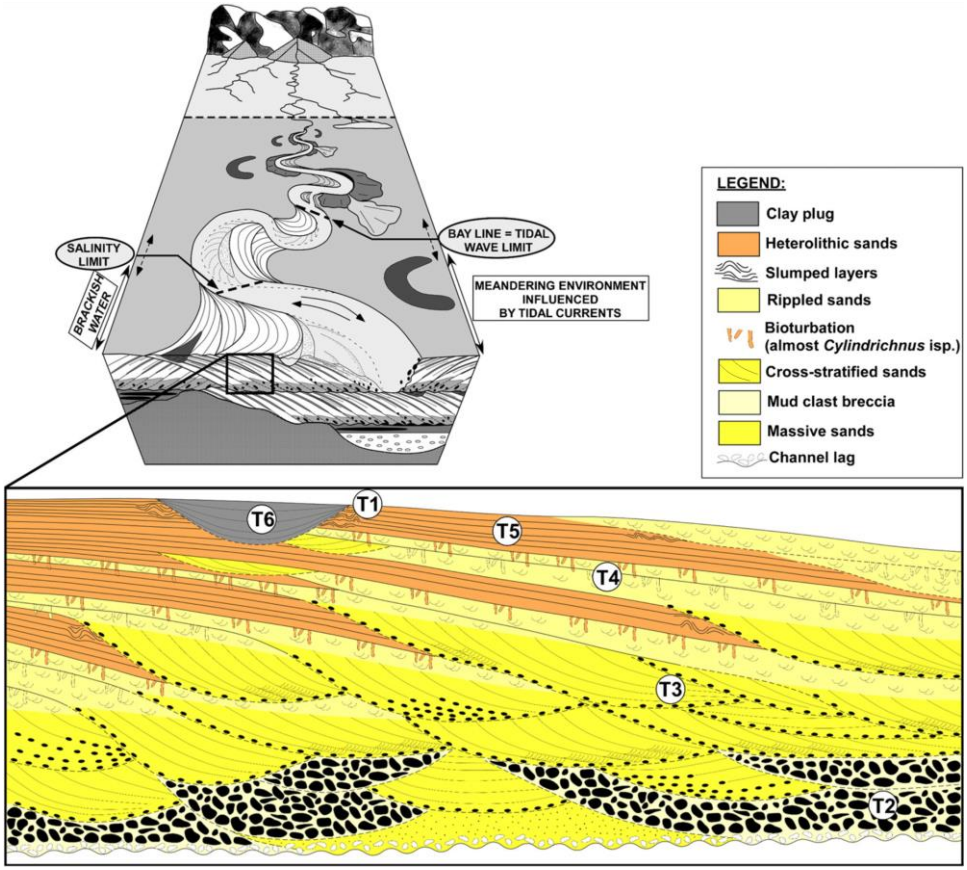

Fig. 1.16. Example of the internal stratigraphy of a tidally influenced point bar in the McMurray Formation, from Musial et al. (2012), with distinction of 6 main facies (T1-6): (T1) slumped layers, (T2) mud-clast in the lag deposit, (T3) cross-stratified sand, (T4) rippled sand, (T5) heterolithic sand, (T6) mud layers.

Point-bar deposits from the fluvio-tidal transition zone display a wider range of grain sizes than in tidal systems (Dalrymple and Choi, 2007; Jablonski and Dalrymple, 2016; Ghinassi et al., 2021), where the dominance of mud is widely documented (de Mowbray, 1983; Fruergaard et al., 2011; Choi and Jo, 2015; Brivio et al., 2016). Overall, morphodynamic and sedimentological observations on point-bar originated in the fluvio-tidal transition zone are documented all over the world, regardless of whether the coast is mesotidal [e.g., Mekong river delta (Gugliotta et al., 2017, 2018)] or macrotidal [e.g., River Seven estuary, UK (Carling et al., 2015), Fraser River, Canada (Dashtgard et al., 2012; Dashtgard and La Croix, 2015)] or microtidal [e.g., James estuary, Virginia (Nichols et al., 1991)].

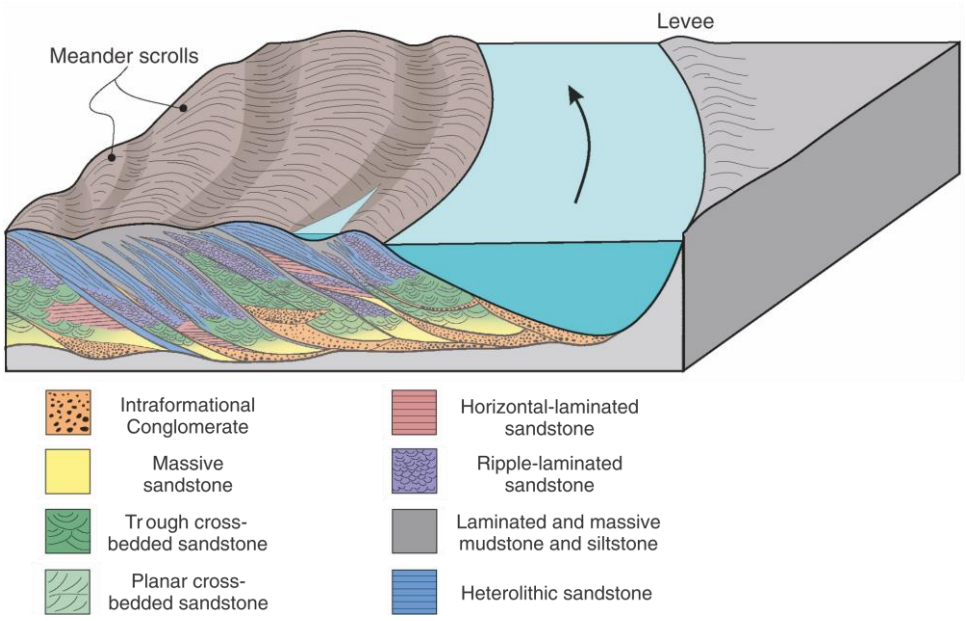

Fig. 1.17. Example of the 3D depositional model of facies and architecture of a tidally influenced point-bar element, (from Shiers et al., 2018).

1.3 Knowledge gaps

FTMC deposits have been widely investigated in modern environments, although a large amount of information about their internal structures derives also from the stratigraphic record. However, a full 3D knowledge of FTMC deposits is not detailed yet. Several models of the sedimentology of FTMC were developed from vertical outcrops (Fig. 1.18) since they are relatively widespread and allow the analysis of the vertical and lateral grain-size changes. On them, sedimentary reconstructions can be made from extensive sedimentary logging (Strobl et al., 1997; Ghinassi et al., 2014; Wu et al., 2015); but a complete 3D analysis of the internal architecture can be barely provided. Planform exposures of FTMC deposits allow for analysing morphological and sedimentological features [e.g., Scalby Formation, UK (Ielpi and Ghinassi, 2014; Ghinassi and Ielpi, 2015), Ellice Formation, Canada (Ielpi and Rainbird, 2015), Ferron Sandstone, USA (Wu et al., 2015)] (Fig. 1.19); however, they are quite uncommon. Recently, the remote-sensing analysis of modern and late Holocene FTMC contributes to the investigation of sedimentary bodies that are visible from satellite and aerial photos, allowing one to reconstruct the planform evolution and the morphometric changes of individual bends (e.g., Strick et al., 2018; Pal and Pani,

2019; Finotello et al., 2020a). Nevertheless, in these cases, the internal structure of related sedimentary bodies cannot be inferred.

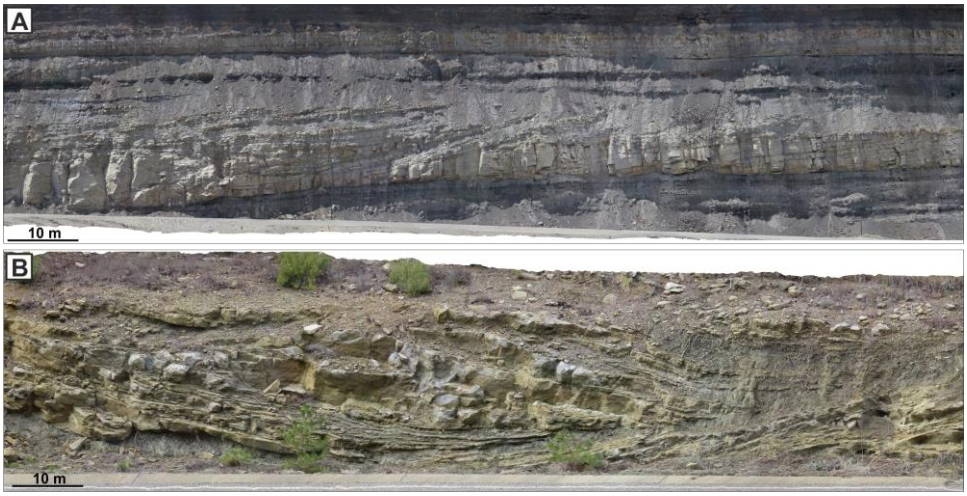

Fig. 1.18. Examples of vertical outcrops: (A) the Mesaverde Formation, Colorado, USA, and (B) the Castigaleu Formation, Spain. Photos: courtesy of Massimiliano Ghinassi.

Fig. 1.19. Example of a planform exposure of a point-bar body, Scalby Formation, Yorkshire, UK. Modified from Ielpi and Ghinassi (2014).

The direct observation of active morphodynamic processes in modern FTMC, through ground and remote-sensing analyses, is a favourable way to study them and understand their deposits (e.g., Langat et al., 2019; Strick et al., 2019; Finotello et al., 2020b) (Fig. 1.20); however, in addition to the limitation of remote-sensing analyses, natural channel systems are quite rare to be found on accessible areas, which are generally strongly impacted by human activities. Sedimentary cores provide the direct solution to investigate sedimentary features (e.g., Brivio et al., 2016), but, due to the spatially limited information that they provide (Baines et al., 2002), they need to be coupled with geophysical investigations (e.g., Hubbard et al., 2011; Labrecque et al., 2011; Durkin et al.,

2017; Ghinassi et al., 2018b). Similar integrations are crucial to provide a detailed understanding of the 3D internal anatomy of point-bar bodies generated by FTMC. However, studies integrating different methodologies to provide complete 3D analyses of FTMC deposits are uncommon, providing an onerous knowledge gap.

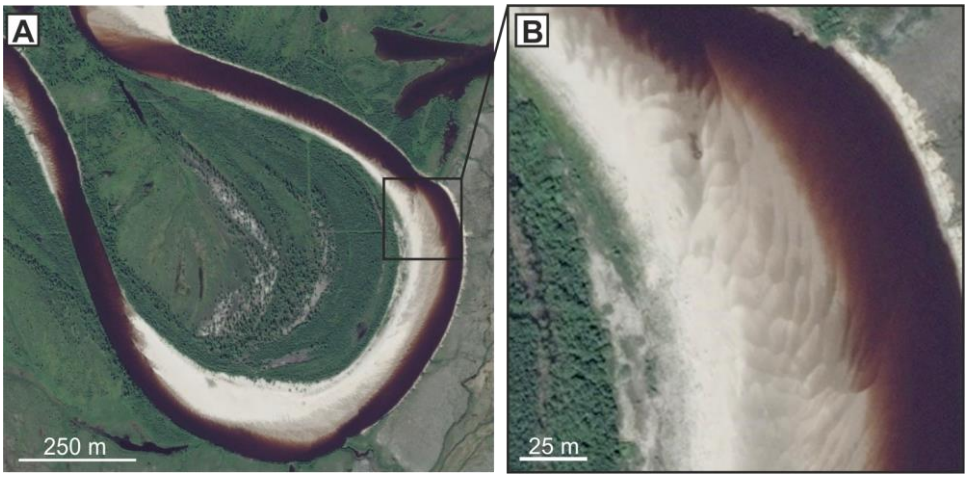

Fig. 1.20. Example of meander bend of a modern river of the Ural Federal District, Russia. (A) The planform evolution can be reconstructed from the scroll bar pattern, and (B) both bedforms and flow dynamic can be directly studied on the meander bend. (Modified after Ghinassi et al., 2016)

At the channel-belt scale (Fig. 1.10), a gap of knowledge occurs about how the fluvial response adapts to floodplain substrate heterogeneities (e.g., sandy vs. muddy substrates) and related microreliefs (e.g., differences in elevation lower than 1 m).

Additionally, still in the fluvial realm, a further knowledge gap arises from the almost scarcity of studies analysing how morphologies and deposits are linked together, since meander bends were commonly studied keeping separated hydraulic (e.g., Dietrich, 1982; Whiting and Dietrich, 1990; Seminara et al., 1997; Ferguson et al., 2003) and sedimentological approaches (e.g., Jackson, 1976; Smith, 1987; Sambrook Smith et al., 2006). This is especially notable for tidal meanders, which receive much less attention compared to their fluvial counterparts, thus highlighting another gap in current knowledge. Going into detail with tidal point bars, the analysis of the planform evolution of tidal meandering channels is not always straightforward as scroll-bar patterns are not preserved (or formed?). Therefore, there is a need for integrated methodologies that can provide an alternative way to carefully reconstruct the evolutive history of tidal meander bends.

Overall, less attention has been paid to the development of meandering tidal channels from microtidal regimes, although this tidal range typifies a large part of coastal areas throughout the world (Fig. 10). Knowledge gaps are even more considerable for subtidal channels, which have been investigated by few studies (e.g. La Croix and Dashtgard, 2015; Ghinassi et al., 2019), despite being widely present in coastal environments [for example, the Geum River estuary (Korea) and Hammocks Beach State Park, North Carolina (USA)].

1.4 Choice of study area and methods

To address these knowledge gaps, this study analyses the FTMC deposits in the north-eastern coastal plain of Italy, an area suitable for integrated 3D analysis and where the coasts are characterised by a microtidal regime. This study is based on a multidisciplinary and integrated approach that provides spatial information on the variability of sedimentary properties in FTMC deposits.

The north-eastern coastal plain of Italy, in the Mediterranean Sea, provides a unique environment to analyse FTMC deposits. Specifically, the Venetian Plain originated due to the aggradation of the main fluvial channels during Holocene time (Fontana et al., 2008), still shows perfectly visible traces of ancient fluvial channels. These ancient rivers mainly developed meandering patterns and meander bends with different morphologies. The southern portion of the plain is the one where the river traces are best preserved, being mainly occupied by crops and sparsely urbanised. Nowadays, this portion is mainly drained by the Adige and Brenta Rivers (Fig. 20A). Both rivers flow eastward into the Adriatic Sea and have their sources in the Trentino Alto Adige region (Italy). The Adige River is the second longest Italian river, after the Po River, with a length of 410 km and a mountain catchment of 11,000 km^2 (Bondesan, 2001). The Brenta River is 174 km long and has a catchment area of 5840 km^2. The visible traces of paleo-meanders belongs mainly to the ancient evolution of these two fluvial channels, along with ancient, poorly-defined branches of the Po River that expanded in the area until about 3000 years ago (Piovan et al., 2012).

The southern portion of the Venetian Plain borders the Venice Lagoon, which offers the possibility to study tidal meandering channels developed in a microtidal regime. The Venice Lagoon is the greatest brackish water body of the Mediterranean Sea and developed over the last 7500 years (McClennen and Housley, 2006; Zecchin et al., 2008). It is characterised by a dense network of tidal channels crossing tidal flats and salt marshes, and a mean tidal range of 1.0

m and 0.75 m around mean sea level (MSL), respectively (D'Alpaos et al., 2013). Being the coasts of the Venetian Plain affected by a microtidal regime, the effect of a reduced tidal range on the dynamics and sedimentation of fluvial channels can be also evaluated.

From a methodological point of view, freely distributed satellite images (i.e., Bing and Google Earth images), covering a range of almost ten years (2010-2021), and aerial photos were used to select ancient channel belts and individual meander bends characterised by different morphologies. The absence of vertical outcrops or/and planform exposures led to the study of the internal architecture and deposits of FTMC through sedimentary cores. A hand auger was chosen to sample muddy deposits (i.e., overbanks and tidal ones) and surficial sandy ones (i.e., upper 2 meters from the ground), as it cheaply allows to recover several cores in moderate time intervals (i.e., 2/3 cores per hour). To reach greater depths, especially in point-bar deposits, a continuous drilling core sampler was used, as it allows to recover sand also at higher depths. Grain-size analyses were performed to quantitively analyse grain-size trends within point-bar deposits. Specifically, the dry-sieving approach was the most appropriate for sandy samples, whereas muddy deposits were analysed through a laser diffractometer, which is suitable for fine materials. To analyse subsurface deposits in a spatial and three-dimensional manner, geophysical surveys were conducted. Although the popularity of ground penetrating radar (GPR) for characterising subsurface fluvial deposits (e.g., Peretti et al., 1999; Lesmes et al., 2002), results from its application would have been compromised by the occurrence of salt-water from the sea (cf. Galgaro et al., 2000). Electromagnetic approaches can overcome this limitation. Thus, to extensively analyse subsurface volumes of deposits in the Venetian Plain, electromagnetic induction (EMI) investigations in the frequency domain (FDEM) were performed (Boaga, 2017), instead of linear tomographic acquisitions. In the Venice Lagoon, acoustic data were treated to reconstruct the subsurface, as they were available from a previous study (Madricardo et al., 2007). Finally, data were statistically analysed through univariate (e.g., 2D plots) and multivariate tools (e.g., Principal Component Analysis), to precisely describe samples and analyse the relationships between morphological and sedimentological elements.

1.5 Goals of the study

Towards the goal of improving the current knowledge of meander-bend deposits from FTMC and providing useful methodologies and data for aquifer management, the present work investigates how sediment properties vary within point-bar bodies developed in different depositional settings, such as purely fluvial and purely tidal ones. A multidisciplinary and integrated approach has been used, combining remote sensing analysis, recovery of sedimentary cores, geophysical investigations, laboratory techniques, literature review and statistical analyses. In this framework, the research questions of this study have been addressed following the main workflow listed below:

1. *What do morphologies and deposits of purely fluvial and purely tidal meandering channels of the Venetian Plain look like? How can they be compared with classical models?*
   Through these general questions, the present work aims to characterise selected point-bar deposits from fluvial and tidal realms, by analysing the origin, development, and abandonment processes of meander-bends and related deposits.

2. *How can we effectively and quantitatively investigate the spatial variability of sediment textural properties within FTMC deposits?*
   Sedimentary cores are essential to internally analyse point-bar deposits but provide local information. Conversely, geophysical analysis supplies 3D-extensive data that however indirectly and qualitatively describe the variability of sediment properties within meander-bend deposits. The present work proposes a method to integrate core and geophysical data to develop quantitative models related to sedimentary-property distribution within point-bar deposits.

3. *How do sedimentary and morphological features of meandering channels vary at the channel-belt scale?*
   Once different types of point-bar deposits were analysed individually, this study focused on the scale of a channel belt located within the fluvio-transition zone, since deposits forming these elements are the major conduits for groundwater flow, defining the subsurface permeability paths.

1.6 Thesis outline

The introductory chapter is followed by six main chapters.

Chapter 2 contains a brief overview of the study sites and the description of methods adopted in the following chapters.

Chapter 3 contributes to answering the first research question by analysing a purely fluvial paleo-meander bend. Sedimentological and geophysical investigations are combined to analyse the impact of genesis and abandonment processes on geometries and sediment properties of a fluvial point-bar body.

Chapter 4 further contributes to addressing the first question by analysing a paleo-meander bend from a purely tidal environment. Sedimentological and geophysical data are coupled together to highlight the relevance of high-resolution 3D reconstructions for linking sedimentary products and paleo-morphodynamic processes.

Chapter 5 focuses on the second research question by proposing a new multidisciplinary approach to extensively investigate the spatial variability of sediment textural properties within paleo-meanders. By statistically analysing geophysical and sedimentological data, the proposed approach can be applied to retrieve the fundamental data required for modelling groundwater flows within surficial aquifers.

Contributing to answering the fourth research question, chapter 6 investigates morphological and sedimentary features at the channel-belt scale, by analysing the dynamic response of a fluvial paleo-channel belt to floodplain micro-morphologies and heterogeneities, and the proximity of the coastline.

A summary of the main results obtained from this thesis is finally traced in the seventh chapter (i.e., the Conclusions).

Appendices A and B include two publications to which I contributed as co-author. Appendix A is an integration of chapter 3, in which the results from the same study area were treated from a remote-sensing and geophysical point of view, highlighting the novelty of the geophysical methodology for the objectives of this thesis. To show the implications of sedimentary heterogeneities of FTMC deposits in controlling groundwater and pollutant flows within surficial aquifers, Appendix B shows an example of the straightforward application of the detailed sedimentological results from chapter 4 to provide numerical modelling simulations of flow propagation in the subsurface.

Appendix A embodies a research paper that was published in *Remote sensing* (Cassiani et al., 2020); Appendix B is a manuscript that has been accepted for publication in *Environmental Modelling and Software* pending minor revision.

References

Abdul Nassir, S.S., Loke, M.H., Lee, C.Y., and Nawawi, M.N.M., 2000, Salt-water intrusion mapping by geoelectrical imaging surveys: Geophysical Prospecting, v. 48, p. 647–661, doi:10.1046/j.1365-2478.2000.00209.x.

Abidin, H., Andreas, H., Gumilar, I., Fukuda, Y., Pohan, Y.E., and Deguchi, T., 2011, Land subsidence of Jakarta (Indonesia) and its relation with urban development: Nature Hazards, v. 59, p. 1753–1771, doi:10.1007/s11069-011-9866-9.

Agoubi, B., 2021, A review: saltwater intrusion in North Africa's coastal areas—current state and future challenges: Environmental Science and Pollution Research, v. 28, p. 17029–17043, doi:10.1007/s11356-021-12741-z.

Ahuja, S., 2008, Arsenic contamination of groundwater: mechanism, analysis, and remediation: Hoboken, New Jersey, John Wiley \& Sons.

Allen, J.R.L., 1965, A review of the origin and characteristics of recent alluvial sediments: Sedimentology, v. 5, p. 89–191, doi:10.1111/j.1365-3091.1965.tb01561.x.

Allen, J.R.L., 1982, Sedimentary structures - Their character and Physical Basis, Volume II: Amsterdam, The Netherlands, Elsevier Scientific Publishing Company, v. 2, 662 p.

Allen, J.R.L., 1970, Studies in fluviatile sedimentation: a comparison of fining-upwards cyclothems, with special reference to coarse-member composition and interpretation: Journal of Sedimentary Research, v. 40, p. 298–323.

Amaya, A.G., Dahlin, T., Barmen, G., and Rosberg, J.E., 2016, Electrical resistivity tomography and induced polarization for mapping the subsurface of alluvial fans: A case study in Punata (Bolivia): Geosciences (Switzerland), v. 6, p. 51, doi:10.3390/geosciences6040051.

Archer, A.W., 2013, World's highest tides: Hypertidal coastal systems in North America, South America and Europe: Sedimentary Geology, v. 284–285, p. 1–25, doi:10.1016/j.sedgeo.2012.12.007.

Awad, S., Araffa, S., and Pek, J., 2014, Delineating Groundwater Aquifer and Subsurface Structures Using Integrated Geophysical Interpretation at the Western Part of Gulf of Aqaba, Sinai, Egypt: International Journal of Water Resources and Arid Environments, v. 3, p. 51–62.

Bagnold, R.A., 1960, Some aspects of the shape of river meanders: U.S. Geological Survey Professional Paper, v. 282-E, p. 371–375, doi:10.1080/00207217608920581.

Baines, D., Smith, D.G., Froese, D.G., Bauman, P., and Nimeck, G., 2002, Electrical resistivity ground imaging (ERGI): A new tool for mapping the

lithology and geometry of channel-belts and valley-fills: Sedimentology, v. 49, p. 441–449, doi:10.1046/j.1365-3091.2002.00453.x.

Barbier, E.B., Hacker, S.D., Kennedy, C., Koch, E.W., Stier, A.C., and Silliman, B.R., 2011, The value of estuarine and coastal ecosystem services: Ecological Monographs, v. 81, p. 169–193, doi:10.1890/10-1510.1.

Barlow, P.M., 2003, Ground water in freshwater-saltwater environments of the Atlantic Coast: 1–113 p., doi:10.3133/cir1262.

Barwis, J.H., 1977, Sedimentology of some South Carolina tidal-creek point bars, and a comparison with their fluvial counterparts: Fluvial Sedimentology, v. 5, p. 129–160.

Berg, M., Tran, H.C., Nguyen, T.C., Pham, H.V., Schertenleib, R., and Giger, W., 2001, Arsenic contamination of groundwater and drinking water in Vietnam: A human health threat: Environmental Science and Technology, v. 35, p. 2621–2626, doi:10.1021/es010027y.

Van den Berg, J.H., Boersma, J.R., and van Gelder, A., 2007, Diagnostic sedimentary structures of the fluvial-tidal transition zone - Evidence from deposits of the Rhine and Meuse: Geologie en Mijnbouw/Netherlands Journal of Geosciences, v. 86, p. 287–306, doi:10.1017/s0016774600077866.

Bhattacharyya, P., Bhattacharya, J.P., and Khan, S.D., 2015, Paleo-channel reconstruction and grain size variability in fluvial deposits, Ferron Sandstone, Notom Delta, Hanksville, Utah: Sedimentary Geology, v. 325, p. 17–25, doi:10.1016/j.sedgeo.2015.05.001.

Bluck, B.J., 1971, Sedimentation in the meandering river Endrick: Scottish Journal of Geology, v. 7, p. 93–138, doi:10.1144/sjg07020093.

Blum, M.D., and Valastro, S., 1994, Late Quaternary sedimentation, lower Colorado River, Gulf Coastal Plain of Texas: Geological Society of America Bulletin, v. 106, p. 1002–1016, doi:10.1130/0016-7606(1994)106<1002:LQSLCR>2.3.CO;2.

Boaga, J., 2017, The use of FDEM in hydrogeophysics: A review: Journal of Applied Geophysics, v. 139, p. 36–46, doi:10.1016/j.jappgeo.2017.02.011.

Bondesan, M., 2001, Hydrography, *in* Castiglioni, G.B. and Pellegrini, G.B. eds., Illustrative Notes of the Geomorphological Map of Po Plain (Italy)., Geografia Fisica Dinamica Quaternaria, 4, p. 33–44.

Boyer, P., Roberts, N., and Baird, D., 2006, Holocene environment and settlement on the {Ç}arşamba alluvial fan, south-central {T}urkey: Integrating geoarchaeology and archaeological field survey: Geoarchaeology, v. 21, p. 675–698, doi:10.1002/gea.20133.

De breuck, G., and De moor, G., 1969, The water-table aquifer in the eastern coastal area of belgium: International Association of Scientific Hydrology. Bulletin, v. 14, p. 137–155, doi:10.1080/02626666909493739.

Brice, J.C., 1975, Airphoto interpretation of the form and behavior of alluvial rivers.:

Brice, J.C., 1974, Evolution of meander loops: Geological Society of America Bulletin, v. 85, p. 581–586, doi:10.1130/0016-

7606(1974)85<581:EOML>2.0.CO;2.

Bridge, J.S., 2003, Rivers and floodplains. Forms, Processes and Sedimentary Record: Blackwell Science, v. 491.

Bridge, J.S., Alexander, J.A.N., Collier, R.E.L., Gawthorpe, R.L., and Jarvis, J., 1995, Ground-penetrating radar and coring used to study the large-scale structure of point-bar deposits in three dimensions: Sedimentology, v. 42, p. 839–852, doi:10.1111/j.1365-3091.1995.tb00413.x.

Bridges, P.H., and Leeder, M.R., 1976, Sedimentary model for intertidal mudflat channels, with examples from the Solway Firth, Scotland: Sedimentology, v. 23, p. 533–552, doi:10.1111/j.1365-3091.1976.tb00066.x.

Brivio, L., Ghinassi, M., D'Alpaos, A., Finotello, A., Fontana, A., Roner, M., and Howes, N., 2016, Aggradation and lateral migration shaping geometry of a tidal point bar: An example from salt marshes of the Northern Venice Lagoon (Italy): Sedimentary Geology, v. 343, p. 141–155, doi:10.1016/j.sedgeo.2016.08.005.

Burge, L.M., and Smith, D.G., 1999, Confined Meandering River Eddy Accretions: Sedimentology, Channel Geometry and Depositional Processes, *in* Fluvial Sedimentology VI, International Association of Sedimentologists, Special Publication, v. 28, p. 113–130, doi:10.1002/9781444304213.ch9.

Cabello, P., Domínguez, D., Murillo-López, M.H., López-Blanco, M., García-Sellés, D., Cuevas, J.L., Marzo, M., and Arbués, P., 2018, From conventional outcrop datasets and digital outcrop models to flow simulation in the Pont de Montanyana point-bar deposits (Ypresian, Southern Pyrenees): Marine and Petroleum Geology, v. 94, p. 19–42, doi:10.1016/j.marpetgeo.2018.03.040.

Cao, T., Han, D., and Song, X., 2021, Past, present, and future of global seawater intrusion research: A bibliometric analysis: Journal of Hydrology, v. 603, p. 126844, doi:10.1016/j.jhydrol.2021.126844.

Carling, P.A., Chateau, C.. C., Leckie, D.A., Langdon, C.T., Scaife, R.G., and Parsons, D.R., 2015, Sedimentology of a tidal point-bar within the fluvial-tidal transition: River Severn Estuary, UK, *in* Ashworth, P.J., Best, J.L., and Parsons, D.R. eds., Fluvial-Tidal Sedimentology. Developments in Sedimentology., Elsevier B.V., v. 68, p. 149–189, doi:10.1016/B978-0-444-63529-7.00008-0.

Carraro, A., Fabbri, P., Giaretta, A., Peruzzo, L., Tateo, F., and Tellini, F., 2013, Arsenic anomalies in shallow Venetian Plain (Northeast Italy) groundwater: Environmental Earth Sciences, v. 70, p. 3067–3084, doi:10.1007/s12665-013-2367-2.

Cartwright, K., and McComas, M.R., 1968, Geophysical Surveys in the Vicinity of Sanitary Landfills in Northeastern Illinois: Groundwater, v. 6, p. 23–30, doi:10.1111/j.1745-6584.1968.tb01661.x.

Choi, K., 2011, Tidal rhythmites in a mixed-energy, macrotidal estuarine channel, Gomso Bay, west coast of Korea: Marine Geology, v. 280, p. 105–115, doi:10.1016/j.margeo.2010.12.004.

Choi, K.S., and Dalrymple, R.W., 2004, Recurring tide-dominated sedimentation

in Kyonggi Bay (west coast of Korea): Similarity of tidal deposits in late Pleistocene and Holocene sequences: Marine Geology, v. 212, p. 81–96, doi:10.1016/j.margeo.2004.07.008.

Choi, K.S., Dalrymple, R.W., Chun, S.S., and Kim, S.P., 2004, Sedimentology of modern, Inclined Heterolithic Stratification (IHS) in the macrotidal Han River Delta, Korea: Journal of Sedimentary Research, v. 74, p. 677–689, doi:10.1306/030804740677.

Choi, K., Hong, C.M., Kim, M.H., Oh, C.R., and Jung, J.H., 2013, Morphologic evolution of macrotidal estuarine channels in Gomso Bay, west coast of Korea: Implications for the architectural development of inclined heterolithic stratification: Marine Geology, v. 346, p. 343–354, doi:10.1016/j.margeo.2013.10.005.

Choi, K., and Jo, J., 2015, Morphodynamics and stratigraphic architecture of compound dunes on the open-coast macrotidal flat in the northern Gyeonggi Bay, west coast of Korea: Marine Geology, v. 366, p. 34–48, doi:10.1016/j.margeo.2015.05.002.

Choi, K.S., and Park, Y.A., 2000, Late pleistocene silty tidal rhythmites in the macrotidal flat between Youngjong and Yongyou Islands, west coast of Korea: Marine Geology, v. 167, p. 231–241, doi:10.1016/S0025-3227(00)00037-2.

Choudhury, K., and Saha, D.K., 2004, Integrated Geophysical and Chemical: Ground Water, v. 42, p. 671–677.

Christensen, B.A., and Hatfield, K., 1994, In situ restoration of contaminated surficial aquifers. Part I: The flow process, *in* IAHS Publications - Series of Proceedings and Reports-Intern . Assoc. Hydrological Sciences, p. 313–322.

Constantine, A., Dunne, T., Piégay, H., and Kondolfs, G.M., 2010, Controls on the alluviation of oxbow lakes by bed-material load along the Sacramento River, California: Sedimentology, v. 57, p. 389–407, doi:10.1111/j.1365-3091.2009.01084.x.

Cosma, M., Finotello, A., Ielpi, A., Ventra, D., Oms, O., D'Alpaos, A., and Ghinassi, M., 2020, Piracy-controlled geometry of tide-dominated point bars: Combined evidence from ancient sedimentary successions and modern channel networks: Geomorphology, v. 370, p. 107402, doi:10.1016/j.geomorph.2020.107402.

Cosma, M., Ghinassi, M., D'Alpaos, A., Roner, M., Finotello, A., Tommasini, L., and Gatto, R., 2019, Point-bar brink and channel thalweg trajectories depicting interaction between vertical and lateral shifts of microtidal channels in the Venice Lagoon (Italy): Geomorphology, v. 342, p. 37–50, doi:10.1016/j.geomorph.2019.06.009.

La Croix, A.D., and Dashtgard, S.E., 2015, A synthesis of depositional trends in intertidal and upper subtidal sediments across the tidal–fluvial transition in the Fraser River, Canada.: Journal of Sedimentary Research, v. 85, p. 683–698, doi:10.2110/jsr.2015.47.

D'Alpaos, A., Carniello, L., and Rinaldo, A., 2013, Statistical mechanics of wind wave-induced erosion in shallow tidal basins: Inferences from the Venice

Lagoon: Geophysical Research Letters, v. 40, p. 3402–3407, doi:10.1002/grl.50666.

D'Alpaos, A., Ghinassi, M., Finotello, A., Brivio, L., Bellucci, L.G., and Marani, M., 2017, Tidal meander migration and dynamics: A case study from the Venice Lagoon: Marine and Petroleum Geology, v. 87, p. 80–90, doi:10.1016/j.marpetgeo.2017.04.012.

Dalrymple, R.W., and Choi, K., 2007, Morphologic and facies trends through the fluvial-marine transition in tide-dominated depositional systems: A schematic framework for environmental and sequence-stratigraphic interpretation: Earth-Science Reviews, v. 81, p. 135–174, doi:10.1016/j.earscirev.2006.10.002.

Dalrymple, R.W., Kurcinka, C.E., Jablonski, B.V.J., Ichaso, A.A., and Mackay, D.A., 2015, Deciphering the relative importance of fluvial and tidal processes in the fluvial-marine transition, *in* Ashworth, P.J., Best, J.L., and Parsons, D.R. eds., Fluvial-Tidal Sedimentology. Developments in Sedimentology, Elsevier B.V., v. 68, p. 3–45, doi:10.1016/B978-0-444-63529-7.00002-X.

Van Dam, J.C., and Meulenkamp, J.J., 1967, Some results of the geo-electrical resistivity method in ground water investigations in the Netherlands: Geophysical Prospecting, v. 15, p. 92–115, doi:10.1111/j.1365-2478.1967.tb01775.x.

Daniel, J.F., 1971, Channel movement of meandering Indiana streams: Washington D.C., US Government Printing Office.

Dashtgard, S.E., and La Croix, A.D., 2015, Sedimentological trends across the tidal–fluvial transition, Fraser River, Canada: A review and some broader implications, *in* Ashworth, P.J., Best, J.L., and Parsons, D.R. eds., Fluvial - Tidal Sedimentology. Developments in Sedimentology, Elsevier, v. 68, p. 111–126, doi:10.1016/B978-0-444-63529-7.00005-5.

Dashtgard, S.E., Venditti, J.G., Hill, P.R., Johnson, S.M., and La Croix, A.D., 2012, Sedimentation across the tidal-fluvial transition in the Lower Fraser River , Canada: The Sedimentary Record, v. 10, p. 4–9, doi:10.2110/sedred.2012.4.4.

Davies, J.L., 1964, A morphogenic approach to world shorelines: Zeitschrift für Geomorphologie, v. 8, p. 127–142, doi:10.1127/zfg/mortensen/8/1964/127.

Davies, J.L., 1980, Geographical Variation in Coastal Development (Longman, Ed.): Berkeley, 212 p.

Delagnes, A., Tribolo, C., Bertran, P., Brenet, M., Crassard, R., Jaubert, J., Khalidi, L., Mercier, N., Nomade, S., Peigné, S., Sitzia, L., Tournepiche, J.F., Al-Halibi, M., Al-Mosabi, A., MacChiarelli, R., 2012, Inland human settlement in southern Arabia 55,000 years ago. New evidence from the Wadi Surdud Middle Paleolithic site complex, western Yemen: Journal of Human Evolution, v. 63, p. 452–474, doi:10.1016/j.jhevol.2012.03.008.

Deng, Y., Wang, Y., and Ma, T., 2009, Isotope and minor element geochemistry of high arsenic groundwater from Hangjinhouqi, the Hetao Plain, Inner Mongolia: Applied Geochemistry, v. 24, p. 587–599,

doi:10.1016/j.apgeochem.2008.12.018.

Desbarats, A.J., Koenig, C.E.M., Pal, T., Mukherjee, P.K., and Beckie, R.D., 2014, Groundwater flow dynamics and arsenic source characterization in an aquifer system of West Bengal, India: Water Resources Research, v. 50, p. 4974–5002, doi:10.1002/2013WR014034.

Dietrich, W.E., 1982, Mechanics of a river meander: Journal of Chemical Information and Modeling, v. 53, p. 18–29.

Dietrich, W.E., and Smith, J.D., 1983, Influence of the point bar on flow through curved channels: Water Resources Research, v. 19, p. 1173–1192, doi:10.1029/WR019i005p01173.

Dietrich, W.E., and Smith, J.D., 1984, Processes controlling the equilibrium bed morphology in river meanders, *in* River Meandering: Proceedings of the Conference Rivers '83, p. 759–769.

Dillon, P., 2005, Future management of aquifer recharge: Hydrogeology Journal, v. 13, p. 313–316, doi:10.1007/s10040-004-0413-6.

Dunne, T., and Aalto, R.E., 2013, Large River Floodplains, *in* Schroder, J.E. and Wohl, E. eds., Treatise on Geomorphology, Elsevier Ltd., v. 9, p. 645–678, doi:10.1016/B978-0-12-374739-6.00258-X.

Durkin, P.R., Boyd, R.L., Hubbard, S.M., Shultz, A.W., and Blum, M.D., 2017, Three-dimensional reconstruction of meander-belt evolution, Cretaceous McMurray Formation, Alberta foreland basin, Canada: Journal of Sedimentary Research, v. 87, p. 1075–1099, doi:10.2110/jsr.2017.59.

Durkin, P.R., Hubbard, S.M., Smith, D.G., and Leckie, D.A., 2018, Predicting heterogeneity in meandering fluvial and tidal-fluvial deposits: The point bar to counter point bar transition, *in* Ghinassi, M., Colombera, L., Mountney, N.P., and Reesink, J.H. eds., Fluvial Meanders and Their Sedimentary Products in the Rock Record. Int. Assoc. Sedimentol. Spec. Publ., John Wiley & Sons, v. 48, p. 231–250, doi:10.1002/9781119424437.ch9.

Ebraheem, A.-A.M., Senosy, M.M., and Dahab, K. a., 1997, Geoelectrical and hydrogeochemical studies for delineating ground-water contamination due to salt water intrusion: Ground Water, v. 35, p. 216–222.

Fagherazzi, S., 2008, Self-organization of tidal deltas: Proceedings of the National Academy of Sciences of the United States of America, v. 105, p. 18692–18695, doi:10.1073/pnas.0806668105.

Fagherazzi, S., Gabet, E.J., and Furbish, D.J., 2004, The effect of bidirectional flow on tidal channel planforms: Earth Surface Processes and Landforms, v. 29, p. 295–309, doi:10.1002/esp.1016.

Fenies, H., and Faugères, J.C., 1998, Facies and geometry of tidal channel-fill deposits (Arcachon Lagoon, SW France): Marine Geology, v. 150, p. 131–148, doi:10.1016/S0025-3227(98)00049-8.

Fennema, R.J., and Newton, V.P., 1982, Ground water resources of the Eastern Shore of Virginia: State Water Control Board, Commonwealth of Virginia, v. 332, 74 p.

Ferguson, R.I., Parsons, D.R., Lane, S.N., and Hardy, R.J., 2003, Flow in meander

bends with recirculation at the inner bank: Water resources research, v. 39, p. 1322, doi:10.1029/2003WR001965.

Fielding, C.R., and Crane, R.C., 1987, An application of statistical modelling to the prediction of hydrocarbon recovery factors in fluvial reservoir sequences:

Finotello, A., 2017, Tidal channel patterns: field investigations, numerical modelling and laboratory experiments: University of Padova, 211 p.

Finotello, A., D'Alpaos, A., Bogoni, M., Ghinassi, M., and Lanzoni, S., 2020a, Remotely-sensed planform morphologies reveal fluvial and tidal nature of meandering channels: Scientific Reports, v. 10, p. 1–13, doi:10.1038/s41598-019-56992-w.

Finotello, A., Ghinassi, M., Carniello, L., Belluco, E., Pivato, M., Tommasini, L., and D'Alpaos, A., 2020b, Three-dimensional flow structures and morphodynamic evolution of microtidal meandering channels: Water Resources Research, v. 56, p. e2020WR027822, doi:10.1029/2020WR027822.

Fisk, H.N., 1947, Fine-grained alluvial deposits and their effects on Mississippi River activity. Vols 1 & 2: Vicksburg, Mississippi, Mississippi River Commission, doi:10.1086/625561.

Fontana, A., Mozzi, P., and Bondesan, A., 2008, Alluvial megafans in the Venetian-Friulian Plain (north-eastern Italy): Evidence of sedimentary and erosive phases during Late Pleistocene and Holocene: Quaternary International, v. 189, p. 71–90, doi:10.1016/j.quaint.2007.08.044.

De Franco, R., Biella, G., Tosi, L., Teatini, P., Lozej, A., Chiozzotto, B., Giada, M., Rizzetto, F., Claude, C., Mayer, A., Bassan, V., Gasparetto-Stori, G., 2009, Monitoring the saltwater intrusion by time lapse electrical resistivity tomography: The Chioggia test site (Venice Lagoon, Italy): Journal of Applied Geophysics, v. 69, p. 117–130, doi:10.1016/j.jappgeo.2009.08.004.

Friend, P.F., and Sinha, R., 1993, Braiding and meandering parameters, *in* Best, J.L. and Bristow, C.S. eds., Braided Rivers, London, Special Publications, Geological Society, v. 75, p. 105–111, doi:10.1144/GSL.SP.1993.075.01.05.

Frings, R.M., 2008, Downstream fining in large sand-bed rivers: Earth-Science Reviews, v. 87, p. 39–60, doi:10.1016/j.earscirev.2007.10.001.

Frohlich, R.K., Urish, D.W., Fuller, J., and O'Reilly, M., 1994, Use of geoelectrical methods in groundwater pollution surveys in a coastal environment: Journal of Applied Geophysics, v. 32, p. 139–154, doi:10.1016/0926-9851(94)90016-7.

Frothingham, K.M., and Rhoads, B.L., 2003, Three-dimensional flow structure and channel change in an asymmetrical compound meander loop, Embarras River, Illinois: Earth Surface Processes and Landforms: The Journal of the British Geomorphological Research Group, v. 28, p. 625–644, doi:10.1002/esp.471.

Fruergaard, M., Andersen, T.J., Nielsen, L.H., Madsen, A.T., Johannessen, P.N., Murray, A.S., Kirkegaard, L., and Pejrup, M., 2011, Punctuated sediment record resulting from channel migration in a shallow sand-dominated

micro-tidal lagoon, Northern Wadden Sea, Denmark: Marine Geology, v. 280, p. 91–104, doi:10.1016/j.margeo.2010.12.003.

Fustic, M., Strobl, R., Ghinassi, M., and Zhang, S., 2018, Unsuccessful cut offs--origin and partial preservation of enigmatic channel fills encased within a large-scale point-bar deposit--The McMurray Formation type section, Alberta, Canada, *in* Ghinassi, M., Colombera, L., Mountney, N.P., and Reesink, J.H. eds., Fluvial Meanders and Their Sedimentary Products in the Rock Record. Int. Assoc. Sedimentol. Spec. Publ. 48, John Wiley & Sons, Ltd Chichester, UK, p. 321–348, doi:10.1002/9781119424437.ch13.

Galgaro, A., Finzi, E., and Tosi, L., 2000, An experiment on a sand-dune environment in Southern Venetian coast based on GPR, VES and documentary evidence: Annals of Geophysics, v. 43, p. 289–295, doi:10.4401/ag-3643.

Garcés-Vargas, J., Schneider, W., Pinochet, A., Piñones, A., Olguin, F., Brieva, D., and Wan, Y., 2020, Tidally forced saltwater intrusions might impact the quality of drinking water, the Valdivia river (40°s), Chile estuary case: Water, v. 12, doi:10.3390/W12092387.

Ghinassi, M., D'alpaos, A., Gasparotto, A., Carniello, L., Brivio, L., Finotello, A., Roner, M., Franceschinis, E., Realdon, N., Howes, N., Cantelli, A., 2018a, Morphodynamic evolution and stratal architecture of translating tidal point bars: Inferences from the northern Venice Lagoon (Italy): Sedimentology, v. 65, p. 1354–1377, doi:10.1111/sed.12425.

Ghinassi, M., Brivio, L., D'Alpaos, A., Finotello, A., Carniello, L., Marani, M., and Cantelli, A., 2018b, Morphodynamic evolution and sedimentology of a microtidal meander bend of the Venice Lagoon (Italy): Marine and Petroleum Geology, v. 96, p. 391–404, doi:10.1016/j.marpetgeo.2018.06.011.

Ghinassi, M., D'Alpaos, A., Tommasini, L., Brivio, L., Finotello, A., and Stefani, C., 2019, Tidal currents and wind waves controlling sediment distribution in a subtidal point bar of the Venice Lagoon (Italy): Sedimentology, v. 66, p. 2926–2949, doi:10.1111/sed.12616.

Ghinassi, M., and Ielpi, A., 2015, Stratal architecture and morphodynamics of downstream-migrating fluvial point bars (Jurassic Scalby Formation, UK): Journal of Sedimentary Research, v. 85, p. 1123–1137, doi:10.2110/jsr.2015.74.

Ghinassi, M., Ielpi, A., Aldinucci, M., and Fustic, M., 2016, Downstream-migrating fluvial point bars in the rock record: Sedimentary Geology, v. 334, p. 66–96, doi:10.1016/j.sedgeo.2016.01.005.

Ghinassi, M., Nemec, W., Aldinucci, M., Nehyba, S., Özaksoy, V., and Fidolini, F., 2014, Plan-form evolution of ancient meandering rivers reconstructed from longitudinal outcrop sections: Sedimentology, v. 61, p. 952–977, doi:10.1111/sed.12081.

Ghinassi, M., Oms, O., Cosma, M., Finotello, A., and Munari, G., 2021, Reading tidal processes where their signature is cryptic: The Maastrichtian meandering channel deposits of the Tremp Formation (Southern Pyrenees,

Spain): Sedimentology, v. 68, p. 2009–2042, doi:10.1111/sed.12840.
Giacomelli, S., Rossi, V., Amorosi, A., Bruno, L., Campo, B., Ciampalini, A., Civa, A., Hong, W., Sgavetti, M., and de Souza Filho, C.R., 2018, A mid-late Holocene tidally-influenced drainage system revealed by integrated remote sensing, sedimentological and stratigraphic data: Geomorphology, v. 318, p. 421–436, doi:10.1016/j.geomorph.2018.07.004.
Gibling, M.R., Nanson, G.C., and Maroulis, J.C., 1998, Anastomosing river sedimentation in the Channel Country of central Australia: Sedimentology, v. 45, p. 595–619, doi:10.1046/j.1365-3091.1998.00163.x.
Goodell, H.G., 1986, A study of saltwater intrusion into the surface aquifer and the underlying of Yorktown Aquifer of Coastal Virginia: Final Report to Virginia Environmental Endowment Richmond, VA, p. 14.
Gorycki, M.A., 1973, Hydraulic drag: A meander-initiating mechanism: Reply: Bulletin of the Geological Society of America, v. 84, p. 3119–3122, doi:10.1130/0016-7606(1973)84<3119:HDAMMR>2.0.CO;2.
Gray, A.B., Pasternack, G.B., Watson, E.B., and Goñi, M.A., 2016, Abandoned channel fill sequences in the tidal estuary of a small mountainous, dry-summer river: Sedimentology, v. 63, p. 176–206, doi:10.1111/sed.12223.
Gugliotta, M., 2016, The Fluvial To Marine Transition Zone and Its Stratigraphic Significance: The University of Manchester(United Kingdom), 241 p.
Gugliotta, M., Flint, S.S., Hodgson, D.M., and Veiga, G.D., 2016, Recognition criteria, characteristics and implications of the fluvial to marine transition zone in ancient deltaic deposits (Lajas Formation, Argentina): Sedimentology, v. 63, p. 1971–2001, doi:10.1111/sed.12291.
Gugliotta, M., Saito, Y., Nguyen, V.L., Ta, T.K.O., Nakashima, R., Tamura, T., Uehara, K., Katsuki, K., and Yamamoto, S., 2017, Process regime, salinity, morphological, and sedimentary trends along the fluvial to marine transition zone of the mixed-energy Mekong River delta, Vietnam: Continental Shelf Research, v. 147, p. 7–26, doi:10.1016/j.csr.2017.03.001.
Gugliotta, M., Saito, Y., Nguyen, V.L., Ta, T.K.O., Tamura, T., and Fukuda, S., 2018, Tide- and River-Generated Mud Pebbles from the Fluvial To Marine Transition Zone of the Mekong River Delta, Vietnam: Journal of Sedimentary Research, v. 88, p. 981–990, doi:10.2110/jsr.2018.54.
Gupta, A., 2008, Large rivers: geomorphology and management: Chichester, UK, John Wiley & Sons, 661 p.
Hagstrom, C.A., Hubbard, S.M., Leckie, D.A., and Durkin, P.R., 2019, The Effects of Accretion-package Geometry On Lithofacies Distribution in Point-bar Deposits: Journal of Sedimentary Research, v. 89, p. 381–398, doi:10.2110/jsr.2019.23.
Harvey, C.F., Ashfaque, K.N., Yu, W., Badruzzaman, A.B.M., Ali, M.A., Oates, P.M., Michael, H.A., Neumann, R.B., Beckie, R., Islam, S., Ahmed, M.F., 2006, Groundwater dynamics and arsenic contamination in Bangladesh: Chemical Geology, v. 228, p. 112–136, doi:10.1016/j.chemgeo.2005.11.025.
Hickin, E.J., 1986, Concave-Bank Benches in the Floodplains of Muskwa and Fort

Nelson Rivers, British Columbia: Canadian Geographer / Le Géographe canadien, v. 30, p. 111–122, doi:10.1111/j.1541-0064.1986.tb01036.x.

Hickin, E.J., 1974, The development of meanders in natural river-channels: American Journal of Science, v. 274, p. 414–442, doi:10.2475/ajs.274.4.414.

Hickin, E.J., and Nanson, G.C., 1975, The character of channel migration on the Beatton River, Northeast British Columbia, Canada: Bulletin of the Geological Society of America, v. 86, p. 487–494, doi:10.1130/0016-7606(1975)86<487:TCOCMO>2.0.CO;2.

Hubbard, S.M., Smith, D.G., Nielsen, H., Leckie, D.A., Fustic, M., Spencer, R.J., and Bloom, L., 2011, Seismic geomorphology and sedimentology of a tidally influenced river deposit, Lower Cretaceous Athabasca oil sands, Alberta, Canada: AAPG Bulletin, v. 95, p. 1123–1145, doi:10.1306/12131010111.

Hughes, Z.J., 2012, Tidal Channels on Tidal Flats and Marshes, *in* Davis, R.A. and Dalrymple, R.W. eds., Principles of Tidal Sedimentology, New York, Springer, p. 269–300, doi:10.1007/978-94-007-0123-6_11.

Hussain, M.S., Abd-Elhamid, H.F., Javadi, A.A., and Sherif, M.M., 2019, Management of Seawater Intrusion in Coastal Aquifers: A Review: Water, v. 11, p. 1–20, doi:10.3390/w11122467.

Ibrahim, H.A., Al Gabery, A.S., and Abdulqader, A.A., 2011, Use of Vertical Electrical Sounding for Delineating Groundwater Contamination in the Uplands Wadi Rasyan, Taiz, Yemen.: Journal of King Abdulaziz University Earth Sciences, v. 22, p. 131–154, doi:10.4197/ear.22-2.6.

Ielpi, A., and Ghinassi, M., 2014, Planform architecture, stratigraphic signature and morphodynamics of an exhumed Jurassic meander plain (Scalby Formation, Yorkshire, UK): Sedimentology, v. 61, p. 1923–1960, doi:10.1111/sed.12122.

Ielpi, A., and Rainbird, R.H., 2015, Architecture and morphodynamics of a 1.6 Ga fluvial sandstone: Ellice Formation of Elu Basin, Arctic Canada: Sedimentology, v. 62, p. 1950–1977, doi:10.1111/sed.12211.

Ikeda, S., Parker, G., and Sawai, K., 1981, Bend theory of river meanders. Part 1. Linear development: Journal of Fluid Mechanics, v. 112, p. 363–377, doi:10.1017/S0022112081000451.

Jablonski, B.V.J., and Dalrymple, R.W., 2016, Recognition of strong seasonality and climatic cyclicity in an ancient, fluvially dominated, tidally influenced point bar: Middle McMurray Formation, Lower Steepbank River, north-eastern Alberta, Canada: Sedimentology, v. 63, p. 552–585, doi:10.1111/sed.12228.

Jackson, R.G., 1976, Depositional model of point bars in the lower Wabash River: Journal of Sedimentary Research, v. 46, p. 579–594, doi:10.1306/212F6FF5-2B24-11D7-8648000102C1865D.

Johnson, S.M., and Dashtgard, S.E., 2014, Inclined heterolithic stratification in a mixed tidal--fluvial channel: differentiating tidal versus fluvial controls on sedimentation: Sedimentary Geology, v. 301, p. 41–53,

doi:10.1016/j.sedgeo.2013.12.004.
Jordan, D.W., and Pryor, W.A., 1992, Hierarchical levels of heterogeneity in a Mississippi River meander belt and application to reservoir systems: American Association of Petroleum Geologists Bulletin, v. 76, p. 1601–1624, doi:10.1306/BDFF8A6A-1718-11D7-8645000102C1865D.
Kayan, I., 1999, Holocene stratigraphy and geomorphological evolution of the Aegean coastal plains of Anatolia: Quaternary Science Reviews, v. 18, p. 541–548, doi:10.1016/S0277-3791(98)90095-6.
Kearney, W.S., and Fagherazzi, S., 2016, Salt marsh vegetation promotes efficient tidal channel networks: Nature Communications, v. 7, doi:10.1038/ncomms12287.
Kellerhals, R., Church, M., and Bray, D.I., 1976, Classification and analysis of river processes: Journal of the Hydraulics Division, v. 102, p. 813–829.
Klassen, J., and Allen, D.M., 2017, Assessing the risk of saltwater intrusion in coastal aquifers: Journal of Hydrology, v. 551, p. 730–745, doi:10.1016/j.jhydrol.2017.02.044.
Knighton, A.D., 1999, Downstream variation in stream power: Geomorphology, v. 29, p. 293–306, doi:10.1016/S0169-555X(99)00015-X.
Labrecque, P.A., Jensen, J.L., Hubbard, S.M., and Nielsen, H., 2011, Sedimentology and stratigraphic architecture of a point bar deposit, Lower Cretaceous McMurray Formation, Alberta, Canada: Bulletin of Canadian Petroleum Geology, v. 59, p. 147–171, doi:10.2113/gscpgbull.59.2.147.
Langat, P.K., Kumar, L., and Koech, R., 2019, Monitoring river channel dynamics using remote sensing and GIS techniques: Geomorphology, v. 325, p. 92–102, doi:10.1016/j.geomorph.2018.10.007.
Lanzoni, S., and D'Alpaos, A., 2015, On funneling of tidal channels: Journal of Geophysical Research: Earth Surface, v. 120, p. 433–452, doi:10.1002/2014JF003203.
Leopold, L.B., and Wolman, M.G., 1957, River channel patterns: braided, meandering, and straight: US Government Printing Office.
Leopold, L.B., and Wolman, M.G., 1960, River Meanders: Geological Soceity of America Bulletin, v. 71, p. 769–793, doi:10.1130/0016-7606(1960)71[769:RM]2.0.CO;2.
Lesmes, D.P., Decker, S.M., and Roy, D.C., 2002, A multiscale radar-stratigraphic analysis of fluvial aquifer heterogeneity: Geophysics, v. 67, p. 1452–1464, doi:10.1190/1.1512745.
Lewin, J., 1976, Initiation of bed forms and meanders in coarse-grained sediment: Bulletin of the Geological Society of America, v. 87, p. 281–285, doi:10.1130/0016-7606(1976)87<281:IOBFAM>2.0.CO;2.
Da Lio, C., Carol, E., Kruse, E., Teatini, P., and Tosi, L., 2015, Saltwater contamination in the managed low-lying farmland of the Venice coast, Italy: An assessment of vulnerability: Science of the Total Environment, v. 533, p. 356–369, doi:10.1016/j.scitotenv.2015.07.013.
Mackey, S.D., and Bridge, J.S., 1995, Three-dimensional model of alluvial stratigraphy: theory and application: Journal of Sedimentary Research B:

Stratigraphy & Global Studies, v. B65, p. 7–31, doi:10.1306/d42681d5-2b26-11d7-8648000102c1865d.

Madricardo, F., Donnici, S., Lezziero, A., De Carli, F., Buogo, S., Calicchia, P., and Boccardi, E., 2007, Palaeoenvironment reconstruction in the Lagoon of Venice through wide-area acoustic surveys and core sampling: Estuarine, Coastal and Shelf Science, v. 75, p. 205–213, doi:10.1016/j.ecss.2007.02.031.

Makaske, B., and Weerts, H.J.T., 2005, Muddy lateral accretion and low stream power in a sub-recent confined channel belt, Rhine-Meuse delta, central Netherlands: Sedimentology, v. 52, p. 651–668, doi:10.1111/j.1365-3091.2005.00713.x.

Martínez, M.L., Intralawan, A., Vázquez, G., Pérez-Maqueo, O., Sutton, P., and Landgrave, R., 2007, The coasts of our world: Ecological, economic and social importance: Ecological Economics, v. 63, p. 254–272, doi:10.1016/j.ecolecon.2006.10.022.

Martinius, A.W., Fustic, M., Garner, D.L., Jablonski, B.V.J., Strobl, R.S., MacEachern, J.A., and Dashtgard, S.E., 2017, Reservoir characterization and multiscale heterogeneity modeling of inclined heterolithic strata for bitumen-production forecasting, McMurray Formation, Corner, Alberta, Canada: Marine and Petroleum Geology, v. 82, p. 336–361, doi:10.1016/j.marpetgeo.2017.02.003.

Martinius, A.W., and Gowland, S., 2011, Tide-influenced fluvial bedforms and tidal bore deposits (Late Jurassic Lourinhã Formation, Lusitanian Basin, Western Portugal): Sedimentology, v. 58, p. 285–324, doi:10.1111/j.1365-3091.2010.01185.x.

Martinius, A.W., Jablonski, B.V.J., Fustic, M., Strobl, R., and Van den Berg, J.H., 2015, Fluvial to tidal transition zone facies in the McMurray Formation (Christina River, Alberta, Canada), with emphasis on the reflection of flow intensity in bottomset architecture, *in* Ashworth, P.J., Best, J.L., and Parsons, D.R. eds., Fluvial-Tidal Sedimentology. Developments in Sedimentology., Elsevier, p. 445–480, doi:10.1016/B978-0-444-63529-7.00019-5.

McClennen, C.E., and Housley, R.A., 2006, Late-Holocene Channel Meander Migration and Mudflat Accumulation Rates, Lagoon of Venice, Italy: Journal of Coastal Research, v. 22, p. 930–945, doi:10.2112/03-0113.1.

Mehdi, S.M., Pant, N.C., Saini, H.S., Mujtaba, S.A.I., and Pande, P., 2016, Identification of palaeochannel configuration in the Saraswati River basin in parts of Haryana and Rajasthan, India, through digital remote sensing and GIS: Episodes, v. 39, p. 29–38, doi:10.18814/epiiugs/2016/v39i1/89234.

Miall, A.D., 1985, Architectural-element analysis: A new method of facies analysis applied to fluvial deposits: Earth Science Reviews, v. 22, p. 261–308, doi:10.1016/0012-8252(85)90001-7.

Miall, A.D., 1988, Reservoir heterogeneities in fluvial sandstones: lessons from outcrop studies: AAPG bulletin, v. 72, p. 682–697, doi:10.1306/703C8F01-

1707-11D7-8645000102C1865D.

de Mowbray, T., 1983, The genesis of lateral accretion deposits in recent intertidal mudflat channels, Solway Firth, Scotland: Sedimentology, v. 30, p. 425–435, doi:10.1111/j.1365-3091.1983.tb00681.x.

Mulrennan, M.E., and Woodroffe, C.D., 1998, Saltwater intrusion into the coastal plains of the Lower Mary River, Northern Territory, Australia: Journal of Environmental Management, v. 54, p. 169–188, doi:10.1006/jema.1998.0229.

Musial, G., Reynaud, J.Y., Gingras, M.K., Féniès, H., Labourdette, R., and Parize, O., 2012, Subsurface and outcrop characterization of large tidally influenced point bars of the Cretaceous McMurray Formation (Alberta, Canada): Sedimentary Geology, v. 279, p. 156–172, doi:10.1016/j.sedgeo.2011.04.020.

Myrick, R.M., and Leopold, L.B., 1963, Hydraulic geometry of a small tidal estuary: US Government Printing Office, 18 p.

Nanson, G.C., 1980, Point bar and floodplain formation of the meandering Beatton River, northeastern British Columbia, Canada: Sedimentology, v. 27, p. 3–29, doi:10.1111/j.1365-3091.1980.tb01155.x.

Nanson, G.C., and Page, K., 1983, Lateral accretion of fine-grained concave benches on meandering rivers, *in* Collinson, J.D. and Lewin, J. eds., Modern and ancient fluvial systems. Int. Assoc. Sedimentol. Spec. Publ., Wiley-Blackwell, v. 6, p. 133–143, doi:/10.1002/9781444303773.ch10.

Narayan, K. a, Schleeberger, C., Charlesworth, P.B., and Bristow, K.L., 1993, Effects Of Groundwater Pumping On Saltwater Intrusion In The Lower Burdekin Delta , North Queensland: Delta, p. 224–229.

Nichols, M.M., Johnson, G.H., and Peebles, P.C., 1991, Modern sediments and facies model for a microtidal coastal plain estuary, the James Estuary, Virginia: Journal of Sedimentary Petrology, v. 61, p. 883–899, doi:10.1306/D42677F8-2B26-11D7-8648000102C1865D.

Nicoll, T.J., and Hickin, E.J., 2010, Planform geometry and channel migration of confined meandering rivers on the Canadian prairies: Geomorphology, v. 116, p. 37–47, doi:10.1016/j.geomorph.2009.10.005.

Nofal, E.R., Amer, M.A., El-Didy, S.M., and Fekry, A.M., 2015, Delineation and modeling of seawater intrusion into the Nile Delta Aquifer: A new perspective: Water Science, v. 29, p. 156–166, doi:10.1016/j.wsj.2015.11.003.

Nowroozi, A.A., Horrocks, S.B., and Henderson, P., 1999, Saltwater intrusion into the freshwater aquifer in the eastern shore of Virginia: A reconnaissance electrical resistivity survey: Journal of Applied Geophysics, v. 42, p. 1–22, doi:10.1016/S0926-9851(99)00004-X.

Oomkems, E., and Terwindt, J.H.J., 1960, Inshore estuarine sediments in the Haringvliet, Netherlands: Geologie en Mijnbouw, v. 39, p. 701–710.

Pal, R., and Pani, P., 2019, Remote sensing and GIS-based analysis of evolving planform morphology of the middle-lower part of the Ganga River, India: Egyptian Journal of Remote Sensing and Space Science, v. 22, p. 1–10,

doi:10.1016/j.ejrs.2018.01.007.

Paniconi, C., Khlaifi, I., Lecca, G., Giacomelli, A., and Tarhouni, J., 2001, Modeling and analysis of seawater intrusion in the coastal aquifer of Eastern Cap-Bon, Tunisia: Transport in Porous Media, v. 43, p. 3–28, doi:10.1023/A:1010600921912.

Pearson, N.J., and Gingras, M.K., 2006, An Ichnological and Sedimentological Facies Model for Muddy Point-Bar Deposits: Journal of Sedimentary Research, v. 76, p. 771–782, doi:10.2110/jsr.2006.070.

Peretti, W.R., Knoll, M.D., Clement, W.P., and Barrash, W., 1999, 3-D GPR imaging of complex fluvial stratigraphy at the Boise Hydrogeophysical Research Site, *in* 12th EEGS Symposium on the Application of Geophysics to Engineering and Environmental Problems, p. cp--202.

Piovan, S., Mozzi, P., and Stefani, C., 2010, Bronze age paleohydrography of the southern Venetian Plain: Geoarchaeology, v. 25, p. 6–35, doi:10.1002/gea.20300.

Piovan, S., Mozzi, P., and Zecchin, M., 2012, The interplay between adjacent Adige and Po alluvial systems and deltas in the late Holocene (Northern Italy): Géomorphologie: relief, processus, environnement, v. 18, p. 427–440, doi:10.4000/geomorphologie.10034.

Polya, D.A., Gault, A.G., Diebe, N., Feldman, P., Rosenboom, J.W., Gilligan, E., Fredericks, D., Milton, A.H., Sampson, M., Rowland, H.A.L., Lythgoe, P.R., Jones, J.C., Middleton, C., Cooke, D.A., 2005, Arsenic hazard in shallow Cambodian groundwaters: Mineralogical Magazine, v. 69, p. 807–823, doi:10.1180/0026461056950290.

Pousa, J., Tosi, L., Kruse, E., Guaraglia, D., Bonardi, M., Mazzoldi, A., Rizzetto, F., and Schnack, E., 2007, Coastal processes and environmental hazards: The Buenos Aires (Argentina) and Venetian (Italy) littorals: Environmental Geology, v. 51, p. 1307–1316, doi:10.1007/s00254-006-0424-9.

Qahman, K., and Larabi, A., 2006, Evaluation and numerical modeling of seawater intrusion in the Gaza aquifer (Palestine): Hydrogeology Journal, v. 14, p. 713–728, doi:10.1007/s10040-005-003-2.

Qi, S.Z., and Qiu, Q.L., 2011, Environmental hazard from saltwater intrusion in the Laizhou Gulf, Shandong Province of China: Natural Hazards, v. 56, p. 563–566, doi:10.1007/s11069-010-9686-3.

Ravenscroft, P., Burgess, W.G., Ahmed, K.M., Burren, M., and Perrin, J., 2005, Arsenic in groundwater of the Bengal Basin, Bangladesh: Distribution, field relations, and hydrogeological setting: Hydrogeology Journal, v. 13, p. 727–751, doi:10.1007/s10040-003-0314-0.

Rice, S.P., and Church, M., 2001, Longitudinal profiles in simple alluvial systems: Water Resources Research, v. 37, p. 417–426, doi:10.1029/2000WR900266.

Rinaldo, A., Fagherazzi, S., Lanzoni, S., Marani, M., and Dietrich, W.E., 1999, Tidal networks 2. Watershed delineation and comparative network morphology: Water Resources Research, v. 35, p. 3905–3917, doi:10.1029/1999WR900237.

Rodriguez-Iturbe, I., and Rinaldo, A., 1997, Fractal river basins: chance and self-organization: New York, Cambridge University Press.

Rossetti, D. de F., 2010, Multiple remote sensing techniques as a tool for reconstructing late Quaternary drainage in the Amazon lowland: Earth Surface Processes and Landforms, v. 35, p. 1234–1239, doi:10.1002/esp.1996.

Rossetti, D.F., and Valeriano, M.M., 2007, Evolution of the lowest amazon basin modeled from the integration of geological and SRTM topographic data: Catena, v. 70, p. 253–265, doi:10.1016/j.catena.2006.08.009.

Sambrook Smith, G.H., Ashworth, P.J., Best, J.L., Woodward, J., and Simpson, C.J., 2006, The sedimentology and alluvial architecture of the sandy braided South Saskatchewan River, Canada: Sedimentology, v. 53, p. 413–434, doi:10.1111/j.1365-3091.2005.00769.x.

Schumm, S.A., 1985, Patterns of alluvial rivers: Annual review of Earth and planetary sciences, v. 13, p. 5–27, doi:10.1146/annurev.earth.13.1.5.

Seminara, G., 2010, Fluvial Sedimentary Patterns: Annual Review of Fluid Mechanics, v. 42, p. 43–66, doi:10.1146/annurev-fluid-121108-145612.

Seminara, G., 2006, Meanders: Journal of Fluid Mechanics, v. 554, p. 271–297, doi:10.1017/S0022112006008925.

Seminara, G., Solari, L., and Tubino, M., 1997, Finite amplitude scour and grain sorting in wide channel bends, *in* Environmental and Coastal Hydraulics: Protecting the Aquatic Habitat, San Francisco, California, p. 1445–1450.

Shiers, M.N., Mountney, N.P., Hodgson, D.M., and Cobain, S.L., 2014, Depositional controls on tidally influenced fluvial successions, Neslen Formation, Utah, USA: Sedimentary Geology, v. 311, p. 1–16, doi:10.1016/j.sedgeo.2014.06.005.

Shiers, M.N., Mountney, N.P., Hodgson, D.M., and Colombera, L., 2018, Controls on the depositional architecture of fluvial point-bar elements in a coastal-plain succession, *in* Ghinassi, M., Colombera, L., Mountney, N.P., and Reesink, A.J.H. eds., Fluvial Meanders and Their Sedimentary Products in the Rock Record, John Wiley & Sons, Ltd Chichester, UK, p. 15–46, doi:10.1002/9781119424437.ch2.

Smith, D.G., 1987, Meandering river point bar lithofacies models: modern and ancient examples compared, *in* Ethfidge, F.G., Flores, M.R., and Harvey, M.D. eds., Recent Developments in Fluvial Sedimentology, Tulsa, SEPM, v. SP39, p. 83–91, doi:10.2110/pec.87.39.0083.

Smith, D.G., Hubbard, S.M., Lavigne, J.R., Leckie, D.A., and Fustic, M., 2011, Stratigraphy of counter-point-bar and eddy-accretion deposits in low-energy meander belts of the Peace-Athabasca Delta, northeast Alberta, Canada, *in* Davidson, S.K., Leleu, S., and North, C.P. eds., From River to Rock Record: The preservation of fluvial sediments and their subsequent interpretation, SEPM Special Publication, p. 143–152, doi:10.2110/sepmsp.097.143.

Smith, D.G., Hubbard, S.M., Leckie, D.A., and Fustic, M., 2009, Counter point bar deposits: Lithofacies and reservoir significance in the meandering modern

peace river and ancient McMurray formation, Alberta, Canada: Sedimentology, v. 56, p. 1655–1669, doi:10.1111/j.1365-3091.2009.01050.x.

Strick, R.J.P., Ashworth, P.J., Awcock, G., and Lewin, J., 2018, Morphology and spacing of river meander scrolls: Geomorphology, v. 310, p. 57–68, doi:10.1016/j.geomorph.2018.03.005.

Strick, R.J.P., Ashworth, P.J., Sambrook Smith, G.H., Nicholas, A.P., Best, J.L., Lane, S.N., Parsons, D.R., Simpson, C.J., Unsworth, C.A., and Dale, J., 2019, Quantification of bedform dynamics and bedload sediment flux in sandy braided rivers from airborne and satellite imagery: Earth Surface Processes and Landforms, v. 44, p. 953–972, doi:10.1002/esp.4558.

Strobl, R.S., Wightman, D.M., Muwais, W.K., Cotterill, D.K., and Yuan, L., 1997, Geological modelling of McMurray Formation reservoirs based on outcrop and subsurface analogues, *in* Pemberton, S.G. and James, D.P. eds., Petroleum Geology of the Cretaceous Mannville Group, Western Canada, Canadian Society of Petroleum Geologists, Memoir 18, p. 292–311.

Tappe, W., Groeneweg, J., and Jantsch, B., 2002, Diffuse atrazine pollution in German aquifers: Biodegradation, v. 13, p. 3–10, doi:10.1023/A:1016325527709.

Tessier, B., 1993, Upper intertidal rhythmites in the Mont-Saint-Michel Bay (NW France): Perspectives for paleoreconstruction: Marine Geology, v. 110, p. 355–367, doi:10.1016/0025-3227(93)90093-B.

Thomas, R.G., Smith, D.G., Wood, J.M., Visser, J., Calverley-range, E.A., and Koster, E.H., 1987, Inclined heterolithic stratification—terminology, description, interpretation and significance: Sedimentary Geology, v. 53, p. 123–179, doi:10.1016/S0037-0738(87)80006-4.

Tirsgaard, H., 1993, The architecture of precambrian high energy tidal channel deposits: an example from the lyell land group (eleonore bay supergroup), northeast Greenland: Sedimentary Geology, v. 88, p. 137–152, doi:10.1016/0037-0738(93)90154-W.

Toonen, W.H.J., Kleinhans, M.G., and Cohen, K.M., 2012, Sedimentary architecture of abandoned channel fills: Earth Surface Processes and Landforms, v. 37, p. 459–472, doi:10.1002/esp.3189.

Tularam, G.A., and Krishna, M., 2009, Long term consequences of groundwater pumping in Australia: A review of impacts around the globe: Journal of Applied Sciences in Environmental Sanitation, v. 04, p. 151–166.

UNEP, 2005, Freshwater Ecosystem Services, *in* Programme, U.N.E. ed., Millennium Ecosystem Assessment, Washington, DC, Island Press, v. 1, p. 165–207.

Vietz, G.J., Stewardson, M.J., and Finlayson, B.L., 2006, Flows that form: The hydromorphology of concave-bank bench formation in the Ovens River, Australia: IAHS Publication, p. 267–276.

Voudouris, K., Panagopoulos, A., and Koumantakis, I., 2004, Nitrate pollution in the coastal aquifer system of the korinthos prefecture (Greece): Global Nest Journal, v. 6, p. 31–38, doi:10.30955/gnj.000236.

Werner, A.D., 2010, A review of seawater intrusion and its management in Australia: Hydrogeology Journal, v. 18, p. 281–285, doi:10.1007/s10040-009-0465-8.

Whiting, P.J., and Dietrich, W.E., 1990, Boundary Shear Stress and Roughness over Mobile Alluvial Beds: Journal of Hydraulic Engineering, v. 116, p. 1495–1511, doi:10.1061/(ASCE)0733-9429(1990)116:12(1495).

Willis, B.J., 1993, Interpretation of Bedding Geometry within Ancient Point-Bar Deposits, *in* Marzo, M. and Puigdefàbregas, C. eds., Alluvial Sedimentation. Int. Assoc. Sedimentol. Spec. Publ. 17, Wiley Online Books, p. 101–114, doi:10.1002/9781444303995.ch9.

Willis, B.J., 1989, Palaeochannel reconstructions from point bar deposits: a three-dimensional perspective: Sedimentology, v. 36, p. 757–766, doi:10.1111/j.1365-3091.1989.tb01744.x.

Willis, B.J., and Tang, H., 2010, Three-Dimensional Connectivity of Point-Bar Deposits: Journal of Sedimentary Research, v. 80, p. 440–454, doi:10.2110/jsr.2010.046.

Wray, R.A.L., 2009, Palaeochannels of the Namoi River Floodplain, New South Wales, Australia: The use of multispectral Landsat imagery to highlight a Late Quaternary change in fluvial regime: Australian Geographer, v. 40, p. 29–49, doi:10.1080/00049180802656952.

Wu, C., Bhattacharya, J.P., and Ullah, M.S., 2015, Paleohydrology and 3D facies architecture of ancient point bars, Ferron Sandstone, Notom Delta, south-central Utah, USA: Journal of Sedimentary Research, v. 85, p. 399–418, doi:10.2110/jsr.2015.29.

Yang, J.H., and Lee, K.K., 2012, Locating plume sources of multiple chlorinated contaminants in groundwater by analyzing seasonal hydrological responses in an industrial complex, Wonju, Korea: Geosciences Journal, v. 16, p. 301–311, doi:10.1007/s12303-012-0028-1.

Yang, Y.S., Lin, X.Y., Elliot, T., and Kalin, R.M., 2001, A natural-gradient field tracer test for evaluation of pollutant-transport parameters in a porous-medium aquifer: Hydrogeology Journal, v. 9, p. 313–320, doi:10.1007/s100400100127.

Zecchin, M., Baradello, L., Brancolini, G., Donda, F., Rizzetto, F., and Tosi, L., 2008, Sequence stratigraphy based on high-resolution seismic profiles in the late Pleistocene and Holocene deposits of the Venice area: Marine Geology, v. 253, p. 185–198, doi:10.1016/j.margeo.2008.05.010.

Zeidan, B.A., 2017, Groundwater degradation and remediation in the Nile Delta aquifer, *in* Handbook of Environmental Chemistry, v. 55, p. 159–232, doi:10.1007/698_2016_128.

Zohdy, A.A.R., 1969, The use of Schlumbergerand Equatorial soundings in groundwater investigations near El Paso, Texas: Geophysics, v. 34, p. 713–728, doi:10.1190/1.1440042.

Zohdy, A.A.R., Eaton, G.P., and Mabey, D.R., 1974, Application of surface geophysics to ground-water investigations, *in* Techniques of Water-Resources Investigations of the United States Geological Survey, p. 123,

doi:10.3133/twri02D1.

2

MATERIALS AND METHODS

2.1 Overview of the study sites

The Venetian Plain is sited in northeast Italy and is a low gradient plain bordered by the Adriatic Sea (Fig. 2.1A). The present landscape of the plain, characterised by a dense network of abandoned meander belts, originated during Late Holocene time through the aggradation of different alluvial systems (Piovan et al., 2012). These alluvial deposits form the upper part of a transgressive-regressive cycle, which includes a regressive part documenting the transition from lagoonal-deltaic to fluvial environments (Fontana et al., 2008, 2010). Specifically, the southern portion of the Venetian Plain, whose southern boundary fades with the northern boundary of the Po Plain, still shows evidence for the avulsion and relocation history of ancient fluvial meandering channels, which are mainly related to the eastward flowing Brenta and Adige Rivers (Fig. 2.1A).

Since meander bends and channel belts of different morphologies and scales can be identified in the southern Venetian Plain (e.g., meander bends with symmetric to asymmetric shapes, and radius of curvature from 30 to 400 m; channel-belt widths ranging between 200 and more than 1000 m), eight paleo-meander bends and one paleo-channel belt have been selected for detailed investigations of deposits accumulated on the fluvial realm (Fig. 2.1B). These meander bends were selected to have a representative group, in terms of morphologies, of the meander traces visible in the plain. The selected paleo-channel belt is one of the most well-visible and trackable (from satellite images) belts of the plain, allowing for morphometric analyses. Additionally, logistic constrains were also considered, such as the possibility of reaching them easily

and acquiring data. Each paleo-meander bends extends for about 0.2 km^2, whereas the paleo-channel belt extends for 14 km and has a surficial area of about 11 km^2.

The coastal sector of the Venetian Plain hosts the Venice Lagoon, which represents the largest brackish water body of the Mediterranean Sea (Fig. 2.1C). In the northern part of the Venice Lagoon, which is the most naturally preserved area within the lagoon, three consecutive paleo-meanders, belonging to the same ancient tidal channel, have been selected for investigations on tidal channel deposits (Fig. 2.1D). This study site has an area of 1.1 km^2.

The prevalence of fluvial study cases compared to the tidal one reflects the dominance of fluvial channel forms and deposits on the plain and arises from the need to mainly investigate permeable deposits that effectively host surficial aquifers in coastal plains.

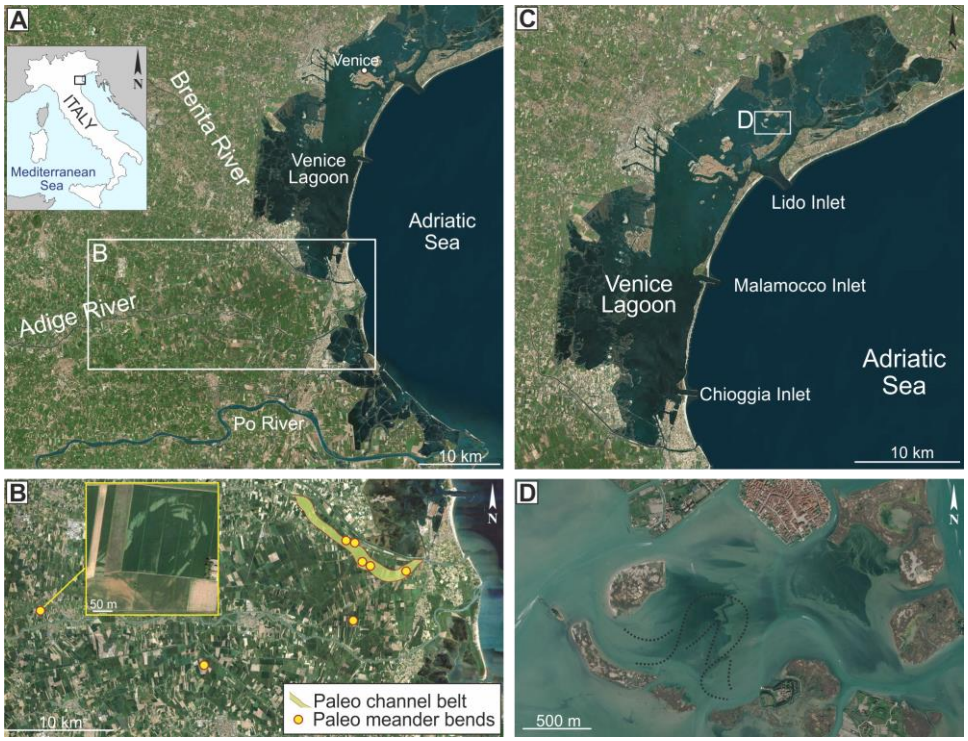

Fig. 2.1. Study sites. (A) The southern portion of the Venetian Plain (NE, Italy), (B) with the study sites selected for investigations on deposits accumulated by fluvial meandering channels. (C) The Venice Lagoon and (D) the paleo meander bends (dashed lines) selected for investigations on tidal meandering channel deposits.

2.2 Data and Methods

To select and analyse deposits of FTMC, different methodologies have been adopted following different needs.

2.2.1 Remote sensing

Satellite images and aerial photos depicting the landscape of the southern Venetian Plain in different years (i.e., from 2011 to 2015), were fundamental for the selection of the study sites. Specifically, satellite images like Sentinel and Landsat images allow for remote-sensing analysis, by considering the solar radiation captured and emitted by each element on the image. Specifically, the different frequencies and wavelengths of the solar radiation emitted by the vegetation and the bare soil provide information about the lithological and sedimentological characteristics of the subsurface. Indeed, through colour combinations (e.g., RGB) and indexes [e.g., vegetation indexes as NDVI, the Normalised Difference Vegetation Index, and NDMI, the Normalised Difference Moisture Index (Bannari et al., 1995; Piedelobo et al., 2019)], remote-sensing analysis with the QGis software can suggest the occurrence of more or less permeable soils, thus providing an excellent starting approach to select and analyse FTMC deposits (e.g., Wray, 2009; Giacomelli et al., 2018).

Once the major morphometric features of different bends were qualitatively identified through satellite images and aerial photos, the morphometric analysis on different bends has been performed by means of a Matlab code, which identifies apex and inflection points of each meander-bend in a semi-automatic way (Finotello et al., 2020). The parameters that can be quantified are sinuosity, amplitude, radius of curvature, bend curvature, intrinsic wavelength, cartesian wavelength, curvature skewness and kurtosis.

2.2.2 Sedimentary cores

Sedimentary cores allow the investigation of the internal stratigraphy of FTMC deposits and perform detailed sedimentological analyses. Different techniques can be adopted to recover sedimentary cores. In this thesis, an Eijkelkamp hand auger and a continuous drilling core sampler with rotary technique (Fig. 2.2A) have been adopted. The hand auger allows the recovery of cores with a diameter of 3 cm through a 1 m-long gouge sampler. It allows to core muddy deposits up to 10 m; however, it is limited in the investigation depth in case of sandy deposits, as the gouge sampler is not able to recover sand sited below groundwater, as the sand slips downwards during the recovery phase. With the

continuous drilling core sampler, instead, cores have a diameter of 10 cm and can be recovered up to 10 m depth on both mud and sand sediments. Compared to the percussion corer, which is another type of drilling core sampler, the rotary technique allows the recovery of cores suffering less deformation. On the whole study sites, 21 and 60 cores have been recovered through the continuous drilling core sampler and the hand auger, respectively. In addition to those acquired, 15 sedimentary cores from previous studies (Madricardo et al., 2007; Madricardo and Donnici, 2014) have been analysed for the tidal environment, as they were located in strategic sites. To investigate the recovered sediments, cores have been cut longitudinally with a knife, photographed, and sampled for grain-size analysis (Fig. 2.2B). High-resolution photos have been taken with photogrammetry to obtain a detailed 3D model of each core, to be digitally stored and analysed. Through the grain-size analysis, sediments were quantitatively studied allowing for a precise characterisation of grain-size trend within point-bar bodies. Specifically, for sandy samples (i.e., 42 samples that were taken from sedimentary cores to precisely characterise a sand body), the dry-sieving technique has been adopted. Six sieves with progressive halved meshes have been used (i.e., 2 mm, 1 mm, 0.5 mm, 0.25 mm, 0.125 mm, 0.063 mm) to characterise sandy deposits by weighting the main sandy classes (i.e., very coarse, coarse, medium, fine, very fine) and the muddy one (i.e., < 0.063 mm). A vibrating screen can be used to facilitate the movement of the grains, instead of moving manually the sieves. For muddy samples (i.e., 29 samples for tidal deposits), a laser diffractometer [located at a laboratory in the Department of Pharmacy in Padua (IT)] has been used, as it is more sensitive to fine grains than the dry-sieve technique. Through the diffraction patterns of a laser beam passed through the grains, the laser diffraction analysis allows to quickly measure the abundance of different grain-size classes.

Cores have been studied following the basic principles of facies analysis to highlight sediment grain size, colour, oxidation, and sedimentary structures. The descriptive sedimentological terminology, including clast fabric notation, is after Harms et al. (1975, 1982) and Collinson and Thompson (1982). Facies are considered to be the main types of sedimentary deposits, distinguished macroscopically as the basic building blocks of a sedimentary succession (Harms et al., 1975) and providing information on the depositional processes involved. Facies associations are assemblages of spatially and genetically related facies, distinguished as the basic building mega-blocks of the sedimentary succession

and representing specific sedimentary environments (Nemec, 1996). This analysis allows to identify different facies associations and compare them to literature observations.

To create a suitable archive, most of the recovered cores have been treated with epoxy resins, which once dry allows preserving the sediment structure and sediment texture (Fig. 2.2C).

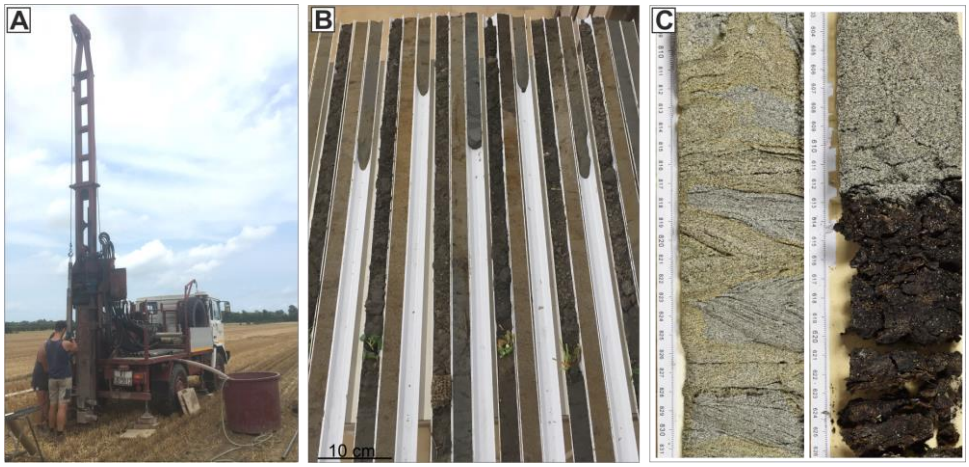

Fig. 2.2. Sedimentary cores. (A) recovery of sedimentary cores with the drilling core sampler. (B) Example of cores recovered with the hand auger. (C) Examples of cores recovered with the drilling core sampler that have been treated with the epoxy resin.

2.2.3 Sediment textural properties and statistical analyses

Grain-size and sediment-sorting data have been analysed through a principal component analysis (PCA), which was run through a Matlab code. The PCA is a multivariate statistical tool allowing for the complete description of the internal variability of the input samples (Davies, 1992). Indeed, the PCA transforms high-dimensional datasets of possibly correlated variables into lower-dimensional subspaces defined by new variables called principal components (PC). Commonly, the first few principal components (e.g., the first three ones) can greatly describe the samples. By running a PCA, loading and score plots are provided: the former allows to observe the weight and importance of the input variables in the new PC-space, whereas the latter shows how the samples distribute in the new PC-space. For instance, grain-size samples (input samples) differ based on their percentage of each grain-size class (input variables). The PCA finds new independent variables (PC) that can explain the variability within samples by considering together the weight of all input variables (e.g., Copelli et al., 2018).

2.2.4 Geophysical investigations: FDEM maps

Electromagnetic induction surveys are a well-established technique that allows for extensive noncontact subsurface analysis ranging in depth from very shallow to tens of kilometres (Telford et al., 1990). For small-scale measurements, as in the case of the study deposits, Electromagnetic induction investigations are conducted in the frequency domain (FDEM), whose results map the variability of the electrical conductivity (Fig. 2.3). This geophysical parameter depends on different soil properties, like texture, temperature, moisture content and water salinity. For acquisition on the study sites, a GF Instruments CMD-Explorer probe has been adopted, which consists of a six-coil system operating at 10 kHz (Fig. 2.4). The probe allows the investigation of the subsurface up to almost 7 m depth thanks to the possibility to acquire data on two coplanar configurations (i.e., horizontal HMD and vertical VMD ones) (Um and Alumbaugh, 2007). The probe can acquire a data point every 0.5 seconds.

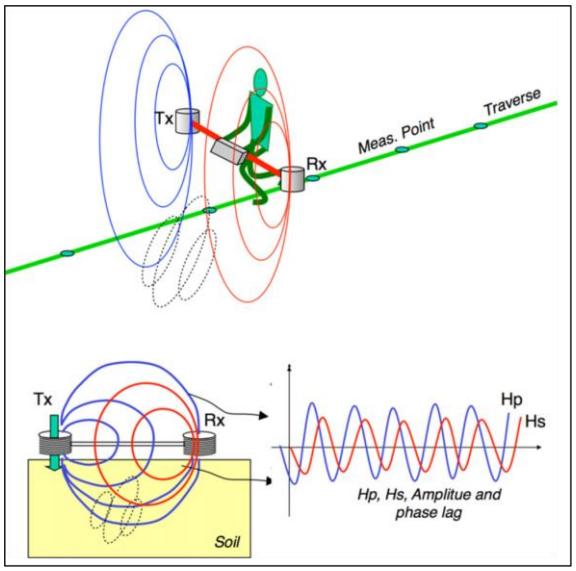

Fig. 2.3. FDEM principles, after Boaga (2017). The tool emits an alternating current from the transmitter coil Tx to induce an alternating primary magnetic field (Hp). The Hp produces secondary electrical Eddy currents (dotted lines), which, in turn, cause, a secondary magnetic field (Hs) that is recorded at the receiver coil Rx. The Hs is a function of coils configuration and electromagnetic properties of the soil. The Rx receives two signals, the real component (in-phase) and the imaginary one (quadrature), which is related to the ground electrical conductivity.

To efficiently investigate study sites at high resolution (i.e., metric scale), the probe has been mounted on a specifically designed wooden carriage and towed by a small tractor that proceeded by straight lines on the fields. To georeference the measured points, a Trimble 5800 GPS has been connected to the probe for continuous positioning. Data have been then inverted to obtain electrical conductivity values of the subsurface by using the EMagPy, which is an open-source software for 1D electromagnetic induction inversion (McLachlan et al., 2021). Through this method, horizontal maps of electrical conductivity values can be produced at different depths, providing useful information about the

morphologies and sediment properties of the investigated deposits (Fig. 2.4). In the Venetian Plain, almost 80 km of lines have been acquired with the FDEM probe, acquiring overall 160.000 data points.

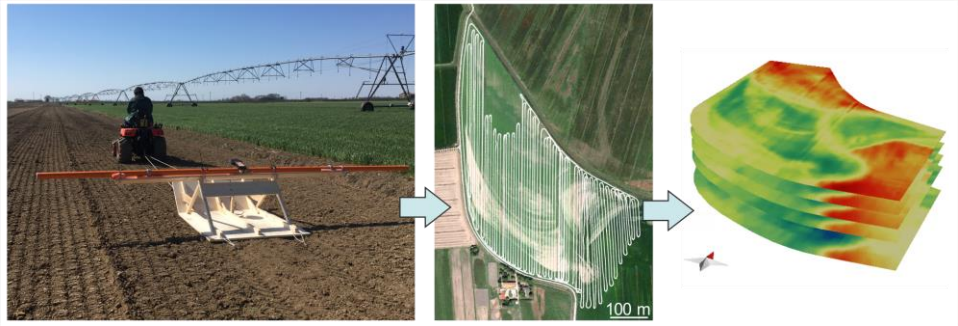

Fig. 2.4. The FDEM probe mounted on the wooden carriage and dragged by the tractor, to acquire data points on straight lines, to finally provide maps of electrical conductivity values.

2.2.5 Geophysical investigations: acoustic images

In the Venice Lagoon, previously acquired acoustic vertical images (Madricardo et al., 2007) have been analysed to reconstruct the architecture of the subsurface deposits (Fig. 2.5). These images were acquired using a single beam echosounder, modified for shallow waters (e.g., 0.5 m). With the echosounder, sound waves are emitted in short pulses (τ = 0,15 ms) at a frequency of 30 kHz, propagating in the water down to the sea bottom. There, part of the waves is reflected, and another penetrates the bottom sediments. The acoustic signals reflected from the sea-bottom are detected by the instrument, and the same happens for the reverberations produced to the interfaces between sediments with different properties. Sediments differing in physical characteristics originate different acoustic responses. The transducer is composed of seven piezoelectric elements organised in a hexagonal matrix with a diameter of 18.2 cm. In shallow waters, it is characterised by signals with a low lateral resolution; however, signals have a high vertical resolution, of the order of a decimetre, being useful for the purposed of this work. The echosounder was set with a repetition rate of 50 pulses/s and constant compressional wave velocity of v = 1530 m/s, determined based on the average measured values of the Venice Lagoon. It was mounted on a small boat with a flat bottom, along with a DGPS system (Trymble DSM12), which allows a sub-metric positioning accuracy. The measured signals were treated to reduce the noise and improve visibility, and finally visualized as reflection profiles. Between 2003 and 2004, a total of 980 images, ca. 500 km of acoustic profiles, were acquired in the study site, to

investigate the first 6 m of the lagoonal subsoil (Madricardo et al., 2007). For this thesis, 201 equally spaced (2.5 to 10 m) images have been selected for reconstructing the subsurface architecture (Fig. 2.5B). To interpolate and visualize the electromagnetic data the QGis software has been used, and both FDEM maps and acoustic images have been analysed in the 3D space provided by the Move 2018.2TM (Midland Valley) software (Fig. 2.5B).

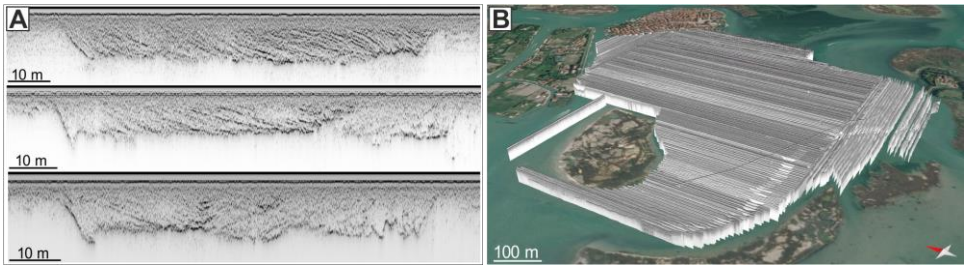

Fig. 2.5. The acoustic images: (A) examples of three acoustic images and (B) a 3D view of the acoustic images in the area in the 3D space provided by the Move software.

References

Bannari, A., Morin, D., Bonn, F., and Huete, A.R., 1995, A review of vegetation indices: Remote sensing reviews, v. 13, p. 95–120, doi:10.1080/02757259509532298.

Boaga, J., 2017, The use of FDEM in hydrogeophysics: A review: Journal of Applied Geophysics, v. 139, p. 36–46, doi:10.1016/j.jappgeo.2017.02.011.

Collinson, J.D., and Thompson, D.B., 1982, Sedimentary structures: London, UK, George Allen and Unwin, 194 p.

Copelli, D., Cavecchi, A., Merusi, C., and Leardi, R., 2018, Multivariate evaluation of the effect of the particle size distribution of an Active Pharmaceutical Ingredient on the performance of a pharmaceutical drug product: a real-case study: Chemometrics and Intelligent Laboratory Systems, v. 178, p. 1–10, doi:10.1016/j.chemolab.2018.04.013.

Davies, T., 1992, Principal Components of Principal Component Analysis: Spectroscopy World, v. 4, p. 38–39.

Finotello, A., D'Alpaos, A., Bogoni, M., Ghinassi, M., and Lanzoni, S., 2020, Remotely-sensed planform morphologies reveal fluvial and tidal nature of meandering channels: Scientific Reports, v. 10, p. 1–13, doi:10.1038/s41598-019-56992-w.

Fontana, A., Mozzi, P., and Bondesan, A., 2008, Alluvial megafans in the Venetian-Friulian Plain (north-eastern Italy): Evidence of sedimentary and erosive phases during Late Pleistocene and Holocene: Quaternary International, v. 189, p. 71–90, doi:10.1016/j.quaint.2007.08.044.

Fontana, A., Mozzi, P., and Bondesan, A., 2010, Late Pleistocene evolution of the

Venetian-Friulian Plain: Rendiconti Lincei, v. 21, p. 181–196, doi:10.1007/s12210-010-0093-1.

Giacomelli, S., Rossi, V., Amorosi, A., Bruno, L., Campo, B., Ciampalini, A., Civa, A., Hong, W., Sgavetti, M., and de Souza Filho, C.R., 2018, A mid-late Holocene tidally-influenced drainage system revealed by integrated remote sensing, sedimentological and stratigraphic data: Geomorphology, v. 318, p. 421–436, doi:10.1016/j.geomorph.2018.07.004.

Harms, J.C., Southard, J.B., Spearing, D.R., and Walker, R.G., 1975, Depositional environments as interpreted from primary sedimentary structures and stratification sequences: SEPM Short Course No. 2, Lecture Notes,.

Harms, J.C., Southard, J.B., and Walker, R.G., 1982, Structures and Sequences in Clastic Rocks, *in* SEPM Short Course No. 9, Lecture Notes, Tulsa, Oklohoma (USA), Society of Economic Palaeontologists and Mineralogists.

Madricardo, F., and Donnici, S., 2014, Mapping past and recent landscape modifications in the Lagoon of Venice through geophysical surveys and historical maps: Anthropocene, v. 6, p. 86–96, doi:10.1016/j.ancene.2014.11.001.

Madricardo, F., Donnici, S., Lezziero, A., De Carli, F., Buogo, S., Calicchia, P., and Boccardi, E., 2007, Palaeoenvironment reconstruction in the Lagoon of Venice through wide-area acoustic surveys and core sampling: Estuarine, Coastal and Shelf Science, v. 75, p. 205–213, doi:10.1016/j.ecss.2007.02.031.

McLachlan, P., Blanchy, G., and Binley, A., 2021, EMagPy: Open-source standalone software for processing, forward modeling and inversion of electromagnetic induction data: Computers and Geosciences, v. 146, p. 104561, doi:10.1016/j.cageo.2020.104561.

Nemec, W., 1996, Principles of lithostratigraphic logging and facies analysis: University of Bergen.

Piedelobo, L., Taramelli, A., Schiavon, E., Valentini, E., Molina, J.L., Xuan, A.N., and González-Aguilera, D., 2019, Assessment of green infrastructure in Riparian zones using copernicus programme: Remote Sensing, v. 11, doi:10.3390/rs11242967.

Piovan, S., Mozzi, P., and Zecchin, M., 2012, The interplay between adjacent Adige and Po alluvial systems and deltas in the late Holocene (Northern Italy): Géomorphologie: relief, processus, environnement, v. 18, p. 427–440, doi:10.4000/geomorphologie.10034.

Telford, W.M., Geldart, L.P., and Sheriff, R.E., 1990, Applied geophysics: Cambridge, UK, Cambridge University Press, 770 p.

Um, E.S., and Alumbaugh, D.L., 2007, On the physics of the marine controlled-source electromagnetic method: Geophysics, v. 72, p. WA13–WA26, doi:10.1190/1.2432482.

Wray, R.A.L., 2009, Palaeochannels of the Namoi River Floodplain, New South Wales, Australia: The use of multispectral Landsat imagery to highlight a Late Quaternary change in fluvial regime: Australian Geographer, v. 40, p. 29–49, doi:10.1080/00049180802656952.

3

GEOMETRIES AND GRAIN-SIZE DISTRIBUTION IN FLUVIAL POINT BARS

This chapter is published as a paper in *Marine and Petroleum Geology* (2021, v. 127, p. 104951, doi: 10.1016/j.marpetgeo.2021.104951) under the title "Impact of genesis and abandonment processes of a fluvial meander on geometry and grain-size distribution of the associated point bar (Venetian Plain, Italy)".

E.B. and M.G. designed the study. E.B., J.B. and M.G. developed the methodology. E.B., A.F., M.G. collected the data. E.B. annotated and maintained the research data. E.B. was responsible for data creation and presentation. E.B. and M.G. were the project administrator. J.B and G.C. applied computational techniques to analyse study data. J.B and M.G. provided the instrumentation and analysis tools. A.F. and A.D. verified the reproducibility of the results. All the authors discussed the data and agreed on their interpretation. E.B., J.B. and A.F. wrote the original draft. A.D., G.C. and M.G. provided comments and suggestions to improve the original draft. All the co-authors contributed to the final polishing of the manuscript.

Impact of genesis and abandonment processes of a fluvial meander on geometry and grain-size distribution of the associated point bar (Venetian Plain, Italy)

Elena Bellizia[1], Jacopo Boaga[1], Alessandro Fontana[1], Andrea D'Alpaos[1], Giorgio Cassiani[1], Massimiliano Ghinassi[1]

[1]Department of Geosciences, University of Padova, Via G. Gradenigo 6, IT-35131 Padova, Italy

ABSTRACT

Sedimentary sand bodies originated by Holocene meandering fluvial channels are widespread in modern alluvial plains, and their planform morphometry and evolution can be easily detected from satellite images. Results from the combination of different approaches, including remote sensing, geophysical investigations and sedimentary cores contribute to understanding sedimentary facies distribution and reservoir connectivity of these deposits and provide a crucial contribution for developing models predicting fluid migration within them, with relevant implications for reservoir development and management. The present study focuses on a Late-Holocene meander bend of the southern Venetian Plain (Italy) and aims to analyse depositional patterns and grain-size variability of the related sedimentary bodies by integrating morphological evidence with geophysical and sedimentological investigations.

The investigated paleomeander has a sinuosity of about 2.2 and is associated with a 15-20 m wide paleochannel. Electromagnetic surveys coupled with sedimentary core description allow depicting a 3D stratigraphy of the related point-bar that is characterised by low conductivity values (i.e., 0-40 mS/m) compared to the surrounding overbank deposits (i.e., 80-250 mS/m). Point-bar deposits form an arcuate shape, which started accreting from a newly-formed sinuous channel. Sedimentary cores revealed that point-bar deposits mainly consist of sands, with minimal vertical and lateral grain-size changes. Channel-fill deposits are mainly sandy and document a gradual abandonment of the channel, which caused a progressive decrease of the channel width. The residual channel is detectable from satellite images and appears to be disproportionally narrow in comparison with other morphometric features of the bend. Such a disproportion can be used to predict infill styles of meandering channels from aerial images. This work highlights how the genesis and

abandonment processes of a fluvial meander bend can impact the geometry and sediment properties of the associated point-bar body.

Keywords: Channel avulsion; Lateral accretion; Oxbow lake; Meander cut-off.

3.1 Introduction

Morphology of modern coastal alluvial plains has been largely shaped by meandering channels through the complex interaction between erosion, aggradation and avulsion (Allen, 1965; Nanson, 1980; Plint, 1983; Bridge et al., 1986; Wood, 1989; Khan et al., 1997; Gibling et al., 1998; Bondesan et al., 2003; Bridge, 2003; Page et al., 2003; Zecchin et al., 2008). In coastal alluvial plains, the evolution of late Holocene fluvial meanders is likely similar to ancient systems that hold notable hydrocarbon reservoirs, such as the McMurray Formation in Canada (Strobl et al., 1997; Smith et al., 2009; Hubbard et al., 2011; Labrecque et al., 2011b, 2011a; Fustic et al., 2012b), the Sorrento field in Colorado (Sonnenberg et al., 1990), the Gudao field in China (Wu et al., 2008) and the Campbell-Namao field in Canada (Edie and Andrichuk, 2005). Holocene meandering fluvial channels are widespread and well-studied by high-resolution satellite images (Wray, 2009; Rossetti, 2010; Mehdi et al., 2016; Giacomelli et al., 2018) which further allow for studying their morphology and planform evolution through detection of the scroll-bar patterns (Strick et al., 2018). If located in anthropized areas, these paleo-channels are easily accessible and can be studied by integrating different approaches, such as remote sensing, geophysical investigations and sedimentary cores. This peculiar setting provides the opportunity to understand sedimentary facies distribution and connectivity within fluvial point-bar bodies, contributing to developing models predicting fluid propagation within them, with implications for reservoir development and management.

Point bars originate after lateral migration of a meandering channel (Bagnold, 1960; Leopold and Wolman, 1960; Dietrich et al., 1979; Blanckaert and de Vriend, 2004; Seminara, 2006; Ghinassi et al., 2014; Bhattacharyya et al., 2015), which progressively increase its sinuosity, starting from a slightly sinusoidal shape (Leopold and Wolman, 1960; Daniel, 1971; Willis and Tang, 2010) or a relatively straight one (Brice, 1974; Lewin, 1976; Nanson and Page, 1983; Ghinassi et al., 2014; Wu et al., 2015). By acquiring a sinuous shape, the channel bend develops a helical flow that governs sediment deposition in the associated

point-bar body (Bagnold, 1960; Dietrich, 1987; Seminara, 2006; Camporeale et al., 2007). This helical flow forms at the bend apex zone, where the main streamflow is forced toward the outer bank by the centrifugal acceleration induced by the bend curvature. To balance this disequilibrium, water moves downward and toward the inner bank triggering a helical circulation. Due to gravitational and fluid drag forces in the inner-bank zone, this helical flow leads to the deposition of larger and smaller particles toward the channel thalweg and the point bar, respectively (Hooke, 1975; Dietrich et al., 1979; Dietrich and Whiting, 1989). This helical circulation explains the classical fining-upward grain size trend of point-bar bodies (Allen, 1965, 1970; Brice, 1974; Jackson, 1976; Nanson, 1980), and also accounts for the development of an overall downstream grain-size distribution along the meander bend (Bluck, 1971; Bridge et al., 1995; Willis and Tang, 2010; Ielpi and Ghinassi, 2014; Hagstrom et al., 2019). In sharp meander bends, the accumulation of fine-grained deposits in the downstream side of the bend can be promoted by the local development of a dead zone, where a weak reverse flow produces slough-water conditions (Leeder and Bridges, 1975; Riley and Taylor, 1978; Ferguson et al., 2003; Ghinassi et al., 2016; Finotello et al., 2020b). Point-bar bodies are usually bounded by abandoned channel deposits, which form after the deactivation of the meander bend (Fisk, 1947; Hooke, 1995; Constantine et al., 2010; Toonen et al., 2012). Deposits filling the abandoned channel are generally mud-rich but their internal stratigraphy is dictated by abandonment mechanisms (i.e., avulsion, neck cut-off, chute cut-off), sediment availability in the systems, and the angle between the new channel and the upstream entrance of the old one (Lindner, 1953; Bridge et al., 1986; Fustic et al., 2018). The aforementioned notions suggest that the development and abandonment of a fluvial meander generate a point-bar body, which: i) occupies the whole area delimited by the bend; ii) shows a vertical and downstream decrease in grain size, and iii) is rimmed by mud-rich, channel-fill deposits. Because these basic principles are widely used to constrain geometries of meandering-river deposits in the subsurface, the study of point-bar bodies differing from these classical models deserves particular attention, being able to provide insights to subsurface investigations, with implications for reservoir development (Miall, 1988; Pranter et al., 2007; Martinius et al., 2017).

The present study focuses on a late-Holocene fluvial point bar of the southern Venetian Plain (Italy), where, during Holocene time, aggradation of a complex network of fluvial meandering channels built up the modern coastal landscape

(Bondesan et al., 2008; Piovan et al., 2012). This work built on a previous geophysical study (Cassiani et al., 2020) that highlights the approach followed to detect the main morphometric features of a buried meander bend. The planform morphometry of the study meander bend can be constrained using satellite images, which are integrated here with sedimentary core data and non-invasive geophysical investigations to define 3D geometry and grain-size distribution of the associated bar. This work focuses on sedimentological features of this bend and discusses data that provide insights to compare sedimentology of the studied bar with classical point bar facies models, with particular emphasis on morphometries associated with the origin and abandonment of the bend.

3.2 Geological setting

3.2.1 The southern Venetian Plain

The studied bar is located at the boundary between the Venetian Plain and the Po River Delta, in Northern Italy (Fig. 3.1). This area is part of a foreland basin located between Northern Apennines and the Southern Alps, that, during Quaternary (Ghielmi et al., 2010), was filled with ca. 700 m of coastal, alluvial and lagoon deposits, with the top 100 m formed since Late Pleistocene (Fontana et al., 2010; Veneto, 2012; Amorosi et al., 2017). During the Last Glacial Maximum (LGM), the investigated area was part of the distal sector of the alluvial megafan of the Adige River and the coastline was over 250 km south of the present one due to the marine lowstand (Fontana et al., 2014). The top of the LGM alluvial plain is found at 6 - 9 m depth and is covered by Holocene fluvial deposits, which, few kilometers east of the study site, interfinger with lagoon and paralic sediments (Piovan et al., 2010, 2012). The present-day coastal plain is located on top of a succession consisting of a basal Early to Middle Holocene transgressive sequence that is covered by regressive deltaic deposits, which accumulated after an eastward coastline shift of about 20 km (Favero and Serandrei Barbero, 1980; Amorosi et al., 2008). Channel belts developed on the deltaic succession are visible in most of the available aerial images because of the light colour of their sandy deposits that contrasts with the dark tone of the surrounding organic-rich floodplain (cf. Bondesan et al., 2004). Moreover, late-Holocene channel belts formed under highstand aggradational conditions and built well-defined fluvial ridges (Piovan et al., 2012).

Since the Roman period, the entire Venetian Plain and parts of the Po Delta experienced a strong anthropogenic activity related to the development of extensive reclamation systems (Piovan et al., 2010). In the 16th century, for instance, the Venetian Republic started the management of the surface hydrography by developing a dense network of dikes, canals, and ditches. In 1604 the Po River was artificially diverted in its present channel, leading to the formation of the modern Po Delta (Stefani, 2017). During the first decades of the 20th century, reclamation was extended to the coastal plain where large portions of swamps were drained through canals and pumping stations. All these improvements made the entire area available for agricultural activities, although the reclamation also induced land subsidence that, in the last century, reached rates of about 2-5 mm/yr with large sectors up to 10 mm/yr (Teatini et al., 2011).

3.2.2 The study site

The studied site is located in a typical lowland landscape that is characterized by a dense network of abandoned meander belts. In this case, meander belts generated during late Holocene by avulsions of the Adige and Po Rivers (Fig. 3.1) (Piovan et al., 2010), which were characterized by overall eastward flowing drainages.

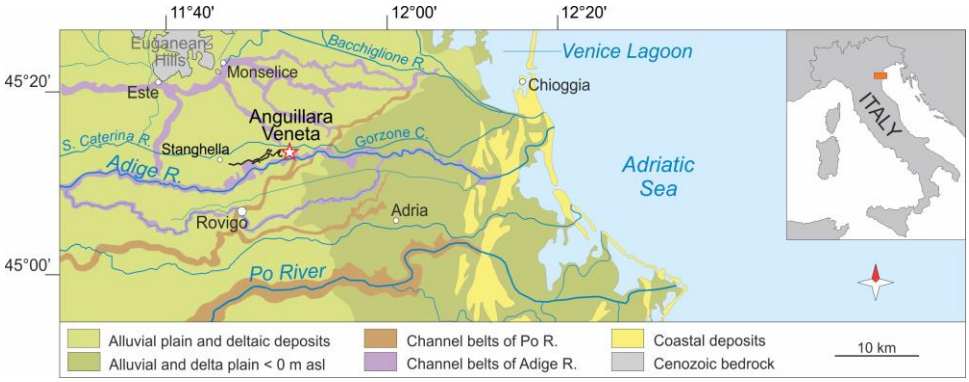

Fig. 3.1. Location of the investigated area (white star) with an indication of the main geological units of the southern Venetian Plain and the Po Delta (after Mozzi et al., 2020). The black lines correspond to the investigated channel belt.

The Adige River has a mountain catchment of 11,000 km^2 with an annual average discharge of 220 m^3/s and a peak flood of 4000 m^3/s (Bondesan, 2001). The Po River is the major Italian river and has a catchment of about 70,000 km^2, an average discharge of 1565 m^3/s and a peak flood of 11,800 m^3/s (Stefani and Vincenzi, 2005). The investigated site is located about 1 km north of the Adige

River, at an altitude ranging between 0.7 and 2.0 m asl (above sea level). In this area, several paleomeanders define a roughly continuous belt, which can be followed for about 7 km from Stanghella to Anguillara Veneta (Fig. 3.1). Close to Anguillara Veneta, satellite images clearly show two main channel reaches, named here Reach A and B (Fig. 3.2); Reach A is composed by two meander bends, called Bend 1 and 2, both defined by an 18-m wide paleochannel (Fig. 3.2B).

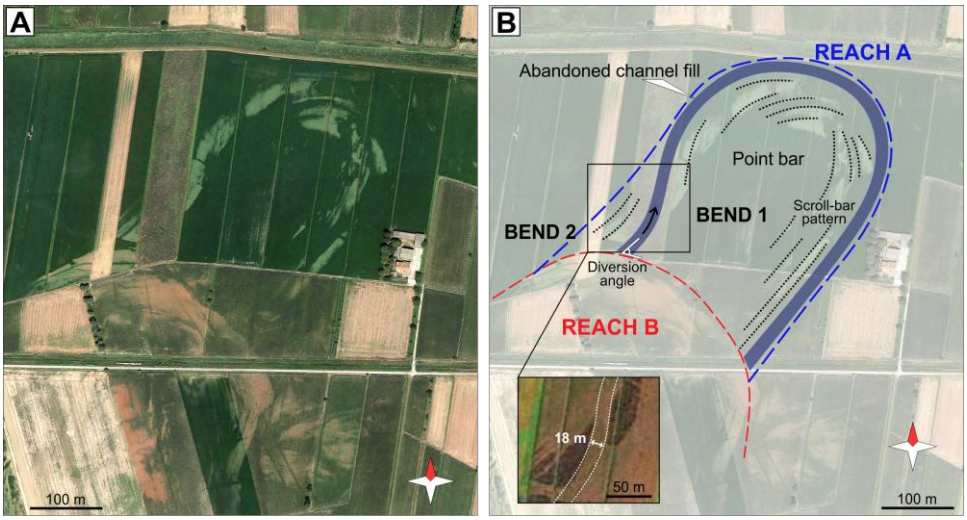

Fig. 3.2. The study site. (A) Satellite image from Google Earth and related interpretation (B) of the studied meander bend (Reach A, Bend 1), highlighting fluvial morphologies from different vegetation colours (see Cassiani et al., 2020). Green areas are associated with good health of cultivated plants due to the high moisture content in the mud-rich soil.

The meander Bend 1 has a sinuosity of ca. 2.2, a radius of curvature of about 140 m and a riffle-to-riffle distance of 260 m. The axis of the bend trends SSW-NNE, and the scroll-bar pattern of the associated point bar highlights an expansional growth style (*sensu* Ghinassi et al., 2016). Bend 2 developed in the upstream portion of Reach A by an expansional growth and has an axis trending NW-SE. It is a low sinuosity bend (i.e., 1.12) characterised by a radius of curvature and riffle-to-riffle distance of 135 m and 230 m, respectively. Reach B overlaps Reach A in its southern part and forms a bend, with the axis trending SW-NE. Geometric relationships between these two reaches suggest that Reach B developed following a shortcutting of Reach A. Diversion angle (*sensu* Constantine *et al.*, 2010) between the upstream reach of Reach A and that of Reach B is ca. 50° (Fig. 3.2B).

3.3 Methods and terminology

3.3.1 Geophysical survey

To evaluate the electrical ground conductivity, Electromagnetic Induction (EMI) investigations were collected in the frequency domain (Frequency Domain Electro-Magnetics of FDEM) (Corwin and Rhoades, 1982) using a GF Instruments CMD-Explorer probe ("GF Instruments s.r.o."). The FDEM method is based on the generation and recording of electromagnetic fields to estimate the subsoil electrical conductivities (McNeill, 1980). FDEM survey is considered part of the contactless geophysical methods since the FDEM probe does not need galvanic contact with the ground (Cassiani et al., 2015). The CMD-Explorer probe is a multi-coil system (three co-planar pairs) operating at a single frequency equal to 10 kHz. It has three internal coils, which allow one to estimate the apparent conductivity at three different depths simultaneously, and it can be operated in both horizontal co-planar (HMD) and vertical co-planar (VMD) configurations (Um and Alumbaugh, 2007), providing six apparent depths of exploration. The probe has to acquire data at almost the same location twice (once for each coil orientation) in the studied field. The FDEM probe was connected to a Trimble 5800 GPS for continuous position measurements ("Trimble - Transforming the Way the World Works") and on a wooden sledge dragged by a small tractor that was specifically designed for this research. The adopted drag acquisition is useful to cover large areas of exploration in relatively small time keeping the re-occupation of the same locations thanks to the GPS centimetric precision. This way the probe height from the ground is kept constant, avoiding drift problems due to height changes. Moreover, the dragging system allowed for shortening the time of the acquisition to avoid temperature changes during the survey, which can cause relevant data drift (Allred et al., 2008; Delefortrie et al., 2014). We collected about 20.000 FDEM data points in the study area by acquiring about one point every 0.5 m and 1 s, each in both in HMD and VMD modes. FDEM data were then inverted to retrieve real soil conductivity values by using the Interpex IX1D inversion software ("Interpex Limited - Specialists in PC Based Geophysical Software"). The inversion was conducted at all locations using a smooth model constrained according to Occam's inversion approach (Constable et al., 1987). The approach is used iteratively to repeatedly improve the model until 9 iterations are used up or until the improvement in fitting error is negligible from one iteration to the next. Interpolation of the acquired data allowed us to generate eight 2D conductivity maps at eight different depths (Fig.

3.3A). These maps were then used to create 3D surfaces, by linear method, and Tetravolumes of the architectural elements in the 3D space provided by the *Move 2018.2*^{TM} (Petroleum Experts) ("MOVE Suite - Petroleum Experts") software.

3.3.2 Sedimentary cores

Sedimentary cores were recovered in the investigated area to integrate and calibrate geophysical data and analyse the sedimentary features of the study deposits. A total of 17 cores were recovered, whose locations are shown in figure 3.3B. Three cores were recovered using a continuous drilling core sampler with a rotary technique that allowed us to reach a depth of 10 m and collect cores with a diameter of 10 cm. These cores were sampled in the upstream, central and downstream portion of the studied bar, respectively (green triangles in Fig. 3.3B). Additional cores (yellow dots in Fig. 3.3B), spanning in depth between 2.5 and 6 m, were successively recovered at 14 sites using an Eijkelkamp hand auger, through a gouge sampler with a length of 1 m and a diameter of 30 mm. This technique did not allow to recover the whole thickness of point bar deposits.

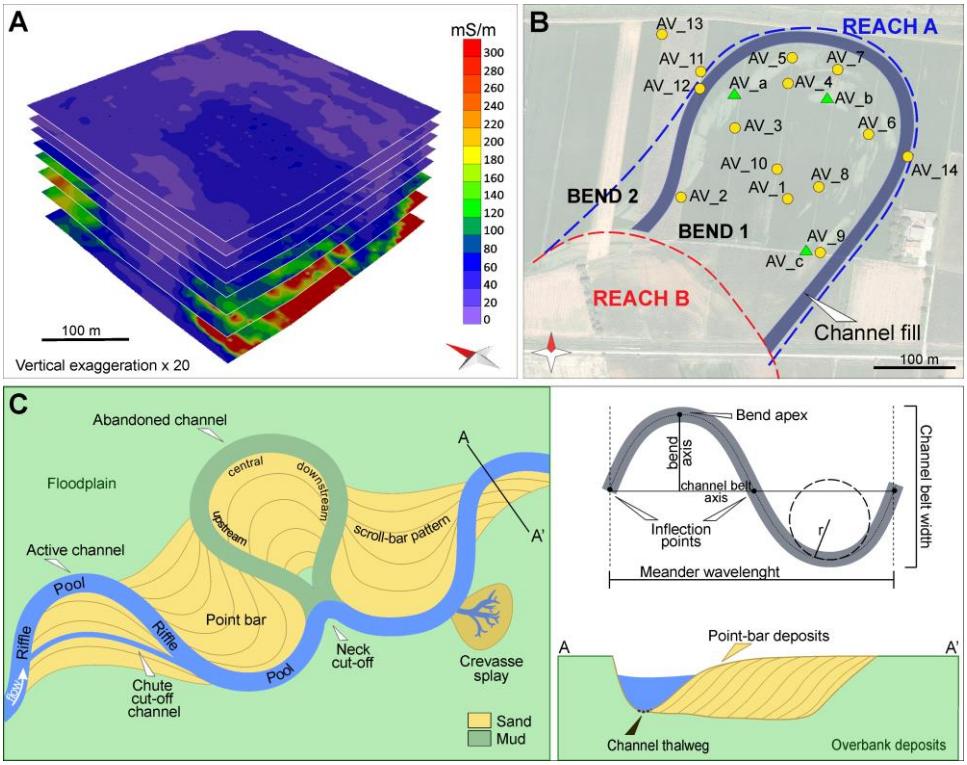

Fig. 3.3. Methods and terminology. (A) Vertical stacking of electrical conductivity maps provided by EMI acquisition, with x20 vertical exaggeration. (B) Position of the recovered cores. Yellow dots indicate hand auger cores, whereas green triangles point to cores obtained with rotary technique. (C) Descriptive terminology for the fluvial environment, meander-bend morphometry and related deposits.

Cores were cut longitudinally, measured, photographed and sampled every meter for grain-size analysis. Dry peels with epoxy were made to preserve grain-size texture and sedimentary structures.

Core logging was carried out following the basic principles of facies analysis, to highlight sediment grain size, colour, oxidation, and sedimentary structures. In the bar deposits, the vertical and streamwise variability of grain size was defined through grain-size analyses on the cores AV_a – c. A total of 15 samples were collected from undisturbed portions of these cores and grain-size analyses were carried out by dry sieving through a vibrating screen. Each sample has a total volume of ca. 45 cm^3. The terminology adopted in this work is reported in figure 3.3C.

3.4 Results

3.4.1 Geophysical sediment properties

The inversion of FDEM survey data provided measured electrical conductivity values σ (mS/m) for different depth intervals (Fig. 3.4). Maps spanning between 1 and 6 m from the ground level highlight the occurrence of an arcuate sedimentary body with a low conductivity pattern. The internal boundary of this arcuate body shows a radius of curvature of about 60 m and a sinuosity value of 2.3, whereas the external boundary is characterised by a radius of curvature and a sinuosity of about 135 m and 2.2, respectively (Fig. 3.4). The position and orientation of this arcuate body adapt mainly to that of meander Bend 1 of Reach A, suggesting that these low-resistivity deposits belong to the point-bar body associated with Bend 1. Consistency between the orientation of the arcuate body and the scroll-pattern of the bar (Fig. 3.2B) strongly supports this hypothesis. The arcuate bar body is characterised by very low conductivity values (i.e., $\sigma < 20$ mS/m) in shallower slices (i.e., 1 to 5), whereas they get close to 40 mS/m at about 5 - 6 m below the ground level (slices 6, 7; Fig. 3.4). At higher depths (i.e., slice 8) conductivity values rise to 180 mS/m, defining the base of the bar body, although these values are obtained at the resolution limits of the instrument (Fig. 3.4).

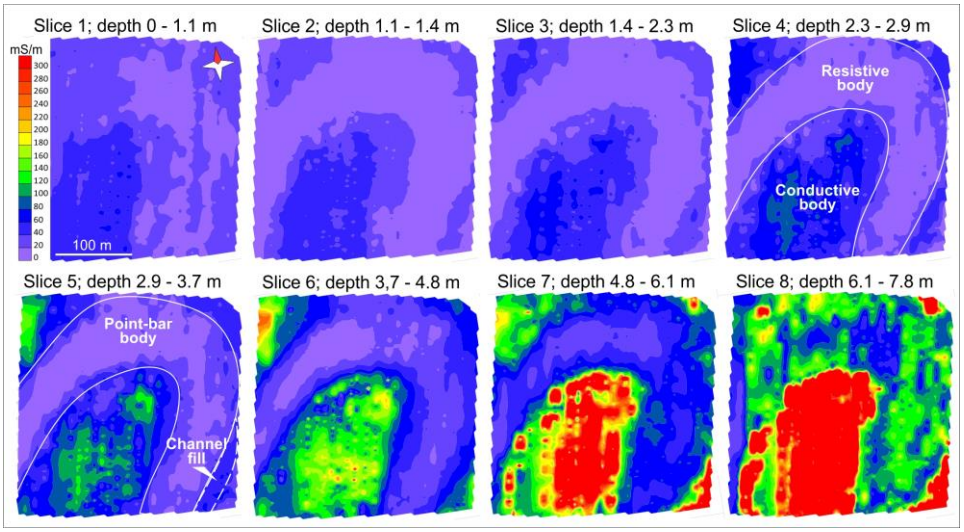

Fig. 3.4. Conductivity slice maps.

Although the point-bar body is characterised by an almost uniform resistivity, subtle differences are enhanced, for a selected area, by narrowing the range of conductivity scale (Fig. 3.5A).

This procedure visually highlights a subtle increase in conductivity from the upstream to the downstream sector of the bar (Fig. 3.5A), along with the occurrence of two zones of higher conductivity within the overall resistive domain (Fig. 3.5B).

These two zones are located in the upstream and downstream limb of Bend 1 and overlap with the planform trend of its paleochannel (Fig. 3.2 and 3.5B), suggesting these higher conductivity values are associated with channel-fill deposits associated with Bend 1. Specifically, upstream channel fill deposits (inset B.1 in figure 3.5B) appear slightly more resistive than those in the downstream part of the bend (inset B.2 in figure 3.5B), which seem to bound a third bend (Bend 3) in the eastern termination of Reach 1 (Fig. 3.5B.1). Deposits surrounding the point-bar body show electrical resistivity values spanning from 80 to 250 mS/m. Specifically, the resistivity of these deposits is close to 100 mS/m until -3 m from the ground, and increases to 250 mS/m between a depth of 3.0 and 7.8 m. By comparing geophysical data and satellite images (Fig. 3.2 and 3.4), these conductive sediments are interpreted as the floodplain deposits through which meander Bend 1 of Reach A was cut.

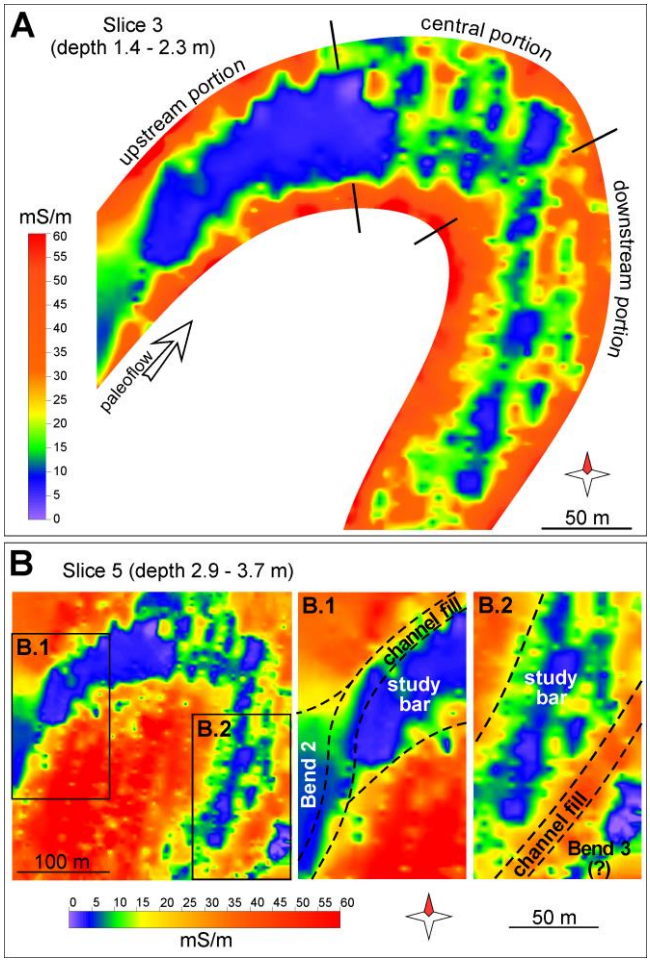

Fig. 3.5. Conductivity slice maps with enhanced resolution. (A) Subtle changes in conductivity within the study bar between 1.4 and 2.3 m from the ground. (B) Channel-fill deposits in the upstream (inset B.1) and downstream (inset B.2) portion of the investigated channel bend.

3.4.2 Sedimentary facies and meander architecture

Once the planform morphology of Bend 1 and related point-bar deposits were defined, sedimentary cores were recovered. Core data show that the first 80 cm below the ground surface has been severely reworked by agricultural activities. These reworked deposits are made of very fine sand with a moderate to a high amount of mud. Point-bar deposits are up to 4.2 m thick, occurring from 0.8 to a maximum depth of 5.4 m (core AV_b) below the ground surface, and are mainly made of poorly structured sand with a low percentage of mud. Point-bar deposits are paved by a channel lag, consisting of structureless sands (Fig. 3.6B) with scattered gravel-sized mudclasts (Fig. 3.6C). Lower bar deposits are 1.0 to 1.5 m thick and are characterised by well-sorted, mud-free sand, which ranges

from massive to roughly plane-parallel stratified (Fig. 3.6D). Upper bar deposits, 2.5 – 3 m thick, are made of sand with plane-parallel to ripple cross-laminations (Fig. 3.6E). These sand deposits show a higher intergranular mud content, which is ca. 12%, 21% and 20% in the upstream, central and downstream cores, respectively. Subordinate 0.5 – 2.0 cm-thick mud layers occur in the upper part of the bar (Fig. 3.6F).

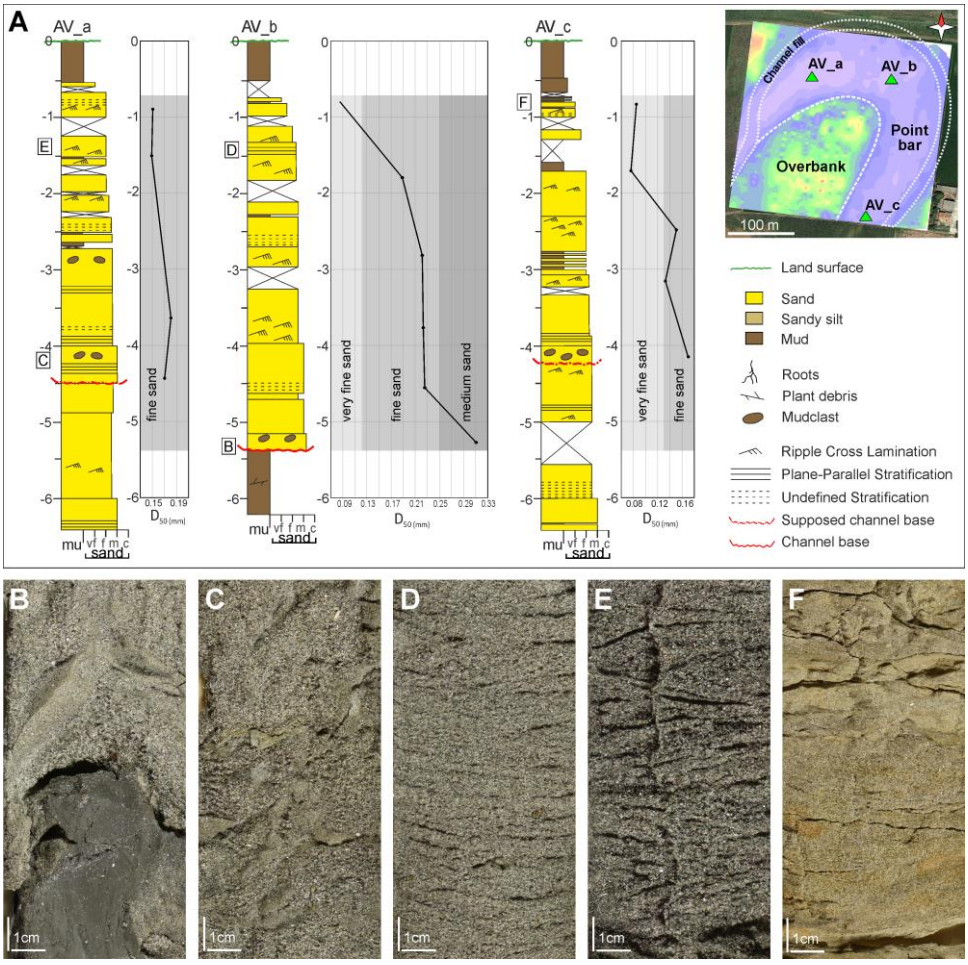

Fig. 3.6. Point-bar deposits. (A) Upstream (AV_a), central (AV_b) and downstream (AV_c) bar deposits and related grain size. (B) Fine to medium sand lag deposits with pebble-sized mudclasts (C). (D) Plane parallel stratification and (E) ripple-cross lamination in upper bar sands. (F) Mud layers in the upper bar portion.

Grain size (D_{50}) of the bar sand ranges between very-fine and medium sand, although most of the samples are made of fine sand (Fig. 3.6A and 3.7). The D_{50} grain size of the upstream-bar deposits corresponds to fine-grained sand, and no relevant vertical grain-size changes occur in the cored deposits (Fig. 3.6A and

3.7A). Central bar deposits show the widest range of sand size (Fig. 3.6A and 3.7B), and their D_{50} spans from medium to very-fine sand, although these values occur only in the lowermost and uppermost parts of the bar, respectively. The D_{50} of the downstream-bar deposits corresponds to fine- and very-fine grained sand in the lower and upper part of the bar, respectively (Fig. 3.6A and 3.7C). The coarsest and finest sand deposits (i.e., averaged value through the bar) are observed in the central and downstream bar zone, respectively (Fig. 3.7D).

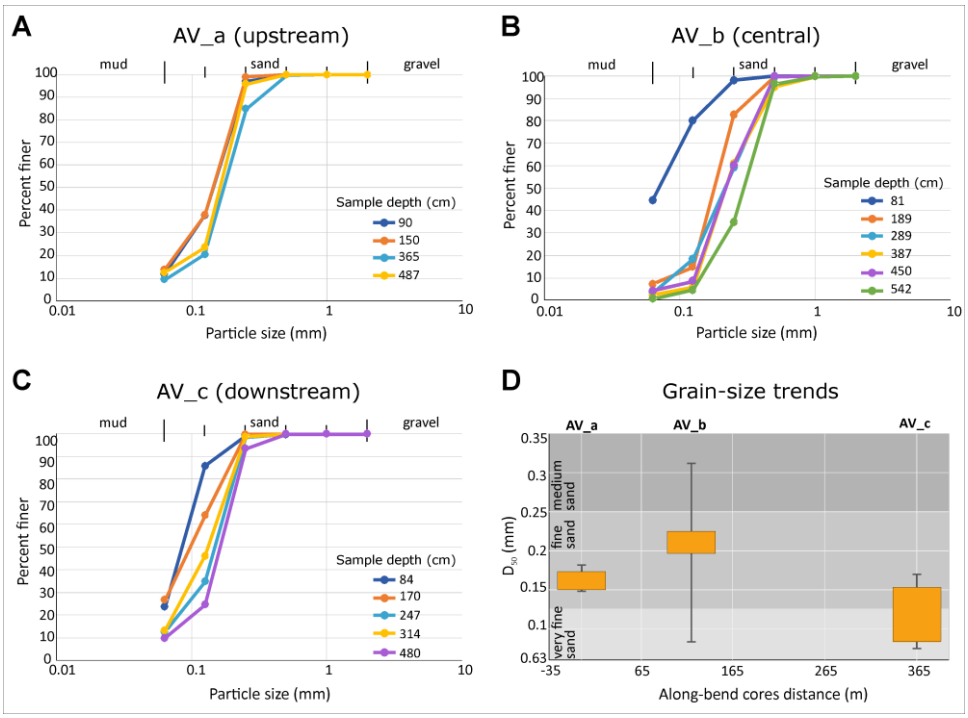

Fig. 3.7. Grain-size analysis. (A - C) Cumulative curves of grain size analysis performed in upstream (A), central (B) and downstream (C) bar deposits. (D) Grain-size distribution in three cores located in upstream, central and downstream point-bar sides.

Channel-fill deposits have been recovered at core AV_12 (Fig. 3.8) and are almost 4 m thick. They consist of very fine to fine sand forming well-defined beds (Fig. 3.8B) raging in thickness between 1 and 3 cm. Sand is commonly ripple-cross and plane-parallel laminated, although cross-stratification occurs in the lowermost part of the core (Fig. 3.8A). In the upper part of the channel-fill succession, muddy intercalations become common (Fig. 3.8C), along with the occurrence of oxidations and root traces, which probably pertain to the post-depositional activity of plant living on the present surface (Fig. 3.8D).

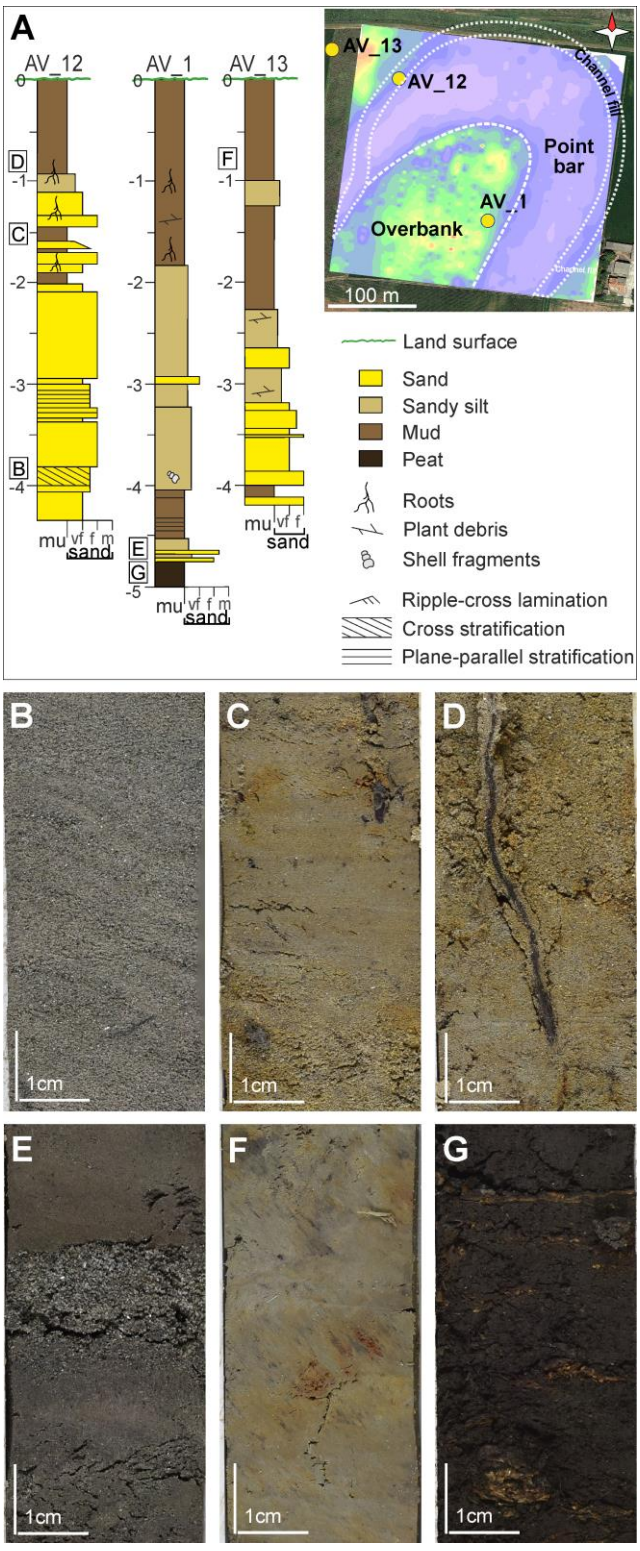
A
AV_12
AV_1
AV_13
D
C
B
F
E
G
-1
-2
-3
-4
-5
mu vf f m
sand
AV_13
AV_12
AV_1
Point bar
Channel fill
Overbank
100 m
Land surface
Sand
Sandy silt
Mud
Peat
Roots
Plant debris
Shell fragments
Ripple-cross lamination
Cross stratification
Plane-parallel stratification
B
C
D
E
F
G
1cm

Fig. 3.8. Channel-fill and overbank deposits. (A) Core logs of channel fill and overbank elements. (B – D) Channel-fill deposits showing cross-stratified very-fine sand layers (B), massive mud layer (C), and oxidized mud with roots (D). (E – G) Overbank deposits consisting of horizontal-bedded mud with a massive sand layer (E), oxidized massive mud (F), and massive organic-rich mud with wood fragments (G).

Overbank areas, where geophysical investigations disclose conductive sediments, are characterised by horizontal bedding and are principally made of silt-rich mud with centimetric to decimetric sandy layers (Fig. 3.8E). Mud is massive and locally oxidized (Fig. 3.8F) or organic-rich (Fig. 3.8G).

At a few sites, organic content almost exceeds the inorganic clastic fraction becoming peat (Fig. 3.8G). Sandy layers are commonly sharp-based (Fig. 3.8E), consist of fine sand and range in thickness between 1 and 2 cm. These sandy intercalations are commonly massive or plane-parallel stratified. Small shell fragments locally occur and they are mainly related to freshwater gastropods (i.e., Pulmonata).

Study bar deposits cover both organic-rich mud (core AV_b) or sandy deposits (cores AV_a and AV_c), which are at least 0.8 and 5 m thick, respectively. Sandy deposits are comparable with those of the investigated bar in terms of grain size, sedimentary structures and presence of mudclasts, suggesting they were also probably formed in a channelized setting. Organic-rich mud is massive, dark grey with peat layers, and bears sedimentary features consistent with those of overbank deposits.

3.5 Discussions

The comparison between geomorphological evidence and integrated geophysical and sedimentological data shows that the investigated paleochannel formed a sandy point bar (Bend 1) with a characteristic horseshoe planform shape. The bar body is homogeneously made of fine sand, although slightly coarser sand occurs in the central part of the bar. Abandoned channel-fill deposits are sand-rich and plug a 15-20 m wide channel. These elements are discussed here in terms of genesis of the meander bend, intra-bar grain-size variability, and style of channel bend abandonment.

3.5.1 Bar shape and genesis of the bend

The external boundary of the studied point bar fits with that of point bars generated by a uniform increase in bend radius and sinuosity and shows a "simple asymmetrical" planform following the classification proposed by Hooke

(2013). The geometry of the point bar differs from that of most point bars for the arcuate shape of its inner boundary, which suggests that the bar started to accrete from a channel with a sinuosity of ca 2.3 (Fig. 3.4). This evidence challenges the paradigm suggesting that point bars originate from the increase in sinuosity of a straight channel (Brice, 1974; Lewin, 1976; Nanson and Page, 1983; Ghinassi et al., 2014; Wu et al., 2015; Finotello et al., 2018). The onset of accretion from a sinuous reach forced the channel to accumulate a reduced volume of bar sediments in comparison with that produced by bar growth from a relatively straight channel. A 3D reconstruction of the bar body, obtained by interpolating boundaries of the point-bar body between conductivity maps, estimates that ca. 1.8 x 10^6 m^3 of sand were stored in the study bar (Fig. 3.9A), whereas a volume of ca. 3.1 x 10^6 m^3 would have been produced by bar growing from a straight channel (Fig. 3.9B). This observation, although based on the analyses of a single study site, provides insights for the reconstruction of the effective volume of point-bar sandbodies.

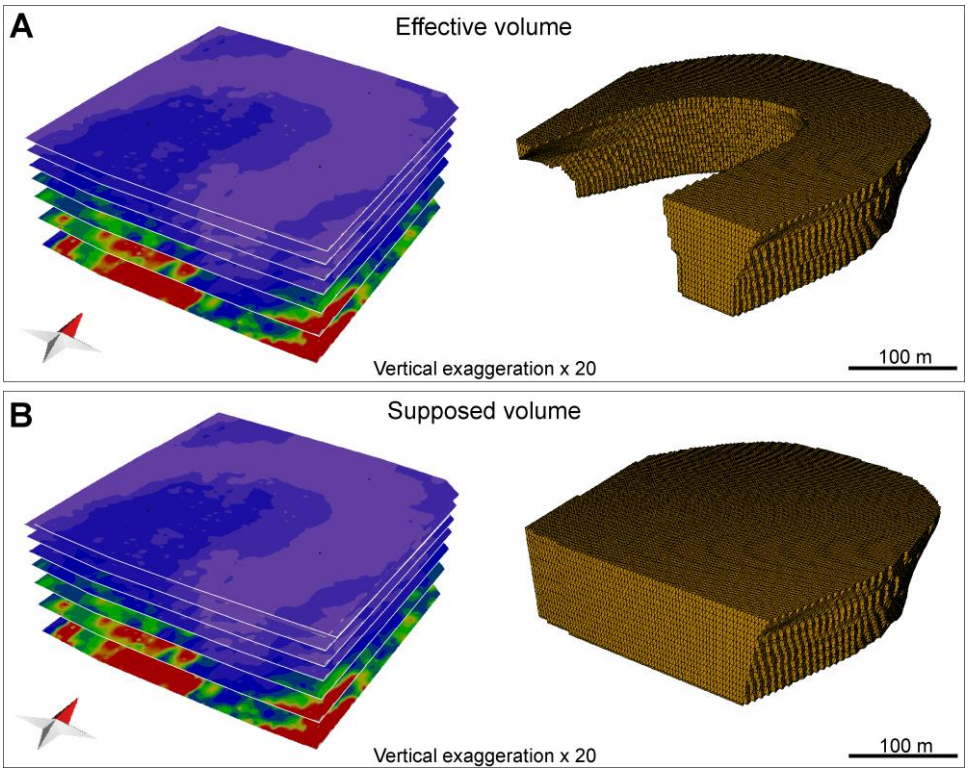

Fig. 3.9. 3D reconstructed volumes for the investigated point bar. (A) Effective 3D morphology of the bar is inferred through the integration between geophysical and sedimentary evidence. (B) Reconstructed morphology of the point-bar body assuming onset of bar accretion from a straight channel.

The onset of bar deposition from a sinuous channel is discussed concerning floodplain morphologies. Although floodplains are considered as low-relief landscapes, a wide variety of local morphologies are generated in association with the development of depositional sub-elements, including levees, crevasse splays, abandoned channels and flood basins (Wolman and Leopold, 1957; Leopold et al., 1964; Bluck, 1971; Nanson, 1980; Mjøs et al., 1993; Khan et al., 1997; Smith and Rogers, 1999; Kemp, 2004; Gibling, 2006; Ielpi and Ghinassi, 2014; Burns et al., 2017; Gugliotta et al., 2018). These sub-elements commonly occur in the southern Venetian Plain, where late Holocene interaction between the Po and Adige rivers gave rise to a complex network of alluvial landforms (Fontana et al., 2008; Piovan et al., 2010, 2012; Mozzi et al., 2020). These different alluvial sub-environments produced a wide spectrum of deposits and lithological heterogeneities (Güneralp and Rhoads, 2011; Motta et al., 2012; Bogoni et al., 2017), which promoted differential compaction that, in turn, enhanced the primary depositional morphologies (Gambolati and Teatini, 1998; Gambolati et al., 1998; Teatini et al., 2011; Bruno et al., 2019). Floodplain morphologies forced the newly-formed watercourse to connect adjacent depressed areas (Aslan and Blum, 1999; Morozova and Smith, 1999; Taylor, 1999) defining an irregular track with local bends of different shapes.

The onset of the studied channel is consistent with its relocation on the floodplain following an avulsion event (e.g., Slingerland and Smith, 1998, 2004; Jones and Schumm, 1999; Mohrig *et al.*, 2000). Relocation of the channel after an avulsion event can occur following different processes (Flood and Hampson, 2014), including i) avulsion by annexation, when the new channel is relocated in the depression left by a pre-existing channel (Slingerland and Smith, 2004); ii) avulsion by progradation, where emplacement of the channel is heralded in the overbank succession by progradation of precursor crevasse deposits (Slingerland and Smith, 2004); and, iii) avulsion by incision, occurring where relocation of the channels is abrupt and leads to local incision of the floodplain (Mohrig et al., 2000). The presence of overbank deposits in the area enclosed by the investigated point bar suggests that the channel did not reoccupy the depression left by a pre-existing sinuous channel, which would have accumulated sandy bar deposits along its inner bank. Overbank deposits forming the substrate for embanking of the study channel show an overall fining upward grain-size trend, which consists of 2.0-2.5 m of organic-rich mud covering 2-3 m of silty to very fine sandy layers (Fig. 3.8). This trend rules out a gradual progradation of a newly-formed fluvial channel into a topographically

low zone (i.e., avulsion by progradation), a process that commonly produces coarsening-upward stacking of overbank splay deposits. The establishment of the studied channel likely followed an avulsion by incision where the stemming channel was originated by headward erosion of a knickpoint (Mohrig et al., 2000) that moved in the alluvial plain connecting different topographic lows. Propagation of such stemming channel in the floodplain is consistent with isolation of overbank mud within the convex side of the bend, where the bar started to grow once a certain amount of bedload started to be conveyed within the channel.

3.5.2 Point bar grain-size variability

The investigated bar is largely made of sandy deposits, which are loose and possibly formed the unrecovered part of some of the cores. The sand is ubiquitously fine in grain size, and only subtle grain-size variations locally occur (Fig. 3.6 and 3.7D). Although fluvial point-bars are described as fining upward units (Nanson, 1980; Nanson and Page, 1983; Ghinassi et al., 2013; Bhattacharyya et al., 2015; Durkin et al., 2018), variability in the vertical grain-size distribution has also been documented (Jackson, 1976; Ielpi and Ghinassi, 2014; Swan et al., 2018). The upstream part of the study bar does not show any vertical change in grain size and fits with cases where point-bar head deposits provide a 'blocky' well log pattern (Willis, 1989; Willis and Sech, 2018). Accumulation of fine-grained deposits is hindered in the upstream bar by the approaching of the main flow toward the bar during its shift from the inner toward the outer bank of the bend (Dietrich and Smith, 1983; Frothingham and Rhoads, 2003). A subtle vertical decrease in grain size occurs downstream of the bar head and is slightly better expressed in the central bar zone, where medium and very fine sand occurs in the lowermost and uppermost part of the bar, respectively (Fig. 3.6A). Although this trend is weak, it represents the stratigraphic signature of the secondary helical flows (Blanckaert, 2018) that, in the bend apex zone, is more effective in providing a vertical zonation of grain size along the inner bank (Frothingham and Rhoads, 2003). The overall along-bar distribution of grain size is also fairly uniform, although slightly coarser sand occurs in the central bar zone (Fig. 3.7D). The sand fining occurring downstream of the bend apex fits with the downstream decrease of depth-averaged flow velocity and bed shear stress (Dietrich and Smith, 1983; Frothingham and Rhoads, 2003; Seminara, 2006; Kasvi et al., 2013). The paucity of muddy deposits in the downstream bar zone can also account for the lack of the

establishment of a low-energy recirculation zone (i.e., “dead zone”; Leeder and Bridges, 1975; Ferguson *et al.*, 2003; Riley *et al.*, 2015) that is originated by a flow separation in sharply curved bends (Hickin and Nanson, 1975; Leeder and Bridges, 1975; Ferguson et al., 2003), where the ratio between the radius of curvature and the channel width is commonly less than two (Bagnold, 1960; Hickin and Nanson, 1975; Finotello et al., 2019). The occurrence of coarser deposits in the point-bar apex zone has also been recently documented in large-scale point bars of the McMurray Fm. (see figure 10 in Hagstrom et al., 2019), and might suggest that fluid drag forces developed by the helical flow are the highest of the whole bend.

Although flow configurations occurring in different parts of the bend cause variations in grain-size distribution, these changes are very subtle and differ from vertical and along-bend grain-size trends which are commonly ascribed to fluvial point-bar deposits (Bluck, 1971; Hooke, 1975; Bridges and Leeder, 1976; Nanson, 1980; Nanson and Page, 1983; Bridge et al., 1995; Ghinassi et al., 2013; Bhattacharyya et al., 2015; Durkin et al., 2018). This overall homogenous sand-size distribution fits with the uniform values of conductivity values in the bar body and can be ascribed to a combination of a narrow spectrum of grain size for available bedload transport and limited variability of river discharge capability (Plink-Björklund, 2015).

3.5.3 Infill and morphometry of the residual channel

Channel bounding the studied bar is ca. 15-20 m wide (Figs. 3.4 and 3.5B), and its infill consists of sand with subordinate mud in the upper infill succession (Fig. 3.8A). An overall fining-upward grain-size trend characterizes the infill of an abandoned meandering channel (Díaz-Molina and Muñoz-García, 2010; Toonen et al., 2012), although grain size can vary according to morphodynamic processes causing the abandonment. Channel-fill deposits are most likely muddy in case of neck cut-off (Fisk, 1947; Allen, 1965; Russell, 2017) and contain an increasing amount of sand in case of chute cut off (Fisk, 1947; Allen, 1965; Toonen et al., 2012; Fustic et al., 2018). Channel-fills are commonly sand-dominated, where avulsion takes place (Allen, 1965; Mackey and Bridge, 1995; Toonen et al., 2012). The sand-rich infill of the study channel suggests that it was not abruptly deactivated (cf. Toonen, Kleinhans and Cohen, 2012) and that river currents promoted tractional deposition of sand, preventing mud settling until the latest stage of infill. Planform distribution of Reach A and B (Fig. 3.2) shows that deactivation of Reach A was not caused by a neck cut off but

followed the connection of two closely-spaced reaches of Bend 1 that was probably initiated by a floodplain channel during major floods (Gay et al., 1998; Ghinassi, 2011). The diversion angle (*sensu* Constantine et al., 2010) between the entrance of the abandonment channel (Reach A) and the new channel (Reach B) is ca. 50°, and promoted bed-material load mobility within the abandoned channel allowing for a more coarse-grained infill, especially in the upstream reach of the channel. This mechanism is consistent with a downstream increase in conductivity values (i.e., mud content) within the abandoned channel (Fig. 3.5B). A gradual abandonment accounts for the development of a residual channel and fits with the limited width of the channel (i.e., 15-20 m) shown by satellite images (Fig. 3.2). Accordingly, the studied channel appears to be disproportionally narrow in comparison with its depth, which is recorded by the overall 4 m-thick associated point bar. An aspect ratio in the range of 10-100 typifies meandering fluvial channels (Gibling, 2006; Cuevas Martínez et al., 2010; Ielpi et al., 2017; Finotello et al., 2020a), whereas values close to 4 characterize delta distributary channels (Gibling, 2006). A discrepancy arises between channel width and meander bend wavelength for Bend 1 since meander wavelength is commonly 10 to 14 times the width of the related channel (Leopold and Wolman, 1960; Lagasse et al., 2004; Finotello et al., 2020a), whereas this value is ca. 30 for the investigated bend. Finally, the radius of curvature is ca. 8 times the width of the study channel, whereas most of the fluvial bends tend to reach a radius of curvature that is 2 to 3 times the channel width to get the most efficient hydraulic shape (Leopold and Wolman, 1960; Thorne, 1997; Lagasse et al., 2004; Ielpi et al., 2017; Finotello et al., 2019). The disproportional narrowness of channel-forming Bend 1 suggests that the width measurable from satellite images is referred to that of the channel at its residual stage when it was almost filled and mud settling caused vertical thalweg aggradation and channel narrowing (Fisk, 1947; Allen, 1965; Toonen et al., 2012). Identification of similar disproportionally narrow channels from 3D seismic images can provide insights to infer the infill style of abandoned channels, allowing to predict inter-bar connectivity within fluvial reservoirs generated by meandering channels. Muddy channel fills, generated by a sudden abandonment, preserve the aspect ratio of the active channel and limit inter-bar connectivity, with strong implication for oil charge that arises from the mechanism of fill and spill in a compartmentalized reservoir (e.g., McMurray Fm., Fustic et al., 2012a). Disproportionally narrow channel fills, like that

reconstructed in this study, do not hinder the oil charge of adjacent point bars allowing for the development of a poorly compartmentalized reservoir.

3.6 Conclusions

The morphodynamic evolution and the internal distribution of sedimentary facies of a fluvial paleomeander in the southern Venetian Plain (Italy) were analysed through the integration of morphological evidence, sedimentary core data, and non-invasive geophysical investigations.

The main conclusions stemming from this study are as follows:

1) Geophysical investigations allow us to define the 3D stratigraphy of the study area up to ca. 6 m from the ground. Conductivity maps enhance the occurrence of a buried paleomeander body, as suggested by marked electric contrast between the fluvial body and the surrounding floodplain deposits. The fluvial body, indeed, is characterised by low conductivity values of about 20 mS/m, whereas the floodplain varies in conductivity between 80 and 250 mS/m, in surficial and deeper portions, respectively. Allowing to quickly collect high-quality data, the geophysics approach proposed here represents a powerful tool to detect paleo-morphologies in similar coastal plains, even where landforms are poorly visible from remote sensing.

2) Although it is commonly assumed that point bars initiate from almost straight channels, the studied point bar is characterised by an unusual curved shape of its inner boundary, which suggests the onset of lateral migration from a channel with a sinuosity of ca. 2.3. This process is explained as a post-avulsion relocation of the channel, which defined its first track connecting adjacent topographic lows developed within the floodplain.

3) The investigated point bar is ubiquitously made of fine sand, and only subtle vertical and lateral grain-size variations occur. The classical fining-upward grain size trend is slightly defined only in the central bar zone, and a downstream fining of bar deposits barely occurs.

4) Channel-fill deposits associated with the studied bar are mainly sandy and document a gradual abandonment of the channel that allows the tractional deposition of sand and prevents mud settling until the latest stage of infill. Gradual abandonment causes the width of the residual channel, visible from satellite images, to be disproportionally low in comparison with other morphometric features of the bend (e.g., wavelength). Detection of disproportionally narrow meandering channels from aerial images can allow

predicting the infill style of abandoned channels and, consequently, inter-bar connectivity within channel belt bodies.

Acknowledgments

This work was supported by "HYDROSEM: Fluvial and tidal meanders of the Venetian-Po plain: from hydrodynamics to stratigraphy" project (Progetto di Eccellenza CARIPARO 2017, PI Massimiliano Ghinassi), and the University of Padova (SID2016 project, titled "From channels to rock record: morphodynamic evolution of tidal meanders and related sedimentary products" PI Massimiliano Ghinassi). We thank Studio Tecnico Drago (Monselice, Italy) for logistic support, I. Rizzi for help in the laboratory and M. Cosma for her contribution to data collection. We would like to acknowledge R. Bonato for allowing us the investigations in his properties and kindly provide information about the investigated area. The manuscript benefits from the constructive comments from M. Fustic and an anonymous reviewer. We are indebted with the Editor in Chief M. Zecchin for his editorial assistance.

Data Availability

Datasets related to this article can be found at https://data.mendeley.com/datasets/drp7gj7mbb/draft?a=6eb3ddf0-3bd2-4ecf-9f49-75ba4ae499f3, an open-source online data repository hosted at Mendeley Data (Bellizia et al., 2021).

References

Allen, J.R.L., 1965, A review of the origin and characteristics of recent alluvial sediments: Sedimentology, v. 5, p. 89–191, doi:10.1111/j.1365-3091.1965.tb01561.x.

Allen, J.R.L., 1970, Studies in fluviatile sedimentation: a comparison of fining-upwards cyclothems, with special reference to coarse-member composition and interpretation: Journal of Sedimentary Research, v. 40, p. 298–323.

Allred, B., Daniels, J.J., and Reza Ehsani, M., 2008, Handbook of Agricultural Geophysics: USA, CRC Press, 432 p.

Amorosi, A., Bruno, L., Cleveland, D.M., Morelli, A., and Hong, W., 2017, Paleosols and associated channel-belt sand bodies from a continuously subsiding late quaternary system (Po basin, Italy): New insights into

continental sequence stratigraphy: Bulletin of the Geological Society of America, v. 129, p. 449–463, doi:10.1130/B31575.1.

Amorosi, A., Fontana, A., Antonioli, F., Primon, S., and Bondesan, A., 2008, Post-LGM sedimentation and Holocene shoreline evolution in the NW Adriatic coastal area: GeoActa, v. 7, p. 41–67.

Aslan, A., and Blum, M.D., 1999, Contrasting styles of Holocene avulsion, Texas Gulf coastal plain, USA, *in* Smith, N.D. and Rogers, J. eds., Fluvial sedimentology VI: International Association of Sedimentologists Special Publication, Wiley Online Library, v. 28, p. 193–209, doi:10.1002/9781444304213.ch15.

Bagnold, R.A., 1960, Some aspects of the shape of river meanders: U.S. Geological Survey Professional Paper, v. 282-E, p. 371–375, doi:10.1080/00207217608920581.

Bhattacharyya, P., Bhattacharya, J.P., and Khan, S.D., 2015, Paleo-channel reconstruction and grain size variability in fluvial deposits, Ferron Sandstone, Notom Delta, Hanksville, Utah: Sedimentary Geology, v. 325, p. 17–25, doi:10.1016/j.sedgeo.2015.05.001.

Blanckaert, K., 2018, Hydro-sedimentological processes in meandering rivers: A review and some future research directions, *in* Ghinassi, M., Colombera, L., Mountney, N.P., Reesink, A.J., and Bateman, M. eds., Fluvial Meanders and Their Sedimentary Products in the Rock Record (Int. Assoc. Sedimentol. Spec. Publ. 48, John Wiley & Sons, p. 297–320, doi:10.1002/9781119424437.ch12.

Blanckaert, K., and de Vriend, H.J., 2004, Secondary flow in sharp open-channel bends: Journal of Fluid Mechanics, v. 498, p. 353–380, doi:10.1017/S0022112003006979.

Bluck, B.J., 1971, Sedimentation in the meandering river Endrick: Scottish Journal of Geology, v. 7, p. 93–138, doi:10.1144/sjg07020093.

Bogoni, M., Putti, M., and Lanzoni, S., 2017, Modeling meander morphodynamics over self-formed heterogeneous floodplains: Water Resources Research, v. 53, p. 5137–5157, doi:10.1002/2017WR020726.

Bondesan, M., 2001, Hydrography, *in* Castiglioni, G.B. and Pellegrini, G.B. eds., Illustrative Notes of the Geomorphological Map of Po Plain (Italy)., Geografia Fisica Dinamica Quaternaria, 4, p. 33–44.

Bondesan, A., Meneghel, M., Miola, A., and Valentini, G., 2003, Paleoenvironmental reconstruction from LGM to historical time in the lower coastal plain of the Piave River. Preliminary pollen analysis on a 20 m core of lagoon and fluvial sediments: Il Quaternario, v. 16, p. 183–192.

Bondesan, A., Meneghel, M., Rosselli, R., and Vitturi, A., 2004, La carta geomorfologica della Provincia di Venezia, scala 1:50,000: Firenze, LAC, v. 5.

Bondesan, A., Primon, S., Bassan, V., and Vitturi, A., 2008, Carta delle unità geologiche della provincia di Venezia: Verona, Italy, Cierre, 160 p.

Brice, J.C., 1974, Evolution of meander loops: Geological Society of America Bulletin, v. 85, p. 581–586, doi:10.1130/0016-

7606(1974)85<581:EOML>2.0.CO;2.

Bridge, J.S., 2003, Rivers and floodplains. Forms, Processes and Sedimentary Record: Blackwell Science, v. 491.

Bridge, J.S., Alexander, J.A.N., Collier, R.E.L., Gawthorpe, R.L., and Jarvis, J., 1995, Ground-penetrating radar and coring used to study the large-scale structure of point-bar deposits in three dimensions: Sedimentology, v. 42, p. 839–852, doi:10.1111/j.1365-3091.1995.tb00413.x.

Bridge, J.S., Smith, N.D., Trent, F., Gabel, S.L., and Bernstein, P., 1986, Sedimentology and morphology of a low-sinuosity river: Calamus River, Nebraska Sand Hills: Sedimentology, v. 33, p. 851–870, doi:10.1111/j.1365-3091.1986.tb00987.x.

Bridges, P.H., and Leeder, M.R., 1976, Sedimentary model for intertidal mudflat channels, with examples from the Solway Firth, Scotland: Sedimentology, v. 23, p. 533–552, doi:10.1111/j.1365-3091.1976.tb00066.x.

Bruno, L., Campo, B., Di Martino, A., Hong, W., and Amorosi, A., 2019, Peat layer accumulation and post-burial deformation during the mid-late Holocene in the Po coastal plain (Northern Italy): Basin Research, v. 31, p. 621–639, doi:10.1111/bre.12339.

Burns, C.E., Mountney, N.P., Hodgson, D.M., and Colombera, L., 2017, Anatomy and dimensions of fluvial crevasse-splay deposits: Examples from the Cretaceous Castlegate Sandstone and Neslen Formation, Utah, U.S.A.: Sedimentary Geology, v. 351, p. 21–35, doi:10.1016/j.sedgeo.2017.02.003.

Camporeale, C., Perona, P., Porporato, A., and Ridolfi, L., 2007, Hierarchy of models for meandering rivers and related morphodynamic processes: Reviews of Geophysics, v. 45, p. 1–28, doi:10.1029/2005RG000185.

Cassiani, G., Bellizia, E., Fontana, A., Boaga, J., D'Alpaos, A., and Ghinassi, M., 2020, Geophysical and Sedimentological Investigations Integrate Remote-Sensing Data to Depict Geometry of Fluvial Sedimentary Bodies: An Example from Holocene Point-Bar Deposits of the Venetian Plain (Italy): Remote Sensing, v. 12, p. 2568, doi:10.3390/rs12162568.

Cassiani, G., Boaga, J., Vanella, D., Perri, M.T., and Consoli, S., 2015, Monitoring and modelling of soil-plant interactions: The joint use of ERT, sap flow and eddy covariance data to characterize the volume of an orange tree root zone: Hydrology and Earth System Sciences, v. 19, p. 2213–2225, doi:10.5194/hess-19-2213-2015.

Constable, S.C., Parker, R.L., and Constable, C.G., 1987, Occam's inversion: A practical algorithm for generating smooth models from electromagnetic sounding data: Geophysics, v. 52, p. 289–300, doi:10.1190/1.1442303.

Constantine, A., Dunne, T., Piégay, H., and Kondolfs, G.M., 2010, Controls on the alluviation of oxbow lakes by bed-material load along the Sacramento River, California: Sedimentology, v. 57, p. 389–407, doi:10.1111/j.1365-3091.2009.01084.x.

Corwin, D.L., and Rhoades, J.D., 1982, An Improved Technique for Determining Soil Electrical Conductivity-Depth Relations from Above-ground Electromagnetic Measurements: Soil Science Society of America Journal, v.

46, p. 517–520, doi:10.2136/sssaj1982.03615995004600030014x.

Cuevas Martínez, J.L., Cabrera Pérez, L., Marcuello, A., Arbués Cazo, P., Marzo Carpio, M., and Bellmunt, F., 2010, Exhumed channel sandstone networks within fluvial fan deposits from the Oligo-Miocene Caspe Formation, South-east Ebro Basin (North-east Spain): Sedimentology, v. 57, p. 162–189, doi:10.1111/j.1365-3091.2009.01096.x.

Daniel, J.F., 1971, Channel movement of meandering Indiana streams: Washington D.C., US Government Printing Office.

Delefortrie, S., De Smedt, P., Saey, T., Van De Vijver, E., and Van Meirvenne, M., 2014, An efficient calibration procedure for correction of drift in EMI survey data: Journal of Applied Geophysics, v. 110, p. 115–125, doi:10.1016/j.jappgeo.2014.09.004.

Díaz-Molina, M., and Muñoz-García, M.B., 2010, Sedimentary facies and three-dimensional reconstructions of upper Oligocene meander belts from the Loranca Basin, Spain: AAPG Bulletin, v. 94, p. 241–257, doi:10.1306/07210909010.

Dietrich, W.E., 1987, Mechanics of flow and sediment transport in river bends, *in* Richards, K.S. ed., River channels: Environment and process, Oxford, UK, Basil Blackwell, v. 18, p. 179–227.

Dietrich, W.E., and Smith, J.D., 1983, Influence of the point bar on flow through curved channels: Water Resources Research, v. 19, p. 1173–1192, doi:10.1029/WR019i005p01173.

Dietrich, W.E., Smith, J.D., and Dunne, T., 1979, Flow and sediment transport in a sand bedded meander: The Journal of Geology, v. 87, p. 305–315, doi:10.1086/628419.

Dietrich, W.E., and Whiting, P., 1989, Boundary shear stress and sediment transport in river meanders of sand and gravel, *in* Ikeda, S. and Whiting, P. eds., River Meandering, American Geophysical Union, v. 12, p. 1–50, doi:10.1029/wm012p0001.

Durkin, P.R., Hubbard, S.M., Smith, D.G., and Leckie, D.A., 2018, Predicting heterogeneity in meandering fluvial and tidal-fluvial deposits: The point bar to counter point bar transition, *in* Ghinassi, M., Colombera, L., Mountney, N.P., and Reesink, J.H. eds., Fluvial Meanders and Their Sedimentary Products in the Rock Record. Int. Assoc. Sedimentol. Spec. Publ., John Wiley & Sons, v. 48, p. 231–250, doi:10.1002/9781119424437.ch9.

Edie, R.W., and Andrichuk, J.M., 2005, Meander Belt Entrapment of Hydrocarbons, Campbell-Namao Field, Alberta: Search and Discovery, v. 20027, p. 1–32, http://searchanddiscovery.comwww.searchanddiscovery.com/documents/2005/edie/images/edie.pdf.

Favero, V., and Serandrei Barbero, R., 1980, Origine ed evoluzione della laguna di Venezia: bacino meridionale: Lavori della Società Veneziana di Scienze Naturali, v. 5, p. 49–71.

Ferguson, R.I., Parsons, D.R., Lane, S.N., and Hardy, R.J., 2003, Flow in meander

bends with recirculation at the inner bank: Water resources research, v. 39, p. 1322, doi:10.1029/2003WR001965.

Finotello, A., D'Alpaos, A., Bogoni, M., Ghinassi, M., and Lanzoni, S., 2020a, Remotely-sensed planform morphologies reveal fluvial and tidal nature of meandering channels: Scientific Reports, v. 10, p. 1–13, doi:10.1038/s41598-019-56992-w.

Finotello, A., D'Alpaos, A., Lazarus, E.D., and Lanzoni, S., 2019, High curvatures drive river meandering: Comment: Geology, v. 47, p. e486, doi:10.1130/G45608.1/4639675/g45608.pdf.

Finotello, A., Ghinassi, M., Carniello, L., Belluco, E., Pivato, M., Tommasini, L., and D'Alpaos, A., 2020b, Three-dimensional flow structures and morphodynamic evolution of microtidal meandering channels: Water Resources Research, v. 56, p. e2020WR027822, doi:10.1029/2020WR027822.

Finotello, A., Lanzoni, S., Ghinassi, M., Marani, M., Rinaldo, A., and D'Alpaos, A., 2018, Field migration rates of tidal meanders recapitulate fluvial morphodynamics: Proceedings of the National Academy of Sciences, v. 115, p. 1463–1468, doi:10.1073/pnas.1711330115.

Fisk, H.N., 1947, Fine-grained alluvial deposits and their effects on Mississippi River activity. Vols 1 & 2: Vicksburg, Mississippi, Mississippi River Commission, doi:10.1086/625561.

Flood, Y.S., and Hampson, G.J., 2014, Facies and architectural analysis to interpret avulsion style and variability: Upper Cretaceous Blackhawk Formation, Wasatch Plateau, Central Utah, USA: Journal of Sedimentary Research, v. 84, p. 743–762, doi:10.2110/jsr.2014.59.

Fontana, A., Mozzi, P., and Bondesan, A., 2008, Alluvial megafans in the Venetian-Friulian Plain (north-eastern Italy): Evidence of sedimentary and erosive phases during Late Pleistocene and Holocene: Quaternary International, v. 189, p. 71–90, doi:10.1016/j.quaint.2007.08.044.

Fontana, A., Mozzi, P., and Bondesan, A., 2010, Late Pleistocene evolution of the Venetian-Friulian Plain: Rendiconti Lincei, v. 21, p. 181–196, doi:10.1007/s12210-010-0093-1.

Fontana, A., Mozzi, P., and Marchetti, M., 2014, Alluvial fans and megafans along the southern side of the Alps: Sedimentary Geology, v. 301, p. 150–171, doi:10.1016/j.sedgeo.2013.09.003.

Frothingham, K.M., and Rhoads, B.L., 2003, Three-dimensional flow structure and channel change in an asymmetrical compound meander loop, Embarras River, Illinois: Earth Surface Processes and Landforms: The Journal of the British Geomorphological Research Group, v. 28, p. 625–644, doi:10.1002/esp.471.

Fustic, M., Bennett, B., Huang, H., and Larter, S., 2012a, Differential entrapment of charged oil - New insights on McMurray Formation oil trapping mechanisms: Marine and Petroleum Geology, v. 36, p. 50–69, doi:10.1016/j.marpetgeo.2012.05.004.

Fustic, M., Hubbard, S.M., Spencer, R., Smith, D.G., Leckie, D.A., Bennett, B., and

Larter, S., 2012b, Recognition of down-valley translation in tidally influenced meandering fluvial deposits, Athabasca Oil Sands (Cretaceous), Alberta, Canada: Marine and Petroleum Geology, v. 29, p. 219–232, doi:10.1016/j.marpetgeo.2011.08.004.

Fustic, M., Strobl, R., Ghinassi, M., and Zhang, S., 2018, Unsuccessful cut offs--origin and partial preservation of enigmatic channel fills encased within a large-scale point-bar deposit--The McMurray Formation type section, Alberta, Canada, *in* Ghinassi, M., Colombera, L., Mountney, N.P., and Reesink, J.H. eds., Fluvial Meanders and Their Sedimentary Products in the Rock Record. Int. Assoc. Sedimentol. Spec. Publ. 48, John Wiley & Sons, Ltd Chichester, UK, p. 321–348, doi:10.1002/9781119424437.ch13.

Gambolati, G., Giunta, G., Putti, M., Teatini, P., Tomasi, L., Betti, I., Morelli, M., Berlamont, J., De Backer, K., Decouttere, C., Monbaliu, J., Yu, C.S., Br0ker, I., Christensen, E.D., Elfrink, B., Dante, A., Gonella, M., 1998, Coastal Evolution of the Upper Adriatic Sea due to Sea Level Rise and Natural and Anthropic Land Subsidence, *in* Gambolati, G. ed., CENAS, Coastline Evolution of the Upper Adriatic Sea due to Sea Level Rise and Natural and Anthropic Land Subsidence, Kluwer Academic Publishers, p. 1–34, doi:10.1007/978-94-011-5147-4_1.

Gambolati, G., and Teatini, P., 1998, Numerical analysis of land subsidence due to natural compaction of the Upper Adriatic Sea basin (G. Gambolati, Ed.): CENAS, Coastline Evolution of the Upper Adriatic Sea due to Sea Level Rise and Natural and Anthropic Land Subsidence, p. 103–132, doi:10.1007/978-94-011-5147-4_5.

Gay, G.R., Gay, H.H., Gay, W.H., Martinson, H.A., Meade, R.H., and Moody, J.A., 1998, Evolution of cutoffs across meander necks in Powder River, Montana, USA: Earth Surface Processes and Landforms, v. 23, p. 651–662, doi:10.1002/(SICI)1096-9837(199807)23:7<651::AID-ESP891>3.0.CO;2-V.

GF Instruments s.r.o., www.gfinstruments.cz (accessed February 2020).

Ghielmi, M., Minervini, M., Nini, C., Rogledi, S., Rossi, M., and Vignolo, A., 2010, Sedimentary and tectonic evolution in the eastern Po-Plain and northern Adriatic Sea area from Messinian to Middle Pleistocene (Italy): Rendiconti Lincei, v. 21, p. 131–166, doi:10.1007/s12210-010-0101-5.

Ghinassi, M., 2011, Chute channels in the Holocene high-sinuosity river deposits of the Firenze plain, Tuscany, Italy: Sedimentology, v. 58, p. 618–642, doi:10.1111/j.1365-3091.2010.01176.x.

Ghinassi, M., Billi, P., Libsekal, Y., Papini, M., and Rook, L., 2013, Inferring fluvial morphodynamics and overbank flow control from 3D outcrop sections of a Pleistocene point bar, Dandiero Basin, Eritrea: Journal of Sedimentary Research, v. 83, p. 1065–1083, doi:10.2110/jsr.2013.80.

Ghinassi, M., Ielpi, A., Aldinucci, M., and Fustic, M., 2016, Downstream-migrating fluvial point bars in the rock record: Sedimentary Geology, v. 334, p. 66–96, doi:10.1016/j.sedgeo.2016.01.005.

Ghinassi, M., Nemec, W., Aldinucci, M., Nehyba, S., Özaksoy, V., and Fidolini, F., 2014, Plan-form evolution of ancient meandering rivers reconstructed

from longitudinal outcrop sections: Sedimentology, v. 61, p. 952–977, doi:10.1111/sed.12081.

Giacomelli, S., Rossi, V., Amorosi, A., Bruno, L., Campo, B., Ciampalini, A., Civa, A., Hong, W., Sgavetti, M., and de Souza Filho, C.R., 2018, A mid-late Holocene tidally-influenced drainage system revealed by integrated remote sensing, sedimentological and stratigraphic data: Geomorphology, v. 318, p. 421–436, doi:10.1016/j.geomorph.2018.07.004.

Gibling, M.R., 2006, Width and Thickness of Fluvial Channel Bodies and Valley Fills in the Geological Record: A Literature Compilation and Classification: Journal of Sedimentary Research, v. 76, p. 731–770, doi:10.2110/jsr.2006.060.

Gibling, M.R., Nanson, G.C., and Maroulis, J.C., 1998, Anastomosing river sedimentation in the Channel Country of central Australia: Sedimentology, v. 45, p. 595–619, doi:10.1046/j.1365-3091.1998.00163.x.

Gugliotta, M., Saito, Y., Ben, B., Sieng, S., and Oliver, T.S.N., 2018, Sedimentology of late Holocene fluvial levee and point-bar deposits from the Cambodian tract of the Mekong river: Journal of the Geological Society, v. 175, p. 176–186, doi:10.1144/jgs2017-047.

Güneralp, Í., and Rhoads, B.L., 2011, Influence of floodplain erosional heterogeneity on planform complexity of meandering rivers: Geophysical Research Letters, v. 38, p. 2–7, doi:10.1029/2011GL048134.

Hagstrom, C.A., Hubbard, S.M., Leckie, D.A., and Durkin, P.R., 2019, The Effects of Accretion-package Geometry On Lithofacies Distribution in Point-bar Deposits: Journal of Sedimentary Research, v. 89, p. 381–398, doi:10.2110/jsr.2019.23.

Hickin, E.J., and Nanson, G.C., 1975, The character of channel migration on the Beatton River, Northeast British Columbia, Canada: Bulletin of the Geological Society of America, v. 86, p. 487–494, doi:10.1130/0016-7606(1975)86<487:TCOCMO>2.0.CO;2.

Hooke, R.L.B., 1975, Distribution of Sediment Transport and Shear Stress in a Meander Bend: The Journal of geology, v. 83, p. 543–565.

Hooke, J.M., 1995, River channel adjustment to meander cutoffs on the River Bollin and River Dane, northwest England: Geomorphology, v. 14, p. 235–253, doi:10.1016/0169-555X(95)00110-Q.

Hooke, J.M., 2013, River Meandering, *in* Schroder, J.E. and Wohl, E. eds., Teatise on Geomorphology, San Diego, CA, Academic Press, v. 9, p. 260–288.

Hubbard, S.M., Smith, D.G., Nielsen, H., Leckie, D.A., Fustic, M., Spencer, R.J., and Bloom, L., 2011, Seismic geomorphology and sedimentology of a tidally influenced river deposit, Lower Cretaceous Athabasca oil sands, Alberta, Canada: AAPG Bulletin, v. 95, p. 1123–1145, doi:10.1306/12131010111.

Ielpi, A., and Ghinassi, M., 2014, Planform architecture, stratigraphic signature and morphodynamics of an exhumed Jurassic meander plain (Scalby Formation, Yorkshire, UK): Sedimentology, v. 61, p. 1923–1960, doi:10.1111/sed.12122.

Ielpi, A., Rainbird, R.H., Ventra, D., and Ghinassi, M., 2017, Morphometric convergence between Proterozoic and post-vegetation rivers: Nature Communications, v. 8, p. 1–8, doi:10.1038/ncomms15250.

Interpex Limited - Specialists in PC Based Geophysical Software, www.interpex.com (accessed February 2020).

Jackson, R.G., 1976, Depositional model of point bars in the lower Wabash River: Journal of Sedimentary Research, v. 46, p. 579–594, doi:10.1306/212F6FF5-2B24-11D7-8648000102C1865D.

Jones, L.S., and Schumm, S.A., 1999, Causes of avulsion: an overview, *in* Fluvial sedimentology VI, International Association of Sedimentologists Special Publication, Wiley Online Library, v. 28, p. 171–178, doi:10.1002/9781444304213.ch13.

Kasvi, E., Vaaja, M., Alho, P., Hyyppä, H., Hyyppä, J., Kaartinen, H., and Kukko, A., 2013, Morphological changes on meander point bars associated with flow structure at different discharges: Earth Surface Processes and Landforms, v. 38, p. 577–590, doi:10.1002/esp.3303.

Kemp, J., 2004, Flood channel morphology of a quiet river, the Lachlan downstream from Cowra, southeastern Australia: Geomorphology, v. 60, p. 171–190, doi:10.1016/j.geomorph.2003.07.007.

Khan, I.A., Bridge, J.S., Kappelman, J., and Wilson, R., 1997, Evolution of Miocene fluvial environments, eastern Potwar plateau, northern Pakistan: Sedimentology, v. 44, p. 221–251, doi:10.1111/j.1365-3091.1997.tb01522.x.

Labrecque, P.A., Jensen, J.L., and Hubbard, S.M., 2011a, Cyclicity in Lower Cretaceous point bar deposits with implications for reservoir characterization, Athabasca Oil Sands, Alberta, Canada: Sedimentary Geology, v. 242, p. 18–33, doi:10.1016/j.sedgeo.2011.06.011.

Labrecque, P.A., Jensen, J.L., Hubbard, S.M., and Nielsen, H., 2011b, Sedimentology and stratigraphic architecture of a point bar deposit, Lower Cretaceous McMurray Formation, Alberta, Canada: Bulletin of Canadian Petroleum Geology, v. 59, p. 147–171, doi:10.2113/gscpgbull.59.2.147.

Lagasse, P.F., Spitz, W.J., and Zevenbergen, L.W., 2004, Handbook for Predicting Stream Meander Migration: Washington D.C., National Cooperative Highway Research Program, v. Report 533, 98 p.

Leeder, M.R., and Bridges, P.H., 1975, Flow Separation in Meander Bends: Nature, v. 253, p. 338–339.

Leopold, L.B., and Wolman, M.G., 1960, River Meanders: Geological Soceity of America Bulletin, v. 71, p. 769–793, doi:10.1130/0016-7606(1960)71[769:RM]2.0.CO;2.

Leopold, L.B., Wolman, M.G., and Miller, J.P., 1964, Fluvial processes in geomorphology.: San Francisco, California, W. H. Freeman & Company, 522 p.

Lewin, J., 1976, Initiation of bed forms and meanders in coarse-grained sediment: Bulletin of the Geological Society of America, v. 87, p. 281–285, doi:10.1130/0016-7606(1976)87<281:IOBFAM>2.0.CO;2.

Lindner, C.P., 1953, Diversions from alluvial streams: Transactions of the American Society of Civil Engineers, v. 118, p. 245–288.

Mackey, S.D., and Bridge, J.S., 1995, Three-dimensional model of alluvial stratigraphy: theory and application: Journal of Sedimentary Research B: Stratigraphy & Global Studies, v. B65, p. 7–31, doi:10.1306/d42681d5-2b26-11d7-8648000102c1865d.

Martinius, A.W., Fustic, M., Garner, D.L., Jablonski, B.V.J., Strobl, R.S., MacEachern, J.A., and Dashtgard, S.E., 2017, Reservoir characterization and multiscale heterogeneity modeling of inclined heterolithic strata for bitumen-production forecasting, McMurray Formation, Corner, Alberta, Canada: Marine and Petroleum Geology, v. 82, p. 336–361, doi:10.1016/j.marpetgeo.2017.02.003.

McNeill, J.D., 1980, Electromagnetic Terrain Conductivity Measurement at Low Induction Numbers: Technical note TN6, p. 15, doi:http://www.geonics.com/pdfs/technicalnotes/tn6.pdf.

Mehdi, S.M., Pant, N.C., Saini, H.S., Mujtaba, S.A.I., and Pande, P., 2016, Identification of palaeochannel configuration in the Saraswati River basin in parts of Haryana and Rajasthan, India, through digital remote sensing and GIS: Episodes, v. 39, p. 29–38, doi:10.18814/epiiugs/2016/v39i1/89234.

Miall, A.D., 1988, Reservoir heterogeneities in fluvial sandstones: lessons from outcrop studies: AAPG bulletin, v. 72, p. 682–697, doi:10.1306/703C8F01-1707-11D7-8645000102C1865D.

Mjøs, R., Walderhaug, O., and Prestholm, E., 1993, Crevasse Splay Sandstone Geometries in the Middle Jurassic Ravenscar Group of Yorkshire, UK, *in* Marzo, M. and Puigdefabregas, C. eds., Alluvial Sedimentation, Int. Assoc. Sedimentol. Spec. Publ., Oxford, Blackwell Scientific Publication, v. 17, p. 167–184, doi:10.1002/9781444303995.ch13.

Mohrig, D., Heller, P.L., Paola, C., and Lyons, W.J., 2000, Interpreting avulsion process from ancient alluvial sequences: Guadalope-Matarranya system (Northern Spain) and Wasatch formation (Western Colorado): Geological Society of America Bulletin, v. 112, p. 1787–1803, doi:10.1130/0016-7606(2000)112<1787:IAPFAA>2.0.CO;2.

Morozova, G.S., and Smith, N.D., 1999, Holocene Avulsion History of the Lower Saskatchewan Fluvial System, Cumberland Marshes, Saskatchewan-Manitoba, Canada, *in* Smith, N.D. and Rogers, J. eds., Fluvial Sedimentology VI: International Association of Sedimentologists Special Publication., v. 28, p. 231–249, doi:10.1002/9781444304213.ch18.

Motta, D., Abad, J.D., Langendoen, E.J., and García, M.H., 2012, The effects of floodplain soil heterogeneity on meander planform shape: Water Resources Research, v. 48, p. 1–17, doi:10.1029/2011WR011601.

MOVE Suite - Petroleum Experts, https://www.petex.com/products/move-suite/ (accessed May 2020).

Mozzi, P., Piovan, S., and Corrò, E., 2020, Long-term drivers and impacts of abrupt river changes in managed lowlands of the Adige River and northern

Po delta (Northern Italy): Quaternary International, v. 538, p. 80–93, doi:10.1016/j.quaint.2018.10.024.

Nanson, G.C., 1980, Point bar and floodplain formation of the meandering Beatton River, northeastern British Columbia, Canada: Sedimentology, v. 27, p. 3–29, doi:10.1111/j.1365-3091.1980.tb01155.x.

Nanson, G.C., and Page, K., 1983, Lateral accretion of fine-grained concave benches on meandering rivers, *in* Collinson, J.D. and Lewin, J. eds., Modern and ancient fluvial systems. Int. Assoc. Sedimentol. Spec. Publ., Wiley-Blackwell, v. 6, p. 133–143, doi:/10.1002/9781444303773.ch10.

Page, K.J., Nanson, G.C., and Frazier, P.S., 2003, Floodplain Formation and Sediment Stratigraphy Resulting from Oblique Accretion on the Murrumbidgee River, Australia: Journal of Sedimentary Research, v. 73, p. 5–14, doi:10.1306/070102730005.

Piovan, S., Mozzi, P., and Stefani, C., 2010, Bronze age paleohydrography of the southern Venetian Plain: Geoarchaeology, v. 25, p. 6–35, doi:10.1002/gea.20300.

Piovan, S., Mozzi, P., and Zecchin, M., 2012, The interplay between adjacent Adige and Po alluvial systems and deltas in the late Holocene (Northern Italy): Géomorphologie: relief, processus, environnement, v. 18, p. 427–440, doi:10.4000/geomorphologie.10034.

Plink-Björklund, P., 2015, Morphodynamics of rivers strongly affected by monsoon precipitation: Review of depositional style and forcing factors: Sedimentary Geology, v. 323, p. 110–147, doi:10.1016/j.sedgeo.2015.04.004.

Plint, A.G., 1983, Sandy fluvial point-bar sediments from the Middle Eocene of Dorset, England: Modern and ancient fluvial systems. Special Publications of the International Association of Sedimentologists, v. 6, p. 355–368, doi:10.1016/0037-0738(84)90031-9.

Pranter, M.J., Ellison, A.I., Cole, R.D., and Patterson, P.E., 2007, Analysis and modeling of intermediate-scale reservoir heterogeneity based on a fluvial point-bar outcrop analog, Williams Fork Formation, Piceance Basin, Colorado: AAPG Bulletin, v. 91, p. 1025–1051, doi:10.1306/02010706102.

Riley, J.D., Rhoads, B.L., Parsons, D.R., and Johnson, K.K., 2015, Influence of junction angle on three-dimensional flow structure and bed morphology at confluent meander bends during different hydrological conditions: Earth Surface Processes and Landforms, v. 40, p. 252–271, doi:10.1002/esp.3624.

Riley, S.J., and Taylor, G., 1978, The geomorphology of the upper Darling River system with special reference to the present fluvial system: Proceedings of the Royal Society of Victoria, v. 90, p. 89–102.

Rossetti, D. de F., 2010, Multiple remote sensing techniques as a tool for reconstructing late Quaternary drainage in the Amazon lowland: Earth Surface Processes and Landforms, v. 35, p. 1234–1239, doi:10.1002/esp.1996.

Russell, C.E., 2017, Prediction of sedimentary architecture and lithological

heterogeneity in fluvial point-bar deposits: University of Leeds.
Seminara, G., 2006, Meanders: Journal of Fluid Mechanics, v. 554, p. 271–297, doi:10.1017/S0022112006008925.
Slingerland, R., and Smith, N.D., 1998, Necessary conditions for a meandering-river avulsion: Geology, v. 26, p. 435–438, doi:10.1130/0091-7613(1998)026<0435:NCFAMR>2.3.CO;2.
Slingerland, R., and Smith, N.D., 2004, River Avulsions and Their Deposits: Annual Review of Earth and Planetary Sciences, v. 32, p. 257–285, doi:10.1146/annurev.earth.32.101802.120201.
Smith, D.G., Hubbard, S.M., Leckie, D.A., and Fustic, M., 2009, Counter point bar deposits: Lithofacies and reservoir significance in the meandering modern peace river and ancient McMurray formation, Alberta, Canada: Sedimentology, v. 56, p. 1655–1669, doi:10.1111/j.1365-3091.2009.01050.x.
Smith, N.D., and Rogers, J. (Eds.), 1999, Fluvial Sedimentology VI: Blackwell Science, v. 53, 478 p., doi:10.1002/9781444304213.
Sonnenberg, S.A., McKenna, D.J., and McKenna, P.J., 1990, Sorrento field, Denver basin, Colorado, *in* Sonnenberg, S.A., Shannon, L.T., Rader, K., von Drehle, W.F., and Martin, G.W. eds., Morrow Sandstones of Southeast Colorado and Adjacent Areas, Denver, Rocky Mountain Association of Geologists, p. 79–90.
Stefani, M., 2017, The Po Delta Region: Depositional Evolution, Climate Change and Human Intervention Through the Last 5000 Years, *in* Soldati, M. and Marchetti, M. eds., Landscapes and Landforms of Italy, Springer, p. 193–202.
Stefani, M., and Vincenzi, S., 2005, The interplay of eustasy, climate and human activity in the late Quaternary depositional evolution and sedimentary architecture of the Po Delta system: Marine Geology, v. 222–223, p. 19–48, doi:10.1016/j.margeo.2005.06.029.
Strick, R.J.P., Ashworth, P.J., Awcock, G., and Lewin, J., 2018, Morphology and spacing of river meander scrolls: Geomorphology, v. 310, p. 57–68, doi:10.1016/j.geomorph.2018.03.005.
Strobl, R.S., Wightman, D.M., Muwais, W.K., Cotterill, D.K., and Yuan, L., 1997, Geological modelling of McMurray Formation reservoirs based on outcrop and subsurface analogues, *in* Pemberton, S.G. and James, D.P. eds., Petroleum Geology of the Cretaceous Mannville Group, Western Canada, Canadian Society of Petroleum Geologists, Memoir 18, p. 292–311.
Swan, A., Hartley, A.J., Owen, A., and Howell, J., 2018, Reconstruction of a sandy point-bar deposit: implications for fluvial facies analysis, *in* Ghinassi, M., Colombera, L., Mountney, N.P., Reesink, A.J., and Betaman, M. eds., Fluvial Meanders and Their Sedimentary Products in the Rock Record. Int. Assoc. Sedimentol. Spec. Publ. 48, Ltd, John Wiley & Sons, v. 48, p. 445–474, doi:10.1002/9781119424437.ch17.
Taylor, C.F.H., 1999, The role of overbank flow in governing the form of an anabranching river: the Fitzroy River, northwestern Australia, *in* Smith,

N.D. and Rogers, J. eds., Fluvial Sedimentology VI. Special Publication of the International Association of Sedimentologists, Wiley Online Library, v. 28, p. 77–91, doi:10.1002/9781444304213.ch7.

Teatini, P., Tosi, L., and Strozzi, T., 2011, Quantitative evidence that compaction of Holocene sediments drives the present land subsidence of the Po Delta, Italy: Journal of Geophysical Research: Earth Surface, v. 116, p. 1–10, doi:10.1029/2010JB008122.

Thorne, C.R., 1997, Channel Types and Morphological Classification, *in* Thorne, C.R., Hey, R.D., and Newsom, M.D. eds., Applied Fluvial Geomorphology for River Engineering and Management, Chichester, UK, John Wiley & Sons, p. 175–122.

Toonen, W.H.J., Kleinhans, M.G., and Cohen, K.M., 2012, Sedimentary architecture of abandoned channel fills: Earth Surface Processes and Landforms, v. 37, p. 459–472, doi:10.1002/esp.3189.

Trimble - Transforming the Way the World Works, www.trimble.com (accessed February 2020).

Um, E.S., and Alumbaugh, D.L., 2007, On the physics of the marine controlled-source electromagnetic method: Geophysics, v. 72, p. WA13–WA26, doi:10.1190/1.2432482.

Veneto, R., 2012, Note illustrative del Foglio 147 Monselice. Carta Geologica d'Italia alla scala 1:50.000 (M. Cucato, G. De Vecchi, P. Mozzi, T. Abbà, G. Paiero, & R. Sedea, Eds.): Treviso, Land Technologies & Services, 1 map, 215 p.

Willis, B.J., 1989, Palaeochannel reconstructions from point bar deposits: a three-dimensional perspective: Sedimentology, v. 36, p. 757–766, doi:10.1111/j.1365-3091.1989.tb01744.x.

Willis, B.J., and Sech, R.P., 2018, Emergent facies patterns within fluvial channel belts, *in* Ghinassi, M., Colombera, L., Mountney, N.P., Reesink, A.J.H., and Bateman, M. eds., Fluvial Meanders and Their Sedimentary Products in the Rock Record. Int. Assoc. Sedimentol. Spec. Publ., John Wiley & Sons, Ltd, v. 48, p. 509–542, doi:10.1002/9781119424437.ch19.

Willis, B.J., and Tang, H., 2010, Three-Dimensional Connectivity of Point-Bar Deposits: Journal of Sedimentary Research, v. 80, p. 440–454, doi:10.2110/jsr.2010.046.

Wolman, M.G., and Leopold, L.B., 1957, River flood plains: some observations on their for- mation: U.S. Geological Survey, Professional Paper, v. 282C, p. 86–109.

Wood, J.M., 1989, Alluvial architecture of the Upper Cretaceous Judith River Formation, Dinosaur Provincial Park, Alberta, Canada: Bulletin of Canadian Petroleum Geology, v. 37, p. 169–181.

Wray, R.A.L., 2009, Palaeochannels of the Namoi River Floodplain, New South Wales, Australia: The use of multispectral Landsat imagery to highlight a Late Quaternary change in fluvial regime: Australian Geographer, v. 40, p. 29–49, doi:10.1080/00049180802656952.

Wu, C., Bhattacharya, J.P., and Ullah, M.S., 2015, Paleohydrology and 3D facies

architecture of ancient point bars, Ferron Sandstone, Notom Delta, south-central Utah, USA: Journal of Sedimentary Research, v. 85, p. 399–418, doi:10.2110/jsr.2015.29.

Wu, S.H., Yue, D.L., Liu, J.M., Shu, Q.L., Fan, Z., and Li, Y.P., 2008, Hierarchy modeling of subsurface palaeochannel reservoir architecture: Science in China, Series D: Earth Sciences, v. 51, p. 126–137, doi:10.1007/s11430-008-0624-0.

Zecchin, M., Baradello, L., Brancolini, G., Donda, F., Rizzetto, F., and Tosi, L., 2008, Sequence stratigraphy based on high-resolution seismic profiles in the late Pleistocene and Holocene deposits of the Venice area: Marine Geology, v. 253, p. 185–198, doi:10.1016/j.margeo.2008.05.010.

4

GEOMETRIES AND GRAIN-SIZE DISTRIBUTION IN TIDAL POINT BARS

This chapter is published as a paper in *Sedimentology* (2022, v. 69, p. 1399-1423, doi: 10.1111/sed.12956) under the title "Ontogeny of a subtidal point bar in the microtidal Venice Lagoon (Italy) revealed by three-dimensional architectural analyses".

E.B. and M.G. designed the study. E.B., F.M. and M.G. developed the methodology. E.B., F.M, S.D. and M.G. collected the data. E.B. annotated and maintained the research data. E.B. was responsible for data creation and presentation. E.B. and M.G. were the project administrator. A.F. provided and applied a designed code to analyse study data. S.D., F.M. and M.G. provided the instrumentation and analysis tools. A.F. and A.D. verified the reproducibility of the results. All the authors discussed the data and agree on their interpretation. E.B. wrote the original draft. All the co-authors provided comments and suggestions to improve the original draft. All the co-authors contributed to the final polishing of the manuscript. A.D. and M.G. were responsible for the research activity. M.G. acquired the financial support for the project.

Ontogeny of a subtidal point bar in the microtidal Venice Lagoon (Italy) revealed by three-dimensional architectural analyses

Elena Bellizia[1], Sandra Donnici[2], Fantina Madricardo[3], Alvise Finotello[4], Andrea D'Alpaos[1], Massimiliano Ghinassi[1]

[1] Department of Geosciences, University of Padova, Via G. Gradenigo 6, IT-35131 Padova, Italy
[2] National Research Council of Italy, Institute of Geosciences and Earth Resources (CNR-IGG), Padova, Via G. Gradenigo 6, IT-35131 Padova, Italy
[3] National Research Council of Italy, Institute of Marine Sciences (CNR–ISMAR), Venezia, Tesa 104 – Arsenale, Castello 2737/F, IT-30122 Venezia, Italy
[4] Department of Environmental Sciences, Informatics, and Statistics, Ca' Foscari University of Venice, via Torino 155, IT-30172 Mestre, Venice, Italy

ABSTRACT

Sedimentological and architectural features of meandering subtidal channels are relatively unexplored, and their deposits are commonly investigated based on facies models set up for intertidal meandering channels. The Venice Lagoon (northern Adriatic Sea, Italy) is affected by a micro-tidal regime and hosts a dense network of active and buried tidal channels. It represents an excellent natural laboratory to improve the current knowledge on subtidal meander morphodynamics and related deposits. In this study, the integration of high-resolution geophysical images and core data allows reconstruction of the architectural three-dimensional model of a meandering subtidal palaeochannel, which is buried below a modern subtidal flat. The study palaeochannel was 35 m wide and 3 m deep and formed three adjacent meander bends and related point bars. A detailed three-dimensional architectural reconstruction was carried out for deposits associated with one of these meander bends, that was crossed by a minor, low-sinuosity channel with two minor bank-attached bars. This reconstruction highlights that the study point bar has a horseshoe shape, which arose from the onset of bar accretion from an already-sinuous channel. Reconstructed growth stages of the studying bends show that point-bar accretion can follow different styles of planform transformation, also experiencing simultaneously landward (or seaward) deposition according to the dominant flow direction (i.e., local tidal asymmetry). The analyses show that planform transformations occurred in parallel with elevation changes of the related channel thalweg, which shaped pools with geometry varying with the

radius of curvature of the bend. The present study highlights the relevance of high-resolution three-dimensional reconstructions to link palaeomorphodynamic processes with related sedimentary products.

Keywords: Meander genesis, Planform transformations, Subtidal channel, Tidal asymmetry, Tidal point bars

4.1 Introduction

The study of meandering-channel evolution and related deposits is a fascinating issue of clastic sedimentology, especially for modern and ancient fluvial systems (Visher, 1964; Allen, 1965; Bluck, 1971; Brice, 1974; Jackson, 1976a; Willis, 1989; Bridge, 1993; Nicoll and Hickin, 2010; Smith et al., 2011; Ielpi and Ghinassi, 2014). Starting from an almost straight or slightly sinuous planform, channels increase their sinuosity by migrating laterally on the floodplain and evolve according to a wide spectrum of planform transformations (Leopold and Wolman, 1960; Daniel, 1971; Brice, 1974; Jackson, 1976a; Lewin, 1976; Nanson and Page, 1983; Ghinassi et al., 2014, 2016; Durkin et al., 2017). The evolution of fluvial meandering channels produces laterally-extensive point-bar bodies, which can become important hydrocarbon reservoirs (for example, the McMurray Formation, Hubbard *et al.*, 2011; Fustic *et al.*, 2012), or targets for carbon capture and storage (Issautier et al., 2014; Gershenzon et al., 2015), and host most of the surficial aquifers in modern coastal plains (Clement and Barrash, 2006; Fabbri et al., 2012).

Meandering channels also occur in subaqueous settings, both as well-known turbiditic channels (e.g. Posamentier, 2003; Kolla *et al.*, 2007; Janocko *et al.*, 2013) and as less-documented subtidal channels (e.g. Flemming, 2012) in lagoons and estuaries. Most of the current knowledge on tidal meanders and related point bars has been developed for intertidal meanders, which have been commonly assumed to slowly migrate laterally (Gabet, 1998) and generate tabular point-bar bodies (Bridges and Leeder, 1976; Barwis, 1977). Distinctive sedimentary features of these bar deposits are classically considered to be (Allen, 1982): (i) a shell-rich channel lag; (ii) bedforms diagnostic of bidirectional flows; (iii) alternation between sandy and silty layers, and (iv) intense bioturbation. Recent studies provided new insights on the morphometry and sedimentology of intertidal meanders (Fagherazzi et al., 2004; Pearson and Gingras, 2006; Choi, 2011; Hughes, 2012; Choi et al., 2013; Choi and Jo, 2015;

Brivio et al., 2016; Ghinassi et al., 2018a, 2018b; Cosma et al., 2019, 2021; Finotello et al., 2019), revealing that: (i) intertidal-meander migration rates are comparable to those of their fluvial counterparts, once properly normalized by the channel width (Finotello et al., 2018); (ii) geometry of intertidal point bars is the result of the interaction between channel-migration rate and aggradation rate of the surrounding marsh platform (Brivio et al., 2016; Cosma et al., 2019, 2021); (iii) morphometry of intertidal meanders can differ from that of their fluvial counterparts (Finotello et al., 2019); and (iv) complex flow configurations, due to the occurrence of mutually evasive currents and recirculation zones, can prevent portions of bar deposits from experiencing bidirectional currents, thereby inhibiting the formation of bedforms retaining the signatures of bidirectional flows (Dalrymple and Choi, 2007; Li et al., 2008; Choi et al., 2013; Finotello et al., 2020a).

Despite these recent new findings, several gaps still exist in the understanding of tidal meanders and the related point-bar deposits. One of these gaps is mostly due to the absence of scroll-bar patterns that typically characterize the present-day morphology of most tidal meanders worldwide. These patterns would allow for detailed reconstructions of meander planform evolution, in a fashion similar to fluvial meanders where well-developed scroll bars are widespread and clearly visible from aerial images (Brice, 1974; Nanson, 1980; Strick et al., 2018). Indeed, correlations between planform evolution (i.e. scroll-bar pattern) and related point-bar geometries were carried out for fluvial meanders (Pranter et al., 2007; Ghinassi et al., 2013, 2014, 2019a; Ielpi and Ghinassi, 2014; Ghinassi and Ielpi, 2015; Yan et al., 2017, 2019; Willis and Sech, 2018b; Parquer et al., 2019) along with models concerning along-bend grain-size distribution (Purkait, 2002; Frings, 2008; Smith et al., 2009, 2011; Bhattacharyya et al., 2015; Ghinassi and Ielpi, 2015; Clift et al., 2019; Hagstrom et al., 2019). Comparable insights are conversely missing for intertidal meanders, whose planform evolution has been inferred only for short-time intervals (Choi et al., 2013; Ghinassi et al., 2018a) and for which the spatial distribution of sediment grain size was mainly investigated with vertical, rather than along-channel, trends (de Mowbray, 1983; Dalrymple et al., 1990; Pearson and Gingras, 2006; Choi, 2011; Choi et al., 2013; Choi and Jo, 2015).

Knowledge gaps are even more relevant for subtidal channels, which have been investigated by few studies (e.g. La Croix & Dashtgard, 2015; Ghinassi *et al.*, 2019b) in spite of the fact of their widespread presence in coastal environments [for example, the Geum River estuary (Korea) and Hammocks Beach State Park,

North Carolina (USA)]. Subtidal meandering channels can be found in the most seaward portion of tidal basins (Rieu et al., 2005), where current velocities are higher because of the inlets, and they are permanently submerged. They usually develop on top of tidal flood deltas and their hydrodynamics is complex (Rieu et al., 2005; Ghinassi et al., 2019b) since the flow within the channels can be influenced by the currents flowing on the surrounding subtidal platforms and by the wind-induced wave winnowing (Carniello et al., 2012; Tommasini et al., 2019). Subtidal meanders can migrate laterally accumulating point bars that thereby do not experience any subaerial exposure. Therefore, defining the internal architecture and the sediment distribution within subtidal point-bar deposits is a critical step to deepen current knowledge on the genesis and evolution of subtidal meanders.

The present study aims at improving current understanding on the morphodynamic evolution and internal architecture of subtidal point-bar deposits, focusing on a Holocene tidal meandering channel cutting through a subtidal mudflat of the northern Venice Lagoon (Adriatic Sea, Italy; Fig. 4.1). With its complex network of tidal channels developed in a microtidal regime, the Venice Lagoon represents a key site to study facies distribution and architectural features of a microtidal system, where effects of tidal currents are amplified by meteorological forcings. By integrating geophysical and sedimentological data with morphological characteristics of a previously-detected Holocene palaeochannel (Madricardo et al., 2007), this work reconstructs the detailed 3D architectural model of a subtidal meander and investigates: (i) the onset of tidal meanders and following planform transformations, and (ii) the related changes in bend morphometry and channel bathymetry.

4.2 Geological setting

4.2.1 The Venice Lagoon

Covering an area of about 550 km^2, the Venice Lagoon is the largest brackish water body of the Mediterranean Sea; with its north-east/south-west oriented oblong and arched shape, the lagoon is 50 km long and on average 10 km wide (Zecchin et al., 2008), and exchanges water with the Adriatic Sea through the Lido-San Nicolò, Malamocco and Chioggia inlets (Fig. 4.1A). The lagoon is affected by a semidiurnal microtidal range, with a mean tidal range and maximum astronomical oscillation of 1.0 m and 0.75 m around mean sea-level

(MSL), respectively (D'Alpaos et al., 2013), which can be amplified by local meteorological conditions. Low (high) atmospheric pressure can produce considerably high (low) tides. Surge events strongly contribute to enhance the astronomical tides, especially those associated with the Sirocco wind (Mel et al., 2019). The Venice Lagoon is part of the Venetian foreland basin (north-east Italy), which developed between the Apennine and the South-Alpine chains (Massari et al., 1986; Zecchin et al., 2008). Since the Early Pleistocene, the Venice area was characterized by a shallowing-upward depositional trend from deep-water to deltaic and shoreface sediments (Massari et al., 2004). These deposits were overlain by a cyclical alternation of continental and shallow-marine facies (Kent et al., 2002). The Venice Lagoon developed over the last 7500 years during Holocene transgression (McClennen and Housley, 2006; Zecchin et al., 2008; Rizzetto et al., 2009) and consists of tidal flats, salt marshes, and subtidal and intertidal channel deposits. Sediment ranges in grain size between mud and fine sand, although mud is largely dominant (Brivio et al., 2016; Ghinassi et al., 2018b, 2019b). The channel network comprises tidal channels with different cross sections, from almost 400 m to less than 1 m wide as the distance from the inlets rises up. Mean cross-sectional velocities within the channels can vary widely depending on the distance from the inlets and their channel width. At *ca* 6 km from the Lido inlet (Fig. 4.1B), the Gaggian channel and its two major tributaries (100 m and 30 to 40 m wide, respectively) shows mean cross-sectional velocities of ±0.6 and ±0.4 m/s, respectively (Finotello et al., 2019).

During the last centuries, human interventions contributed to modify the local tidal regime and morphologies within the lagoon (D'Alpaos, 2010; Ferrarin et al., 2015). The building of massive jetties at the inlets led to their deepening and the modification of the hydrodynamic regime. The diversion of all major rivers debouching into the northern part of the Lagoon dramatically decreased the fluvial sediment input (XV to XVIII century; Tosi *et al.*, 2009; D'Alpaos, 2010; Bondesan & Furlanetto, 2012). Recently, the activation of the mobile gates (Project Mo.S.E.), designed to protect the lagoon settlements from extensive flooding, has changed the lagoon hydrodynamics (Mel et al., 2021) and, consequently, the sediment transport, contributing to the deepening of the tidal flats and reducing salt-marsh sedimentation (Tognin et al., 2021).

4.2.2 The study area

The study area is located in the northern part of the Venice Lagoon (Fig. 4.1B) and it is relatively close to the present-day coastline (i.e., 4 km inland). The area is right behind the S. Erasmo island, which represented the littoral strip until the end of the XIX century (Bonardi et al., 1997; Balletti, 2006; Busato, 2007). Specifically, the study area, named *Palude Santa Caterina,* is sited between the Burano, Mazzorbo and San Francesco del Deserto islands (Fig. 4.1C); it is about 1.15 km^2 and shows water depths ranging between 3.0 m and 0.5 m. The area is currently crossed by the *Canale San Francesco*, a 35 m wide navigable channel that exhibits three meander bends with radii of curvature ranging between 210 m and 250 m (yellow lines in Fig. 4.1C).

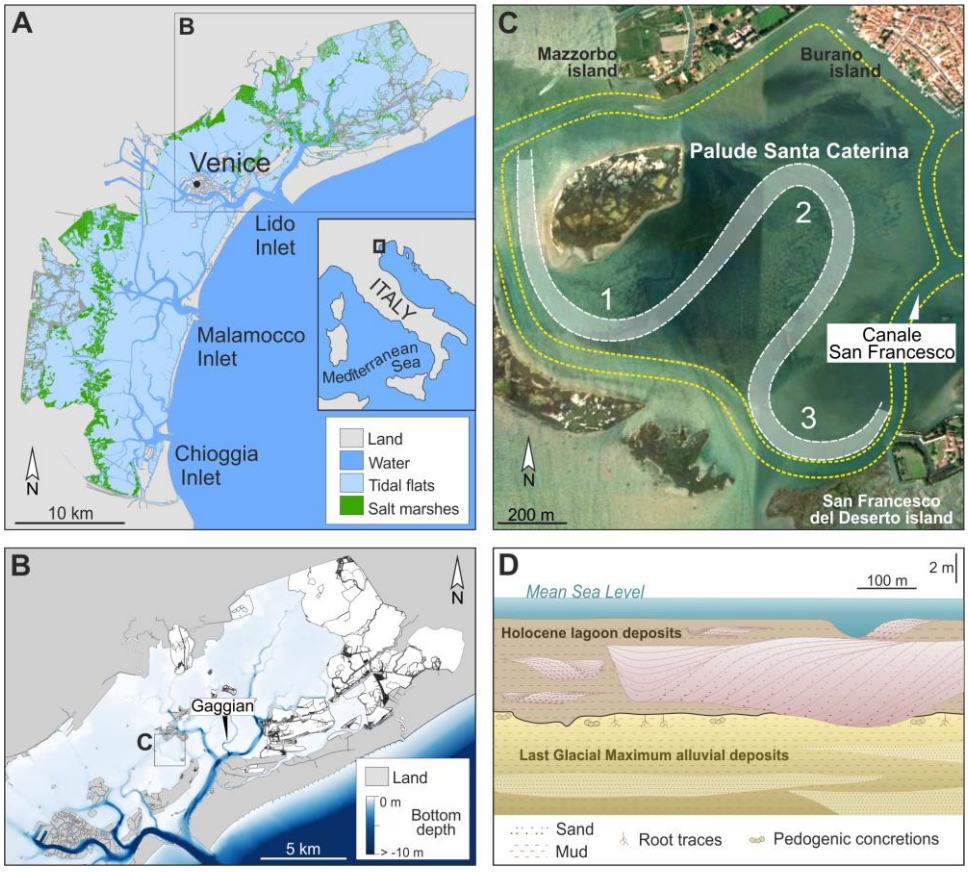

Fig. 4.1. The study area: (A) geographic location of the study site in the Venice Lagoon (IT); (B) bathymetric map (blue-white scale for lagoon bottom depth) of the northern Venice Lagoon; (C) BingTM satellite image of the Palude Santa Caterina with the three main buried meander bends reconstructed in Madricardo et al. (2007); and (D) hypothetical stratigraphic section of the northern Lagoon.

Previous geophysical and sedimentological investigations (see Madricardo *et al.*, 2007, 2012, for more details) reveal that in the study area the lagoonal Holocene succession is up to 8 m thick and covers a pedogenized alluvial substrate accumulated during the Last Glacial Maximum (Fig. 4.1D). The alluvial deposits consist of massive clay and fine sand layers that grade upward into over-consolidated silt, with pedogenetic nodules and roots. The lagoon deposits mainly consist of tidal-flat mud with isolated sandy to silty channelized bodies, which range in thickness between 0.5 to 4.0 m.

Three buried palaeomeanders forming a north-west/south-east oriented belt (bends 1 to 3 in Fig. 4.1C) were documented in the study area (Madricardo et al., 2007, 2012). These palaeomeanders were framed into a lagoonal depositional environment and associated with three sandy to silty, clinostratified point bars, which were buried by and cut into organic-rich lagoonal mud. Specifically, point-bar deposits consist of a shell-rich lag covered by an almost 3 m thick alternation of silty-sand and sandy-silt deposits. Shells belong to lagoonal faunas, including gastropods (for example, *Bittium scabrum*) and bivalves (for example, *Acanthocardia tubercolata* and *Scrobicularia plana*) (Cosma et al., 2019). The foraminiferal assemblage of bar deposits reveals that they accumulated in a subtidal setting of intermediate to inner-lagoon environment (Madricardo et al., 2007, 2012), in the absence of significant riverine input. Bar-top deposits are muddy and do not show diagnostic sedimentary features of subaerial exposure in a salt marsh environment (for example, root traces and oxidation). Accordingly, their foraminiferal assemblage indicated a permanently submerged setting. Radiocarbon ages from channel lag shells date *ca* 4500 years BP (Madricardo et al., 2007, 2012).

4.3 Methods and terminology

4.3.1 Geophysical data

The acoustic data were acquired using a single beam echosounder, modified to improve its resolution in extreme shallow waters (down to 0.5 m depth in some portions). The echosounder emits sound waves in short pulses (τ = 0.15 ms) with a frequency fixed on 30 kHz, which propagate in the water down to the sea-bottom interface where the sound waves are partly reflected and partly penetrate the bottom sediments. The echosounder detects the intensity of the acoustic signals reflected from the interfaces between sediments with different properties. Despite generating a low-lateral single beam resolution in shallow

water conditions, the transducer used for acquisitions provided useful data for qualitative studies thanks to its high vertical resolution, of the order of a decimetre (see Madricardo et al., 2007, for more technical details). A DGPS (differential global positioning system; Trimble DSM12®; Trimble Inc., Sunnyvale, CA, USA) was associated with the echosounder, to allow a positioning accuracy of the acoustic lines below 1 m. Line spacing was set to 2.5 m and, a total of 980 sections (i.e. about 500 km of acoustic profiles in 256-level greyscale) were acquired between 2003 and 2004, allowing for investigation of the upper 6 m of the Holocene lagoonal succession. In the frame of this work, 201 sections, 2.5 to 10 m apart from one another, have been selected to reconstruct a 3D model of the subsurface succession (Fig. 4.2A). The *Move 2018.2™* software was used to visualize and correlate different sections in a georeferenced space. The main acoustic surfaces (for example, horizons) separating different depositional elements (for example, channel-fills, channel-bars and overbank deposits) were traced for each section. Three-dimensional surfaces were created with the Ordinary Kriging method, by interpolating categories of horizons representing the same depositional element. This approach allowed the reconstruction of different stages of channel evolution and related planform configurations. Meander morphometric properties were investigated using an automatic procedure based on the computation of the channel-axis signed curvature (see Marani *et al.*, 2002; Finotello *et al.*, 2020b, for a detailed description of the methodology). Inflection points of the channel centreline, defined as curvature zero-crossings, were employed to delimit individual meander bends and allowed to determine the relevant morphometric parameters. Specifically, this study derived measures of: (i) meander Cartesian length (*Lxy*), defined as the Euclidean distance between meander endpoints; (ii) meander intrinsic length (*Ls*), i.e. computed along the channel centreline; (iii) meander sinuosity, defined as the ratio between *Ls and Lxy;* (iv) meander radius of curvature (*R*) derived from the meander best-fitting circle (see Heo *et al.*, 2009; Finotello *et al.*, 2018); and (v) meander amplitude (*A*) defined as the maximum distance between the channel axis and the line through the two inflection points (Fig. 4.2B). Changes through time of the above parameters were analysed in relation to bend 2, since the available acoustic lines did not always allow to reconstruct the complete planform of bends 1 and 3. In addition to meander planform features, thalweg depths at different bar growth stages were also marked from the acoustic sections.

4.3.2 Core data

A total of 21 sediment cores was used to validate geophysical data and define the spatial distribution of sedimentary facies (Fig. 4.2A). A hydraulic probe and a wire-line corer placed on a floating platform were used to recover 15 cores between 2004 and 2005 (Madricardo et al., 2007, 2012). These cores are 10 cm in diameter and their depth spans from 8.0 to 9.1 m. The grain size was defined *in situ*, whereas lithology, sedimentary structures and Munsell colour were successively detected through laboratory analyses, where cores were sampled for micropalaeontological and radiocarbon analyses (see Madricardo et al., 2012, 2007).

Six additional sedimentary cores were recovered in 2018 using an Eijkelkamp hand auger (Eijkelkamp Soil & Water, Giesbeek, The Netherlands), through a gouge sampler with a length of 1 m and a diameter of 3 cm. Coring sites were planned after preliminary results of the 3D model to analyse point-bar deposits. Coring depth spans from 4.0 to 5.8 m. Collected cores were kept humid in PVC liners and successively cut longitudinally, photographed and logged. Core logging was carried out following the basic principles of facies analysis (Walker, 1992), emphasizing sediment grain size, presence of sedimentary structures and bioturbation, vertical grain-size trends, and occurrence of plant debris and shell fragments. To verify the along-bend grain-size trend, grain-size analyses were carried out through a Mastersizer 2000 (Version 5.40, Malvern Instruments, Malvern, UK).

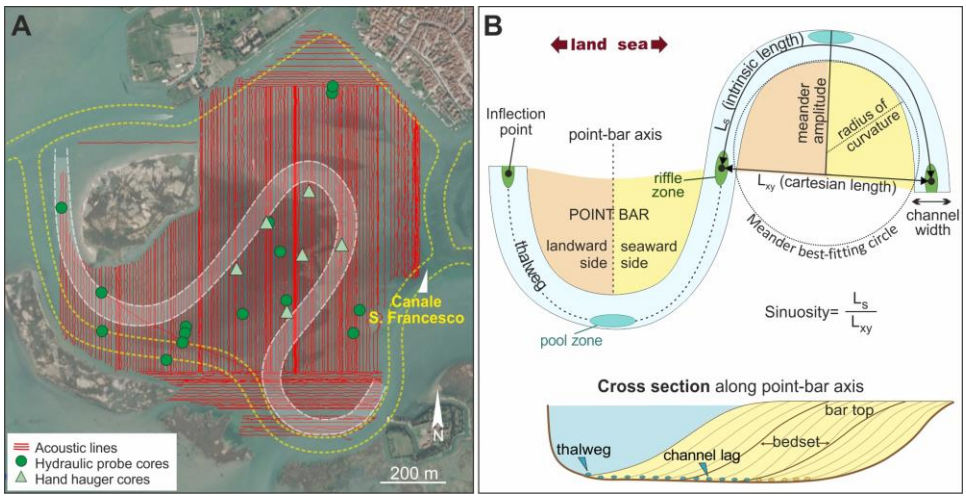

Fig. 4.2. Methods and terminology. (A) Location and orientation of cores and acoustic lines used in this work. (B) Main morphological, morphometric and depositional features of tidal meander bends.

The terminology used in the present work is recalled in Fig. 4.2B and is analogous to that used for fluvial point bars and related deposits, although some modifications are required to adjust to the tidal environment (cf. Brivio *et al.*, 2016).

4.4 Results

4.4.1 Acoustic data and architectural elements

Interpretation of acoustic profiles allowed to identify distinct acoustic facies that can be linked to three main architectural elements: channel fill, channel bar and overbank. The acoustic reflectors are interpreted to represent primary accretion and boundary surfaces (cf. Sambrook Smith *et al*., 2006; Skelly *et al*., 2003).

Channel bar

The channel bars are characterized by sets of packages of inclined reflectors, defined by a poorly detectable planar top and a well-marked concave-up base (Fig. 4.3A). They range in thickness between 2.0 and 3.0 m starting from -1.0 m under the lagoon surface, and the inclined reflectors dip between 6° and 22° showing lateral extent up to 390 m. Channel bars show three main stratal geometries: (i) sets of packages with no internal dip changes, with cross-layered and/or oblique configuration (*sensu* Roksandic, 1978) (i.e. clinoforms) (Fig. 4.3A); (ii) laterally offset packages of inclined reflections showing abrupt variations either of the dip angles or in the acoustic response (Fig. 4.3B), with a sigmoid layer configuration (*sensu* Roksandic, 1978); and (iii) mounded packages geometry with a concave-downward shape of the inclined reflections (Fig. 4.3C). The clinostratified surfaces document processes of point-bar accretion related to lateral channel shift. The three stratal geometries are related to different orientations of the acoustic sections with respect to the main accretion/channel migration direction. The first geometry shows the real dip angles of the inclined reflections, in cases where the direction of accretion remained parallel to that of the acoustic section. Changes in inclination angle of acoustic reflectors document variations of the direction of accretion relative to the acoustic section. Bar accretion parallel and transverse to acoustic section generated inclined (i.e. true dip angle) and sub-horizontal reflectors, respectively.

Mounded reflectors occur in sections cutting through the whole point bar and highlight its positive topographic relief.

Channel fill

Channel fills show concave-upward reflectors (Fig. 4.3E) and range in thickness between 1.7 m and 3.0 m, with the top surface located at approximately 1.0 m below the ground. Dip angles vary from 5° to 20°. Channel-fill reflectors can show two main geometries: (i) the asymmetrical configuration (i.e. semi-elliptic trend), which is the more common one and is always found between sets of bar reflection and overbank deposits (Fig. 4.3D); and (ii) the symmetrical configuration (i.e. semi-cylindrical or concentric) that is found between sets of bar reflection dipping in opposite directions (Fig. 4.3E).

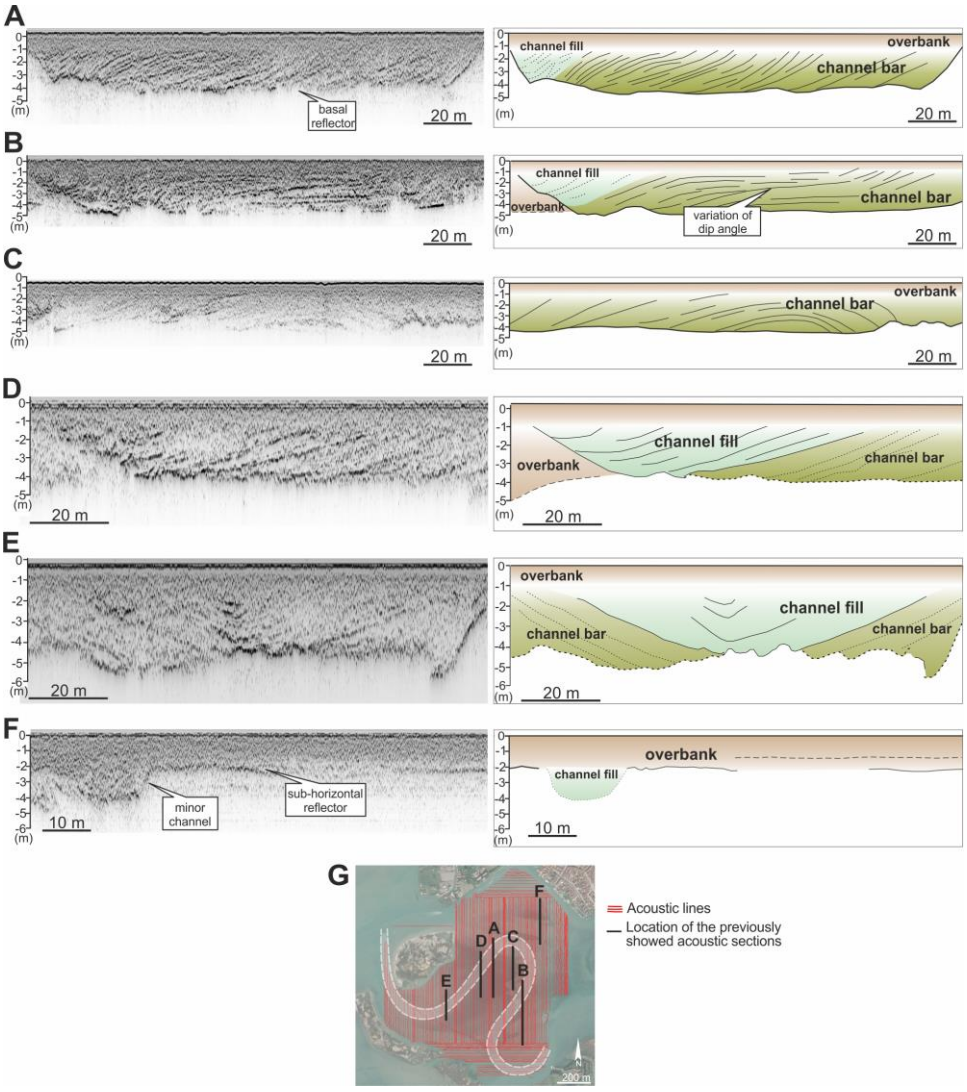

Fig. 4.3. Acoustic facies in the acoustic images (on the left) and with line-drawing of the preserved geometries (on the right). (A) to (C) The channel bars showing: (A) bedset packages with no internal dip changes; (B) laterally offset packages with abrupt variations of the dip angles; and (C) mounded packages. (D) and (E) The channel fills with (D) asymmetrical and (E) symmetrical shapes. (F) The overbank with a minor channel. (G) Location of the acoustic sections chosen for the acoustic facies.

Concave-upward reflectors testify to the progressive infill of the abandoned channel. The two geometries result from the combination between the channel orientation and that of the acoustic sections. Asymmetrical shapes are indicative of sections that are slightly oblique to the axis of the abandoned channel, whereas symmetrical ones appear in sections that are transverse to the main channel. The occurrence of symmetrical shapes between adjacent point bars is a coincidence (Fig. 4.3E).

Overbank

Overbanks are characterized by parallel sub-horizontal reflectors with moderate to good continuity (Fig. 4.3F). Localized lensoidal geometries with a basal concave upward surface can occur. These sub-horizontal reflectors represent tidal flat deposits and include localized minor channels that are too small to be imaged distinctly.

4.4.2 Three-dimensional reconstruction

Three-dimensional surfaces delimiting channel fills and channel bars were created to reconstruct the morphologies and orientation of the study sedimentary bodies (Fig. 4.4A).

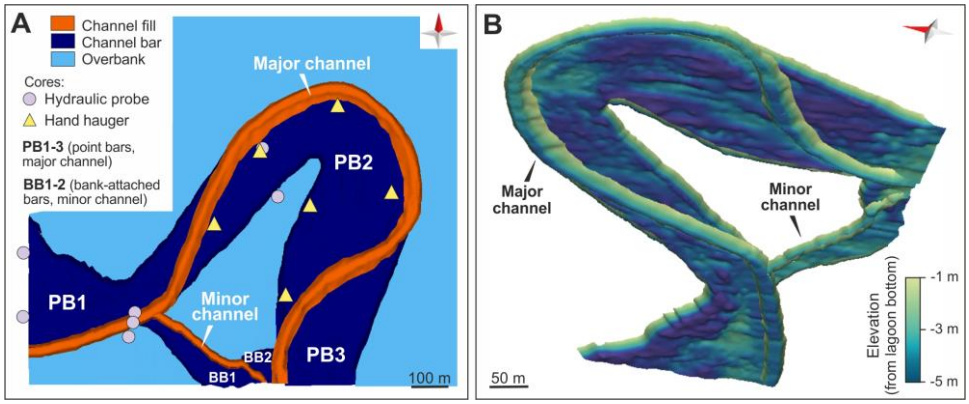

Fig. 4.4. Three-dimensional model. (A) Plan view of all the reconstructed surfaces and position of the analysed cores. (B) Oblique view of the palaeomeanders with elevation scale on bar surfaces.

Minor channelized bodies (i.e. less than 2 m thick), though locally detected, were not modelled due to their discontinuous lateral documentation. Two channelized elements are included in the proposed 3D reconstruction and are named here as 'major' and 'minor' channels, respectively.

The major channel is that identified by Madricardo *et al.* (2007) and forms three adjacent bends with associated point-bar bodies, are hereinafter named PB1, PB2 and PB3 (Figs 4.1C and 4.4). The channel is on average 35 m wide and channel-fill depths in pools and riffles are *ca* 3.0 m and 2.0 m, respectively.

PB1 is located in the western portion (i.e. landward sector) of the study area, but it is only partially visible and its complete geometry cannot be characterized (Figs 4.4A and 4.5A). Bar axis trends *ca* north-east/south-west and deposits forming the observed part of this bar are *ca* 132,000 m^3. PB1 is on average 2.6 m thick, and its thickest (3.6 m) and thinnest (1.7 m) parts occur towards the innermost and outermost part of the bar, respectively (Fig. 4.5A). These changes in thickness are associated with a progressive upward-shift of the bar basal surface along the direction of bar accretion, with the channel becoming shallower through time (Fig. 4.5A). Inclined beds forming PB1 are organized into three major bedsets (Fig. 4.5B) and document an overall south-west accretion of at least 200 m.

PB2 is associated with a meander bend showing an amplitude of *ca* 400 m and a radius of curvature of about 225 m. The bend axis trends north-east/south-west. The cartesian length and the intrinsic length of meander bend 2 measure *ca* 360 m and 1065 m, respectively, defining a sinuosity of 2.9. Bar deposits occupy only a limited area within the meander loop and form a U-shaped body surrounding overbank tabular beds (Fig. 4.4A). PB2 is on average 3 m thick, and its thickest (3.9 m) and thinnest (2.2 m) parts occur in correspondence with its major depressions and ridges, respectively (Figs 4.5C and 4.6). As for PB1, these differences in thickness are associated with an overall progressive upward-shift of the bar basal surface (Fig. 4.5A). The volume of sediment stored in this bar is *ca* 316,000 m^3. Inclined beds of this bar are organized to form four major bedsets (BS1 to BS4 in Fig. 4.5D), which form arcuate bodies with a variable lateral extent on different sides of the bar. BS1 and BS2 occur along the eastward side of the bar. BS1 covers only the eastward side of the bend, whereas BS2 occurs also in the bend apex zone but shows its maximum downdip extent along the eastward side. BS3 is sited along the western side of the bar, whereas BS4 surrounds almost the whole bar, reaching its maximum downdip extent in the bar apex zone (Fig. 4.5D). Reconstructed morphologies of

the bar basal surface show the occurrence of alternating ridges and swales, which follow the overall curvature of the associated bar and related bedsets (Fig. 4.5C). The major depression defined by this surface occurs below BS2, whereas its maximum elevation is associated with BS4 (Fig. 4.6).

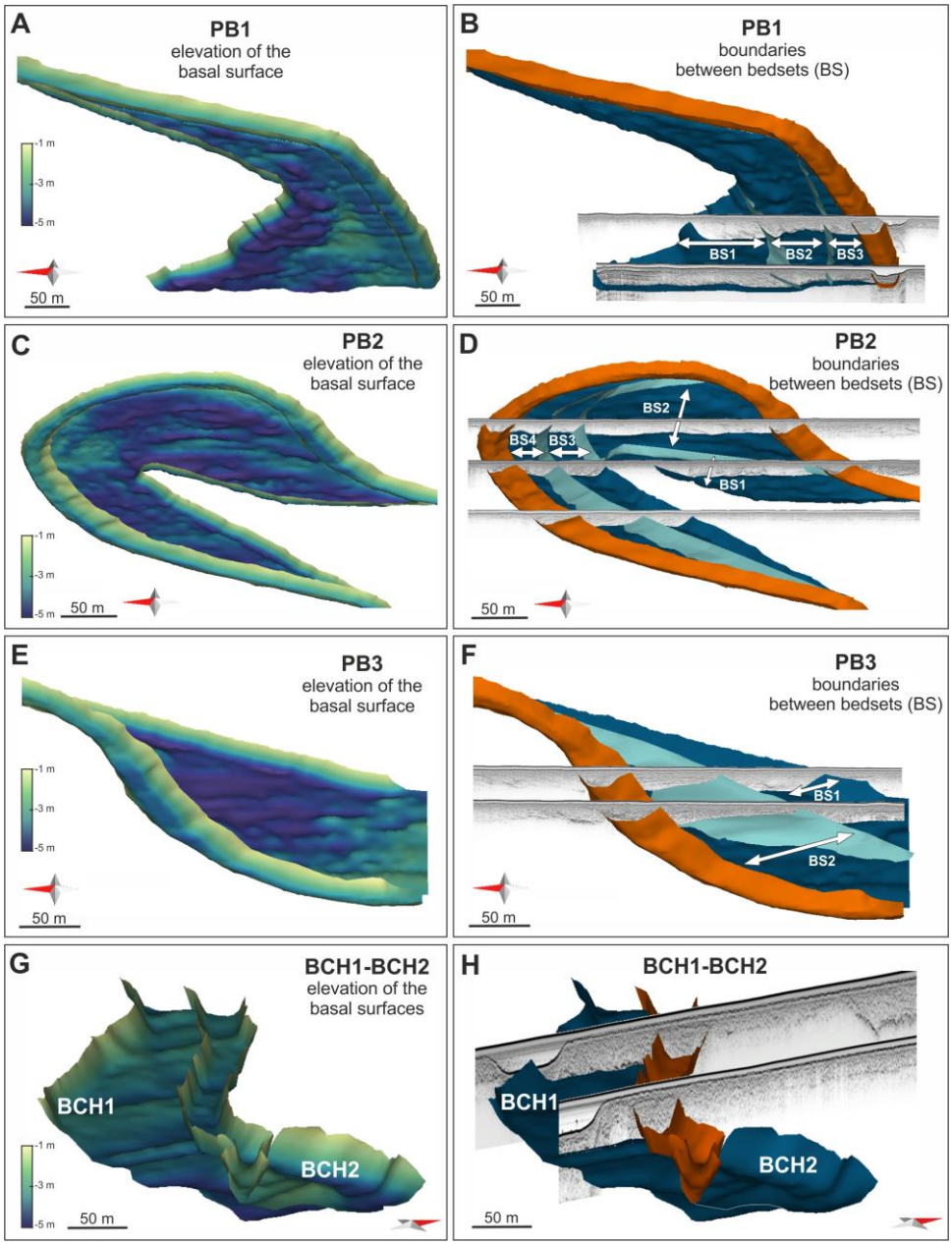

Fig. 4.5. Three-dimensional surfaces. (A) to (F) Point bars of the major channel with elevation scale and the corresponding portion of palaeochannel (on the left), and related internal bedsets with acoustic profiles (on the right). (G) and (H) Oblique view of the bars of the minor channel with elevation scale (G) and acoustic profiles (H).

PB3 is located in the easternmost portion (i.e. seaward sector) of the study area, and, as for PB1, it is only partially visible (Figs 4.4A and 4.5A). Its axis trends *ca* ENE–SSW. The volume of sediments forming the observed part of PB3 is *ca* 107,000 m^3. PB3 is, on average, 3 m thick, and its thickest (3.5 m) and thinnest (2.0 m) parts occur towards the innermost and outermost parts of the bar, respectively (Fig. 4.5E). A progressive upward-shift of the bar basal surface along the direction of accretion occurs also in PB3 (Fig. 4.5E). The overall direction of bar accretion is towards the west and produced two laterally offset bedsets (Fig. 4.5F).

The minor channel is slightly sinuous and trends north-west/south-east connecting meanders 1 and 3 of the major channel (Fig. 4.4B). The minor channel is 20 m wide and the channel fill ranges in depth between 1.7 m and 2.0 m. This channel contains two bank-attached bars, which are sited along its southern (BB1) and norther (BB2) flank, respectively (Fig. 4.4B). This bar typology can be found in low-sinuosity channels that do not migrate laterally enough to develop point bars but accumulate sediment along the banks. BB1 and BB2 are characterized by north-dipping and south-dipping internal clinoforms, respectively. BB1 extends for 300 m along the entire channel (Fig. 4.5G). The mean thickness is 2.2 m, and it decreases to less than 1 m moving northward (Fig. 4.5H). BB2 is the smallest bar of the study area and is found at the confluence between the minor and the major channels (Fig. 4.4A), extending laterally for *ca* 100 m. BB2 is 3 m thick and thins to 1.7 m thick southward, where overlaps BB1. The reconstructed volumes of BB1 and BB2 are *ca* 27,000 m^3 and 6,700 m^3, respectively (Fig. 4.5H).

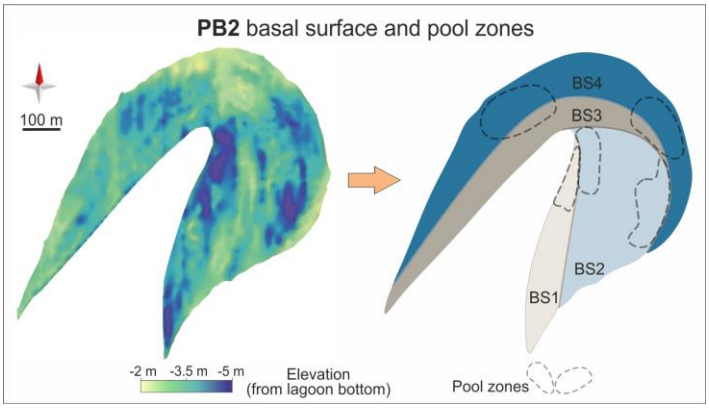

Fig. 4.6. Basal surface of PB2 with elevation scale to emphasize the position of pool zones within the different bedsets.

4.4.3 Core data

Sedimentary cores recovered in the area delimited by meander bend 2 allow depicting sedimentary features of the PB2 and related channel-fill, along with those of the surrounding overbank deposits (Fig. 4.4A).

Channel-bar deposits are floored by a massive channel lag consisting of mud-free, fine sand characterized by a high content in shell fragments, with plant debris and sporadic mudclasts (Fig. 4.7A). Bar deposits are essentially made of silty-rich mud with subordinate 1 to 5 cm thick intervals of mud-rich very fine sand. Beds are thinly laminated with dominance of plane-parallel stratification (Fig. 4.7C) and local evidence of ripple cross-lamination in the sandy-rich layers (Fig. 4.7B). These deposits also appear locally deformed, possibly by slump processes (Fig. 4.7D). Scattered centimetric mudclasts are locally concentrated in sandy intervals (Fig. 4.7E). Plant debris is common and locally forms 1 to 5 mm thick layers (Fig. 4.7F). The upper part of bar deposits consists of silty-rich mud with a moderate content of plant debris (Fig. 4.7G) and burrows (Fig. 4.7H). Bar deposits are overlaid by massive tidal flat mud that is characterized by a high content of mollusc shells (*Cerastoderma glaucum* and *Bittium reticulatum*), and both bioturbations and plant debris are common (Fig. 4.7I).

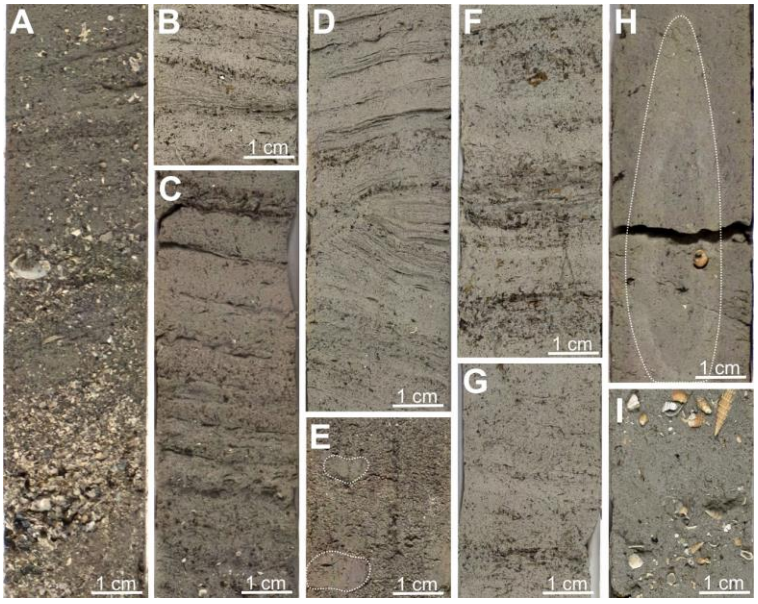

Fig. 4.7. Sedimentary facies of point-bar deposits. (A) Lag deposits with shell fragments, plant debris and sporadic mudclasts; (B) silty-rich mud body with ripple cross-lamination in mud-rich sandy layers, (C) plane-parallel stratification and (D) slump evidence. (E) Centimetric mudclasts in sandy-rich laminae and (F) plant debris layers. (G) Upper-bar silty mud deposits with moderate content of plant debris, (H) and burrows in structureless portions. (I) Massive muddy bar-top deposits with shells (*Cerastoderma glaucum*).

Sedimentary cores recovered at different sites along the bar (Fig. 4.4A) highlight that the whole bar body does not show any relevant vertical grain-size change. Grain-size analyses from cores recovered from BS4 in the landward and seaward part of the bar do not reveal any relevant vertical or lateral (i.e., seaward or landward) change in grain size (i.e., cores SC1 to SC4 in Fig. 4.8).

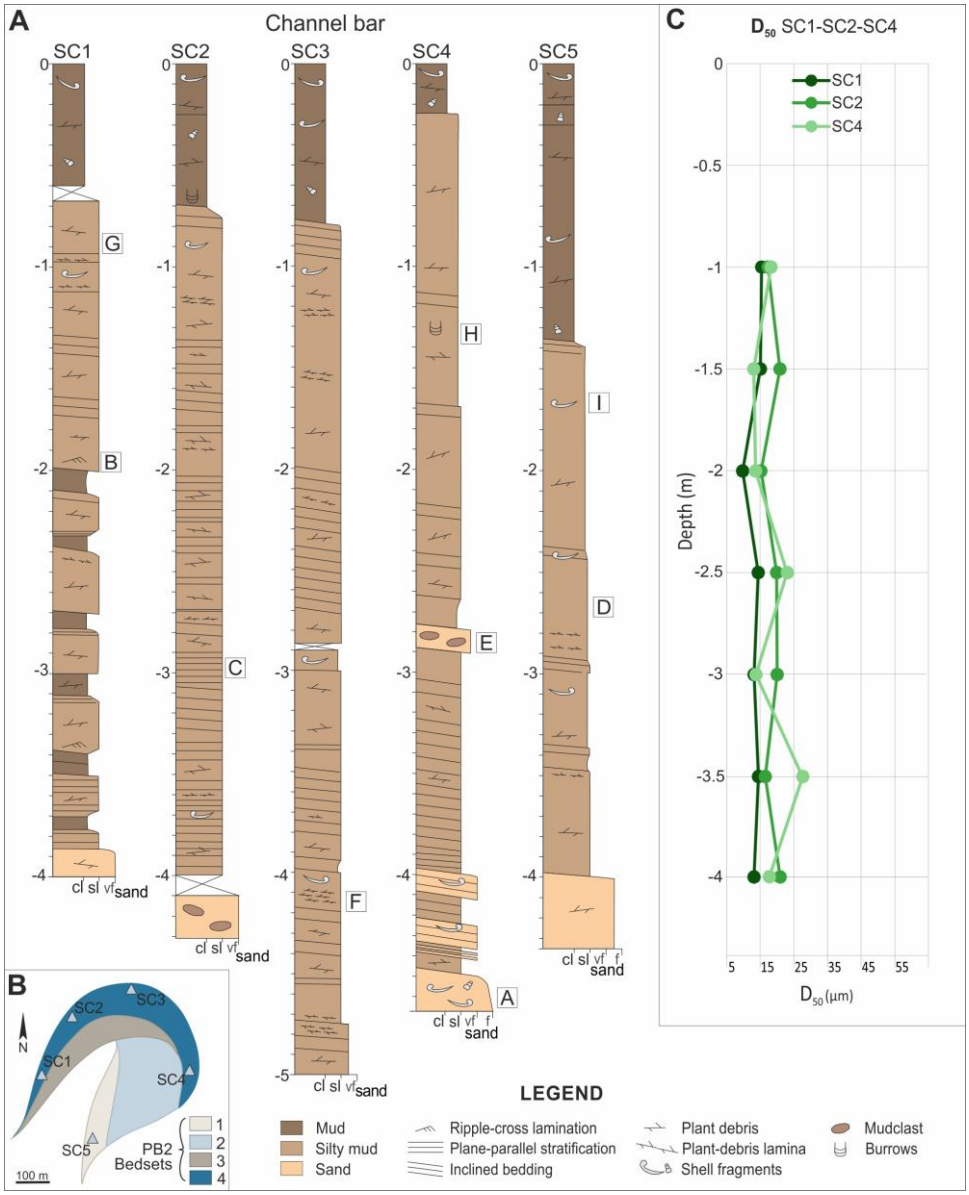

Fig. 4.8. Point-bar cores. (A) Stratigraphic logs and (B) core position on PB2. In inset (A), letters in squares indicate the position of the facies shown in Fig. 4.7. (C) Grain-size values (i.e. D50) of cores SC1, SC2 and SC4.

Channel-fill deposits cover a basal silty lag and grade upward to structureless mud. Channel-fill deposits contain sporadic plant remains and mollusc shells (*B. reticulatum and C. glaucum*) (Fig. 4.9B).

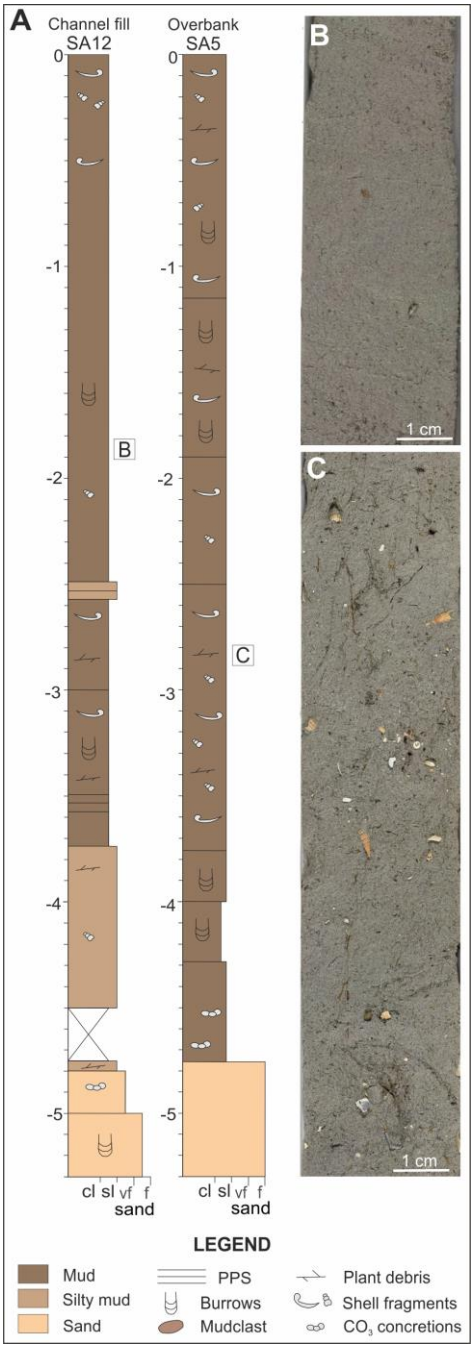

Fig. 4.9. Channel-fill and overbank deposits. (A) Stratigraphic logs of cores recovered within channel fill and overbank deposits; sedimentary facies of channel fill (B) and overbank (C) deposits.

Overbank deposits are mostly made of structureless mud with a high content of mollusc shells (*B. reticulatum* and *C. glaucum*) (Fig. 4.9C) and plant debris. These deposits do not show any evidence of subaerial exposure (for example, oxidation and root traces).

4.4.4 Planform evolution

Spatial distribution, orientation and curvature of different bedsets detected within the three study point bars (Fig. 4.5) provide the inferences which are commonly derived from the investigation of bar-top scroll pattern to reconstruct planform evolution of fluvial point bars (Ielpi and Ghinassi, 2014; Durkin et al., 2015; Ielpi et al., 2018; Mason and Mohrig, 2019). Bedsets are considered here as the subsurface expression of bar-top scroll-sets (Ghinassi et al., 2014). Integration between architectural and sedimentological data show that accretion of point bars started from a sinuous channel and continued through four distinct stages (stage 1 to 4 in Fig. 4.10).

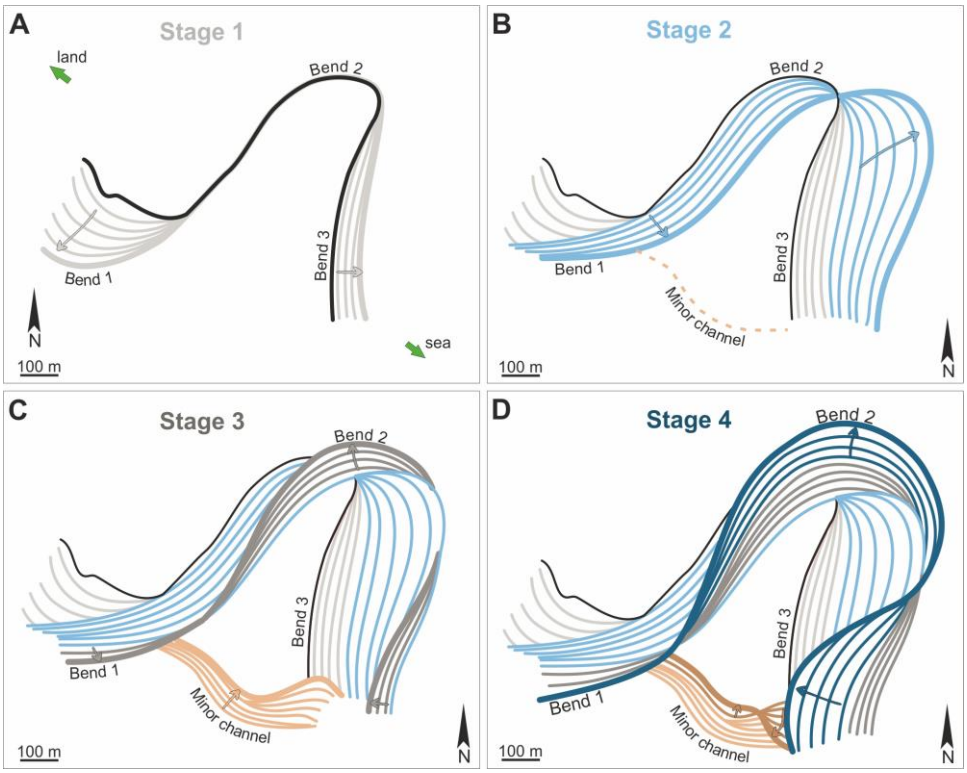

Fig. 4.10. Planform evolution of study channels. (A) to (D) The four stages of the reconstructed depositional evolution: (A) and (B) main seaward migration; (C) and (D) main landward accretion of the major palaeochannel with the development of the minor channel system. Arrows indicate the main directions of migration of the bars at each stage.

The early preserved establishment stage of evolution (T0 in Fig. 4.11), which defined the sinuous initial morphology of the channel and was not depositional, was characterized by Ls and Lxy of meander bend 2 of 440 m and 260 m, respectively, defining a sinuosity of 1.69 (black line, Fig. 4.10). The meander radius of curvature and amplitude measured 134 m and 126 m, respectively, and the thalweg maximum depth value was about 1 m (Fig. 4.11).

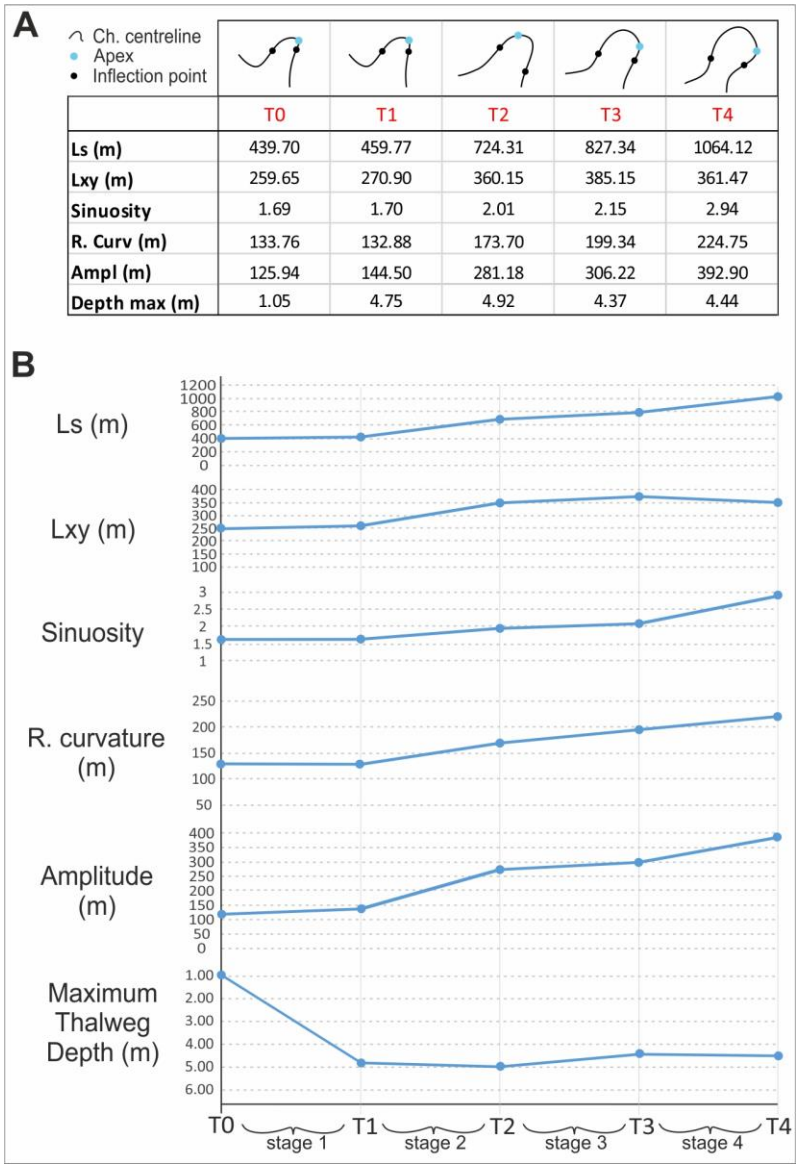

	T0	T1	T2	T3	T4
Ls (m)	439.70	459.77	724.31	827.34	1064.12
Lxy (m)	259.65	270.90	360.15	385.15	361.47
Sinuosity	1.69	1.70	2.01	2.15	2.94
R. Curv (m)	133.76	132.88	173.70	199.34	224.75
Ampl (m)	125.94	144.50	281.18	306.22	392.90
Depth max (m)	1.05	4.75	4.92	4.37	4.44

Fig. 4.11. Morphometric parameters and thalweg depths of meander bend 2 during the four main stages of planform evolution visualized as (A) schematic table (black lines represent the channel centreline; black and light-blue dots represent inflection points and apexes, respectively) and (B) graphs.

During the first stage (light grey lines in Fig. 4.10A), meander bend 1 migrated towards the south-west with a gentle downward shift of its thalweg (Fig. 4.5A) and allowed the expansional accretion (*sensu* Jackson, 1976) of the related bar with the accumulation of its first bedset package (BS1 in Fig. 4.5B). Simultaneously, meander bend 2 shifted eastward allowing seaward accretion (cf. Ghinassi *et al.*, 2018b) of PB2, with deposition of its first bedset, and erosion of the landward side of meander bend 3. During this stage, both *Ls* (*ca* 459 m) and *Lxy* (*ca* 270 m) of meander bend 2 slightly increased relative to the initial bend morphology (T1 in Fig. 4.11A). In contrast, the radius of curvature and sinuosity of the bend remained nearly constant during this stage, showing values of 133 m and 1.69, with an amplitude of 144 m, respectively. During the accumulation of BS1, the channel reached a maximum depth of 4.75 m from the lagoon bottom (T1 in Fig. 4.11A).

During the second stage (light blue lines in Fig. 4.10B), meander bend 1 changed its growth pattern, experiencing an overall SSE shift that allowed PB1 to accrete accordingly and generate its second bedset package (BS2 in Fig. 4.5B). This stage was characterized by a marked rising of the channel thalweg (Fig. 4.5B). Consistently, bend 2 experienced a seaward translation, associated with a north-east migration of the bar apex, that resulted in the deposition of its second bedset package. During this second stage, meander bend 2 modified its radius of curvature from 133 m to almost 173 m, and at the end of the stage, the *Ls* and *Lxy* of meander bend 2 increased to 724 m and 360 m, respectively, producing an overall sinuosity of 2.01. Also, the meander-bend amplitude increased, doubling to 280 m (T2 in Fig. 4.11A). During the accumulation of BS2, the channel reached a maximum depth of 4.92 m from the lagoon bottom (T2 in Fig. 4.11A) and the bar basal topography generated by thalweg shifts during this stage produced two major pool depressions close to the bend-apex zone (Fig. 4.6). Following meander bend 2, meander 3 experienced a seaward migration during this stage. Activation of the minor channel possibly occurred at this stage.

During the third depositional stage (grey lines in Fig. 4.10C) meander bend 1 experienced a minor SSE shift, with a gentle rising of the thalweg that generate its third bedset package (BS3 in Fig. 4.5B). Meander bend 2 experienced an asymmetrical growth characterized by an overall NNW landward shift and consequent accretion of the related bar through deposition of BS3. This process was associated with a partial erosion of the seaward side of bend 1. The meander bend 2 sinuosity remained almost unchanged during stage 3, but the

radius of curvature increased from 173 to 199 m (T3 in Fig. 4.11A) defining a semi-circular and more symmetric morphology of the bend. During this stage, the *Ls* and *Lxy* increased up to 827 m and 385 m, respectively, while the meander-bend amplitude reached a value of 306 m. The maximum thalweg depth slightly rose to 4.37 m (T3 in Fig. 4.11A), though the available data do not offer a clear identification of the pool zone (Fig. 4.6). Meander bend 3 was affected by an asymmetrical growth that caused a landward accretion of the related bar, resulting in a westward shift of the channel and the consequent erosion of PB2 deposits. This growth accumulated the first preserved bedset of PB3 (BS1 in Fig. 4.5F). During stage 3, the minor channel migrated towards the north-east accumulating most of the BB1 deposits (pink lines, Fig. 4.10C).

During stage four (blue lines, Fig. 4.10D), meander bend 1 continued to grow southward. Meander bend 2 was characterized by an asymmetrical growth towards NNE and consequently the final radius of curvature and sinuosity of meander bend 2 are equal to 224 m and 2.94, respectively. This migration leads to the increase in the *Ls* up to 1064 m, and the decrease in the cartesian length up to 361 m, whereas the meander amplitude reached the final value of 392 m (T4 in Fig. 4.11A). During this stage, the thalweg shift shaped two distinct pool depressions (Fig. 4.6), which are separated by a ridge sited in the bend apex zone. This erosional surface floors the fourth bedset forming BD4, during which the maximum depth reached by the channel was 4.44 m from the lagoon bottom (T4 in Fig. 4.11A). In parallel, meander bend 3 shifted landward, leading to the accretion of PB3 and causing the erosion of PB2 deposits and accumulating the second preserved bedset package of PB3 (BS2 in Fig. 4.5F). The fourth depositional stage is also characterized by a minimal northward shift of the western portion of the minor channel, accreting the related deposits of BB1 (brown lines, Fig. 4.10D), and an abrupt growth towards the south-west of the eastern portion of the channel, which implies the deposition of BB2. This south-west shift was characterized by a marked rise of the thalweg and allowed overlap between BB1 and BB2.

Variations of the main morphometric parameters of meander bend 2 during the four morphodynamic stages are summarized in Fig. 4.11B, along with the changes of maximum thalweg depth. Although an increase in the intrinsic length of the bend clearly appears, bend evolution was also associated with a progressive increase in its cartesian length, sinuosity, amplitude and radius of curvature. The maximum thalweg depth increased by *ca* 3.5 m (from -1.0 to -4.75 m from the bottom) during the first accretionary stage (T0–T1 in Fig. 4.11),

reaching the maximum depth during stage 2 (T1–T2 in Fig. 4.11). It decreased during stage 3 (from -4.92 to -4.37 m below the lagoon bottom) and remained almost constant during stage 4 (T3–T4 in Fig 4.11).

4.5 Discussion

4.5.1 Genesis and planform evolution of the bend

The overbank deposits nested within the horseshoe point bar allows to rule out that bar accretion started from an almost straight channel but indicate that the track of the channel was quite already sinuous (black line in Fig. 4.10; T0 in Fig. 4.11) at time of deposition inception. Accretion of PB1, PB2 and PB3 started along the inner bank of a bend, allowing PB2 to grow preserving at its core a relic of overbank mud. A similar contrast between the external geometry of meanders and the architecture of related point bars has been highlighted for fluvial meanders (Russell *et al.*, 2019) through the analysis of their complex scroll-bar patterns. Fluvial and tidal point bars are assumed to arise from a progressive increase in sinuosity of relatively-straight channels (Leopold and Wolman, 1960; Daniel, 1971; Brice, 1974; Lewin, 1976; Nanson and Page, 1983; Knighton et al., 1992; Hughes, 2012; Ghinassi et al., 2014), although the planform patterns of newly-formed channels are commonly irregular, being controlled by adaptation of the flow to local micro-reliefs of the newly-drained areas (Aslan and Blum, 1999; Taylor, 1999; Motta et al., 2012; Cassiani et al., 2020; Bellizia et al., 2021). Although adaptation of the Holocene lagoon mud to the underlying alluvial lowstand topography (Castiglioni and Favero, 1987; Amorosi et al., 2008) could have generated the micro-relief required to trigger wandering of a newly-formed channel, an avulsive relocation (Slingerland and Smith, 1998, 2004; Mohrig et al., 2000) of the study channel is ruled out by the lack of a significant superelevation between sub-tidal channels and surrounding overbanks. Development of such a superelevation was hindered by removal of possible levée-deposits by the combined action of waves and tidal currents (Ghinassi et al., 2019b). The high density which typifies tidal networks (Marani et al., 2003; Passalacqua et al., 2013; Hoitink et al., 2017) promotes interactions between adjacent migrating bends, causing piracies and connection of adjacent branches (Cosma et al., 2020). This latter process allows the development of new creeks with a sinuous shape, which lead to a renewed circulation pattern over a pre-existing network. Where the newly-established formative discharge

resulted increased by the network reorganization, an increase in the cross-sectional area of the creek (D'Alpaos et al., 2010) will occur.

Reconstructed planform evolution of the study channel reveals complex patterns, which are comparable to those characterizing fluvial meanders (Daniel, 1971; Brice, 1974; Jackson, 1976a; Ielpi and Ghinassi, 2014; Yan et al., 2017, 2019; Willis and Sech, 2018a). Apart from confined meanders [for example, Beaver River, Wapiti River, Red Deer River and Fontas River (Canada)] that are almost forced to translate downstream as part of a continuum of planform evolution (Lewin and Brindle, 1977; Nicoll, 2008; Nicoll and Hickin, 2010), fluvial bends behave almost independently experiencing a combination of migration styles, according to local geomorphic and sedimentary constraints, which are mainly represented by floodplain heterogeneities (Güneralp and Rhoads, 2011; Bogoni et al., 2017). The study bends cut into a homogeneous, muddy overbank (Madricardo et al., 2007); this lack of overbank heterogeneities hindered the development of differential planform behaviours and promoted a uniform response of the study bends to the same forcings. The restricted range of discharge, and therefore of the flowing tidal prism, and the lack of any fluvial input did not prevent the style of planform evolution to change in time. The alternation between phases of accretion along the seaward (for example, stage 2) and landward (for example, stage 3) side of the three adjacent bends could be related to the asymmetrical character of the tidal flow. Tambroni *et al.* (2017) demonstrated that point-bar patterns in tidal meandering channels form according to the local tidal asymmetry. Tidal asymmetries control the long-term net sediment transport in tidal environments (Hoitink et al., 2003; Van Maren et al., 2004), with ebb (flood) dominance leading to dominant accretion of the bar along the seaward (landward) side of the bend.

In the study case, phases dominated by flood currents (for example, stage 3) were associated with erosion on the seaward side of PB2 and accretion on its landward side. Conversely, phases of ebb dominance (i.e. stage 2) were associated with erosion on the landward side of PB2 and accretion on its seaward side (cf. Ghinassi *et al.*, 2018b; Finotello *et al.*, 2019). Alternation between landward and seaward shifts of the channel contributes to shaping the planform profile of the overbank relic deposits preserved within the bar (Figs 4.6 and 4.10). Recent studies on meanders of the Venice Lagoon (Finotello et al., 2019, 2020b) corroborated the findings of changes in sedimentation patterns with the local tidal asymmetry, and also demonstrated that morphological adaptation of meander bends to changes in local tidal asymmetry occurs over

relatively short timescales (i.e. decades) even in microtidal regimes. Although this may require further studies, we argue that the planform changes in the documented case study may have occurred at the scale of 10^1-10^2 years. Changes in local tidal asymmetry within tidal channels can arise both from changes in the overall structure of the tidal channel network and from modifications of the overall basin morphology. In the former instance, network modifications can happen due to meander cut-offs (Brivio et al., 2016) or channel piracy events (Cosma et al., 2020; Finotello et al., 2020b). These processes lead to redistribution of the tidal prisms and adjustments of channel cross-section, with channel shallowing (for example, silting and infill) where the prism decreases and cross-section enlarging where the prism increases. Such dynamics are more likely within dense networks of small channels, like those cutting through salt marshes (Marani et al., 2003). Changes in local tidal asymmetry due to modifications of the basin morphology are more likely to affect larger tidal channels, especially if located in proximity of the inlets where tidal currents are more intense (Walton, 2002; Finotello et al., 2019). These modifications are related to the overall morphodynamic evolution of the basin, which depends on a number of features including, for example, the inlet position and morphology, the relative extent of subtidal versus intertidal areas, the depth of tidal flat surfaces, and the position of a given channel within the basin itself, as well as possible anthropogenic influences on morphodynamics (Townend, 2010; Ferrarin et al., 2015; Silvestri et al., 2018; Finotello et al., 2019; Guo et al., 2019). Although the lack of information concerning changes of the palaeo-drainage, the size of the study palaeochannel would suggest that it suffered from the effect of a basin reorganization following a change in the inlet position, especially considering its proximity to the ancient barrier.

During the last stage of bar growth, the reducing tidal asymmetry would be consistent with a more uniform accretion along the inner bank, which was also associated with the lack of relevant changes in grain size along the bar (Fig. 4.8) and the development of two major pool zones along the thalweg (Fig. 4.6). A similar pattern of grain-size distribution and basal bar morphology has been detected in other point bars of the Venice Lagoon (Brivio et al., 2016), and testifies that the seaward and landward sides of the bar alternatively experienced similar intensity of bed shear stresses over a tidal cycle, due to flood and ebb currents.

4.5.2 Channel morphology, thalweg trajectories and pools development

Changes of the main morphometric parameters of bend 2 during the four growth stages (Fig. 4.11A) are compared with changes in thalweg elevation (Fig. 4.11B). The overall descending, ascending and horizontal trends of the thalweg trajectory reflect adaptation of the channel to different growth stages and related flow configurations (cf. Cosma *et al.*, 2019). The initial descending trend of the thalweg (i.e. stages 1 and 2) documents the channel adjustment to its newly-established formative discharge (Cosma et al., 2019). Deep scouring was also probably promoted by the development of a bend with the lowest radius of curvature, which enhanced the erosional effects of a secondary circulation in the bend apex zone (Finotello et al., 2020b). The subsequent gentle rise of the thalweg during stage 3 was probably related to the maintenance of its formative depth, which was reached at the end of stage 2. During this stage, sediments are accumulated in the channel to maintain a constant equilibrium depth in the frame of keeping dynamic equilibrium conditions (*sensu* Allen, 2000) with the surrounding aggradational tidal flats (Cosma et al., 2019, 2021). This process could have also been enhanced by the activation of the minor channel, which connected bends 1 and 3 causing a local drop in the strength of erosional forces within bend 2 (cf. Toonen *et al.*, 2012). The almost sub-horizontal trajectory of stage 4 indicates the achievement of a new tidal prism configuration, which allowed the channel to slightly increase its depth by keeping its thalweg at a constant depth during aggradation of the surrounding tidal flats.

During the different stages of evolution, meander bend 2 developed erosive pools that are identifiable on the basal surface of PB2 as major depressions. Although stage 1 pool is not clearly defined, stage 2 shows a deep pool zone that migrates south-east following the main seaward accretion of PB2 (Fig. 4.6). During stage 3, the pool zone moved northward and started to show two major depocentres, which became evident in stage 4 (Fig. 4.6). The switching from the one-pool configuration (stages 1 and 2) to the double-pool one (stage 4) can be explained by considering the increase in the radius of curvature in a tidal cyclicity scenario. The alternate turnover of the position of impingement zones is associated with curvature-induced secondary flows, rotating in opposite directions (Finotello et al., 2020b). A lower radius of curvature promotes the formation of a sharp bend where the impingement zones of flood and ebb flows against the outer bank almost coincide, causing a localized and intense scouring. In this frame, the more the radius increases, the fewer ebb and flood impingement zones against the outer bank coincide (Fig. 4.12). The increase in

the radius of curvature caused the separation of the ebb and flood impingement zones, with the establishment of two separated zones affected by ebb and flood helical circulation, respectively (Finotello et al., 2020b). Similar findings have been recently documented in a meander bend of an intertidal channel of the Venice Lagoon, sited almost 3 km east from the study area (site SC in Finotello *et al.*, 2020b), where flood and ebb flows impinge along channel banks downstream and upstream of the bend apex, respectively. This double configuration is similar to the one provided by box-shaped meanders (*sensu* Dalrymple *et al.*, 2012), and is responsible for the formation of two distinct scour pools (Hughes, 2012; Finotello, 2017) separated by a localized high (Hughes, 2012; Brivio et al., 2016).

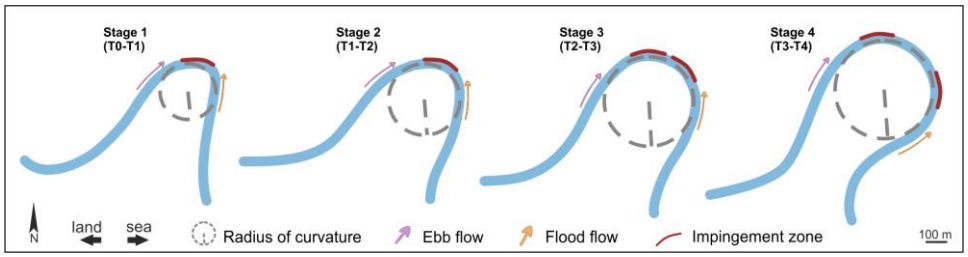

Fig. 4.12. Schematic representation of the variability of the radius of curvature during the four stages of palaeochannel evolution with the related position of the impingement zones.

4.5.3 Aggradation of the minor channel

Acoustic profiles and relative 3D reconstruction also depict the stratigraphic relationship between adjacent bars in the minor channel. Here, BB2 overlaps BB1 below related channel-fill deposits (Fig. 4.5H), suggesting that the channel thalweg shifted southward while aggrading vertically. This vertical aggradation component of the channel trajectory (cf. Cosma *et al.*, 2019, 2020) allowed the preservation of the southern bar (BB1), which was not completely dismantled by the southward channel shift. This ascending trajectory of the channel thalweg highlights that the rate of thalweg rise was sufficiently high to impact the dynamics of lateral shift of the channel. Such a configuration could derive either from the channel tendency to preserve a constant equilibrium depth under intense aggradation of overbank areas (Cosma et al., 2019), or from a gradual decrease in tidal prism (Rieu et al., 2005). In both cases, the occurrence of rising channel trajectories critically increases bar connectivity, as demonstrated by numerical models (Willis and Tang, 2010) and outcrop studies (Ghinassi et al., 2014) for fluvial meandering rivers.

4.5.4 Subtidal versus intertidal point bars from the Venice Lagoon: differences and similarities

Findings of this work contribute to improve the current knowledge about subtidal meanders, by shedding some light on their morphodynamic evolution and through a comparison with their intertidal counterparts. This comparison can be carried in the frame of a similar depositional setting, that is offered here by the backbarrier basin forming the Venice Lagoon. The study case, along with a further subtidal point bar described by Ghinassi *et al*. (2019) in the southern lagoon, provides insights on the comparison with several intertidal counterparts which were recently described (Brivio et al., 2016; Ghinassi et al., 2018b, 2018a). In the Venice Lagoon, although all the intertidal channels are flooded at high tides, only the smaller ones (i.e., shallower than 60–70 cm) can be completely dry at low tides, whereas the deeper ones are still partially to largely flooded. On the contrary, subtidal channels are permanently submerged also at the lowest tides. If the size of channels is similar, the grain size of point bars does not strongly differ from subtidal (Ghinassi et al., 2019b) and intertidal settings (Finotello et al., 2019), and channel-lag deposits seem to be ubiquitously characterized by abundance of shells and shell fragments (Brivio et al., 2016; Ghinassi et al., 2018b, 2018a; Cosma et al., 2019) (Fig. 4.13). Similarly, although bar deposits are laminated, no clear sedimentary structures can be detected, neither in subtidal nor in intertidal settings (Brivio et al., 2016; Ghinassi et al., 2018a; Cosma et al., 2019). Plant-debris laminae are also widespread in both types of point bars (Brivio et al., 2016; Ghinassi et al., 2018a, 2019b; Cosma et al., 2019) (Fig. 4.13). Differences occur essentially in the upper part of the bars, which show contrasting architecture and sedimentary features in subtidal and intertidal setting, respectively. The upper part of intertidal point bars is colonized by halophytic vegetation and consists of plane-parallel laminated mud (Brivio et al., 2016; Ghinassi et al., 2018a; Cosma et al., 2019). Mud is oxidized as consequence of repeated episodes of subaerial exposure, and bears abundant root traces (Brivio et al., 2016; Ghinassi et al., 2018a; Cosma et al., 2019) (Fig. 4.13). Laminations are generally well-preserved, and commonly highlighted by the occurrence of millimetric sandy laminae, which have been commonly related to activity of wind-waves during major storm events (Brivio et al., 2016; Ghinassi et al., 2018a; Cosma et al., 2019). Although geophysical data imaging of the transition between inclined bar slope beds and overlying sub-horizontal bar top layers are missing, this transition is associated with a gradual decrease of dip angle (Brivio et al., 2016), suggesting a sigmoidal

(*sensu* Gobo *et al.*, 2014, 2015) bar top geometry (Cosma et al., 2019) (Fig. 4.13).

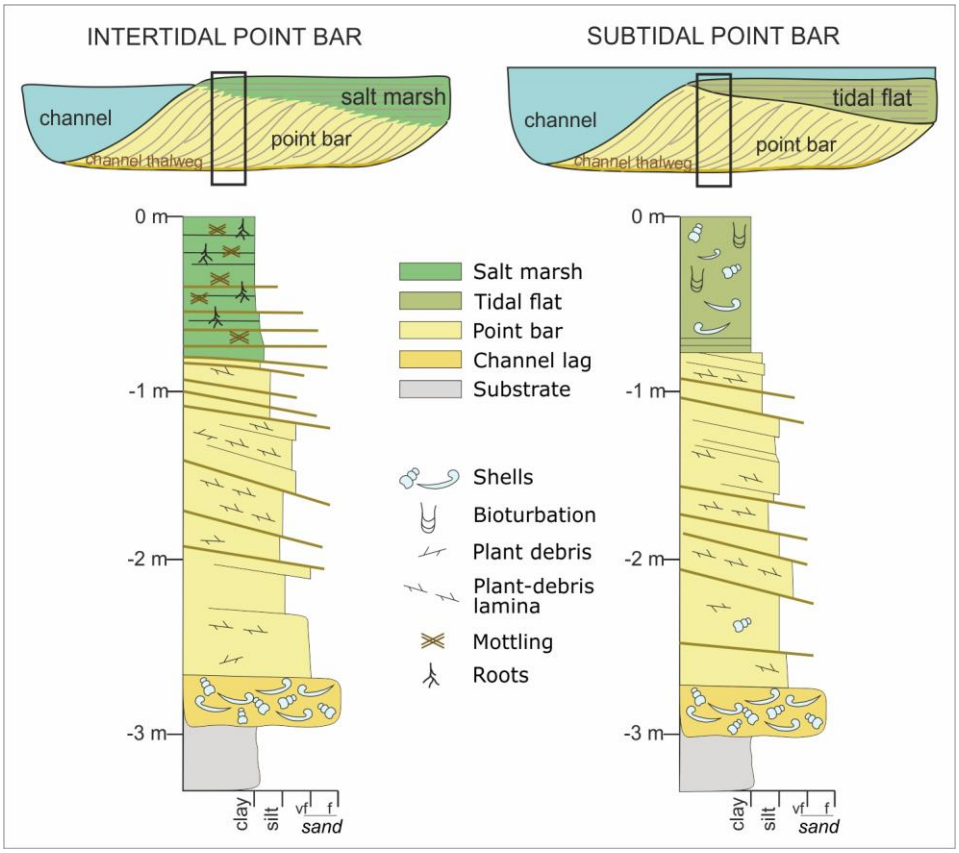

Fig. 4.13. Representative logs of point-bar deposits of the Venice Lagoon from intertidal (left) and subtidal (right) areas.

Bar top deposits in the subtidal counterparts range in grain size from mud (this study, Fig. 4.7l) to very-fine sand (Ghinassi et al., 2019b). Despite this difference, bar-top deposits are always massive due to the intense bioturbation and lack any evidence of oxidation (Fig. 4.13). They appear generally grey to dark grey and contain abundant shells and shell fragments. Bivalves can occur in life position (Ghinassi et al., 2019b). Seismic data from the southern Venice Lagoon (Ghinassi et al., 2019b) show that sub-horizontal bar-top beds abruptly cover inclined bar slope beds (Fig. 4.13). Such an abrupt truncation was ascribed to the erosive effect of wind storm waves, which causes erosion in the bar-top area and also triggers collapses of the bar-slope deposits. Similar features were not imaged in the study site, mainly because of the low resolution of the acoustic data in the bar-top zone, due to the different geophysical approach

used in this study compared to other ones (e.g., Ghinassi et al., 2019b). The dominance of muddy deposits at the study site would be consistent with a lower efficiency of wave activity on the bar-top zone, due to the reduced wind fetch characterizing the study site during the major storm events associated with the north-east blowing Bora wind (Carniello et al., 2009, 2012; D'Alpaos et al., 2013). Large waves affect the southern Venice Lagoon during these storms (Carniello et al., 2009, 2012; D'Alpaos et al., 2013) and account for the occurrence of erosive truncations and sandy deposits in the bar-top deposits.

4.6 Conclusions

Acoustic and sedimentary-core data allowed reconstruction of depositional patterns of deposits associated with a subtidal channel in the microtidal Venice Lagoon (Italy). The study palaeochannel was 35 m wide and 3 m deep and formed three adjacent meander bends and related point bars. A detailed 3D architectural reconstruction was carried out for deposits associated with one of these meander bends, that was crossed by a minor, low-sinuosity channel with two minor bank-attached bars.

The major insights from this 3D sedimentological reconstruction can be summarized as follows:

- The study point bar has an arcuate shape, which preserves at its core tidal-flat mud. Such a peculiar geometry was generated by the onset of bar accretion from an already sinuous channel. This process was probably triggered by the establishment of a new circulation pattern over a pre-existing network, possibly following a piracy event that connected adjacent tidal branches.
- Planform evolution of the study bend occurred through several stages that reflect asymmetrical growth of the point bars, as commonly observed in fluvial systems. This shows that, although the tidal currents work within a restricted and monotonous range of discharge, the style of bend planform evolution can change in time, possibly under the effect of variation in tidal asymmetry. Results show that under asymmetrical tidal flows, subtidal meanders develop depositional patterns according to the dominant flow direction.
- Planform transformations of the investigated bend occurred in parallel with changes in elevation of the related channel thalweg. These changes reflect the tendency of the channel to reach and maintain a specific equilibrium depth. Activation of a subordinate channel could modify the effective discharge of the major channel, influencing the vertical shift of its thalweg.

- Progressive increase in the radius of curvature of the study bend caused the splitting of the related pool scour. While the bend maintained a small radius of curvature, recirculating flows triggered by ebb end flood currents excavated the channel almost in the same area, generating a single pool depression. A progressive increase in meander-bend radius caused flood and ebb currents to create recirculation flows in different areas, with consequent development of two separated pool depressions.
- Bank-attached bars associated with the minor channel developed across the study bend migrated under aggradational conditions. This allowed overlap of these bars, which created a single and well-connected sedimentary body.

Acknowledgements

This work was sponsored by "HYDROSEM: Fluvial and tidal meanders of the Venetian-Po plain: from hydrodynamics to stratigraphy" project (Progetto di Eccellenza CARIPARO 2017, PI Massimiliano Ghinassi) and University of Padova (SID2016 project, titled "From channels to rock record: morphodynamic evolution of tidal meanders and related sedimentary products", PI Massimiliano Ghinassi). Authors are thankful to the "Echos" project supported by the *Ministero delle Infrastrutture e dei Trasporti- Provveditorato Interregionale per le Opere Pubbliche del Veneto – Trentino Alto Adige – Friuli Venezia Giulia tramite il concessionario Consorzio Venezia Nuova*, to provide part of sediment cores and the acoustic data. This manuscript benefits from the constructive comments from Reviewers R. Dalrymple and V. Zuchuat, and from the Associate Editor C. Bristow. Authors are grateful with the Journal Office Manager E. Richardson and the Chief Editor P. Plink-Björklund, for their editorial assistance.

Data Availability

The data that support the findings of this study are openly available in Mendeley Data at http://dx.doi.org/10.17632/jpt2pd8y3h.2

References

Allen, J.R.L., 1965, A review of the origin and characteristics of recent alluvial sediments: Sedimentology, v. 5, p. 89–191, doi:10.1111/j.1365-3091.1965.tb01561.x.

Allen, J.R.L., 2000, Morphodynamics of Holocene salt marshes: a review sketch

from the Atlantic and Southern North Sea coasts of Europe: Quaternary Science Reviews, v. 19, p. 1155–1231, doi:10.1016/S0277-3791(99)00034-7.

Allen, J.R.L., 1982, Sedimentary structures - Their character and Physical Basis, Volume II: Amsterdam, The Netherlands, Elsevier Scientific Publishing Company, v. 2, 662 p.

Amorosi, A., Fontana, A., Antonioli, F., Primon, S., and Bondesan, A., 2008, Post-LGM sedimentation and Holocene shoreline evolution in the NW Adriatic coastal area: GeoActa, v. 7, p. 41–67.

Aslan, A., and Blum, M.D., 1999, Contrasting styles of Holocene avulsion, Texas Gulf coastal plain, USA, *in* Smith, N.D. and Rogers, J. eds., Fluvial sedimentology VI: International Association of Sedimentologists Special Publication, Wiley Online Library, v. 28, p. 193–209, doi:10.1002/9781444304213.ch15.

Balletti, C., 2006, Digital elaborations for cartographic reconstruction: The territorial transformations of Venice harbours in historical maps: e-Perimetron, v. 1, p. 274–286.

Barwis, J.H., 1977, Sedimentology of some South Carolina tidal-creek point bars, and a comparison with their fluvial counterparts: Fluvial Sedimentology, v. 5, p. 129–160.

Bellizia, E., Boaga, J., Fontana, A., D'Alpaos, A., Cassiani, G., and Ghinassi, M., 2021, Impact of genesis and abandonment processes of a fluvial meander on geometry and grain-size distribution of the associated point bar (Venetian Plain, Italy): Marine and Petroleum Geology, v. 127, p. 104951, doi:10.1016/j.marpetgeo.2021.104951.

Bhattacharyya, P., Bhattacharya, J.P., and Khan, S.D., 2015, Paleo-channel reconstruction and grain size variability in fluvial deposits, Ferron Sandstone, Notom Delta, Hanksville, Utah: Sedimentary Geology, v. 325, p. 17–25, doi:10.1016/j.sedgeo.2015.05.001.

Bluck, B.J., 1971, Sedimentation in the meandering river Endrick: Scottish Journal of Geology, v. 7, p. 93–138, doi:10.1144/sjg07020093.

Bogoni, M., Putti, M., and Lanzoni, S., 2017, Modeling meander morphodynamics over self-formed heterogeneous floodplains: Water Resources Research, v. 53, p. 5137–5157, doi:10.1002/2017WR020726.

Bonardi, M., Canal, E., and Cavazzoni, S., 1997, Sedimentological, archeological and historical evidences of paleoclimatic changes during the holocene in the lagoon of Venice (Italy), *in* United States, p. 156.

Bondesan, A., and Furlanetto, P., 2012, Artificial fluvial diversions in the mainland of the Lagoon of Venice during the 16th and 17th centuries inferred by historical cartography analysis: Géomorphologie: relief, processus, environnement, v. 18, p. 175–200, doi:10.4000/geomorphologie.9815.

Brice, J.C., 1974, Evolution of meander loops: Geological Society of America Bulletin, v. 85, p. 581–586, doi:10.1130/0016-7606(1974)85<581:EOML>2.0.CO;2.

Bridge, J.S., 1993, Description and interpretation of fluvial deposits: a critical perspective: Sedimentology, v. 40, p. 801–810, doi:10.1111/j.1365-3091.1993.tb01361.x.

Bridges, P.H., and Leeder, M.R., 1976, Sedimentary model for intertidal mudflat channels, with examples from the Solway Firth, Scotland: Sedimentology, v. 23, p. 533–552, doi:10.1111/j.1365-3091.1976.tb00066.x.

Brivio, L., Ghinassi, M., D'Alpaos, A., Finotello, A., Fontana, A., Roner, M., and Howes, N., 2016, Aggradation and lateral migration shaping geometry of a tidal point bar: An example from salt marshes of the Northern Venice Lagoon (Italy): Sedimentary Geology, v. 343, p. 141–155, doi:10.1016/j.sedgeo.2016.08.005.

Busato, D., 2007, Metamorfosi di un litorale. Origine e sviluppo dell'isola di Sant'Erasmo nella laguna di Venezia: Marsilio, 213 p.

Carniello, L., Defina, A., and D'Alpaos, L., 2012, Modeling sand-mud transport induced by tidal currents and wind waves in shallow microtidal basins: Application to the Venice Lagoon (Italy): Estuarine, Coastal and Shelf Science, v. 102–103, p. 105–115, doi:10.1016/j.ecss.2012.03.016.

Carniello, L., Defina, A., and D'Alpaos, L., 2009, Morphological evolution of the Venice lagoon: Evidence from the past and trend for the future: Journal of Geophysical Research: Earth Surface, v. 114, doi:10.1029/2008JF001157.

Cassiani, G., Bellizia, E., Fontana, A., Boaga, J., D'Alpaos, A., and Ghinassi, M., 2020, Geophysical and Sedimentological Investigations Integrate Remote-Sensing Data to Depict Geometry of Fluvial Sedimentary Bodies: An Example from Holocene Point-Bar Deposits of the Venetian Plain (Italy): Remote Sensing, v. 12, p. 2568, doi:10.3390/rs12162568.

Castiglioni, G.B., and Favero, V., 1987, Linee di costa antiche ai margini orientali della Laguna di Venezia e ai lati della foce attuale del Piave: Istituto Veneto di Scienze Lettere ed Arti, Commissione di Studio dei Provvedimenti per la Conservazione e Difesa della Laguna e della Città di Venezia, p. 17–30.

Choi, K., 2011, Tidal rhythmites in a mixed-energy, macrotidal estuarine channel, Gomso Bay, west coast of Korea: Marine Geology, v. 280, p. 105–115, doi:10.1016/j.margeo.2010.12.004.

Choi, K., Hong, C.M., Kim, M.H., Oh, C.R., and Jung, J.H., 2013, Morphologic evolution of macrotidal estuarine channels in Gomso Bay, west coast of Korea: Implications for the architectural development of inclined heterolithic stratification: Marine Geology, v. 346, p. 343–354, doi:10.1016/j.margeo.2013.10.005.

Choi, K.S., and Jo, J.H., 2015, Morphodynamics of Tidal Channels in the Open Coast Macrotidal Flat, Southern Ganghwa Island in Gyeonggi Bay, West Coast of Korea: Journal of Sedimentary Research, v. 85, p. 582–595, doi:10.2110/jsr.2015.44.

Clement, W.P., and Barrash, W., 2006, Crosshole radar tomography in a fluvial aquifer near Boise, Idaho: Journal of Environmental and Engineering Geophysics, v. 11, p. 171–184, doi:10.2113/JEEG11.3.171.

Clift, P.D., Olson, E.D., Lechnowskyj, A., Moran, M.G., Barbato, A., and Lorenzo,

J.M., 2019, Grain-size variability within a mega-scale point-bar system, False River, Louisiana: Sedimentology, v. 66, p. 408–434, doi:10.1111/sed.12528.

Cosma, M., Finotello, A., Ielpi, A., Ventra, D., Oms, O., D'Alpaos, A., and Ghinassi, M., 2020, Piracy-controlled geometry of tide-dominated point bars: Combined evidence from ancient sedimentary successions and modern channel networks: Geomorphology, v. 370, p. 107402, doi:10.1016/j.geomorph.2020.107402.

Cosma, M., Ghinassi, M., D'Alpaos, A., Roner, M., Finotello, A., Tommasini, L., and Gatto, R., 2019, Point-bar brink and channel thalweg trajectories depicting interaction between vertical and lateral shifts of microtidal channels in the Venice Lagoon (Italy): Geomorphology, v. 342, p. 37–50, doi:10.1016/j.geomorph.2019.06.009.

Cosma, M., Yan, N., Colombera, L., Mountney, N.P., D'Alpaos, A., and Ghinassi, M., 2021, An integrated approach to determine three-dimensional accretion geometries of tidal point bars: Examples from the Venice Lagoon (Italy): Sedimentology, v. 68, p. 449–476, doi:10.1111/sed.12787.

La Croix, A.D., and Dashtgard, S.E., 2015, A synthesis of depositional trends in intertidal and upper subtidal sediments across the tidal–fluvial transition in the Fraser River, Canada.: Journal of Sedimentary Research, v. 85, p. 683–698, doi:10.2110/jsr.2015.47.

D'Alpaos, L., 2010, Fatti e misfatti di idraulica lagunare. La laguna di Venezia dalla diversione dei fiumi alle nuove opere delle bocche di porto (L. D'Alpaos, Ed.): Istituto Veneto di Scienze, Lettere ed Arti, Venice, IVSLA, 355 p.

D'Alpaos, A., Carniello, L., and Rinaldo, A., 2013, Statistical mechanics of wind wave-induced erosion in shallow tidal basins: Inferences from the Venice Lagoon: Geophysical Research Letters, v. 40, p. 3402–3407, doi:10.1002/grl.50666.

D'Alpaos, A., Lanzoni, S., Marani, M., and Rinaldo, A., 2010, On the tidal prism-channel area relations: Journal of Geophysical Research: Earth Surface, v. 115, p. 1–13, doi:10.1029/2008JF001243.

Dalrymple, R.W., and Choi, K., 2007, Morphologic and facies trends through the fluvial-marine transition in tide-dominated depositional systems: A schematic framework for environmental and sequence-stratigraphic interpretation: Earth-Science Reviews, v. 81, p. 135–174, doi:10.1016/j.earscirev.2006.10.002.

Dalrymple, R.W., Knight, R.J., Zaitlin, B.A., and Middleton, G. V., 1990, Dynamics and facies model of a macrotidal sand-bar complex, Cobequid Bay—Salmon River Estuary (Bay of Fundy): Sedimentology, v. 37, p. 577–612, doi:10.1111/j.1365-3091.1990.tb00624.x.

Dalrymple, R.W., Mackay, D.A., Ichaso, A.A., and Choi, K.S., 2012, Processes, Morphodynamics, and Facies of Tide-Dominated Estuaries, *in* Davis, R.A. and Dalrymple, R.W. eds., Principles of Tidal Sedimentology, Springer, p. 79–107, doi:10.1007/978-94-007-0123-6_5.

Daniel, J.F., 1971, Channel movement of meandering Indiana streams: Washington D.C., US Government Printing Office.

Durkin, P.R., Boyd, R.L., Hubbard, S.M., Shultz, A.W., and Blum, M.D., 2017, Three-dimensional reconstruction of meander-belt evolution, Cretaceous McMurray Formation, Alberta foreland basin, Canada: Journal of Sedimentary Research, v. 87, p. 1075–1099, doi:10.2110/jsr.2017.59.

Durkin, P.R., Hubbard, S.M., Boyd, R.L., and Leckie, D.A., 2015, Stratigraphic expression of intra-point-bar erosion and rotation: Journal of Sedimentary Research, v. 85, p. 1238–1257, doi:10.2110/jsr.2015.78.

Fabbri, P., Ortombina, M., and Piccinini, L., 2012, Estimation of Hydraulic Conductivity Using the Slug Test Method in a Shallow Aquifer in the Venetian Plain (NE, Italy): Aqua Mundi, v. 3, p. 125–133, doi:10.4409/Am-045-12-0048.

Fagherazzi, S., Gabet, E.J., and Furbish, D.J., 2004, The effect of bidirectional flow on tidal channel planforms: Earth Surface Processes and Landforms, v. 29, p. 295–309, doi:10.1002/esp.1016.

Ferrarin, C., Tomasin, A., Bajo, M., Petrizzo, A., and Umgiesser, G., 2015, Tidal changes in a heavily modified coastal wetland: Continental Shelf Research, v. 101, p. 22–33, doi:10.1016/j.csr.2015.04.002.

Finotello, A., 2017, Tidal channel patterns: field investigations, numerical modelling and laboratory experiments: University of Padova, 211 p.

Finotello, A., Canestrelli, A., Carniello, L., Ghinassi, M., and D'Alpaos, A., 2019, Tidal Flow Asymmetry and Discharge of Lateral Tributaries Drive the Evolution of a Microtidal Meander in the Venice Lagoon (Italy): Journal of Geophysical Research: Earth Surface, v. 124, p. 3043–3066, doi:10.1029/2019JF005193.

Finotello, A., D'Alpaos, A., Bogoni, M., Ghinassi, M., and Lanzoni, S., 2020a, Remotely-sensed planform morphologies reveal fluvial and tidal nature of meandering channels: Scientific Reports, v. 10, p. 1–13, doi:10.1038/s41598-019-56992-w.

Finotello, A., Ghinassi, M., Carniello, L., Belluco, E., Pivato, M., Tommasini, L., and D'Alpaos, A., 2020b, Three-dimensional flow structures and morphodynamic evolution of microtidal meandering channels: Water Resources Research, v. 56, p. e2020WR027822, doi:10.1029/2020WR027822.

Finotello, A., Lanzoni, S., Ghinassi, M., Marani, M., Rinaldo, A., and D'Alpaos, A., 2018, Field migration rates of tidal meanders recapitulate fluvial morphodynamics: Proceedings of the National Academy of Sciences, v. 115, p. 1463–1468, doi:10.1073/pnas.1711330115.

Flemming, B.W., 2012, Siliciclastic Back-Barrier Tidal Flats, *in* Davis, R.A.J. and Dalrymple, R.W. eds., Principles of Tidal Sedimentology, The Netherlands, Springer, p. 231–267, doi:10.1007/978-94-007-0123-6.

Frings, R.M., 2008, Downstream fining in large sand-bed rivers: Earth-Science Reviews, v. 87, p. 39–60, doi:10.1016/j.earscirev.2007.10.001.

Fustic, M., Hubbard, S.M., Spencer, R., Smith, D.G., Leckie, D.A., Bennett, B., and

Larter, S., 2012, Recognition of down-valley translation in tidally influenced meandering fluvial deposits, Athabasca Oil Sands (Cretaceous), Alberta, Canada: Marine and Petroleum Geology, v. 29, p. 219–232, doi:10.1016/j.marpetgeo.2011.08.004.

Gabet, E., 1998, Lateral Migration and Bank Erosion in a Saltmarsh: Estuaries, v. 21, p. 745–753, doi:10.2307/1353278.

Gershenzon, N.I., Ritzi Jr, R.W., Dominic, D.F., Soltanian, M., and Mehnert, E., Okwen, R.T., 2015, Influence of small-scale fluvial architecture on CO2 trapping processes in deep brine reservoirs: Water Resources Research, v. 51, p. 8240–8256, doi:10.1002/2015WR017638.

Ghinassi, M., D'alpaos, A., Gasparotto, A., Carniello, L., Brivio, L., Finotello, A., Roner, M., Franceschinis, E., Realdon, N., Howes, N., Cantelli, A., 2018a, Morphodynamic evolution and stratal architecture of translating tidal point bars: Inferences from the northern Venice Lagoon (Italy): Sedimentology, v. 65, p. 1354–1377, doi:10.1111/sed.12425.

Ghinassi, M., Billi, P., Libsekal, Y., Papini, M., and Rook, L., 2013, Inferring fluvial morphodynamics and overbank flow control from 3D outcrop sections of a Pleistocene point bar, Dandiero Basin, Eritrea: Journal of Sedimentary Research, v. 83, p. 1065–1083, doi:10.2110/jsr.2013.80.

Ghinassi, M., Brivio, L., D'Alpaos, A., Finotello, A., Carniello, L., Marani, M., and Cantelli, A., 2018b, Morphodynamic evolution and sedimentology of a microtidal meander bend of the Venice Lagoon (Italy): Marine and Petroleum Geology, v. 96, p. 391–404, doi:10.1016/j.marpetgeo.2018.06.011.

Ghinassi, M., Colombera, L., Mountney, N.P., and Reesink, A.J.H., 2019a, Sedimentology of meandering river deposits: advances and challenges, *in* Ghinassi, M., Colombera, L., and Mountney, N.P. eds., Fluvial Meanders and Their Sedimentary Products in the Rock Record, Int. Assoc. Sedimentol. Spec. Publ., Wiley-Blackwell, v. 48, p. 1–14, doi:10.1002/9781119424437.ch1.

Ghinassi, M., D'Alpaos, A., Tommasini, L., Brivio, L., Finotello, A., and Stefani, C., 2019b, Tidal currents and wind waves controlling sediment distribution in a subtidal point bar of the Venice Lagoon (Italy): Sedimentology, v. 66, p. 2926–2949, doi:10.1111/sed.12616.

Ghinassi, M., and Ielpi, A., 2015, Stratal architecture and morphodynamics of downstream-migrating fluvial point bars (Jurassic Scalby Formation, UK): Journal of Sedimentary Research, v. 85, p. 1123–1137, doi:10.2110/jsr.2015.74.

Ghinassi, M., Ielpi, A., Aldinucci, M., and Fustic, M., 2016, Downstream-migrating fluvial point bars in the rock record: Sedimentary Geology, v. 334, p. 66–96, doi:10.1016/j.sedgeo.2016.01.005.

Ghinassi, M., Nemec, W., Aldinucci, M., Nehyba, S., Özaksoy, V., and Fidolini, F., 2014, Plan-form evolution of ancient meandering rivers reconstructed from longitudinal outcrop sections: Sedimentology, v. 61, p. 952–977, doi:10.1111/sed.12081.

Gobo, K., Ghinassi, M., and Nemec, W., 2015, Gilbert-type deltas recording short-term base-level changes: Delta-brink morphodynamics and related foreset facies: Sedimentology, v. 62, p. 1923–1949, doi:10.1111/sed.12212.

Gobo, K., Ghinassi, M., and Nemec, W., 2014, Reciprocal changes in foreset to bottomset facies in a gilbert-type delta: Response to short-term changes in base level: Journal of Sedimentary Research, v. 84, p. 1079–1095, doi:10.2110/jsr.2014.83.

Güneralp, Í., and Rhoads, B.L., 2011, Influence of floodplain erosional heterogeneity on planform complexity of meandering rivers: Geophysical Research Letters, v. 38, p. 2–7, doi:10.1029/2011GL048134.

Guo, L., Wang, Z.B., Townend, I., and He, Q., 2019, Quantification of Tidal Asymmetry and Its Nonstationary Variations: Journal of Geophysical Research: Oceans, v. 124, p. 773–787, doi:10.1029/2018JC014372.

Hagstrom, C.A., Hubbard, S.M., Leckie, D.A., and Durkin, P.R., 2019, The Effects of Accretion-package Geometry On Lithofacies Distribution in Point-bar Deposits: Journal of Sedimentary Research, v. 89, p. 381–398, doi:10.2110/jsr.2019.23.

Heo, J., Duc, T.A., Cho, H.S., and Choi, S.U., 2009, Characterization and prediction of meandering channel migration in the GIS environment: A case study of the Sabine River in the USA: Environmental Monitoring and Assessment, v. 152, p. 155–165, doi:10.1007/s10661-008-0304-8.

Hoitink, A.J.F., Hoekstra, P., and Van Maren, D.S., 2003, Flow asymmetry associated with astronomical tides: Implications for the residual transport of sediment: Journal of Geophysical Research: Oceans, v. 108, p. 1–8, doi:10.1029/2002jc001539.

Hoitink, A.J.F., Wang, Z.B., Vermeulen, B., Huismans, Y., and Kästner, K., 2017, Tidal controls on river delta morphology: Nature Geoscience, v. 10, p. 637–645, doi:10.1038/ngeo3000.

Hubbard, S.M., Smith, D.G., Nielsen, H., Leckie, D.A., Fustic, M., Spencer, R.J., and Bloom, L., 2011, Seismic geomorphology and sedimentology of a tidally influenced river deposit, Lower Cretaceous Athabasca oil sands, Alberta, Canada: AAPG Bulletin, v. 95, p. 1123–1145, doi:10.1306/12131010111.

Hughes, Z.J., 2012, Tidal Channels on Tidal Flats and Marshes, *in* Davis, R.A. and Dalrymple, R.W. eds., Principles of Tidal Sedimentology, New York, Springer, p. 269–300, doi:10.1007/978-94-007-0123-6_11.

Ielpi, A., and Ghinassi, M., 2014, Planform architecture, stratigraphic signature and morphodynamics of an exhumed Jurassic meander plain (Scalby Formation, Yorkshire, UK): Sedimentology, v. 61, p. 1923–1960, doi:10.1111/sed.12122.

Ielpi, A., Ghinassi, M., Rainbird, R.H., and Ventra, D., 2018, Planform sinuosity of Proterozoic rivers: A craton to channel-reach perspective, *in* Ghinassi, M., Colombera, L., Mountney, N.P., Reesink, A.J., and Bateman, M. eds., Fluvial Meanders and Their Sedimentary Products in the Rock Record. Int. Assoc.

Sedimentol. Spec. Publ. 48, Ltd, John Wiley & Sons, p. 81–118, doi:10.1002/9781119424437.ch4.

Issautier, B., Viseur, S., Audigane, P., and Le Nindre, Y.-M., 2014, Impacts of fluvial reservoir heterogeneity on connectivity: Implications in estimating geological storage capacity for CO2: International Journal of Greenhouse Gas Control, v. 20, p. 333–349, doi:10.1016/j.ijggc.2013.11.009.

Jackson, R.G., 1976a, Depositional model of point bars in the lower Wabash River: Journal of Sedimentary Research, v. 46, p. 579–594, doi:10.1306/212F6FF5-2B24-11D7-8648000102C1865D.

Jackson, R.G., 1976b, Largescale ripples of the lower Wabash River: Sedimentology, v. 23, p. 593–623, doi:10.1111/j.1365-3091.1976.tb00097.x.

Janocko, M., Nemec, W., Henriksen, S., and Warchoł, M., 2013, The diversity of deep-water sinuous channel belts and slope valley-fill complexes: Marine and Petroleum Geology, v. 41, p. 7–34, doi:10.1016/j.marpetgeo.2012.06.012.

Kent, D. V., Rio, D., Massari, F., Kukla, G., and Lanci, L., 2002, Emergence of Venice during the Pleistocene: Quaternary Science Reviews, v. 21, p. 1719–1727, doi:10.1016/S0277-3791(01)00153-6.

Knighton, A.D., Woodroffe, C.D., and Mills, K., 1992, The evolution of tidal creek networks, Mary River, northern Australia: Earth Surface Processes and Landforms, v. 17, p. 167–190, doi:10.1002/esp.3290170205.

Kolla, V., Posamentier, H.W., and Wood, L.J., 2007, Deep-water and fluvial sinuous channels-Characteristics, similarities and dissimilarities, and modes of formation: Marine and Petroleum Geology, v. 24, p. 388–405, doi:10.1016/j.marpetgeo.2007.01.007.

Leopold, L.B., and Wolman, M.G., 1960, River Meanders: Geological Soceity of America Bulletin, v. 71, p. 769–793, doi:10.1130/0016-7606(1960)71[769:RM]2.0.CO;2.

Lewin, J., 1976, Initiation of bed forms and meanders in coarse-grained sediment: Bulletin of the Geological Society of America, v. 87, p. 281–285, doi:10.1130/0016-7606(1976)87<281:IOBFAM>2.0.CO;2.

Lewin, J., and Brindle, B.J., 1977, Confined meanders, *in* Gregory, K.J. ed., River Channel Changes, Chichester, UK, John Wiley and Sons, p. 221–233.

Li, C., Chen, C., Guadagnoli, D., and Georgiou, I.Y., 2008, Geometry-induced residual eddies in estuaries with curved channels: Observations and modeling studies: Journal of Geophysical Research, v. 113, p. C01005, doi:10.1029/2006JC004031.

Madricardo, F., Donnici, S., Lezziero, A., De Carli, F., Buogo, S., Calicchia, P., and Boccardi, E., 2007, Palaeoenvironment reconstruction in the Lagoon of Venice through wide-area acoustic surveys and core sampling: Estuarine, Coastal and Shelf Science, v. 75, p. 205–213, doi:10.1016/j.ecss.2007.02.031.

Madricardo, F., Tegowski, J., and Donnici, S., 2012, Automated detection of sedimentary features using wavelet analysis and neural networks on single

beam echosounder data: A case study from the Venice Lagoon, Italy: Continental Shelf Research, v. 43, p. 43–54, doi:10.1016/j.csr.2012.04.018.

Marani, M., Belluco, E., D'Alpaos, A., Defina, A., Lanzoni, S., and Rinaldo, A., 2003, On the drainage density of tidal networks: Water Resources Research, v. 39, p. 1040, doi:10.1029/2001WR001051.

Marani, M., Lanzoni, S., Zandolin, D., Seminara, G., and Rinaldo, A., 2002, Tidal meanders: Water Resources Research, v. 38, p. 7–14, doi:10.1029/2001WR000404.

Van Maren, D.S., Hoekstra, P., and Hoitink, A.J.F., 2004, Tidal flow asymmetry in the diurnal regime: Bed-load transport and morphologic changes around the Red River Delta: Ocean Dynamics, v. 54, p. 424–434, doi:10.1007/s10236-003-0085-0.

Mason, J., and Mohrig, D., 2019, Scroll bars are inner bank levees along meandering river bends: Earth Surface Processes and Landforms, v. 44, p. 2649–2659, doi:10.1002/esp.4690.

Massari, F., Grandesso, P., Stefani, C., and Jobstraibizer, P.G., 1986, A small polyhistory foreland basin evolving in a context of oblique convergence: the Venetian basin (Chattian to Recent, Southern Alps, Italy), *in* Allen, P.A. and Homewood, P. eds., Foreland basins, Oxford, UK, Blackwell Scientific Publication, p. 141–168, doi:10.1002/9781444303810.CH7.

Massari, F., Rio, D., Serandrei Barbero, R., Asioli, A., Capraro, L., Fornaciari, E., and Vergerio, P.P., 2004, The environment of Venice area in the past two million years: Palaeogeography, Palaeoclimatology, Palaeoecology, v. 202, p. 273–308, doi:10.1016/S0031-0182(03)00640-0.

McClennen, C.E., and Housley, R.A., 2006, Late-Holocene Channel Meander Migration and Mudflat Accumulation Rates, Lagoon of Venice, Italy: Journal of Coastal Research, v. 22, p. 930–945, doi:10.2112/03-0113.1.

Mel, R., Carniello, L., and D'Alpaos, L., 2019, Addressing the effect of the Mo.S.E. barriers closure on wind setup within the Venice lagoon: Estuarine, Coastal and Shelf Science, v. 225, p. 106249, doi:10.1016/j.ecss.2019.106249.

Mel, R.A., Viero, D.P., Carniello, L., Defina, A., and D'Alpaos, L., 2021, The first operations of Mo.S.E. system to prevent the flooding of Venice: Insights on the hydrodynamics of a regulated lagoon: Estuarine, Coastal and Shelf Science, v. 261, p. 107547, doi:10.1016/j.ecss.2021.107547.

Mohrig, D., Heller, P.L., Paola, C., and Lyons, W.J., 2000, Interpreting avulsion process from ancient alluvial sequences: Guadalope-Matarranya system (Northern Spain) and Wasatch formation (Western Colorado): Geological Society of America Bulletin, v. 112, p. 1787–1803, doi:10.1130/0016-7606(2000)112<1787:IAPFAA>2.0.CO;2.

Motta, D., Abad, J.D., Langendoen, E.J., and García, M.H., 2012, The effects of floodplain soil heterogeneity on meander planform shape: Water Resources Research, v. 48, p. 1–17, doi:10.1029/2011WR011601.

de Mowbray, T., 1983, The genesis of lateral accretion deposits in recent intertidal mudflat channels, Solway Firth, Scotland: Sedimentology, v. 30, p. 425–435, doi:10.1111/j.1365-3091.1983.tb00681.x.

Nanson, G.C., 1980, Point bar and floodplain formation of the meandering Beatton River, northeastern British Columbia, Canada: Sedimentology, v. 27, p. 3–29, doi:10.1111/j.1365-3091.1980.tb01155.x.

Nanson, G.C., and Page, K., 1983, Lateral accretion of fine-grained concave benches on meandering rivers, *in* Collinson, J.D. and Lewin, J. eds., Modern and ancient fluvial systems. Int. Assoc. Sedimentol. Spec. Publ., Wiley-Blackwell, v. 6, p. 133–143, doi:/10.1002/9781444303773.ch10.

Nicoll, T., 2008, Planform geometry and kinematics of confined meandering rivers on the Canadian Prairies: Simon Fraser University.

Nicoll, T.J., and Hickin, E.J., 2010, Planform geometry and channel migration of confined meandering rivers on the Canadian prairies: Geomorphology, v. 116, p. 37–47, doi:10.1016/j.geomorph.2009.10.005.

Parquer, M., Yan, N., Colombera, L., Mountney, N., Collon, P., and Caumon, G., 2019, Combined inverse and forward numerical models of fluvial meandering-channel evolution and facies distributions, *in* 34th IAS meeting of Sedimentology, v. 1.

Passalacqua, P., Lanzoni, S., Paola, C., and Rinaldo, A., 2013, Geomorphic signatures of deltaic processes and vegetation: The Ganges-Brahmaputra-Jamuna case study: Journal of Geophysical Research: Earth Surface, doi:10.1002/jgrf.20128.

Pearson, N.J., and Gingras, M.K., 2006, An Ichnological and Sedimentological Facies Model for Muddy Point-Bar Deposits: Journal of Sedimentary Research, v. 76, p. 771–782, doi:10.2110/jsr.2006.070.

Posamentier, H.W., 2003, Depositional elements associated with a basin floor channel-levee system: Case study from the Gulf of Mexico: Marine and Petroleum Geology, v. 20, p. 677–690, doi:10.1016/j.marpetgeo.2003.01.002.

Pranter, M.J., Ellison, A.I., Cole, R.D., and Patterson, P.E., 2007, Analysis and modeling of intermediate-scale reservoir heterogeneity based on a fluvial point-bar outcrop analog, Williams Fork Formation, Piceance Basin, Colorado: AAPG Bulletin, v. 91, p. 1025–1051, doi:10.1306/02010706102.

Purkait, B., 2002, Patterns of Grain-Size Distribution in Some Point Bars of the Usri River, India: Journal of Sedimentary Research, v. 72, p. 367–375, doi:10.1306/091001720367.

Rieu, R., Van Heteren, S., Van der Spek, A.J.F., and De Boer, P., 2005, Development and preservation of a mid-Holocene tidal-channel network offshore the western Netherlands: Journal of Sedimentary Research, v. 75, p. 409–419, doi:10.21110/jsr.2005.032.

Rizzetto, F., Tosi, L., Brancolini, G., Zecchin, M., Baradello, L., and Tan, C., 2009, Ancient geomorphological features in shallows of the Venice Lagoon (Italy): Journal of Coastal Research, v. 56, p. 752–756.

Roksandic, M.M., 1978, Seismic facies analysis concepts: Geophysical Prospecting, v. 26, p. 383–398, doi:10.1111/j.1365-2478.1978.tb01600.x.

Russell, C.E., Mountney, N.P., Hodgson, D.M., and Colombera, L., 2019, A novel approach for prediction of lithological heterogeneity in fluvial point-bar

deposits from analysis of meander morphology and scroll-bar pattern, *in* Ghinassi, M., Colombera, L., Mountney, N.P., and Reesink, J.H. eds., Fluvial Meanders and Their Sedimentary Products in the Rock Record. Int. Assoc. Sedimetol. Spec. Publ., v. 48, p. 385–418, doi:10.1002/9781119424437.ch15.

Sambrook Smith, G.H., Ashworth, P.J., Best, J.L., Woodward, J., and Simpson, C.J., 2006, The sedimentology and alluvial architecture of the sandy braided South Saskatchewan River, Canada: Sedimentology, v. 53, p. 413–434, doi:10.1111/j.1365-3091.2005.00769.x.

Silvestri, S., D'Alpaos, A., Nordio, G., and Carniello, L., 2018, Anthropogenic Modifications Can Significantly Influence the Local Mean Sea Level and Affect the Survival of Salt Marshes in Shallow Tidal Systems: Journal of Geophysical Research: Earth Surface, v. 123, p. 996–1012, doi:10.1029/2017JF004503.

Skelly, R.L., Bristow, C.S., and Ethridge, F.G., 2003, Architecture of channel-belt deposits in an aggrading shallow sandbed braided river: The lower Niobrara River, northeast Nebraska: Sedimentary Geology, v. 158, p. 249–270, doi:10.1016/S0037-0738(02)00313-5.

Slingerland, R., and Smith, N.D., 1998, Necessary conditions for a meandering-river avulsion: Geology, v. 26, p. 435–438, doi:10.1130/0091-7613(1998)026<0435:NCFAMR>2.3.CO;2.

Slingerland, R., and Smith, N.D., 2004, River Avulsions and Their Deposits: Annual Review of Earth and Planetary Sciences, v. 32, p. 257–285, doi:10.1146/annurev.earth.32.101802.120201.

Smith, D.G., Hubbard, S.M., Lavigne, J.R., Leckie, D.A., and Fustic, M., 2011, Stratigraphy of counter-point-bar and eddy-accretion deposits in low-energy meander belts of the Peace-Athabasca Delta, northeast Alberta, Canada, *in* Davidson, S.K., Leleu, S., and North, C.P. eds., From River to Rock Record: The preservation of fluvial sediments and their subsequent interpretation, SEPM Special Publication, p. 143–152, doi:10.2110/sepmsp.097.143.

Smith, D.G., Hubbard, S.M., Leckie, D.A., and Fustic, M., 2009, Counter point bar deposits: Lithofacies and reservoir significance in the meandering modern peace river and ancient McMurray formation, Alberta, Canada: Sedimentology, v. 56, p. 1655–1669, doi:10.1111/j.1365-3091.2009.01050.x.

Strick, R.J.P., Ashworth, P.J., Awcock, G., and Lewin, J., 2018, Morphology and spacing of river meander scrolls: Geomorphology, v. 310, p. 57–68, doi:10.1016/j.geomorph.2018.03.005.

Tambroni, N., Luchi, R., and Seminara, G., 2017, Can tide dominance be inferred from the point bar pattern of tidal meandering channels? Journal of Geophysical Research: Earth Surface, v. 122, p. 492–512, doi:10.1002/2016JF004139.

Taylor, C.F.H., 1999, The role of overbank flow in governing the form of an anabranching river: the Fitzroy River, northwestern Australia, *in* Smith,

N.D. and Rogers, J. eds., Fluvial Sedimentology VI. Special Publication of the International Association of Sedimentologists, Wiley Online Library, v. 28, p. 77–91, doi:10.1002/9781444304213.ch7.

Tognin, D., D'Alpaos, A., Marani, M., and Carniello, L., 2021, Marsh resilience to sea-level rise reduced by storm-surge barriers in the Venice Lagoon: Nature Geoscience, v. 14, p. 906–911, doi:10.1038/s41561-021-00853-7.

Tommasini, L., Carniello, L., Ghinassi, M., Roner, M., and D'Alpaos, A., 2019, Changes in the wind-wave field and related salt-marsh lateral erosion: inferences from the evolution of the Venice Lagoon in the last four centuries: Earth Surface Processes and Landforms, v. 44, p. 1633–1646, doi:10.1002/esp.4599.

Toonen, W.H.J., Kleinhans, M.G., and Cohen, K.M., 2012, Sedimentary architecture of abandoned channel fills: Earth Surface Processes and Landforms, v. 37, p. 459–472, doi:10.1002/esp.3189.

Tosi, L., Rizzetto, F., Zecchin, M., Brancolini, G., and Baradello, L., 2009, Morphostratigraphic framework of the Venice Lagoon (Italy) by very shallow water VHRS surveys: Evidence of radical changes triggered by human-induced river diversions: Geophysical Research Letters, v. 36, p. 1–5, doi:10.1029/2008GL037136.

Townend, I., 2010, An exploration of equilibrium in Venice Lagoon using an idealised form model: Continental Shelf Research, v. 30, p. 984–999, doi:10.1016/j.csr.2009.10.012.

Visher, G.S., 1964, Fluvial processes as interpreted from ancient and recent fluvial deposits: AAPG Bulletin, v. 48, p. 550.

Walker, R.G., 1992, Facies, facies models and modern stratigraphic concepts, *in* Walker, R.G. and James, N.P. eds., Facies models: Response to sea-level change, Toronto, Geological Association of Canada, p. 272–14.

Walton, T.L., 2002, Tidal velocity asymmetry at inlets:

Willis, B.J., 1989, Palaeochannel reconstructions from point bar deposits: a three-dimensional perspective: Sedimentology, v. 36, p. 757–766, doi:10.1111/j.1365-3091.1989.tb01744.x.

Willis, B.J., and Sech, R.P., 2018a, Emergent facies patterns within fluvial channel belts, *in* Ghinassi, M., Colombera, L., Mountney, N.P., Reesink, A.J.H., and Bateman, M. eds., Fluvial Meanders and Their Sedimentary Products in the Rock Record. Int. Assoc. Sedimentol. Spec. Publ., John Wiley & Sons, Ltd, v. 48, p. 509–542, doi:10.1002/9781119424437.ch19.

Willis, B.J., and Sech, R.P., 2018b, Quantifying impacts of fluvial intra-channel-belt heterogeneity on reservoir behaviour, *in* Ghinassi, M., Colombera, L., Mountney, N.P., and Reesink, A.J.H. eds., Fluvial Meanders and Their Sedimentary Products in the Rock Record (Int. Assoc. Sedimentol. Spec. Publ. 48), John Wiley & Sons, p. 543–572, doi:10.1002/9781119424437.ch20.

Willis, B.J., and Tang, H., 2010, Three-Dimensional Connectivity of Point-Bar Deposits: Journal of Sedimentary Research, v. 80, p. 440–454, doi:10.2110/jsr.2010.046.

Yan, N., Colombera, L., Mountney, N.P., and Dorrell, R.M., 2019, Fluvial point-bar architecture and facies heterogeneity, and their influence on intra-bar static connectivity in humid coastal-plain and dryland fan systems, *in* Ghinassi, M., Colombera, L., Mountney, N.P., and Reesink, A.J.H. eds., Fluvial Meanders and Their Sedimentary Products in the Rock Record (IAS SP 48), John Wiley & Sons, p. 475–508, doi:10.1002/9781119424437.ch18.

Yan, N., Mountney, N.P., Colombera, L., and Dorrell, R.M., 2017, A 3D forward stratigraphic model of fluvial meander-bend evolution for prediction of point-bar lithofacies architecture: Computers and Geosciences, v. 105, p. 65–80, doi:10.1016/j.cageo.2017.04.012.

Zecchin, M., Baradello, L., Brancolini, G., Donda, F., Rizzetto, F., and Tosi, L., 2008, Sequence stratigraphy based on high-resolution seismic profiles in the late Pleistocene and Holocene deposits of the Venice area: Marine Geology, v. 253, p. 185–198, doi:10.1016/j.margeo.2008.05.010.

5

INTEGRATED ANALYSES OF POINT-BAR SEDIMENT TEXTURAL PROPERTIES

This chapter is published as a paper in *Journal of the Geological Society* (2022, doi: 10.1144/jgs2021-156) under the title "From electromagnetic to sediment textural maps: an integrated approach to unravel the intra-point-bar variability of sediment properties".

E.B., D.T and J.B. designed the study. E.B., D.T. and M.G. developed the methodology. E.B., J.B. and M.G. collected the data. E.B. annotated and maintained the research data. E.B. was responsible for data creation and presentation. E.B. and M.G. were the project administrator. A.F. provided a designed code. J.B and G.C. applied computational techniques to analyse study data. J.B, R.L. and M.G. provided the instrumentation and analysis tools. A.F. and A.D. verified the reproducibility of the results. All the authors discussed the data and agree on their interpretation. E.B. and J.B. wrote the original draft. D.T., R.L., A.D., G.C., A.F. and M.G. provided comments and suggestions to improve the original draft. All the co-authors contributed to the final polishing of the manuscript. A.D. and M.G. were responsible for the research activity. M.G. acquired the financial support for the project.

From electromagnetic to sediment textural maps: an integrated approach to unravel the intra-point-bar variability of sediment properties

Elena Bellizia[1], Davide Tognin[2], Jacopo Boaga[1], Giorgio Cassiani[1], Riccardo Leardi[3], Alvise Finotello[4], Andrea D'Alpaos[1], Massimiliano Ghinassi[1]

[1] Department of Geosciences, University of Padova, Via G. Gradenigo 6, IT-35131 Padova, Italy
[2] Department of Civil, Environmental and Architectural Engineering, University of Padova, Via Marzolo 9, IT-35131 Padova, Italy
[3] Department of Pharmacy, University of Genova, Viale Cembrano 4, IT-16148 Genova, Italy
[4] Department of Environmental Sciences, Informatics, and Statistics, Ca' Foscari University of Venice, via Torino 155, Mestre, Venice, IT-30172, Italy

ABSTRACT

Sedimentary sand bodies that originated by the evolution of meandering channels, such as point bars, host surficial aquifers, providing preferential pathways for groundwater flow in mud-dominated floodplains. These aquifers are a major source of freshwater, yet they can suffer from different environmental issues such as pollution and salt-water intrusion, which can critically damage agriculture and socio-economical activities. Understanding the internal architecture of point-bar bodies is essential to plan proper aquifer management and address environmental issues in coastal plains.

To provide a spatially extensive, cost-effective characterisation of point-bar body architecture, this work proposes a multidisciplinary approach to investigate geophysical and sedimentological data through statistical analyses, with an application to two purely fluvial paleo-meanders in the Venetian Plain, Italy. In this setting, point-bar deposits mainly consist of fine to coarse sand and display lower electromagnetic conductivity values compared to the surrounding muddy overbank deposits. Statistical multivariate analyses on sedimentological and geophysical properties overcome the qualitative direct dependence of electromagnetic conductivity on sediment grain size alone, highlighting a stronger relationship with sediment sorting. By calibrating this relationship on a reasonable number of samples representative of the different depositional bodies, this methodology finally provides maps of sediment textural properties at the meander scale.

5.1 Introduction

In coastal plains, natural rivers shape landscapes, through erosional and depositional processes, and lead to the accumulation of channelised sand bodies, such as channel bars, levees, crevasse splays, within mud-dominated sedimentary successions (Allen, 1965; Khan et al., 1997; Bridge, 2003; Piovan et al., 2012). Among these sand bodies, point-bar deposits, that originated through the evolution of meandering channels, are the major sedimentary units (i.e. with well-defined boundaries within muddy successions). Point bars can grow experiencing different planform behaviours (Daniel, 1971; Brice, 1974; Jackson, 1976), which, together with the helical flows that develop as the sinuosity increases (Bagnold, 1960; Dietrich, 1987), define a wide spectrum of vertical and along-bend changes in sediment properties and sedimentary facies distribution (e.g. Allen 1965, 1970; Bluck 1971; Jackson 1976; Nanson 1980; Bridge *et al.* 1995; Makaske and Weerts 2005; Willis and Tang 2010; Ghinassi *et al.* 2014; Ielpi and Ghinassi 2014; Wu *et al.* 2015; Hagstrom *et al.* 2019). For this reason, point-bar deposits are characterised by variable sediment grain sizes and sorting, along with broad ranges of connectivity between their internal strata (Bowling et al., 2007). However, point-bar deposits are generally characterised by relatively coarser sediment when compared to the surrounding overbank deposits, appearing, therefore, as the most permeable bodies in coastal-plain sedimentary successions. Accordingly, they constitute the preferential pathways for groundwater flows and, thus, host surficial aquifers (i.e. upper 10 m of the subsurface), which represent an important freshwater source in coastal areas. The availability of clean, easily-accessible groundwater, together with the fertile soils and the flat topography of floodplains where these aquifers are hosted, contribute to making coastal areas particularly suitable for urbanisation, agricultural and industrial activities (Boyer et al., 2006; Amorosi et al., 2013). However, coastal surficial aquifers often suffer from saltwater intrusion (Da Lio et al., 2015; Nofal et al., 2015) and pollutant propagation (Harvey et al., 2006; Benner et al., 2008; Carraro et al., 2013; Desbarats et al., 2014), which severely damage groundwater quality, and thus agricultural and other socio-economical activities (e.g. pumping of drinking water). Therefore, there is a pressing need to better understand the internal architecture and the sediment texture of fluvial point-bar bodies to enhance current strategies for aquifer management.

To reconstruct the internal anatomy of point-bar bodies developed in coastal areas, and to understand the related groundwater flow patterns, planform geometries and bar-growth patterns need to be considered. Planform

geometries can be readily traced from aerial photos and satellite images (Wray, 2009; Rossetti, 2010; Giacomelli et al., 2018) and, when scroll-bar patterns are visible, the planform evolution of single bends can also be reconstructed (e.g. Strick *et al.* 2018). Once point-bar deposits are identified through remote sensing analysis, their sedimentological characterisation can be performed by the recovery of sedimentary cores, although this approach is generally time-consuming and spendthrift, and provides only localised information (Baines et al., 2002).

To overcome these limitations, it is possible to combine remote-sensing and sedimentological investigations with geophysical surveys and statistical analyses. This kind of approach provides a unique opportunity to integrate planform geometries with sedimentological data related to the spatial distribution of sedimentary features, including grain size, sorting, and sedimentary facies (Giacomelli et al., 2018; Clift et al., 2019; Bellizia et al., 2021). A predictive, spatially explicit, cost-effective approach would represent a key contribution to analyse the 3D variability of sediment properties, such as grain size and sorting, at the bend scale in meandering-river deposits. This can be extremely useful to predict groundwater flows within point-bar deposits and thus mitigate the effect of environmental threats.

This work proposes an integrated approach encompassing geophysical, sedimentological, and multivariate statistical analyses, and applies it to analyse the variability of texture properties of two paleo-meanders wandering through the Venetian Plain (Italy). In particular, this research focuses on the intra-point-bar variability of sediment grain size and sorting, two key textural quantities which are commonly used to characterise the flow within sedimentary bodies (Weber, 1982; Beard and Weyl, 1993; Willis and Tang, 2010; Willis and Sech, 2018b). The ultimate goal of this study is: (1) to apply an integrated, innovative approach to establish quantitative relationships between sediment properties and electrical conductivity of the subsurface; (2) to discuss results in terms of sedimentary dynamics affecting the study bars and related implications for understanding ancient point-bar deposits. Results provide a spatially extensive, cost-effective methodology, that might potentially be extended beyond the study cases, to characterise channel deposits.

5.2 Setting

The study area is located south of the Venice Lagoon in the southern-east portion of the Venetian Plain, NE Italy (Fig. 5.1). The southern Venetian Plain is part of the foreland basin located between the Apennines and the Southern Alps (Massari et al., 1986), and has recorded the Quaternary deposition of the north Adriatic coast. During the Last Glacial Maximum (LGM), when the coastline of the Adriatic Sea retreated southward hundreds of km, the area experienced a general aggradation thanks to the large amount of sediment produced in the glacial areas (Mozzi, 2005; Fontana et al., 2008, 2010). Successively, between 17000 and 9000 yrs. cal. BP, the fluvial activity was confined within incised valleys (Fontana et al., 2008). From that onward, a marine transgression occurred (i.e. post-glacial sea-level rise), and a highstand phase led to the upbuilding of the main alluvial ridges in the plain (Favero and Serandrei Barbero, 1980), including the Po and Adige Rivers, whose combined evolution built up the southern Venetian Plain (Mozzi, 2005; Piovan et al., 2012). Branches of these rivers, along with numerous minor channel belts, defined an alluvial network flowing towards the east (Rizzetto et al., 2002, 2003) that delivered sand to the Adriatic Sea. Where no channel-related deposition occurred, swamps and marshlands developed, filling up lowland areas with organic-rich muddy deposits. Alluvial sedimentary products are still visible from aerial and satellite images, thanks to the differences in colours of the cropmarks triggered by different degrees of soil moisture (Cassiani et al., 2020).

The selected study site, of about 0.3 km^2, is in the Chioggia Town countryside (Fig. 5.1B) and lies down to almost 2 m below current sea level. Stratigraphic investigations reveal that almost 4500 yrs. BP the coastline reached the studied area from west, and it later moved eastward following the relevant fluvial sediment input (Favero and Serandrei-Barbero, 1978; Bondesan et al., 2001). The study cases are two adjacent paleo-meanders (M1 and M2) (Fig. 5.1C) that belong to the Brenton channel belt, an older course of the Medieval Brenta River that was active between the 4^{th} and the 16^{th} century AD (Bondesan and Furlanetto, 2012). Nowadays, traces of this belt can be followed for about 15 km from Correzzola (PD, NE Italy) to Punta Gorzone in Chioggia Town (VE, NE Italy) (Fig. 5.1B).

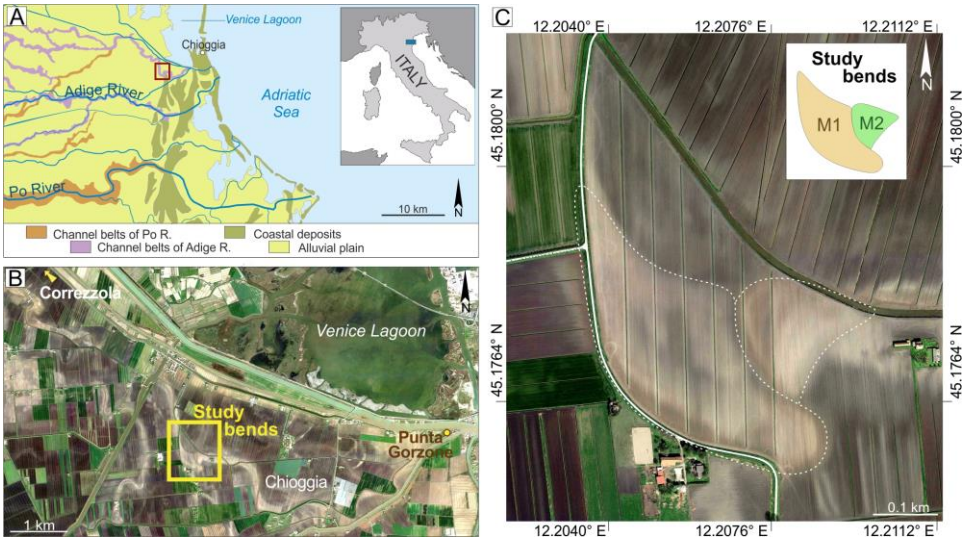

Fig. 5.1. Location of the study area (red square) in the southern Venetian Plain and Po Delta areas (Italy), with main geomorphological elements (A): satellite zoom of the southern Venetian Plain (B) (Map data: ©2015 Google-Landsat/Copernicus, Maxar Technologies), where signatures of paleochannels are still visible from satellite images. (C) Study bends, named M1 and M2, in a Google Earth image of March 2015 (Map data: ©2015 Google-Landsat/Copernicus, Maxar Technologies).

5.3 Method

To develop the research methodology applied here, the required data sets are: (1) satellite images, to identify different depositional elements and reconstruct their morphologies; (2) geophysical data, to detect the electromagnetic properties of the subsurface; (3) sedimentological and grain-size data, to characterise the deposits. Statistical analyses were used to determine relationships between different data sets. The terminology adopted in this paper, to describe morphologies and deposits of the study cases is shown in Figure 5.2A.

Satellite images acquired at different years, where cropmarks highlight paleohydrographic traces of the ancient meanders (e.g. Figs 5.1C and 5.2B), were used to characterise geomorphological elements, and reconstruct morphologies and planform evolution of the investigated paleo-meanders.

Electromagnetic Induction (EMI) surveys in the frequency domain (FDEM) were performed in the selected area to estimate the electrical conductivity of the subsurface (Corwin and Rhoades, 1982). Geophysical investigations were carried out when the fields were not cultivated, to prevent the influence of water irrigation on the electromagnetic response. Geophysical data were collected by using a GF Instruments CMD-Explorer probe ("GF Instruments s.r.o."), which is a

multi-coil system that allows estimating the apparent electrical conductivity at different depths up to almost 7 m, by operating in two configurations (i.e. horizontal [HMD] and vertical [VMD] magnetic dipoles) (Um and Alumbaugh, 2007) and passing twice through the same location. The FDEM probe was connected to a Trimble 5800 GPS for continuous position measurements, and dragged by a small tractor once fixed to a wooden sled that was designed to keep constant the probe height from the ground (see Cassiani et al., 2020 for further details). The selected area was investigated by collecting more than 30.000 FDEM data points, which were then inverted to obtain electrical conductivity values of the subsurface by using the EMagPy, a Python-based open-source software for 1D EMI inversion (McLachlan et al., 2021). EMagPy allows for a variety of forward and inverse model approaches, with full control by the user. In particular, the code is equipped with an option to conduct Full Solution (FS) of the Maxwell equations, a feature not commonly available in commercial EMI inversion software. For the case at hand, the inversion was performed using an FS low-induction number approach (FS_{LIN}) with no Eca linear correction (see McLachlan et al., 2021, for details). In this study, I inversion was constrained to produce 8 layers including an infinite bottom layer from 7.5 metres down. Data were imported into the GIS software ArcMap (version 10.7.1) and their interpolation through the natural neighbour tool provided 2D horizontal conductivity maps at different depths, with average electrical conductivity values σ (mS/m) for depth intervals of 1 m, apart from the first one (i.e. 0 – 1.5 m depth). 2D maps provided information about the spatial variability of electrical conductivity values in M1 and M2 bodies, up to a depth of almost 5 m. Maps at higher depths were not considered as they were too close to the instrument acquisition limit.

In this study, thirty-three sedimentary cores were recovered to analyse sedimentary features of the study deposits (Fig. 5.2B). A continuous drilling core sampler with a rotary technique was used to collect six cores with a diameter of 10 cm, up to 9 m-long, that were recovered in the upstream, central, and downstream portions of M1 and M2 (red dots in Fig. 5.2). The remaining twenty-seven cores were recovered through a 1 m-long gouge sampler and are up to 4 m long and 3 cm in diameter (black dots in Fig. 5.2). They were collected after the electromagnetic survey to better characterise deposits with different conductivity responses. All cores were cut longitudinally and logged in detail to highlight the variability of grain size and sedimentary structures. Fifty samples, covering the sediment grain-size variability of the study area, were collected for

grain-size analyses, which were performed by dry sieving. This procedure determines the fraction of the six diameter classes and the amount of sediment passing through the sieve with the narrowest mesh. The seven classes are representatives of the following grain sizes: (1) gravel (>2 mm); (2) very coarse sand (2-1 mm); (3) coarse sand (1-0.5 mm); (4) medium sand (0.5-0.25 mm); (5) fine sand (0.25-0.125 mm); (6) very fine sand (0.125-0.063 mm); (7) mud (<0.063 mm). From this data, cumulative curves were obtained.

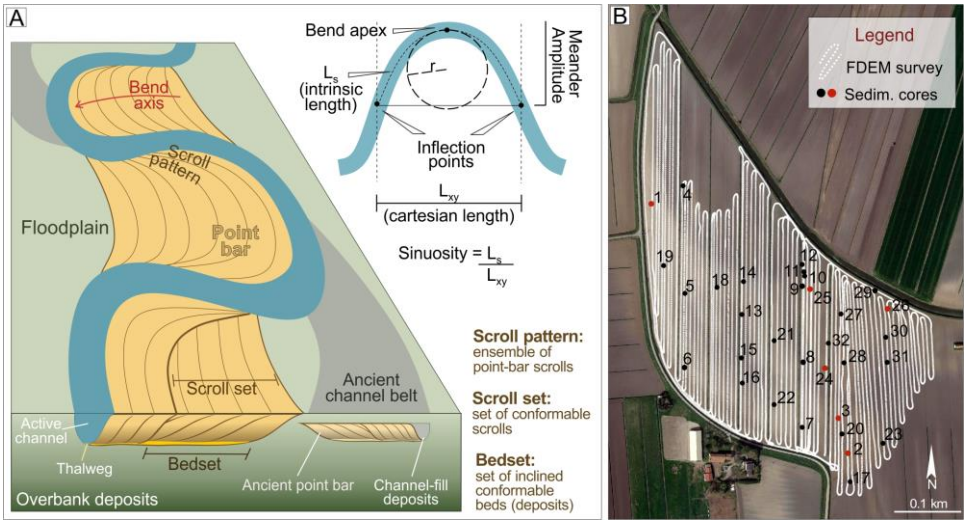

Fig. 5.2. Terminology and methodology. (A) Morphological, depositional, and morphometric terminology adopted in this paper. (B) In small white dots, the survey path of the Frequency Domain Electromagnetics (i.e. FDEM) acquisition; in black and red dots, the sedimentary cores recovered with hand auger and rotary technique, respectively (Map data: ©2015 Google-Landsat/Copernicus, Maxar Technologies).

The MATLAB (R2020b version) software was used for statistical purposes; a Principal Component Analysis (PCA) (Davies, 1992) was performed on the fifty grain-size data described by the seven grain-size variables (50 rows, 7 columns) to find out a limited number of variables reducing the dimensionality of the dataset while maintaining all relevant statistical information on multivariate independent components that can describe the sediment properties of the different depositional elements. The quantitative relationships that allow predicting variability of sediment properties were finally calculated. They were obtained by fitting a linear regression model to the electrical conductivity values of the grain-size samples and their PCA scores. The obtained relationships were applied to all the acquired electromagnetic inverted data to visualise 2D maps of the sediment properties. Linear regression models between PCs and traditional

sedimentological parameters were also calculated to make the interpretation of PCs maps in terms of practical sedimentological meaning easier.

5.4 Results

A brief description of the planform evolution of the study bends based on satellite images will provide the base to frame results obtained from the individual geophysical and sedimentological investigations, and those related to their statistical analysis.

5.4.1 Morphology and planform evolution

Satellite images allow one to distinguish three main geomorphological elements: overbank, abandoned channel fill, and point bars. The abandoned channel fill is ca. 20 m wide and separates point bars associated with bends M1 and M2 (Fig. 5.3A-B). The study paleo-meanders are surrounded by overbank deposits where other ancient paleochannel traces can be locally recognised (Fig. 5.3A-B). M1 is a wide, strongly asymmetric bend, characterised by an amplitude and an estimated riffle-to-riffle distance of about 300 m and 450 m, respectively. This bend occurs at the end of a 1 km long straight reach, has an estimated sinuosity of 2, and a radius of curvature of about 45 m, thus being a relatively sharp bend. M2 is an open, poorly asymmetric bend, showing both amplitude and riffle-to-riffle distance of about 200 m. It has an estimated sinuosity of 2 and a radius of curvature of 60 m. While the M2 bend expanded almost gradually maintaining a SE-NW trending axis, M1 was characterised by a complex evolution that brought the bend axis to finally trend WNW-ESE. Planform evolution of the two-study bends occurred through a combination of expansion and rotation processes and is summarised in Figure 5.3.

5.4.2 Electrical conductivity maps

The electric-conductivity maps allow one to differentiate in-channel and overbank elements and fit well with the geomorphic elements highlighted by satellite images, along with some minor older channelised units (Fig. 5.4F). The M1 and M2 point bars can be identified at different depths as the least conductive bodies (i.e. lower σ), whereas overbank areas are the most conductive ones (i.e. higher σ). Channel-fill deposits are more conductive than point-bar areas, but less than overbank ones. The range of electrical conductivity is generally higher in the first 3 metres below the ground level compared to deeper layers. Specifically, in the upper 3 m, the overbank areas

show conductivity values higher than 160 mS/m, the channel-fill body varies from 160 to 90 mS/m and point-bar bodies vary from 90 to 50 mS/m (Fig. 5.4A-C).

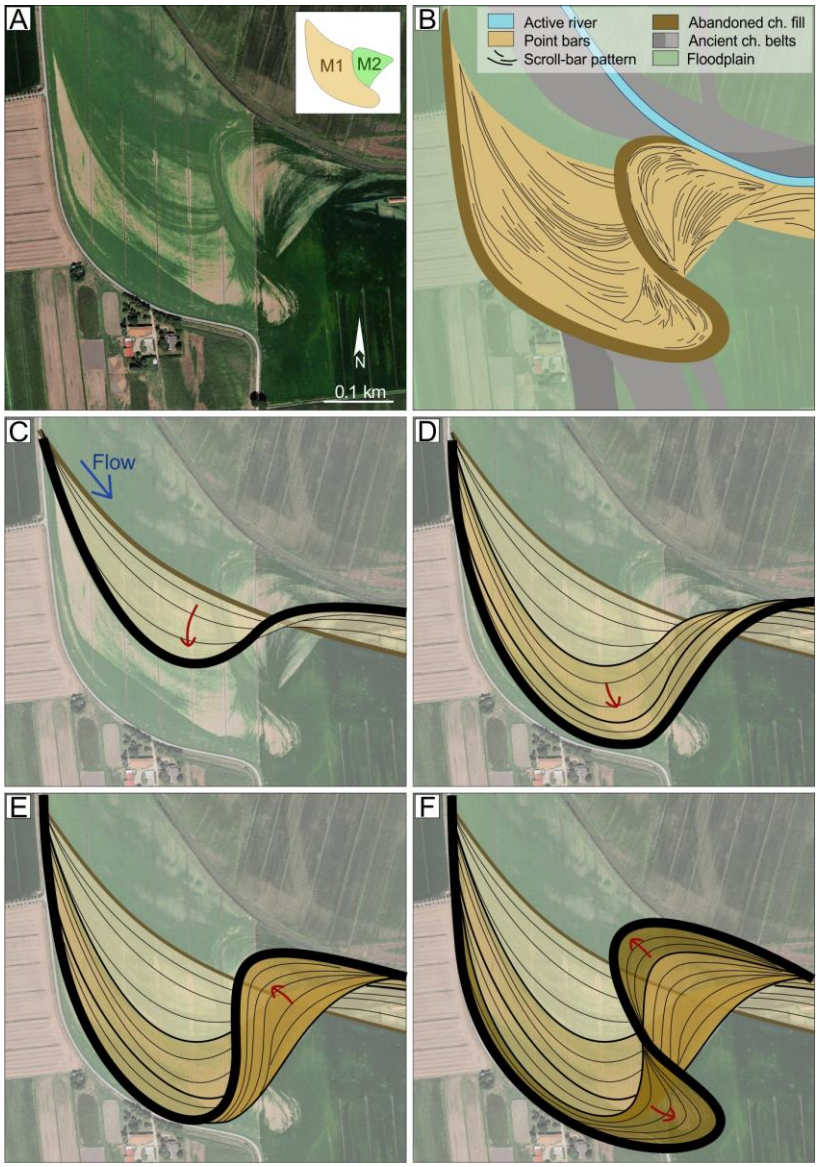

Fig. 5.3. Morphologies and planform evolution of the study bends. (A) Satellite image from Google Earth (Map data: ©2013 Google-Landsat/Copernicus, Maxar Technologies) of the area (B) and interpretation of morphologies and surrounding environment. (C-E) Planform evolution of M1 and M2; (C) from an almost straight starting pattern (brown line), (D) M1 migrated with an expansional transformation style, coupled with rotation and (E) M2 developed partially eroding M1 deposits and causing the rotation of the system which led to a marked channel relocation in M1 bend. (F) Then, both M1 and M2 expanded until the channel abandonment, with M1 experiencing a rotation of the bend apex and partially eroding previously accumulated deposits. Arrows indicate the vector of point-bar accretion.

The electrical conductivity varies significantly within the M1 point bar, whereas is quite uniform within the M2 point-bar body. Specifically, within the M1 point bar, upstream and apex zones exhibit the lowest conductivity values (60 > σ > 50 mS/m). The scroll pattern is clearly highlighted by changes in conductivity values (Fig. 5.4A--C), also revealing areas with the highest conductivity values (i.e. 80-90 mS/m) within the point bar (Fig. 5.4F). At the deepest maps (i.e. 3 to 5 m), conductivity values in overbank areas range between 170 and 90 mS/m, the channel-fill body varies from 90 to 50 mS/m, and point-bar bodies are always lower than 50 mS/m (Fig. 5.4D-E). Variability within the M1 point bar decreases as the depth increases, even if upstream and central zones are still characterised by the lowest electrical conductivity values (σ < 30 mS/m). The M2 point bar shows uniform conductivity values (Fig. 5.4D-E).

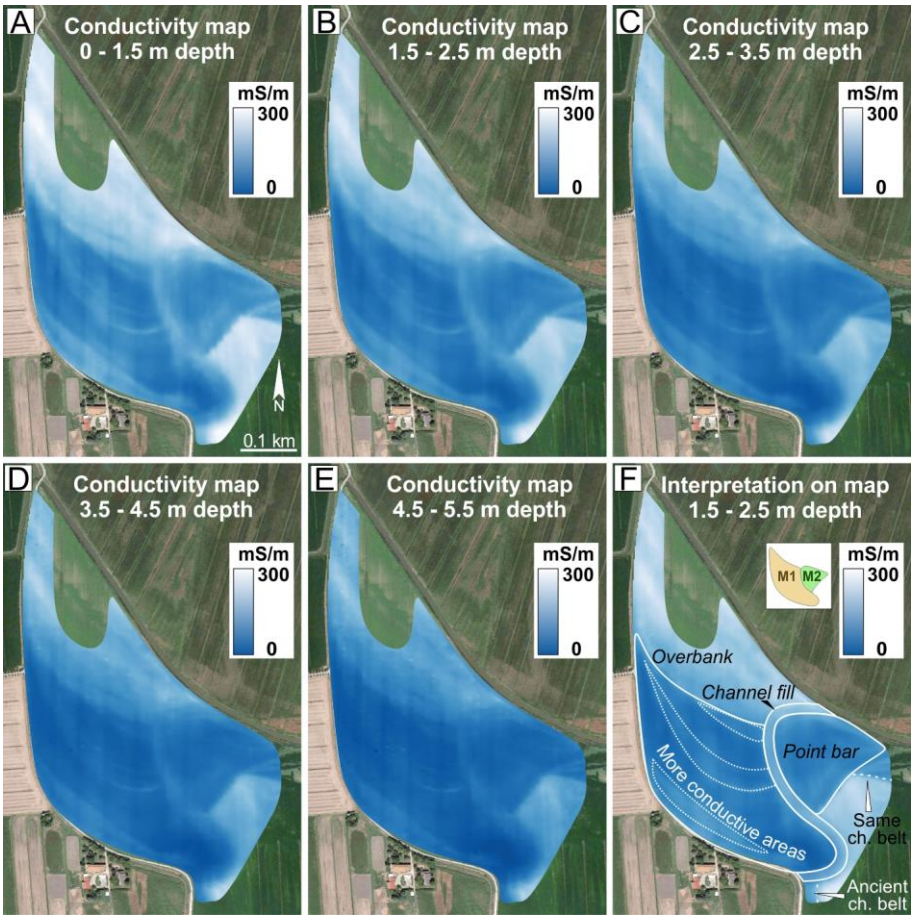

Fig. 5.4. 2D electrical conductivity maps of the 5 depth layers (A-E) on a Google earth image (Map data: ©2013 Google-Landsat/Copernicus, Maxar Technologies), showing differences both between overbank and point-bar bodies, and inside the M1 point-bar body (F).

5.4.3 Sedimentological analyses

Sedimentary cores reveal that at least the first 50 cm below the ground surface are made of structureless mud with a variable amount of fine sand, which is seasonally reworked by agricultural activities (Fig. 5.5A). Overbank deposits consist of poorly laminated mud (Fig. 5.5B) alternated to 10 to 50 cm-thick layers of organic-rich silty clay with wood fragments and plant debris (Fig. 5.5C). Sandy intercalations are common as depth increases and consist of 1-5 cm-thick layers of fine to medium sand. Abandoned channel-fill deposits are made of fine to medium sand, grading upward to organic-rich silt (Fig. 5.5E). In the upper part of the channel-fill deposits oxidised silty layers are common (Fig. 5.5D). Point-bar deposits are up to 6 m thick in the downstream and central sides of the bars, whereas they are 4.5 m thick in upstream portions close to riffle zones (Fig. 5.5A). Although the primary sediment fabric was altered by coring processes, the best-preserved portions mainly consist of fine to coarse sand with plane-parallel stratification (Fig. 5.5G). Upper bar deposits are locally heterolithic, but mainly made of oxidised fine to medium, ripple-cross laminated sands (Fig. 5.5F). Channel-lag deposits underlie the bar bodies and consist of medium to coarse sand with mudclasts and shell fragments (Fig. 5.5H), covering both sand and organic-rich mud. Sandy deposits are comparable with those of the investigated bars suggesting they also probably formed in a channelised setting. Core data reveal that the central and downstream sides of both M1 and M2 point bars show a weak fining upward succession from medium-coarse to fine sand, whilst upstream sides exhibit a blocky (sensu Willis, 1989) to gently coarsening upward trend.

5.4.4 Statistical analyses

PCA results are summarised in Figure 5.6, where the loading and score plots are related to the first two significant components, hereinafter named as PC1 and PC2, which together explain about 75% of the variance of the samples (44.3% PC1, 30.4% PC2). The loading plot shows that grain sizes greater than medium sand have positive loadings on PC1, while finer grain sizes (i.e. from fine sand to mud) have negative ones (Fig. 5.6A). In terms of PC2, fine and medium sand exhibits positive loadings, while the others are characterised by negative loadings (Fig. 5.6A). Grain-size cumulative curves show a gradual increase in PC1 values as sediments become coarser (Fig. 5.6B), whereas steeper and gentler curves show the highest and lowest PC2 values, respectively (Fig. 5.6C).

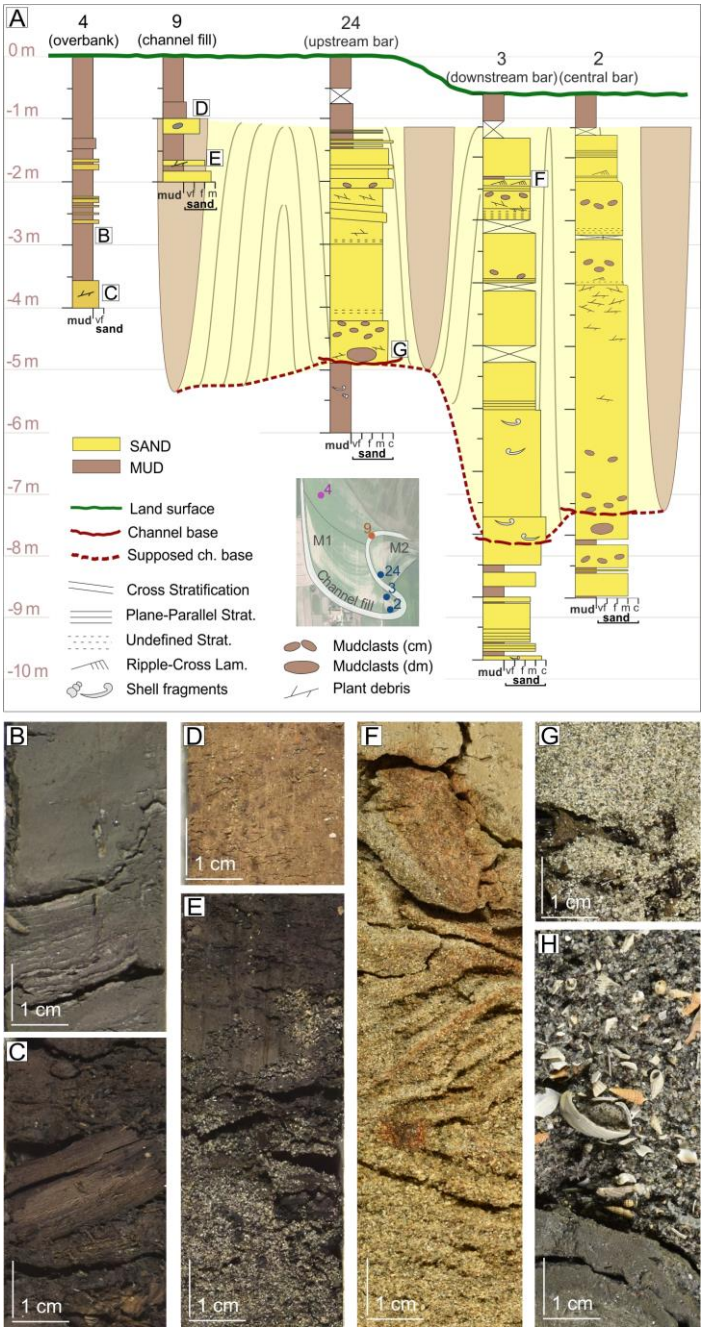

Fig. 5.5. Sedimentary cores. (A) Location (Map data: ©2013 Google-Landsat/Copernicus, Maxar Technologies) and logs of 5 sedimentary cores representing the main depositional elements, where point bars are analysed in upstream, central and downstream bar cores with a schematic representation of paleochannel deposits; (B-G) Deposits of the depositional elements. (B-C) Overbank deposits: (B) poorly laminated clay, (C) organic-rich mud with plant debris. (D-E) Abandoned channel-fill deposits: (D) silty clay and (E) organic-rich silt grading downward to fine sand. (F-H) Point-bar deposits: (F) oxidised mud grading downward to ripple-cross laminated sand, in the upper bar, (G) a fine sand body with plant debris, and (H) shell-rich sandy channel lag.

The score plot yields a clear separation between point-bar and channel-fill/overbank samples (Fig. 5.6D). The latter forms a tight group at negative scores of both components (blue and brown dots, Fig. 5.6D), whereas the former forms a wide cloud (green dots, Fig. 5.6D); with upstream-bar samples mainly having positive scores on PC1 and negative ones on PC2, and downstream-bar samples having PC1 scores around the zero score and positive PC2 ones. PC1 and PC2 scores of central-bar samples do not clearly differ from the upstream and downstream ones together.

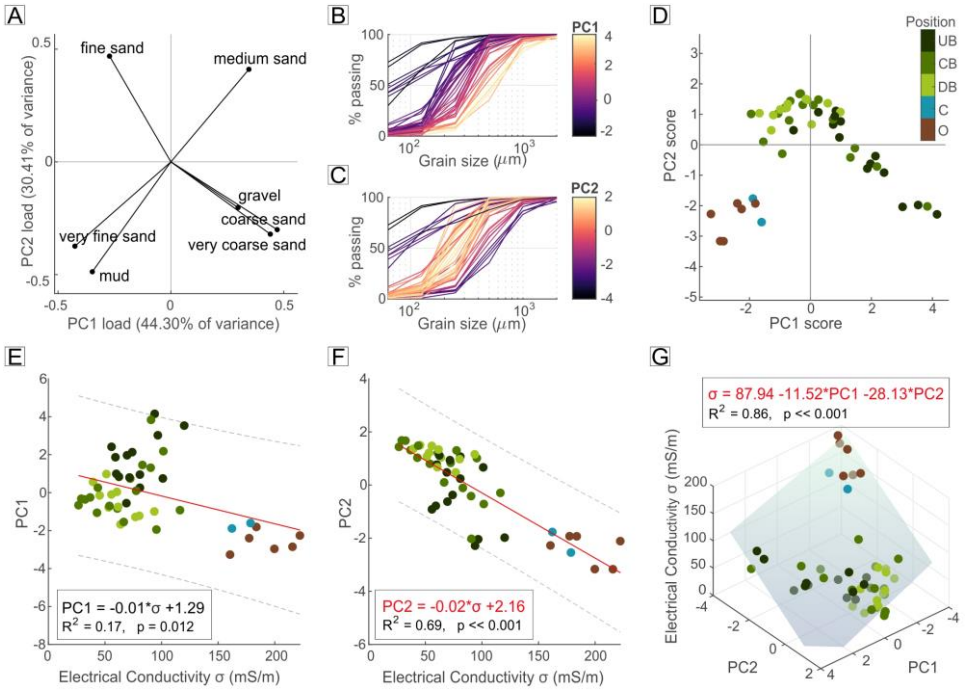

Fig. 5.6. Statistical results; PCA (A-D) and modelling results (E-G). (A) Loading plot of the 7 grain-size variables. (B-C) Cumulative curves of the grain-size samples with colour scale to understand the physical meaning of the 2 Principal Components. (D) Score plot of the grain-size samples represented with different colours based on their location in the study area: UB, CB, DB stand for Upstream, Central and Downstream Bar; C for the abandoned Channel fill, O stands for Overbank. (E-F) Linear relationships between the electrical conductivity and (E) PC1 scores of the grain-size samples, and (F) PC2 scores of analysed samples. (G) The polynomial relationship linking electrical conductivity to PC1 and PC2.

Fitting a linear model, the electrical conductivity is significantly related to PC1 (p-value = 0.012) but the relationship is weak (i.e. has a poor descriptive character [R^2 = 0.17]) (Fig. 5.6E). On the contrary, the relationship with PC2 is statistically significant and strong (i.e. moderate to high descriptive power) (p-

value << 0.001, R^2 = 0.69) (Fig. 5.6F). PC2 linearly decreases as electrical conductivity increases, following the relationship:

$$PC2 = -0.02 \times \sigma + 2.16 \quad (1)$$

Moreover, variations of electrical conductivity due to both PC1 and PC2 are captured by a linear polynomial relationship:

$$\sigma = 84.94 - 11.52 \times PC1 - 28.13 \times PC2 \quad (2)$$

which is significant and strong (p-value << 0.001, R^2 = 0.86) (Fig. 5.6G) and, therefore, can be used to extrapolate PC1 given the electrical-conductivity and PC2 values, the latter obtained with equation 1.

The spatial distributions of PC1 and PC2 (Fig. 5.7), derived from equations 2 and 1 respectively, show the same morphological patterns of electrical-conductivity maps, with overall high PC1 and PC2 values where electric conductivity is low, and vice versa. For instance, at each depth layer, PC2 < -2 and PC1 < 0 are found in overbank areas, -1 > PC2 > -2 and 0 > PC1 > -1 belong to abandoned channel-fill portions, and PC2 > -1 and PC1 > 0 can be found in point-bars areas, where PC2 = 2 and PC1 = 3 are found only in the youngest portions of M1 point bar (Fig. 5.7).

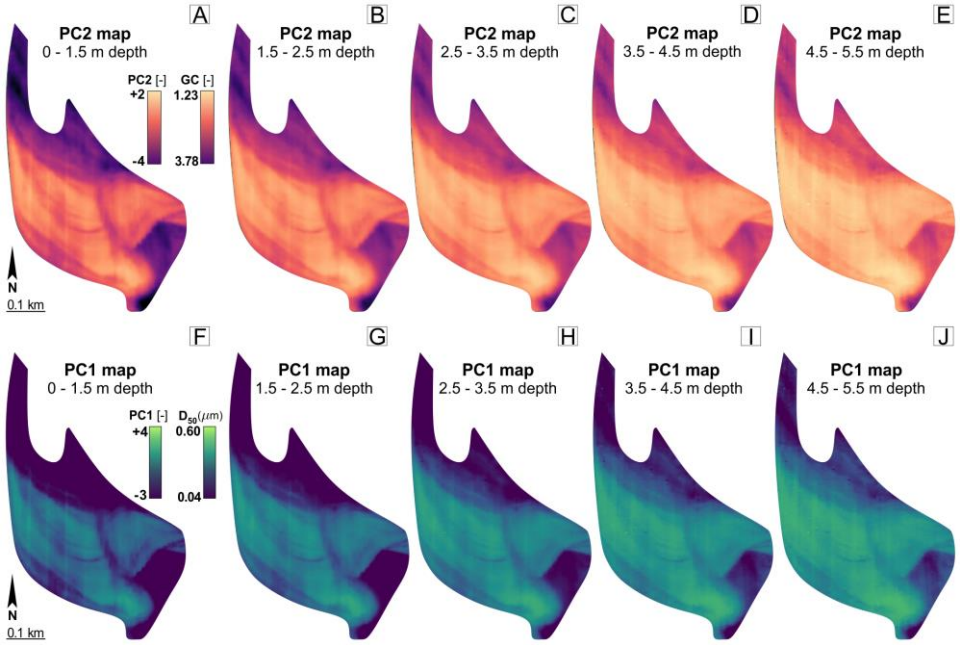

Fig. 5.7. 2D predicting maps. (A-E) PC2-GC maps (maps of sediment sorting) and (F-J) PC1-D50 predicting maps (maps of the average grain size) of the 5 depth layers where electrical conductivity was measured.

Interpretation of PCs' maps in terms of traditional sedimentological parameters is straightforward, as simple linear regressions between PC1 and D_{50} and between PC2 and sediment sorting (expressed as Gradation Coefficient

$$GC = ½ \times \left(\frac{D84}{D50} + \frac{D50}{D16}\right), \quad (3)$$

are both significant and strong (p-value << 0.001, R^2= 0.94 for PC1 and D_{50}; p-value << 0.001, R^2= 0.48 for PC2 and GC). A direct (inverse) proportionality exists between PC1 (PC2) and D_{50} (GC) values (Fig. 5.7).

5.5 Discussions

Results are here discussed to highlight the novelty and efficiency of the proposed methodology and retrieve sedimentological implications on the study cases.

5.5.1 From principal components and electrical properties to sediment textural properties

Ground electrical conductivity depends on different ancillary soil properties, like salinity, soil structure and texture, temperature, and moisture content (Paine, 2003). However, assuming that, in a restricted area (e.g. 0.3 km^2) and at the same depth, temperature, water content, and salinity are almost uniformly distributed, the variability of electrical conductivity can be reasonably correlated to changes in sediment properties (De Smedt et al., 2011; Boaga et al., 2018), with gravelly and muddy deposits linked with low- and high-conductivity values, respectively. However, as individual grain-size classes or synthetic descriptors (i.e. D_{10}, D_{50}, D_{90}, or sorting indexes) are not independent (Copelli et al., 2018), they cannot offer a comprehensive interpretation for the variability of sediment properties. PCA can overcome this shortcoming, considering the properties of the average grain size, and detecting a limited number of uncorrelated variables (i.e. PC1 and PC2) that explain ca. 75% of the sediment textural variability (Fig. 5.6A).

The physical meaning of PC1 and PC2 can be appreciated in terms of their relationship with cumulative grain-size curves (Fig. 5.6B-C). A progressive increase in PC1 values with sediment grain size (Fig. 5.6B) points at a direct tight relation between PC1 and sediment grain size. High and low PC2 values occur where cumulative curves display high and low steepness, respectively (Fig. 5.6C), indicating a direct correlation between PC2 values and sediment sorting. The higher grain-size sorting in sandy-bar deposits coincides with a dominance

of fine to medium sand population, as also observed by previous studies (Hough, 1942; Inman, 1949; Griffiths, 1951). Accordingly, muddy, poorly sorted overbank and channel-fill deposits show negative PC1 and PC2 values (Fig. 5.6D). Point-bar deposit sand is coarser than channel-fill and overbank deposits and shows higher PC1 values (Fig. 5.6D). Intra-point bar variability, both in terms of grain size and sorting, is highlighted by variable values of PC1 and PC2 (Fig. 5.6D). Deposits from upstream-bar portions are made of the coarsest sand (i.e. positive PC1) but show low to medium sorting (negative PC2). In contrast, downstream-bar deposits mostly consist of well-sorted fine-medium sand (intermediate PC1 and positive PC2 scores). Central-bar samples are characterised by an intermediate pattern (Fig. 5.6D).

Linking PC1 and PC2 with electrical conductivity values allows extrapolating punctual data from sedimentary cores through the whole study area. The statistical relationships between principal components and electric conductivity reveal that the latter varies mostly with the sediment sorting (PC2) (Fig. 5.6F), whereas a direct relation between PC1 and electrical conductivity appears to be poorly descriptive (Fig. 5.6E) and can be extrapolated from the linear polynomial relationship (i.e. equation 2) shown in Figure 5.6G.

The application of equations 1 and 2 allows converting electrical conductivity maps obtained at different depths to PC2 (Fig. 5.7A-E) and PC1 (Fig. 5.7F-J) maps which depict the vertical and lateral distribution of sediment sorting and grain size, respectively. The widespread low PC2 and PC1 values in overbank and channel-fill areas (e.g. Fig. 5.7B and G) fit with the muddy composition of related deposits, along with their scarce sorting. The downward increase in PC2 and PC1 values in overbank areas is consistent with the occurrence of transgressive coastal sand (Rizzetto et al., 2002, 2003), which was locally reworked by fluvial channels and spread in the overbank areas (e.g. crevasse splays). The similar pattern occurring in the whole abandoned channel zone is consistent with an upward transition from sandy tractional deposits to residual mud that infilled the abandoned channel (cf. Toonen et al., 2012). The overall high PC1 values of point-bar deposits agree with their sandy composition, and the widespread occurrence of the highest PC1 values in the deep bar zone (i.e. below 4 m) is consistent with core data and classical field studies detecting coarser sand in the lower bar zone (Allen, 1965, 1970; Jackson, 1976; Nanson, 1980; Donselaar and Overeem, 2008; Ghazi and Mountney, 2009; Ielpi and Ghinassi, 2014). Different PC1 and PC2 values within M1 and M2 point-bar bodies document intra-point bar variability (Willis and Sech, 2018a; Clift et al.,

2019) of sand grain size and sorting, and are consistent with scroll-bar patterns, especially in the upper part of bars, where major textural changes are commonly documented (Jackson, 1976; Donselaar and Overeem, 2008; Swan et al., 2018). Given the linear relationship between PC1 and D_{50} and PC2 and Gradation Coefficient, PCs' maps can be directly interpreted in terms of sediment grain size and sorting. Although from a strictly statistical point of view PC1 and PC2 would offer a more comprehensive description of the sediment grain-size properties, the interpretation in terms of traditional sedimentological parameters, like sediment grain size and sorting, provides a straightforward, crucial piece of information for modelling studies of groundwater propagation in surficial aquifers.

5.5.2 Implications for point-bar sedimentation

Reconstructed textural maps allow discussing some implications for the morphodynamical evolution of the study bends and related deposits. Our statistical approach allows the creation of sediment sorting maps (PC2 maps), providing a more comprehensive way to investigate point-bar deposits compared to the sole use of sediment grain-size analysis. The PC maps can be integrated with the reconstructed planform evolution of the study bends, showing that major variability of sediment textural properties occurs in the M1 point bar, whereas the M2 point bar shows a more uniform distribution of PC1-2 values. Such a difference emphasises the crucial role of planform behaviour in controlling sediment distribution along meander bends (Yan et al., 2017, 2019, 2021), furthermore highlighting that marked textural heterogeneities characterise point bars generated by complex bend transformations (Hagstrom et al., 2019; Russell et al., 2019). In contrast, the roughly regular expansional growth of M2 accounts for limited textural variability within the associated point bar, which is characterised by slightly coarser deposits in the central to apex zone (Willis and Sech, 2018a).

The occurrence of the high values of PC1 and 2 in the youngest part of the M1 point bar (Fig. 5.7) is consistent with findings of recent outcrop and modelling studies, where point bars accreted by expansion with more pronounce accretion at apex show either coarser apex deposits (Bhattacharyya et al., 2015; Clift et al., 2019), or apex zone characterised by a high net sand percentage (Hagstrom et al., 2019). Specifically, the scroll pattern of the youngest part of the M1 point-bar defines a sharp bend, which promotes the efficiency of helical circulation that is probably able to deprive deposits of their finer fraction. This mechanism

gives rise to bar deposits characterised by a blocky vertical trend of physical properties, as identified by Willis and Sech (2018), for the grain-size distribution in the central part of point bars generated by an expansional behaviour. Similar conditions could have affected bar M1 during its early stage of development, but cannibalisation of downstream bar deposits due to expansion of M2 bend prevents from detecting the precise geometry of the bend during its early growth phase.

Principal component values are also high in the most upstream part of point bar M1, where a blocky- to lowering-upward vertical trend of conductivity values occurs. As bar M1 is located at the end of a straight channel reach, its upstream side was prone to experience flood currents, which pushed channel sediment over the bar instead of following the major river path (cf. Dietrich and Smith, 1983; Ferguson et al., 2003; Ghinassi et al., 2019). Where point-bar planform configuration can be integrated with vertical grain-size data, this armouring process has been invoked to explain the occurrence of coarsening-upward grain size trends in the upstream point-bar zones (Willis, 1989; Swan et al., 2018; Li et al., 2020). These zones with high PC1-2 values highlight the role of meander planform configuration in controlling local hydraulic sediment sorting (Blanckaert et al., 2013; Blanckaert, 2018), which explains exceptions to the classical vertical decrease in sediment grain size that typifies point-bar bodies (Allen, 1965; Nanson, 1980).

Some scroll sets of the M1 point bar show PC1-2 values that vary along the bend; this is also linked to the along-bend hydrodynamic segregation of sediments, which can produce different grain-size distribution according to the meander morphology (Leopold and Wolman, 1960; Hooke, 1975; Dietrich, 1987). Variations in the bend curvature and sinuosity, during planform evolution, can intimately influence sediment transport and deposition (Leopold and Wolman, 1960; Hooke, 1975; Dietrich, 1987). Overall, coarser sediments are best sorted (Powell, 1998). Thus, deposits accumulated in the upstream and central part of bends accreted by expansion, especially if the latter are quite sharp (i.e. bends with a low radius of curvature of the inner bank), are those with the best reservoir potential, while in the downstream part the sorting commonly worsens and so does the reservoir quality of these deposits (Fig. 5.7) (Folk and Ward, 1957; Clift et al., 2019).

The PC1 and PC2 maps also show that some scroll sets of the M1 point bar show uniformly low values along the whole bar (Figs 5.4F and 5.7). This overall drop of principal component values points out to a widespread decrease in sediment

grain size and sorting along the whole bar, which can be ascribed to factors acting at the spatial scale of the whole channel-belt, such as changes in channel discharge and sediment supply possibly triggered by decadal climate variations (Arnell and Gosling, 2013; Rameshwaran et al., 2021), rather than processes related to site-specific bend geometries. Change in dominant grain size (i.e., fine grained and poorly sorted) from upstream areas could be at the origin of such a widespread accumulation of deposits with low PC1 and PC2 values. Although these localised or widespread textural changes can be ascribed to different processes, they both concur to create intra-bar heterogeneities and develop different pathways for fluid circulations. It is worthwhile recalling that these results would not have been obtained without the integrated methodology developed.

5.5.3 A non-site-specific approach to investigate intra-point-bar sediment properties

The proposed integrated approach allows investigating the spatial variability of sediment properties within paleo-meanders starting from electromagnetic and sedimentary data. The minimum number of samples needed to obtain the regression models is estimated to get a cost-effective approach. Samples of the same depth layer (i.e., 25 samples from 1.5 – 2.5 m-depth layer) are listed in decreasing order of their electric conductivity and subdivided into 5 groups, based on the percentiles 20, 40, 60, and 80. This subdivision allows one to equally represent all the electric-conductivity areas. Then, PCA and relationships between PCs and electrical conductivity are calculated progressively adding one randomly chosen sample per group (i.e., 5, 10, 15, … samples). Only relationships falling within the confidential intervals of the relationships find out with the 50 samples are accepted. Simulations reveal that at least 3 samples per percentile interval of conductivity are required to get the results discussed above.

To extend this methodology beyond the study sites, the approach-to-follow starts with the acquisition and interpolation of the electric conductivity data. Then, conductivity values should be subdivided into percentile intervals, and cores should be retrieved to sample deposits in each individuated interval (e.g. at least 3 cores per area). Then, the next steps follow those described in the previous paragraphs: (1) sedimentological analysis; (2) grain-size analyses; (3) PCA; (4) regression models and their application to electromagnetic data to define maps of sediment properties.

5.6 Conclusions

The innovative approach proposed in this work provides an effective tool to investigate the spatial variability of sediment textural properties within paleo-meanders. This approach can be applied to retrieve the fundamental data required for modelling groundwater flows within surficial aquifers, in order to study and mitigate the damaging effect of environmental issues in coastal areas. Starting from electromagnetic and sedimentary data, this work made use of statistical analyses to improve the current knowledge about geophysical investigations in surficial aquifers and provide an approach to quantitatively study sedimentary bodies efficiently and cost-effectively.

Specifically, the statistical approach allows one to: (1) characterise the sediment properties of the sedimentary bodies by defining uncorrelated components, representing here the sediment grain size and sorting; (2) provide more comprehensive information compared to the qualitative assumption that directly links electric conductivity and sediment grain-size by demonstrating that electric conductivity is indeed influenced by sediment textural properties, but most importantly by sediment sorting; (3) extrapolate local values of a given sediment property with significant reliability, as proved by the comparison between predicted data and classical facies models for point-bar architecture.

The correlation between sediment properties and planform evolution of meandering rivers agrees with previous sedimentological observations, thereby further corroborating the results of this work. In particular, complex dynamics of planform evolution lead to a complex pattern of sediment-properties distribution, which is also highly influenced by autogenic factors at the channel-belt scale, calling for future studies about factors acting at the channel-belt scale that control the variability of sediment properties between consecutive scroll sets. In parallel, differences in terms of sediment properties between consecutive scroll bars could be influenced by allogenic forcings (e.g., sediment provided by upstream reaches).

The proposed innovative approach can be applied beyond the study cases at hand, to characterise sediment properties in channelised deposits in a quantitatively, spatially extensive, and cost-effective way following the criteria suggested here.

Acknowledgements

The authors are grateful to M. Cosma and A. Puppin for their contribution to data collection, I. Rizzi for help in the laboratory analysis, and Studio Tecnico Drago (Monselice, Italy) for logistic support. The authors would like to thank L. Destro for his willingness and help during geophysical acquisitions. N. Boscolo is thanked for his kindness and for allowing the geophysical surveys in his properties. The manuscript benefits from the fruitful suggestions of Prof. A. Moscariello (University of Geneva, Switzerland). The authors would like to acknowledge helpful and critical comments provided by reviewers V. Zuchuat and C. Russell on an early version of this manuscript.

This work was supported by "HYDROSEM: Fluvial and tidal meanders of the Venetian-Po Plain: from hydrodynamics to stratigraphy" project (Progetto di Eccellenza CARIPARO 2017; PI Massimiliano Ghinassi), and the University of Padova (SID2016 project, titled "From channels to rock record: morphodynamic evolution of tidal meanders and related sedimentary products" PI Massimiliano Ghinassi).

Data availability

The data that support the findings of this study are openly available in Mendeley Data at doi: 10.17632/5wshjhrxk7.1

References

Allen, J.R.L., 1965, A review of the origin and characteristics of recent alluvial sediments: Sedimentology, v. 5, p. 89–191, doi:10.1111/j.1365-3091.1965.tb01561.x.

Allen, J.R.L., 1970, Studies in fluviatile sedimentation: a comparison of fining-upwards cyclothems, with special reference to coarse-member composition and interpretation: Journal of Sedimentary Research, v. 40, p. 298–323.

Amorosi, A., Bini, M., Giacomelli, S., Pappalardo, M., Ribecai, C., Rossi, V., Sammartino, I., and Sarti, G., 2013, Middle to late Holocene environmental evolution of the Pisa coastal plain (Tuscany , Italy) and early human settlements: Quaternary International, v. 303, p. 93–106, doi:10.1016/j.quaint.2013.03.030.

Arnell, N.W., and Gosling, S.N., 2013, The impacts of climate change on river flow regimes at the global scale: Journal of Hydrology, v. 486, p. 351–364, doi:10.1016/j.jhydrol.2013.02.010.

Bagnold, R.A., 1960, Some aspects of the shape of river meanders: U.S. Geological Survey Professional Paper, v. 282-E, p. 371–375, doi:10.1080/00207217608920581.

Baines, D., Smith, D.G., Froese, D.G., Bauman, P., and Nimeck, G., 2002, Electrical resistivity ground imaging (ERGI): A new tool for mapping the lithology and geometry of channel-belts and valley-fills: Sedimentology, v. 49, p. 441–449, doi:10.1046/j.1365-3091.2002.00453.x.

Beard, D.C., and Weyl, P.K., 1993, Influence of Texture on Porosity and Permeability of Unconsolidated Sand: AAPG Bulletin, v. 57, p. 349–369, doi:10.1306/819A4272-16C5-11D7-8645000102C1865D.

Bellizia, E., Boaga, J., Fontana, A., D'Alpaos, A., Cassiani, G., and Ghinassi, M., 2021, Impact of genesis and abandonment processes of a fluvial meander on geometry and grain-size distribution of the associated point bar (Venetian Plain, Italy): Marine and Petroleum Geology, v. 127, p. 104951, doi:10.1016/j.marpetgeo.2021.104951.

Benner, S.G., Polizzotto, M.L., Kocar, B.D., Ganguly, S., Phan, K., Ouch, K., Sampson, M., and Fendorf, S., 2008, Groundwater flow in an arsenic-contaminated aquifer, Mekong Delta, Cambodia: Applied Geochemistry, v. 23, p. 3072–3087, doi:10.1016/j.apgeochem.2008.06.013.

Bhattacharyya, P., Bhattacharya, J.P., and Khan, S.D., 2015, Paleo-channel reconstruction and grain size variability in fluvial deposits, Ferron Sandstone, Notom Delta, Hanksville, Utah: Sedimentary Geology, v. 325, p. 17–25, doi:10.1016/j.sedgeo.2015.05.001.

Blanckaert, K., 2018, Hydro-sedimentological processes in meandering rivers: A review and some future research directions, *in* Ghinassi, M., Colombera, L., Mountney, N.P., Reesink, A.J., and Bateman, M. eds., Fluvial Meanders and Their Sedimentary Products in the Rock Record (Int. Assoc. Sedimentol. Spec. Publ. 48, John Wiley & Sons, p. 297–320, doi:10.1002/9781119424437.ch12.

Blanckaert, K., Kleinhans, M.G., Mclelland, S.J., Uijttewaal, W.S.J., Murphy, B.J., van de Kruijs, A., Parsons, D.R., and Chen, Q., 2013, Flow separation at the inner (convex) and outer (concave) banks of constant-width and widening open-channel bends: Earth Surface Processes and Landforms, v. 38, p. 696–716, doi:10.1002/esp.3324.

Bluck, B.J., 1971, Sedimentation in the meandering river Endrick: Scottish Journal of Geology, v. 7, p. 93–138, doi:10.1144/sjg07020093.

Boaga, J., Ghinassi, M., D'Alpaos, A., Deidda, G.P., Rodriguez, G., and Cassiani, G., 2018, Geophysical investigations unravel the vestiges of ancient meandering channels and their dynamics in tidal landscapes: Scientific Reports, v. 8, p. 1–8, doi:10.1038/s41598-018-20061-5.

Bondesan, M., Elmi, C., Marocco, R., and Favero, V., 2001, Forme e depositi di origine litoranea e lagunare, *in* Castiglioni, G.B. and Pellegrini, G.B. eds., Note illustrative della Carta Geomorfologica della Pianura Padana. Suppl. Geogr. Fis. Dinam. Quat. 4, p. 105–118.

Bondesan, A., and Furlanetto, P., 2012, Artificial fluvial diversions in the

mainland of the Lagoon of Venice during the 16th and 17th centuries inferred by historical cartography analysis: Géomorphologie: relief, processus, environnement, v. 18, p. 175–200, doi:10.4000/geomorphologie.9815.

Bowling, J.C., Harry, D.L., Rodriguez, A.B., and Zheng, C., 2007, Integrated geophysical and geological investigation of a heterogeneous fluvial aquifer in Columbus Mississippi: Journal of Applied Geophysics, v. 62, p. 58–73, doi:10.1016/j.jappgeo.2006.08.003.

Boyer, P., Roberts, N., and Baird, D., 2006, Holocene environment and settlement on the Çarşamba alluvial fan, south-central Turkey: Integrating geoarchaeology and archaeological field survey: Geoarchaeology, v. 21, p. 675–698, doi:10.1002/gea.20133.

Brice, J.C., 1974, Evolution of meander loops: Geological Society of America Bulletin, v. 85, p. 581–586, doi:10.1130/0016-7606(1974)85<581:EOML>2.0.CO;2.

Bridge, J.S., 2003, Rivers and floodplains. Forms, Processes and Sedimentary Record: Blackwell Science, v. 491.

Bridge, J.S., Alexander, J.A.N., Collier, R.E.L., Gawthorpe, R.L., and Jarvis, J., 1995, Ground-penetrating radar and coring used to study the large-scale structure of point-bar deposits in three dimensions: Sedimentology, v. 42, p. 839–852, doi:10.1111/j.1365-3091.1995.tb00413.x.

Carraro, A., Fabbri, P., Giaretta, A., Peruzzo, L., Tateo, F., and Tellini, F., 2013, Arsenic anomalies in shallow Venetian Plain (Northeast Italy) groundwater: Environmental Earth Sciences, v. 70, p. 3067–3084, doi:10.1007/s12665-013-2367-2.

Cassiani, G., Bellizia, E., Fontana, A., Boaga, J., D'Alpaos, A., and Ghinassi, M., 2020, Geophysical and Sedimentological Investigations Integrate Remote-Sensing Data to Depict Geometry of Fluvial Sedimentary Bodies: An Example from Holocene Point-Bar Deposits of the Venetian Plain (Italy): Remote Sensing, v. 12, p. 2568, doi:10.3390/rs12162568.

Clift, P.D., Olson, E.D., Lechnowskyj, A., Moran, M.G., Barbato, A., and Lorenzo, J.M., 2019, Grain-size variability within a mega-scale point-bar system, False River, Louisiana: Sedimentology, v. 66, p. 408–434, doi:10.1111/sed.12528.

Copelli, D., Cavecchi, A., Merusi, C., and Leardi, R., 2018, Multivariate evaluation of the effect of the particle size distribution of an Active Pharmaceutical Ingredient on the performance of a pharmaceutical drug product: a real-case study: Chemometrics and Intelligent Laboratory Systems, v. 178, p. 1–10, doi:10.1016/j.chemolab.2018.04.013.

Corwin, D.L., and Rhoades, J.D., 1982, An Improved Technique for Determining Soil Electrical Conductivity-Depth Relations from Above-ground Electromagnetic Measurements: Soil Science Society of America Journal, v. 46, p. 517–520, doi:10.2136/sssaj1982.03615995004600030014x.

Daniel, J.F., 1971, Channel movement of meandering Indiana streams: Washington D.C., US Government Printing Office.

Davies, T., 1992, Principal Components of Principal Component Analysis: Spectroscopy World, v. 4, p. 38–39.

Desbarats, A.J., Koenig, C.E.M., Pal, T., Mukherjee, P.K., and Beckie, R.D., 2014, Groundwater flow dynamics and arsenic source characterization in an aquifer system of West Bengal, India: Water Resources Research, v. 50, p. 4974–5002, doi:10.1002/2013WR014034.

Dietrich, W.E., 1987, Mechanics of flow and sediment transport in river bends, *in* Richards, K.S. ed., River channels: Environment and process, Oxford, UK, Basil Blackwell, v. 18, p. 179–227.

Dietrich, W.E., and Smith, J.D., 1983, Influence of the point bar on flow through curved channels: Water Resources Research, v. 19, p. 1173–1192, doi:10.1029/WR019i005p01173.

Donselaar, M.E., and Overeem, I., 2008, Connectivity of fluvial point-bar deposit: An example from the Miocene Huesca fluvial fan, Ebro Basin, Spain: AAPG Bulletin, v. 92, p. 1109–1129, doi:10.1306/04180807079.

Favero, V., and Serandrei-Barbero, R., 1978, La sedimentazione olocenica nella piana costiera tra Brenta ed Adige, *in* Memorie Società Geologica Italiana, v. 19, p. 337–343.

Favero, V., and Serandrei Barbero, R., 1980, Origine ed evoluzione della laguna di Venezia: bacino meridionale: Lavori della Società Veneziana di Scienze Naturali, v. 5, p. 49–71.

Ferguson, R.I., Parsons, D.R., Lane, S.N., and Hardy, R.J., 2003, Flow in meander bends with recirculation at the inner bank: Water resources research, v. 39, p. 1322, doi:10.1029/2003WR001965.

Folk, R.L., and Ward, W.C., 1957, Brazos river bar: a study in the significance of grain-size parameters: Journalf og Sedimentary Petrology, v. 27, p. 3–26, doi:10.1306/74D70646-2B21-11D7-8648000102C1865D.

Fontana, A., Mozzi, P., and Bondesan, A., 2008, Alluvial megafans in the Venetian-Friulian Plain (north-eastern Italy): Evidence of sedimentary and erosive phases during Late Pleistocene and Holocene: Quaternary International, v. 189, p. 71–90, doi:10.1016/j.quaint.2007.08.044.

Fontana, A., Mozzi, P., and Bondesan, A., 2010, Late Pleistocene evolution of the Venetian-Friulian Plain: Rendiconti Lincei, v. 21, p. 181–196, doi:10.1007/s12210-010-0093-1.

GF Instruments s.r.o., www.gfinstruments.cz (accessed February 2020).

Ghazi, S., and Mountney, N.P., 2009, Facies and architectural element analysis of a meandering fluvial succession: The Permian Warchha Sandstone, Salt Range, Pakistan: Sedimentary Geology, v. 221, p. 99–126, doi:10.1016/j.sedgeo.2009.08.002.

Ghinassi, M., Moody, J., and Martin, D., 2019, Influence of extreme and annual floods on point-bar sedimentation: Inferences from Powder River, Montana, USA: GSA Bulletin, v. 131, p. 71–83, doi:10.1130/B31990.1.

Ghinassi, M., Nemec, W., Aldinucci, M., Nehyba, S., Özaksoy, V., and Fidolini, F., 2014, Plan-form evolution of ancient meandering rivers reconstructed from longitudinal outcrop sections: Sedimentology, v. 61, p. 952–977,

doi:10.1111/sed.12081.

Giacomelli, S., Rossi, V., Amorosi, A., Bruno, L., Campo, B., Ciampalini, A., Civa, A., Hong, W., Sgavetti, M., and de Souza Filho, C.R., 2018, A mid-late Holocene tidally-influenced drainage system revealed by integrated remote sensing, sedimentological and stratigraphic data: Geomorphology, v. 318, p. 421–436, doi:10.1016/j.geomorph.2018.07.004.

Griffiths, J.C., 1951, Size versus Sorting in Some Caribbean Sediments: The Journal of Geology, v. 59, p. 211–243.

Hagstrom, C.A., Hubbard, S.M., Leckie, D.A., and Durkin, P.R., 2019, The Effects of Accretion-package Geometry On Lithofacies Distribution in Point-bar Deposits: Journal of Sedimentary Research, v. 89, p. 381–398, doi:10.2110/jsr.2019.23.

Harvey, C.F., Ashfaque, K.N., Yu, W., Badruzzaman, A.B.M., Ali, M.A., Oates, P.M., Michael, H.A., Neumann, R.B., Beckie, R., Islam, S., Ahmed, M.F., 2006, Groundwater dynamics and arsenic contamination in Bangladesh: Chemical Geology, v. 228, p. 112–136, doi:10.1016/j.chemgeo.2005.11.025.

Hooke, R.L.B., 1975, Distribution of Sediment Transport and Shear Stress in a Meander Bend: The Journal of geology, v. 83, p. 543–565.

Hough, J.L., 1942, Sediments of Cape Cod Bay, Massachusetts: Journal of Sedimentary Research, v. 12, p. 10–30, doi:10.1306/D4269134-2B26-11D7-8648000102C1865D.

Ielpi, A., and Ghinassi, M., 2014, Planform architecture, stratigraphic signature and morphodynamics of an exhumed Jurassic meander plain (Scalby Formation, Yorkshire, UK): Sedimentology, v. 61, p. 1923–1960, doi:10.1111/sed.12122.

Inman, D.L., 1949, Sorting of sediments in the light of fluid mechanics: Journal of Sedimentary Research, v. 19, p. 51–70, doi:10.1306/D426934B-2B26-11D7-8648000102C1865D.

Jackson, R.G., 1976, Depositional model of point bars in the lower Wabash River: Journal of Sedimentary Research, v. 46, p. 579–594, doi:10.1306/212F6FF5-2B24-11D7-8648000102C1865D.

Khan, I.A., Bridge, J.S., Kappelman, J., and Wilson, R., 1997, Evolution of Miocene fluvial environments, eastern Potwar plateau, northern Pakistan: Sedimentology, v. 44, p. 221–251, doi:10.1111/j.1365-3091.1997.tb01522.x.

Leopold, L.B., and Wolman, M.G., 1960, River Meanders: Geological Soceity of America Bulletin, v. 71, p. 769–793, doi:10.1130/0016-7606(1960)71[769:RM]2.0.CO;2.

Li, J., Vandenberghe, J., Mountney, N.P., and Luthi, S.M., 2020, Grain-size variability of point-bar deposits from a fine-grained dryland river terminus, Southern Altiplano, Bolivia: Sedimentary Geology, v. 403, doi:10.1016/j.sedgeo.2020.105663.

Da Lio, C., Carol, E., Kruse, E., Teatini, P., and Tosi, L., 2015, Saltwater contamination in the managed low-lying farmland of the Venice coast,

Italy: An assessment of vulnerability: Science of the Total Environment, v. 533, p. 356–369, doi:10.1016/j.scitotenv.2015.07.013.

Makaske, B., and Weerts, H.J.T., 2005, Muddy lateral accretion and low stream power in a sub-recent confined channel belt, Rhine-Meuse delta, central Netherlands: Sedimentology, v. 52, p. 651–668, doi:10.1111/j.1365-3091.2005.00713.x.

Massari, F., Grandesso, P., Stefani, C., and Jobstraibizer, P.G., 1986, A small polyhistory foreland basin evolving in a context of oblique convergence: the Venetian basin (Chattian to Recent, Southern Alps, Italy), *in* Allen, P.A. and Homewood, P. eds., Foreland basins, Oxford, UK, Blackwell Scientific Publication, p. 141–168, doi:10.1002/9781444303810.CH7.

McLachlan, P., Blanchy, G., and Binley, A., 2021, EMagPy: Open-source standalone software for processing, forward modeling and inversion of electromagnetic induction data: Computers and Geosciences, v. 146, p. 104561, doi:10.1016/j.cageo.2020.104561.

Mozzi, P., 2005, Alluvial plain formation during the Late Quaternary between the southern Alpine margin and the Lagoon of Venice (Northern Italy): Geografia Fisica e Dinamica Quaternaria, v. Suppl. 7, p. 219–229.

Nanson, G.C., 1980, Point bar and floodplain formation of the meandering Beatton River, northeastern British Columbia, Canada: Sedimentology, v. 27, p. 3–29, doi:10.1111/j.1365-3091.1980.tb01155.x.

Nofal, E.R., Amer, M.A., El-Didy, S.M., and Fekry, A.M., 2015, Delineation and modeling of seawater intrusion into the Nile Delta Aquifer: A new perspective: Water Science, v. 29, p. 156–166, doi:10.1016/j.wsj.2015.11.003.

Paine, J.G., 2003, Determining salinization extent, identifying salinity sources, and estimating chloride mass using surface, borehole, and airborne electromagnetic induction methods: Water Resources Research, v. 39, p. 1–10, doi:10.1029/2001WR000710.

Piovan, S., Mozzi, P., and Zecchin, M., 2012, The interplay between adjacent Adige and Po alluvial systems and deltas in the late Holocene (Northern Italy): Géomorphologie: relief, processus, environnement, v. 18, p. 427–440, doi:10.4000/geomorphologie.10034.

Powell, D.M., 1998, Patterns and processes of sediment sorting in gravel-bed rivers: Progress in Physical Geography, v. 22, p. 1–32, doi:10.1177/030913339802200101.

Rameshwaran, P., Bell, V.A., Davies, H.N., and Kay, A.L., 2021, How might climate change affect river flows across West Africa? Climatic Change, v. 169, p. 1–27, doi:10.1007/s10584-021-03256-0.

Rizzetto, F., Tosi, L., Bonardi, M., Gatti, P., Fornasiero, A., Gambolati, G., Putti, M., and Teatini, P., 2002, Geomorphological Evolution of the Southern Catchment of the Venice Lagoon (Italy): the Zennare Basin: Scientific Research and Safeguarding of Venice, Trends in global change processes, p. 217–228.

Rizzetto, F., Tosi, L., Carbognin, L., Bonardi, M., and Teatini, P., 2003,

Geomorphic setting and related hydrogeological implications of the coastal plain south of the Venice Lagoon, Italy, *in* Servat, E., Najem, W., Leduc, C., and Shakeel, A. eds., Hydrology of the Mediterranean and semiarid regions, IAHS Publication 278, p. 463–470.

Rossetti, D. de F., 2010, Multiple remote sensing techniques as a tool for reconstructing late Quaternary drainage in the Amazon lowland: Earth Surface Processes and Landforms, v. 35, p. 1234–1239, doi:10.1002/esp.1996.

Russell, C.E., Mountney, N.P., Hodgson, D.M., and Colombera, L., 2019, A novel approach for prediction of lithological heterogeneity in fluvial point-bar deposits from analysis of meander morphology and scroll-bar pattern, *in* Ghinassi, M., Colombera, L., Mountney, N.P., and Reesink, J.H. eds., Fluvial Meanders and Their Sedimentary Products in the Rock Record. Int. Assoc. Sedimetol. Spec. Publ., v. 48, p. 385–418, doi:10.1002/9781119424437.ch15.

De Smedt, P., Van Meirvenne, M., Meerschman, E., Saey, T., Bats, M., Court-Picon, M., De Reu, J., Zwertvaegher, A., Antrop, M., Bourgeois, J., De Maeyer, P., Finke, P.A., Verniers, J., Crombé, P., 2011, Reconstructing palaeochannel morphology with a mobile multicoil electromagnetic induction sensor: Geomorphology, v. 130, p. 136–141, doi:10.1016/j.geomorph.2011.03.009.

Strick, R.J.P., Ashworth, P.J., Awcock, G., and Lewin, J., 2018, Morphology and spacing of river meander scrolls: Geomorphology, v. 310, p. 57–68, doi:10.1016/j.geomorph.2018.03.005.

Swan, A., Hartley, A.J., Owen, A., and Howell, J., 2018, Reconstruction of a sandy point-bar deposit: implications for fluvial facies analysis, *in* Ghinassi, M., Colombera, L., Mountney, N.P., Reesink, A.J., and Betaman, M. eds., Fluvial Meanders and Their Sedimentary Products in the Rock Record. Int. Assoc. Sedimentol. Spec. Publ. 48, Ltd, John Wiley & Sons, v. 48, p. 445–474, doi:10.1002/9781119424437.ch17.

Toonen, W.H.J., Kleinhans, M.G., and Cohen, K.M., 2012, Sedimentary architecture of abandoned channel fills: Earth Surface Processes and Landforms, v. 37, p. 459–472, doi:10.1002/esp.3189.

Um, E.S., and Alumbaugh, D.L., 2007, On the physics of the marine controlled-source electromagnetic method: Geophysics, v. 72, p. WA13–WA26, doi:10.1190/1.2432482.

Weber, K.J., 1982, Influence of Common Sedimentary Structures on Fluid Flow in Reservoir Models.: JPT, Journal of Petroleum Technology, v. 34, p. 665–672, doi:10.2118/9247-PA.

Willis, B.J., 1989, Palaeochannel reconstructions from point bar deposits: a three-dimensional perspective: Sedimentology, v. 36, p. 757–766, doi:10.1111/j.1365-3091.1989.tb01744.x.

Willis, B.J., and Sech, R.P., 2018a, Emergent facies patterns within fluvial channel belts, *in* Ghinassi, M., Colombera, L., Mountney, N.P., Reesink, A.J.H., and Bateman, M. eds., Fluvial Meanders and Their Sedimentary

Products in the Rock Record. Int. Assoc. Sedimentol. Spec. Publ., John Wiley & Sons, Ltd, v. 48, p. 509–542, doi:10.1002/9781119424437.ch19.

Willis, B.J., and Sech, R.P., 2018b, Quantifying impacts of fluvial intra-channel-belt heterogeneity on reservoir behaviour, *in* Ghinassi, M., Colombera, L., Mountney, N.P., and Reesink, A.J.H. eds., Fluvial Meanders and Their Sedimentary Products in the Rock Record (Int. Assoc. Sedimentol. Spec. Publ. 48), John Wiley & Sons, p. 543–572, doi:10.1002/9781119424437.ch20.

Willis, B.J., and Tang, H., 2010, Three-Dimensional Connectivity of Point-Bar Deposits: Journal of Sedimentary Research, v. 80, p. 440–454, doi:10.2110/jsr.2010.046.

Wray, R.A.L., 2009, Palaeochannels of the Namoi River Floodplain, New South Wales, Australia: The use of multispectral Landsat imagery to highlight a Late Quaternary change in fluvial regime: Australian Geographer, v. 40, p. 29–49, doi:10.1080/00049180802656952.

Wu, C., Bhattacharya, J.P., and Ullah, M.S., 2015, Paleohydrology and 3D facies architecture of ancient point bars, Ferron Sandstone, Notom Delta, south-central Utah, USA: Journal of Sedimentary Research, v. 85, p. 399–418, doi:10.2110/jsr.2015.29.

Yan, N., Colombera, L., and Mountney, N.P., 2021, Controls on fluvial meander-belt thickness and sand distribution: Insights from forward stratigraphic modelling: Sedimentology, v. 68, doi:10.1111/sed.12830.

Yan, N., Colombera, L., Mountney, N.P., and Dorrell, R.M., 2019, Fluvial point-bar architecture and facies heterogeneity, and their influence on intra-bar static connectivity in humid coastal-plain and dryland fan systems, *in* Ghinassi, M., Colombera, L., Mountney, N.P., and Reesink, A.J.H. eds., Fluvial Meanders and Their Sedimentary Products in the Rock Record (IAS SP 48), John Wiley & Sons, p. 475–508, doi:10.1002/9781119424437.ch18.

Yan, N., Mountney, N.P., Colombera, L., and Dorrell, R.M., 2017, A 3D forward stratigraphic model of fluvial meander-bend evolution for prediction of point-bar lithofacies architecture: Computers and Geosciences, v. 105, p. 65–80, doi:10.1016/j.cageo.2017.04.012.

6

FLUVIAL RESPONSE TO MORPHO-SEDIMENTARY HETEROGENEITIES

This chapter is a manuscript in preparation to be submitted to *Sedimentary Geology* under the title "Impact of morpho-sedimentary heterogeneities on the evolution of coastal meandering rivers: insights from the Medieval Brenta River (Italy)".

E.B., P.M. and M.G. designed the study. E.B., J.B., P.M. and M.G. developed the methodology. E.B. and M.G. collected the data. E.B. annotated and maintained the research data. E.B. was responsible for data creation and presentation. E.B. and M.G. were the project administrator. J.B and G.C. applied computational techniques to analyse study data. J.B, P.M. and M.G. provided the instrumentation and analysis tools. A.D. verified the reproducibility of the results. All the authors discussed the data and agreed on their interpretation. E.B. wrote the original draft. P.M., A.D., G.C. and M.G. provided comments and suggestions to improve the original draft. All the co-authors contributed to the final polishing of the manuscript.

Impact of morpho-sedimentary heterogeneities on the evolution of coastal meandering rivers: insights from the Medieval Brenta River (Italy)

Elena Bellizia[1], Jacopo Boaga[1], Paolo Mozzi[1], Giorgio Cassiani[1], Andrea D'Alpaos[1], Massimiliano Ghinassi[1]

[1] Department of Geosciences, University of Padova, Via G. Gradenigo 6, IT-35131 Padova, Italy

ABSTRACT

Alluvial and coastal plains developed through time thanks to the evolution of alluvial systems, which shape the landscape by accumulating a variety of morpho-sedimentary bodies. Such floodplain heterogeneity, which is enhanced by compaction processes, influences river dynamics by providing preferential areas to be eroded, for instance in the case of river avulsion. Although there is literature about river adjustments to active tectonics, which induce morphodynamic changes as uplift and subsidence areas are crossed by a river, less is known about the interaction between rivers and topographic highs and lows in the plain, which slightly differ in elevation respect to the plain and originated from differential compaction of morpho-sedimentary alluvial elements.

The present study contributes to fill this knowledge gap by analysing the fluvial response of an ancient channel belt to the floodplain morphological and sedimentological heterogeneities. A 14 km long paleo-channel belt of the southern Venetian Plain (northeast Italy) was considered for field (e.g., sedimentary cores and geophysical investigations) and morphometric analyses (e.g., remote sensing). Results reveal that the channel belt experienced architectural changes as it crossed the flank of an ancient beach ridge, which appear as a relative topographic high in the floodplain. Changes in the plain gradient and the erodible substrate, as the channel approached the topographic high, induced morphometric and sedimentological changes in both portions of the channel belt above and below the high.

6.1 Introduction

Alluvial plains develop through aggradation, erosion, and deposition of river deposits. During their evolution, rivers may exhibit variable planform styles (i.e.,

expansion, rotation and translation) (Leopold and Wolman, 1957; Schumm, 1985), transforming from one to another through time as the dominant controls on the system change (Hartley et al., 2010). Overall, meandering rivers are more frequently found to characterise low-gradient plains (e.g., Mississippi River on the Louisiana Plain, USA; Amazon River on the Brazil plain), where they can generate sinuous channel bends. These bends can migrate laterally through different mechanisms, since their planform evolution reflects a balance between the erosive power of the streamflow and the erosional resistance provided by their banks (Leopold and Wolman, 1957; Nanson, 1980; Dietrich and Smith, 1984). As meandering rivers evolve, they form different morpho-sedimentary bodies, including point bars, levees, crevasse splays, channel plugs, chute channels and oxbow lakes (Leopold and Wolman, 1957; Allen, 1965). Avulsion events (Russell, 1954; Smith et al., 1989; Posamentier, 2001; Carter, 2003), are fundamental in shaping the landscape of a plain as they lead to the abandonment of a segment of a meander belt to form a new course, which can re-occupy older fluvial traces (i.e., annexation), develop from previously formed forms, such as crevasse channels (i.e., progradation), and create a new reach by eroding the plain (i.e., incision) (Aslan and Blum, 1999; Morozova and Smith, 1999; Slingerland and Smith, 2004).

Avulsive processes, in combination with different styles of bend planform evolution, allow meandering rivers to build up alluvial and coastal plains characterised by heterogeneous sedimentary successions composed of a rich network of inherited morpho-sedimentary elements (Nanson, 1980; Khan et al., 1997; Kemp, 2004; Burns et al., 2017). These elements show different sedimentological architecture and internal features, being consequently characterised by different lithologies and compaction rates (i.e., sandy elements undergo less compaction than muddy ones), which can promote the development of microreliefs on the plain surface (Khan et al., 1997; Kemp, 2004), such as slightly depressed (e.g. muddy) and elevated (e.g. sandy) areas. The architectural complexity of coastal-plain sedimentary successions is increased where alluvial systems interact with other depositional environments, like deltas or strand plains (Gouw, 2007; Ghielmi et al., 2010; Shiers et al., 2014, 2018). Interaction between these environments generates adjacent sedimentary units with contrasting sedimentological properties, that can enhance local microrelief following spatial distribution of different lithologies and related compactional rates.

The role of these microreliefs has been acknowledged in terms of their link with avulsive processes (Slingerland and Smith, 2004; Jones and Hajek, 2007) or with the early phase of meander bend development (Bellizia et al., 2021). However, the fluvial response to micro morphologies induced by lithological heterogeneities of the substrate (e.g., previous floodplain deposits that undergo different compaction rates based on their lithology) has been poorly investigated. Although river response to subtle modifications of floodplain morphologies triggered by tectonics have been studied (Ouchi, 1985; Jorgensen, 1990; Holbrook and Schumm, 1999; Schumm et al., 2000), not much is known about the interaction between rivers and relict floodplain morphologies and related microreliefs. This is especially true in the case of morphologies characterised by topographic elevations that slightly differ from the surrounding plain (i.e., microreliefs), for instance in low-gradient coastal plains.

This study focuses on the fluvial response to relict floodplain morphologies in coastal areas. Specifically, it analyses the effect of morpho-sedimentary heterogeneities on the evolution of a late Holocene channel belt that crossed the southern Venetian Plain (northeast Italy). This plain originated during the Holocene, over a regressive coastal succession, by aggradation and evolution of rivers and still shows a complex network of relict fluvial traces and depositional elements (Bondesan et al., 2008; Fontana et al., 2008; Mozzi et al., 2020). The main goal is to study the morphometry and sedimentology of a 14 km-long paleo-channel belt through remote sensing and statistical analyses, together with field investigations (i.e., sedimentological and geophysical analyses) on five meander bends. Obtained data are discussed in relationship with the architecture of the coastal sedimentary succession sited below the study channel belt. Results highlight the sensitivity of meandering rivers to coastal plain microreliefs, by depicting the morphometric and sedimentological response to floodplain heterogeneities related to relict morpho-sedimentary elements.

6.2 Geological setting

6.2.1 The Venetian Plain

The Venetian Plain is the southern portion of the Venetian-Friulan Plain and is part of the foreland basin occurring between the eastern portion of the Southern Alps and the Northern Apennines (Ghielmi et al., 2010). The Venetian Plain is filled with a 700 m-thick sedimentary succession that originated in the

last 2.5 My (Fontana et al., 2010; Amorosi et al., 2017). During the Last Glacial Maximum (LGM; 30 – 17 ky BP), the Adriatic Sea retreated 400 km from the present-day coastline and the Plain was covered with a considerable amount of alluvial deposits (i.e. up to 25-30 m thick) fed from the retreating glacial fronts (Fontana et al., 2008). A transgressive-regressive cycle followed the LGM, leading late Holocene channel belts to develop under highstand-aggradational conditions. The Plain started experiencing anthropogenic activity in the Roman period when roads and canals were built up, and wide areas were ploughed and cultivated. The major modifications started in the XV century when the Venetian Republic laid down the river diversion and the construction of dikes, canals and ditches that are still recognizable in the Plain.

Since the XVIII century, the rivers were artificially confined, preventing lateral mobility and sedimentation. In the XX century, the reclamation was extended to the coastal plain, where large portions of swamps and lagoons were drained. The Plain is affected by natural subsidence, whose rates are amplified by anthropic activities, reaching maximum values of 10 mm/y (Teatini et al., 2011). The coasts of the Venetian Plain are characterised by a microtidal tidal regime with an average tidal range of 1 m and maximum astronomical tidal excursions of 0.75 m (D'Alpaos et al., 2013).

6.2.2 The study area

The study area is in the southern portion of the Venetian Plain, which is nowadays drained by the eastward-flowing Adige, Bacchiglione and Brenta Rivers (Fig. 6.1A). It is a low gradient (<1‰) plain where satellite images allow for the identification of different geomorphological elements, including fluvial ridges, overbank areas and beach ridges (Fig. 6.1B). Fluvial ridges consist of elongated sand bodies, formed by the aggradation of meandering channel deposits and their natural levees (green areas, Fig 6.1B), in which traces of the last active channels are still visible (brown lines in Fig. 6.1B). On these belts, paleo-channels generally appear with a sinuous shape (Fig. 6.1D-E-F-G), sometimes discontinuous or ending to splay morphologies. The paleo-traces of the belts can be larger than 2 km, whereas the fluvial ridges vary in width from less than 50 m to almost 1 km. Fluvial ridges have a noticeable downdip continuity (i.e., 3 to 15 km) and are surrounded by depressed areas (light brown areas, Fig 6.1B) that host organic-rich mud deposits accumulated in flood-basin swamps, developed between the fluvial ridges (Fig. 6.1G). The easternmost part of the study area is mainly occupied by a beach ridge system (yellow areas, Fig.

6.1B) that were originated by the progradation of the Po and Adige deltaic systems (Fig. 6.1H), thus indicating the position of ancient coastlines (Bondesan et al., 2004).

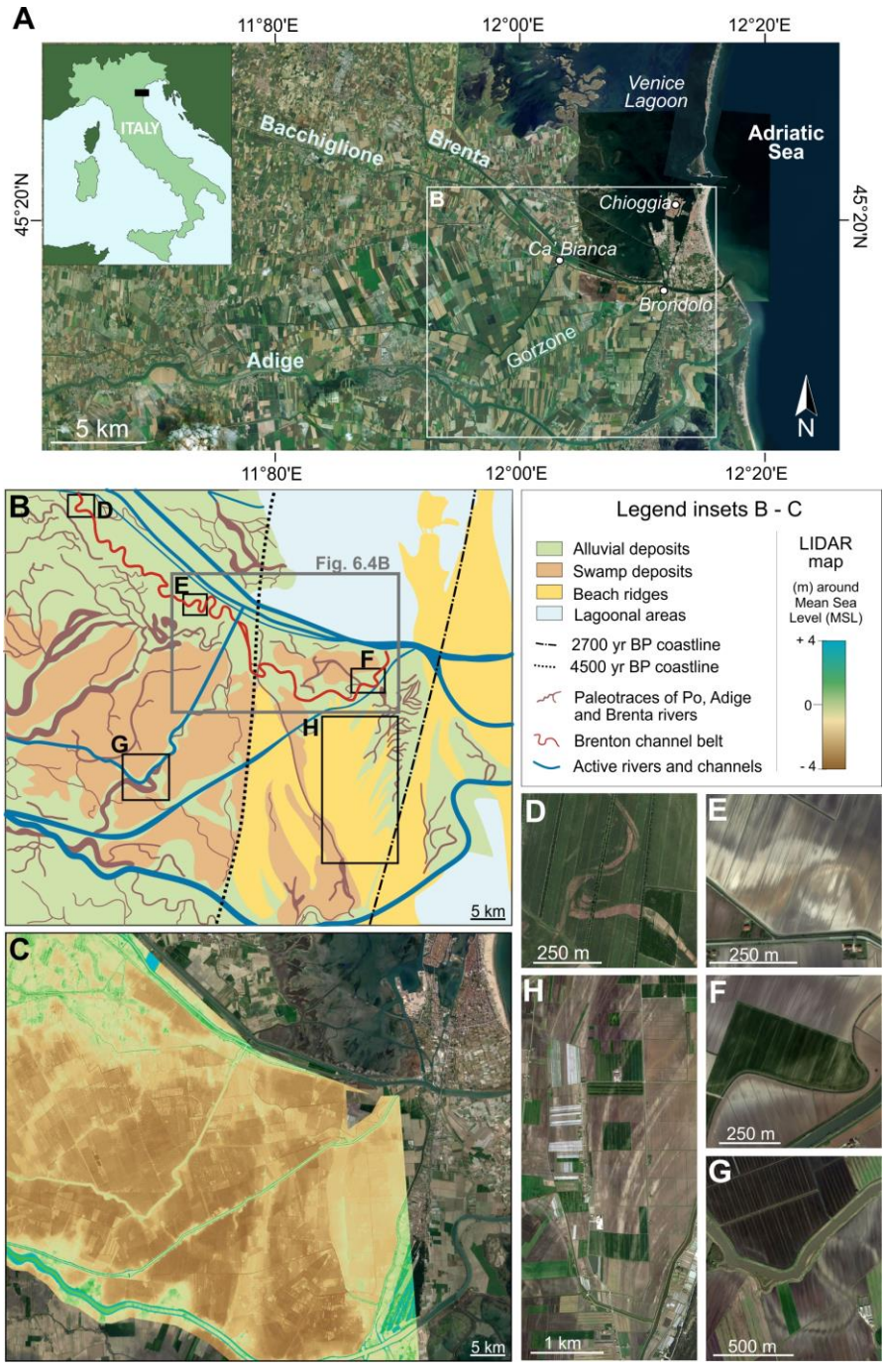

Fig. 6.1. The study area. (A) The southern portion of the Venetian Plain (NE, Italy) with the main active hydrography; (B) The main morpho-sedimentary elements of the study area (modified from

Bondesan et al. 2008). (C) Lidar map (Veneto region, Italy) of the study area (http://www.pcn.minambiente.it/). (D – H) Satellite images of the different elements: alluvial deposits and paleotraces of meander bends (D – G), alluvial swamps (G) and beach ridges (H).

The major fluvial ridges of the study area were generated by the Po and Adige rivers. Between 3.5 and 2.2 ky BP the Po River (Po di Solferino) crossed the area entering the Adriatic Sea at Chioggia (Fig. 6.1B). Sedimentary cores reveal that the main channelized body is up to 6 m thick and mainly consists of medium sand (Bondesan and Meneghel, 2004). The other major fluvial ridges of the area were generated by different reaches of the Medieval Adige River (ca. 1000 yrs. BP), which generated sandy sedimentary bodies up to 5 m thick (Bondesan and Meneghel, 2004).

Swamp deposits characterised an area where the highest subsidence rate of the coastal zone was reconstructed by means of field data and laboratory experiments (e.g. Zennare Basin, Fornasiero *et al.* 2002; Rizzetto *et al.* 2002). Swamp deposits consist of silty clay deposits with plant debris and show a maximum thickness of 2 m (Favero and Serandrei-Barbero, 1978; Bondesan et al., 2004). The beach ridge deposits belong to two different deltaic systems generated by the Po River around 3 and 4 ky BP, respectively. Both beach ridges consist of composite laterally-continuous, and laterally offset, elongated sand bodies (e.g. Ravenna Po, Amorosi *et al.* 1999). The beach ridges are up to 12 m thick and consist of medium-fine sand with abundant shells and shell fragments.

6.2.3 The Brenton paleo-channel belt

The Brenton paleo-channel belt (the focus of this study) is an NW-SE trending, 14 km-long, and 250 m-wide paleo-channel belt (red line, Fig. 6.1B), which ranges in elevation between +1 and -2 m around Mean Sea Level (MSL) from upstream to downstream portions (Fig. 6.1C). The Brenton paleo-channel belt was the southernmost reach of the Medieval Brenta River, which crossed the city of Padova and entered the Adriatic Sea in the Port of Brondolo, where the coastline almost coincided with the present-day one (Favero and Serandrei-Barbero, 1978; Bondesan et al., 2004). The Brenta River is an emissary of the Caldonazzo Lake, in the Trentino Alto Adige region (Italy), and has a catchment area of 5840 km^2 with an average discharge of 71 m^3/s. The study channel belt was active from the IV century a.D. to the 1142 a.D. when it was abandoned because of the diversion of the Brenta River to Fusina, in the Venice Lagoon (Favero and Serandrei-Barbero, 1978; Mozzi et al., 2013). Successively, the Brenta River was diverted repeated times into the sea, to prevent silting of the

Lagoon (Fig. 6.2), but the Brenton reach remained partially active as a secondary branch of the Brenta River until the XVI century (see Bondesan and Meneghel, 2004 for historic maps).

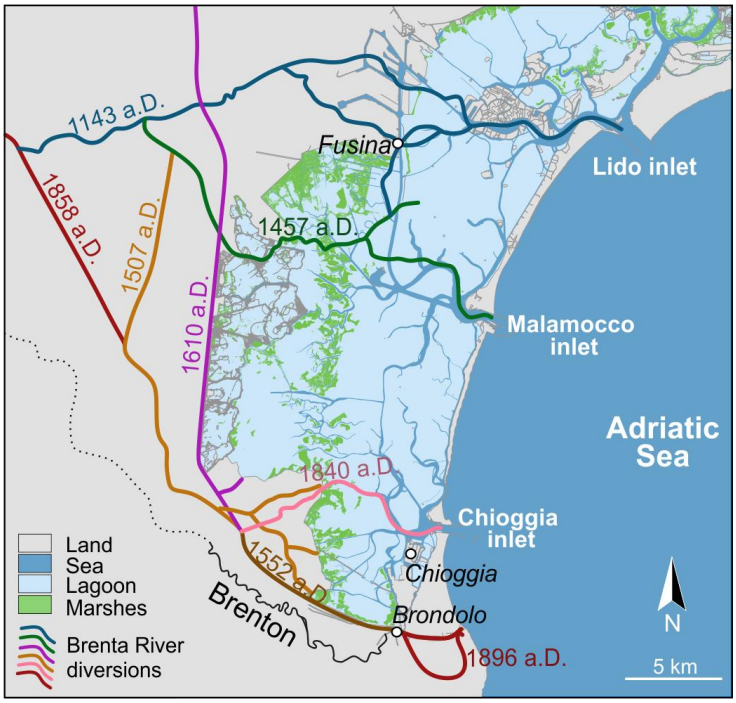

Fig. 6.2. The diversion history of the Brenta River from the XXII century a.D.. The Brenton channel belt is traced in its final portion (solid black line) (i.e., the study area), whereas it is hypothesized toward the inland (dashed black line).

Subsurface and geomorphological data showed that the Brenton belt developed over two different substrate deposits (Bondesan et al., 2008). In the NW sector of the study area, integrated studies highlighted that the Brenton channel developed over the ancient channelised and overbank deposits of the Adige River (i.e. Conselve ridge), which was active during the Roman Age (Tosi et al., 2007; Bondesan et al., 2008). Differently, in the SE part of the study area (i.e., east of Ca' Bianca) the Brenton channel belt drained across deposits forming the old beach-ridge sand (Fig. 6.3). These beach-ridge deposits plunge below the Adige River alluvium in the Ca' Bianca area, where the surface capping the beach-ridge sand forms a westward dipping ramp inclined at ca. 30°.

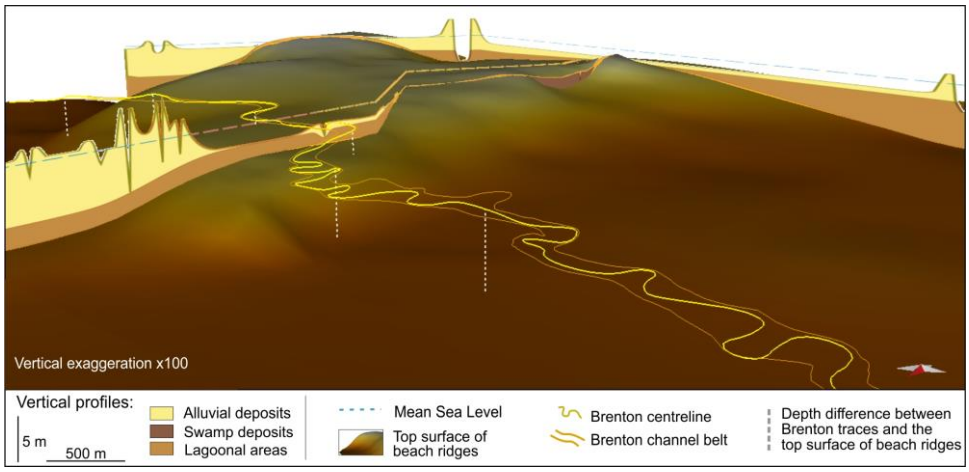

Fig. 6.3. 3D reconstruction of the stratigraphic top of the beach ridges in the study area, with the relative position of available cores in the area and the stratigraphic ones of the Brenton channel belt.

6.3 Methods

Planform evolution of the Brenton paleo-channel belt was reconstructed by comparing Google Earth and Bing™ satellite images acquired at different years, where soil marks and crop marks enhance the subsurface differences in sediment properties due to different humidity content (Cassiani et al., 2020). QGis 3.16.14 were used to image interpretation: following soil marks related to the abandoned channel fill, the analysis of satellite images allows identifying the centreline of the paleo-channel belt, depicting its planform geometries. Satellite images were integrated with the available LIDAR data and aerial photos acquired in 2012 (www.regione.veneto.it). LIDAR data allowed to obtain present-day elevations of the Brenton channel belt. The morphometric, geomorphological, and sedimentological terminology adopted in this work is shown in Figure 6.4A.

The QGis 3.16.14 shapefile of the channel-belt centreline was elaborated with a Matlab code that identifies the apex and inflection points of each bend in a semi-automatic way (Finotello et al., 2020). The code measures the morphometric parameters of each bend (Fig. 6.4A), including sinuosity (Sin), amplitude (Ampl), radius of curvature (R.Curv.), median and maximum curvature (C.med and C.max), intrinsic wavelength (Ls), cartesian wavelength (Lxy), curvature skewness and kurtosis (C.skew and C.kurt). Only bends with sinuosity greater than 1.06 were analysed (Brice, 1975; Kellerhals et al., 1976;

Schumm, 1985; Friend and Sinha, 1993). To observe the variability of each morphometric parameter per bend univariate analyses were performed (Excel statistical tool, Office 365).

Fig. 6.4. Terminology and methodologies. (A) Morphological, depositional, and morphometric terminology adopted in this paper. (B) The position of the sedimentary cores recovered in the five selected meander bends (Cases 1 to 5) belonging to three different localities (see Fig. 6.1B for the location of this view). (C) The geophysical acquisition: in white dots, the data point acquired in Case 1.

Five meander bends (i.e., sinuosity greater than 1.25 (Brice, 1975; Kellerhals et al., 1976; Schumm, 1985) were selected for sedimentological and geophysical

investigations, based on relative position within the 14 km-long channel belt and accessibility of sites (Fig. 6.4B). Fifteen cores were recovered to analyse sedimentary features of point-bar deposits (Fig. 6.4B). A continuous drilling core sampler with a rotary technique was used to collect 10 cm wide cores, up to 9 m-long, that were recovered in the upstream, central, and downstream portions of the five meander bends. Cores were cut longitudinally, logged, photographed, and treated with epoxy resin to preserve sediments and structures.

To characterise the 3D volumes of point bars related to cored bends, Electromagnetic Induction (EMI) surveys in the frequency domain (FDEM) (Corwin and Rhoades, 1982) were performed on different days during an year. A GF Instruments CMD-Explorer probe was used to collect geophysical data; being characterised by a multi-coil system, the tool allows investigation of the apparent electrical conductivity (ECa) at different depths up to – 7 m. This was made possible thanks to the double acquiring configurations in horizontal and vertical coplanar modes (Um and Alumbaugh, 2007), which need a double pass through the same area. To accurately georeferencing the geophysical data, a Trimble 5800 GPS was connected to the FDEM probe, for continuous position measurements; the probe was also fixed to a wooden sled, designed to keep constant the probe height from the ground, and dragged by a small tractor (see Cassiani et al., 2020 for further details). Acquisition of each selected meander bend provides 10’000 to 30’000 points, depending on the spatial extension of the site (e.g., collected data points at site 1, Fig. 6.4C). Acquired data were inverted to obtain real electrical conductivity values of the subsurface by using the EMagPy, a Python-based open-source software for 1D EMI inversion (McLachlan et al., 2021). Eight depth intervals were used to constrain the inversion, producing eight layers. The deepest of these layers is representative of conductivity data from 7.5 meters to down. Data were imported into the QGIS working space and interpolated through the natural neighbour tool to define 2D horizontal conductivity maps at different depths, with average electrical conductivity values σ (mS/m) for depth intervals of 1 m [i.e., 0 – (-1.5 m), (-1.5) – (-2.5) m, (-2.5) – (-3.5) m, up to -7.5 m)]. Only the first five maps from the ground level (up to -5.5 m) per site were considered since the deeper ones were too close to the instrument acquisition limit.

6.4 Results

6.4.1 Morphometric analyses

Morphometric analyses identified 32 bends belonging to the latest phase of channel-belt evolution (Fig. 6.5A), showing that the bend sinuosity averages around 1.57, ranging between 1.10 and 2.9, whereas the mean amplitude of bends is 140 m, with peaks at 325 and 42 m, and the radius of curvature ranges between 54 and 490 m with an average value of 205 m.

From a morphological and descriptive point of view, the study belt was subdivided into an upstream, central and downstream reach (Fig. 6.5A). The central portion includes approximately the bends from number 14 to 21 and differs from the other two reaches for having on average high sinuosity values (i.e., from 1.51 to 2.2) (Fig. 6.5B), linked especially to the presence of overall low values of Lxy (i.e., values from ca. 120 to 310 m) (Fig. 6.5C). The central section also has lower values of the radius of curvature (i.e., between 80 and 150 m), compared to all the bends, where average values are about 200 m (Fig. 6.5D). The Amplitude and Ls of bends do not easily identify the central reach, but rather highlight the downstream stretch, where bends show values with wider ranges for both parameters (Fig. 6.5E-F). For Ls, the downstream reach has values from 200 to 1080 m, while in the previous bends the range varies on average from 200 to 600, with only two bends between 700 and 800 m (Fig. 6.5E). Bends of the downstream reach have amplitude values ranging between 325 and 42 m, while the bends of the other reaches vary on average from 65 to 200 m (Fig. 6.5F). Present-day elevations show that the channel belt varies from 0.8 to -1.5 m above MSL (Fig. 6.5G). The central reach can be easily identified as it breaks the continuity of the upstream gradient, which shows a clear seaward decrease (Fig. 6.5G).

The central zone shows almost uniform elevation values, comparable to those of the distalmost part of the upstream reach. The downstream reach is characterised by the lowest values, with a poorly defined seaward decrease in elevation.

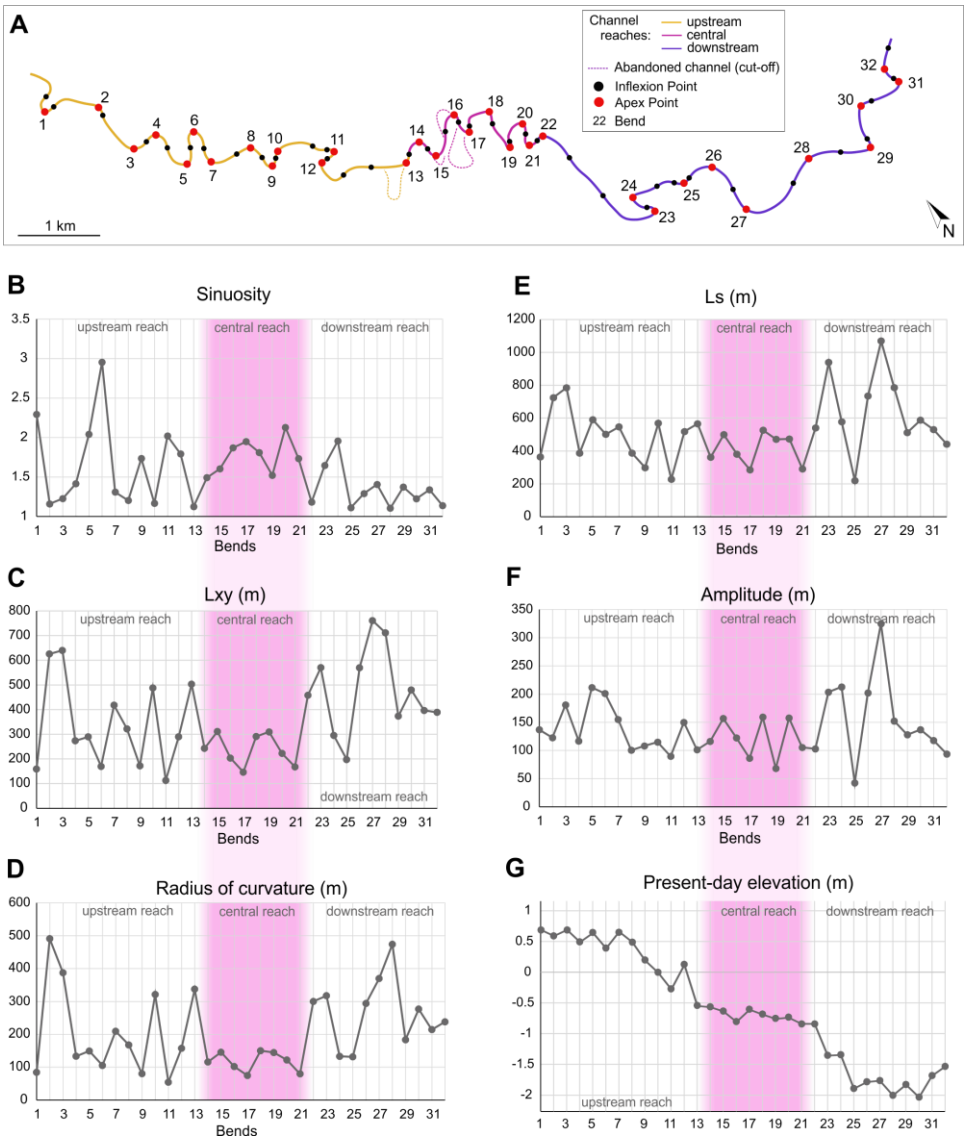

Fig. 6.5. Morphometric and statistical results. (A) Graphical output of the Matlab code, showing the position of apexes (red dots) and inflection points (black dots) of the 32 bends belonging to the channel centreline, which is subdivided in three reaches: yellow, pink and purple for upstream, central and downstream reaches, respectively. Meander cut-offs are also identified. (B - G) Graphs showing variability of Sinuosity (Sin) (B), cartesian wavelength (Lxy) (C), radius of curvature (R.Curv.) (D), intrinsic wavelength (Ls) (E), amplitude (Ampl) (F) and present-day elevations (G) of the 32 bends, with a coloured band to indicate the central reach.

6.4.2 Sedimentological analyses

Sedimentary cores reveal that the first 0.5 m below the ground surface consists of massive sandy mud, which has been intensively reworked by agricultural activities (Figs. 6.6 to 6.8). Point-bar bodies of the five meander bends are on

average 5.5 m thick, ranging between 4.5 and 6.5 m. Point-bar deposits consist of fine to coarse sand (Figs. 6.6 to 6.8), which appears mainly structureless due to the coring process. Occasionally, plane parallel to inclined stratifications in the main body can be observed (Figs. 6.6 to 6.8). Upper-bar deposits are locally heterolithic, with oxidised fine to medium sand that is commonly ripple-cross laminated (Figs. 6.6 to 6.8).

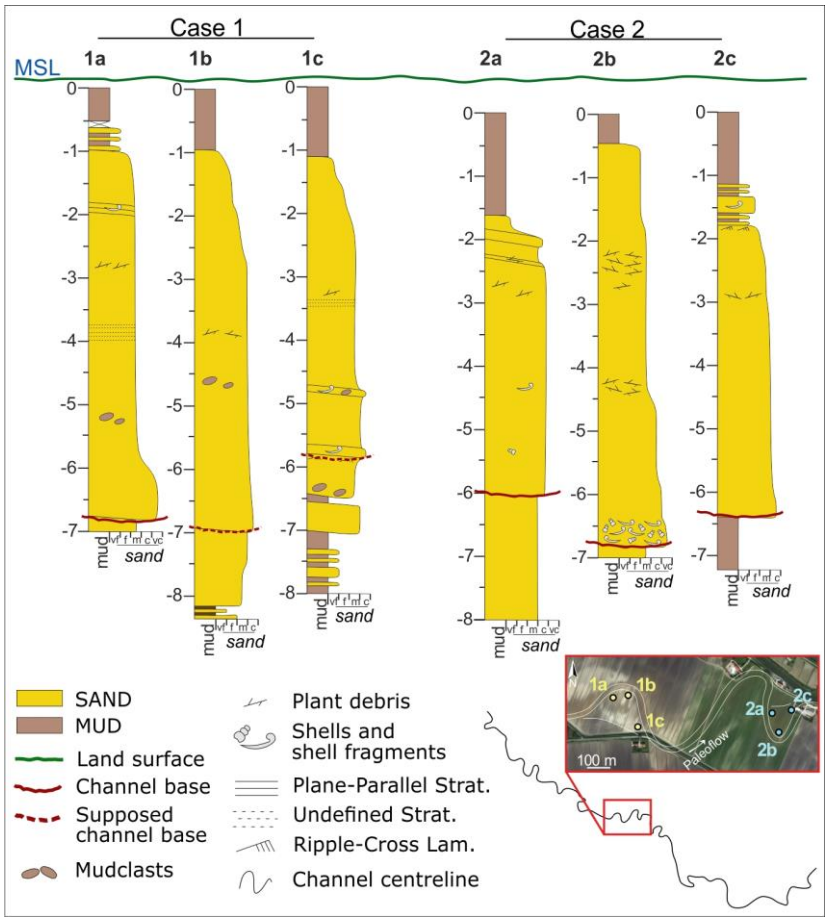

Fig. 6.6. Sedimentological results. Logs of the sedimentary cores from Case 1 and Case 2, (topographically positioned respect to the MSL) with location of each core with respect to each meander bend on a Google Earth image (Map data: ©2012 Google-Landsat/Copernicus, Maxar Technologies) and the Brenton channel.

The channel lag is almost recognizable in all cores and consists of massive medium-to-coarse sand (Fig. 6.9B), which is locally enriched with shells, shell fragments (Fig. 6.9A) and mud clasts. Point-bar deposits erosively cover both laminated mud (Fig. 6.9B) with sandy intercalations (Fig. 6.9C) or massive sandy deposits (Fig. 6.9A). Vertical grain-size distribution highlights that upstream bar

portions show a blocky-(sensu Willis, 1989) to-slightly-coarsening upward trend of grain size (cores 2a, 3a, 4a and 5a in Figs. 6.6 to 6.8), whereas central and downstream cores are characterised by a gentle fining upward trend (cores 1b-c, 2b-c, 3b-c, 4b-c, 5b-c in Figs. 6.6 to 6.8). These vertical grain size trends occur consistently at the different study bends, with no relevant changes occurring moving upstream or downstream along the bend.

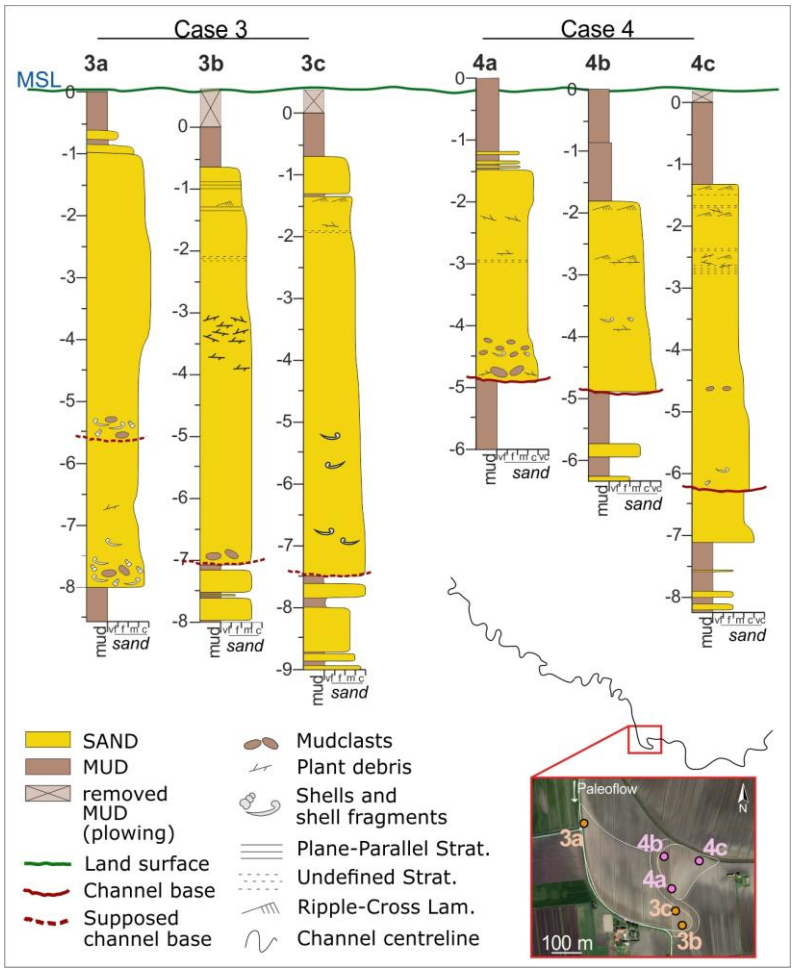

Fig. 6.7. Sedimentological results. Logs of the sedimentary cores from Case 3 and Case 4, (topographically positioned respect to the MSL) with location of each core with respect to each meander bend on a Google Earth image (Map data: ©2012 Google-Landsat/Copernicus, Maxar Technologies) and the Brenton channel.

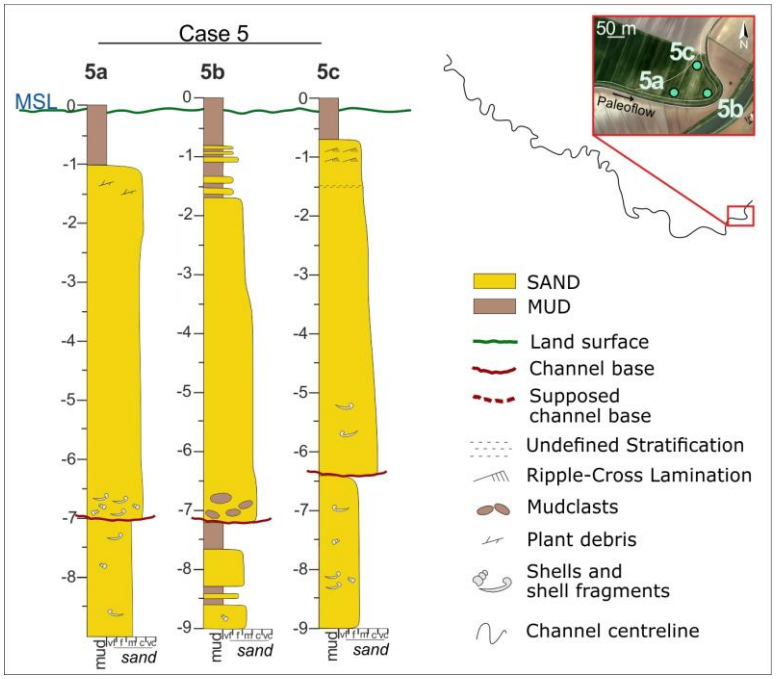

Fig. 6.8. Sedimentological results. Logs of the sedimentary cores from Case 3 and Case 4, (topographically positioned respect to the MSL) with location of each core with respect to each meander bend on a Google Earth image (Map data: ©2012 Google-Landsat/Copernicus, Maxar Technologies) and the Brenton channel.

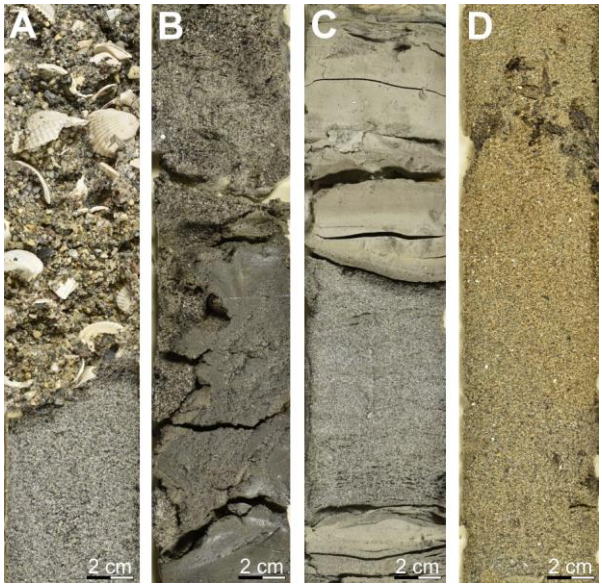

Fig. 6.9. Sedimentary results. Deposits: channel lag with (A) or without (B) shells and shell fragments, overlaying two types of deposits: sandy (A) and muddy (B) ones. (C) Example of the heterogeneous muddy substrate, and (D) massive sandy point-bar body.

6.4.3 Electromagnetic analyses

The 2D electrical conductivity maps show that the conductivity varies between 10 and 500 mS/m (Fig. 6.10). All the maps show spatial changes in conductivity values, which strongly reflect paleo-channel morphologies and planform scroll distribution observable from satellite images, making exception for study case 2, where electrical conductivity shows a remarkably limited spatial variability.

Case 1 (Fig. 6.*10A to F)*. Electrical conductivity values range between 10 and 150 mS/m. The abandoned channel deposits are 40 m wide and show electrical conductivity values ranging between 40 e 57 mS/m. The contrast between conductivity values of the abandoned channel and those of the surrounding deposits allows to depict the abandoned channel unit until 5.5 m below the ground. Conductivity values of point-bar deposits range between 10 and 33 mS/m, and clearly follow scroll-bar geometries in the 2.5 m below the ground (Fig. 6.10B-C), whereas between 2.5 and 5.5 m bar deposits are characterised by more homogeneous conductivity values (Fig. 6.10D-F). Overbank deposits range in conductivity values between 50 to 150 mS/m (Fig. 6.10A to F).

Case 2 (Fig. 6.*10G to L).* Electrical conductivity values range between 20 and 290 mS/m, but both channel-fill and point-bar units are poorly distinguishable (Fig. 6.10H-L), whereas the scroll-bar pattern can be seen from the satellite image (Fig. 6.10G). The abandoned channel-fill deposit is 35 m wide and ranges in conductivity between 50 and 70 mS/m. The point-bar deposit shows electrical conductivity values ranging between 20 and 60 mS/m. Southeast of the point bar, overbank deposits are visible and show conductivity values higher than 70 mS/m.

Case 3 and case 4 (Fig. 6.*10M to R).* The electrical conductivity ranges between 0 and 300 mS/m, highlighting the occurrence of two consecutive point-bar units characterised by conductivity values varying between 0 and 90 mS/m. The abandoned channel-fill unit is 30 m wide and shows conductivity ranging between 70 and 140 mS/m. Surrounding overbank deposits are characterised by conductivity values higher than 130 mS/m.

Case 5 (Fig. 6.*10S to X).* The electrical conductivity varies between 100 and 500 mS/m. The point-bar deposit shows conductivity ranging between 100 and 300 mS/m, whereas in the abandoned channel-fill unit they are higher than 300 mS/m. North-Northwest to the point-bar unit, overbank deposits show the same conductivity interval as channel-fill deposits, particularly below the 3.5 m (Fig. 6.10W-X), testifying to the occurrence of sandy beach ridges.

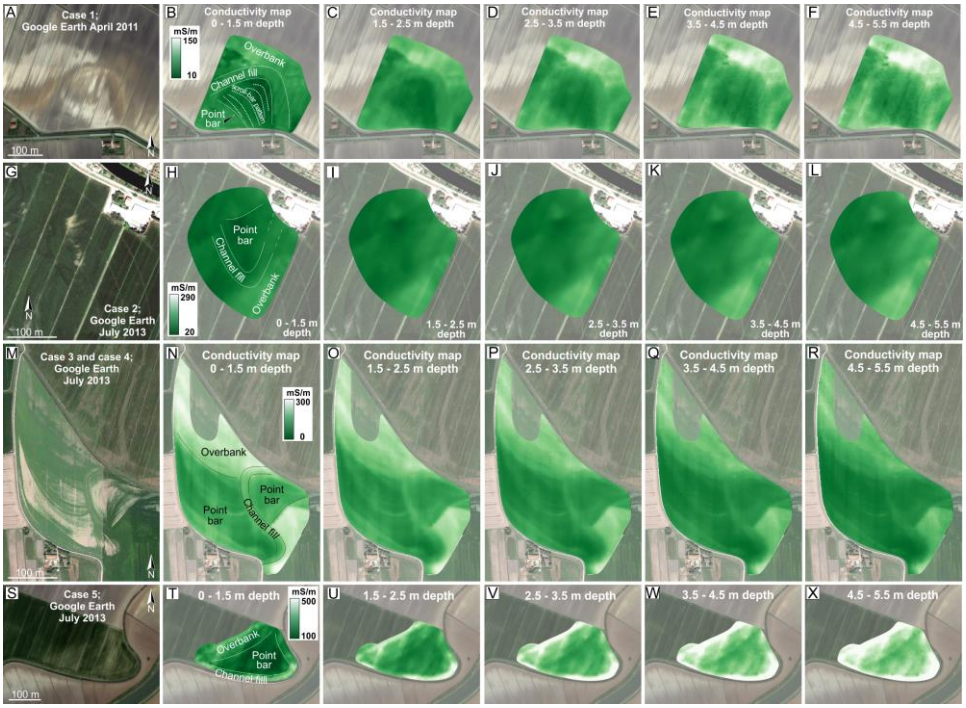

Fig. 6.10. Electromagnetic results. The upper five electrical conductivity maps of each investigated meander bend: (A-F) site 1, (G-L) site 2, (M-R) sites 3 and site 4, (S-X) site 5.

6.5 Discussion

6.5.1 Placing the study reach within a riverine profile

Relevant morphodynamical changes are known to affect riverine systems once they approach the coastline, especially where channels enter the backwater zone (Nittrouer et al., 2012). A river enters the backwater zone when the channel-bed elevation descends below sea level, allowing the properties of the receiving basin to influence the riverine flow (Chow, 1959; Paola and Mohrig, 1996; Li et al., 2006; Nittrouer et al., 2012; Blum et al., 2013). Entering the backwater zone, migration rates and the width-to-depth ratio of a channel can change (Durkin et al., 2017). The backwater zone can extend hundreds of kilometres upstream from the river mouth in low-gradient rivers (Li et al., 2006; Nittrouer et al., 2012; Blum et al., 2013). The upstream portion of the Brenton channel belt is approximately 0.5 m above the modern sea level (MSL); since the average depth of the study paleochannel is 5.5 m, the channel thalweg of the upstream channel belt reach is estimated to be sited at ca. 5 m below the

modern sea level. Considering a subsidence rate ranging between 1 and 2 mm/year (Teatini et al., 2011), and knowing that the sea level of the Adriatic Sea was approximately -1.2 m below the present-day level around the IV century a.D. (Vacchi et al., 2016), emerges that the channel thalweg of the upstream reach of the Brenton belt was about 1.2 m below sea level, placing the whole study belt within the backwater zone.

In the modern Venetian Plain, direct measurements (http://idrometri.agenziapo.it/Aegis/map/map2d) show that water elevation in large rivers (e.g., Po River) is modulated by tides up to several tens of kilometres from the mouth also during floods. Accordingly, since the upstream termination of the study Brenton reach sites at about 15 km from the modern coastline, its flow could have been modulated by the tidal oscillations, indicating that the study reach was placed within the fluvial-marine transition zone.

6.5.2 Morphometric changes in river bends

Morphometric analyses show that moving from the upstream to the central reach of the study belt, bends tend to gain a greater sinuosity, diminish their radius of curvature, amplitude, and wavelength, and generate cut-offs. Differently, in the distal reach, bends are wider and less sinuous and are characterised by higher radius of curvature and amplitudes than in the central reach (Fig. 6.5). Being the study reach entirely placed within the fluvio-tidal transition zone, changes in bend morphometries cannot be ascribed either to the channel's entry into the backwater zone or to relevant changes in fluvial-tidal interaction processes. These changes are here discussed in terms of interaction between riverine dynamics and sedimentological characteristics of the related substrate. Specifically, the study belt developed onto a heterogenous substrate characterised by muddy alluvial elements and sandy coastal ones (Bondesan et al., 2008). Due to their different textural structure, muddy alluvial successions and sandy beach ridges experienced different sin- and post-depositional compaction (Teatini et al., 2011), triggering different spatially-distributed subsidence rates. Differential compaction enhances micro-morphologies of the alluvial plain surface (Gambolati and Teatini, 1998; Gambolati et al., 1998; Bruno et al., 2019), defining morphological 'highs' and 'lows' in the plain, which can differ up to several decimetres in elevation (Teatini et al., 2011). Due to their sandy nature, the beach ridges experienced relatively lower compaction in comparison with the adjacent muddy alluvial succession of the subsiding Zennare Basin (Fornasiero et al., 2002; Rizzetto et al., 2002).

Specifically, the central portion of the study reach is placed where the muddy alluvial units onlap the sandy beach ridge. At this site, the river was forced to cross over a localized counter-slope generated by the reduced compaction of the sandy ridge. Such a morphological setting resembles those generated by epeirogenic movements in tectonically active zones (Holbrook and Schumm, 1999; Schumm et al., 2000), where rivers reorganise their planform to cross localised shoulders (Burnett and Schumm, 1983; Ouchi, 1985; Jin and Schumm, 1987; Holbrook and Schumm, 1999; Schumm et al., 2000). In this setting, the Brenton channel response resembles the longitudinal changes triggered by localized tectonic uplifts (Fig. 6.11). Just upstream of the beach-ridge morphological high, bends tend to increase in sinuosity and generate neck cut-offs in response to the slope decrease and possible local development of counter-slope morphologies (Fig. 6.11). This sensitive decrease in river slope triggered an increase in sinuosity to maintain its bedload transport capability, which culminated in several cut-off events.

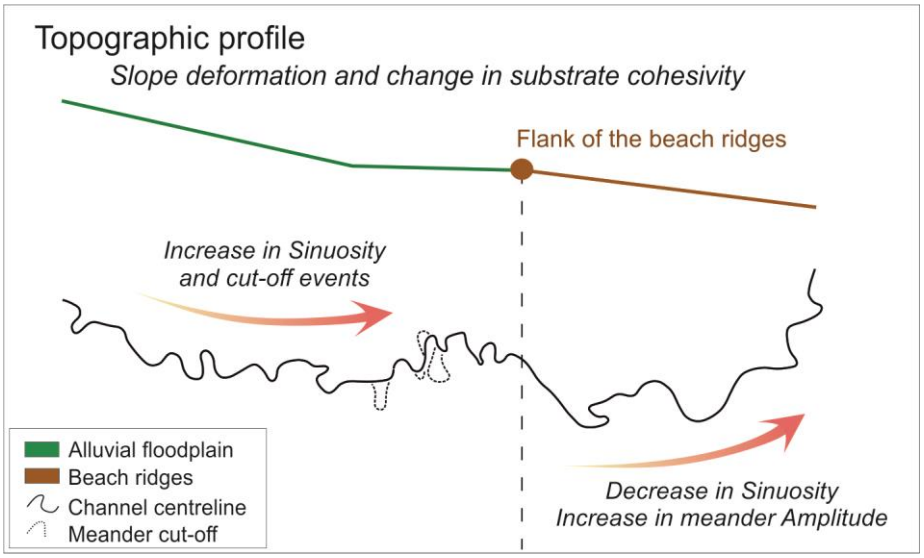

Fig. 6.11. Schematic sketch of the causes that influenced the morphometric changes of the Brenton channel belt: a change in the plain gradient (topographic profile) due to the approaching of the sandy beach ridges, and a change in substrate cohesivity.

Although the unconsolidated nature of the river substrate allowed the river to easily cut through the substrate avoiding local damming (Doornkamp and Temple, 1966; Räsänen et al., 1987; Marple and Talwani, 1993), this decrease in river gradient reasonably increased flow expansion in overbank areas and related mud sedimentation (Ouchi, 1985; Jorgensen, 1990; Bianchi et al., 2015).

Accumulation of mud in overbank zones contributed to developing cohesive banks, which enhanced the increase of channel sinuosity (Schumm, 1960; Hooke, 2007; Lazarus and Constantine, 2013). Further changes in channel-bend morphometries occur in the distal reach of the Brenton channel, where the river flowed above the beach-ridge sand (Fig. 6.11). In this reach, the river tends to define milder bends by decreasing sinuosity and increasing the intrinsic wavelength and amplitude of bends (Fig. 6.11). The relatively uniform gradient of the area did not probably play any relevant role in modifying the morphology of bends, and the origin of these mild bends is consistent with the occurrence of a non-cohesive substrate and erodible banks, which militated against the formation of sharp bends (Gibling, 2006; Davies and Gibling, 2010; Ielpi et al., 2014).

6.5.3 Along-belt variability of sedimentary features

Integration between sedimentological and geophysical data depicts the spatial distribution of different types of sediments within the study point bars. At the bar scale, central and downstream portions of investigated point bars (Figs. 6.6 to 6.8) show a weak fining-upward grain size trend that is consistent with the commonly observed upward trend of grain size in point-bar bodies (Nanson, 1980; Nanson and Page, 1983; Bhattacharyya et al., 2015; Durkin et al., 2018; Clift et al., 2019). The blocky to slightly coarsening-upward grain-size trend occurring in the upstream side of some of the study point bars fits with other documented cases (Jackson, 1976; Willis and Tang, 2010; Ielpi and Ghinassi, 2014; Swan et al., 2018), and can be explained by a sediment transport across-stream from the inner to the outer bank of the bend (Dietrich and Smith, 1983).
Point-bar bodies are also usually characterised by a downstream decrease in grain size (Bluck, 1971; Wood, 1989; Bridge et al., 1995; Willis and Tang, 2010; Hubbard et al., 2011). This trend develops as the result of the along-bend decrease of depth-averaged flow velocity and bed shear stress toward a bend (Dietrich and Smith, 1983; Frothingham and Rhoads, 2003; Seminara, 2006; Kasvi et al., 2013), which commonly leads to accumulation of mud in downstream zones. Although this trend is consolidated in classical facies models (Nanson, 1980; Labrecque et al., 2011; Fustic et al., 2012; Nardin et al., 2013), core and geophysical data reveal that investigated point bars do not show this clear downstream fining trend. A relatively homogenous along-bend distribution of grain size is also clearly highlighted by the electrical conductivity maps (Fig. 6.10). The electrical conductivity response depends on different soil properties

like salinity, soil structure, temperature, and moisture content (Paine, 2003). Since in a restricted area soil properties like salinity, temperature and moisture content can be assumed constant at the same elevation, sediment properties exert a major control on the electrical properties of the study bars (Cassiani et al., 2020; Bellizia et al., 2021, 2022), therefore varying with the grain size. Once conductivity is measured at the same elevation below the ground, the lower conductivity values are related to the coarser sediments, and vice versa. The scarce along-bar variability of conductivity values documented at different depths in all the study point bars (Fig. 6.10) confirms the limited changes in grain size of sediments along the bar. These limited changes in grain size along the study point bars, along with the scarce development of a clear fining upward grain-size trend, depict the study bars as highly homogeneous sedimentary bodies separated by mud-rich channel fills. These homogenous sandy point-bar deposits lead the whole channel belt to lack the general downstream decrease in grain size of point-bar deposits, which is generally caused by a lowering of stream gradient and related flow transport capability occurring where rivers approach the coastline (Knighton, 1999; Rice and Church, 2001; Frings, 2008). The overall paucity of fine-grained sediment in the study channel belt contrast with the abundance of mud in overbank areas (Fig. 6.9C), suggesting a scarce capability of the channelised system to store fine-grained deposits on the bars. It also follows that the morphometric changes triggered by substrate heterogeneities do not find clear expression on sedimentary patterns of related deposits, indicating that the river managed to cross over different substrates adjusting its planforms without changing its transport capability. The widespread homogeneity of bar deposits could be ascribed to the fact that observations are limited to a restricted portion of the Brenton watercourse, making changes in the downstream grain-size trend not appreciable. Nevertheless, although tides can modulate river water elevation, the limited tidal range could have not been able to significantly slow down the river flows to promote the settling of relevant volumes of mud within the channel. Finally, erosion of ancient sand-dominated depositional elements, like abandoned fluvial channel belts or beach ridges, could have promoted entrainment of the relevant volume of sand within the Brenton River, contributing to a significant increase in the sand-to-mud ratio within the channel.

6.6 Conclusions

Morphometry and sedimentology of a late Holocene channel belt were analysed through remote-sensing, sedimentological and geophysical investigations, to provide insights into the planform evolution of meandering rivers that flow through coastal lowlands where lithological and topographic heterogeneities occur. Morphological analyses allow subdividing the study belt into three reaches, where bends with different morphometries occur. These different reaches lay on different substrates, consisting of mud-rich alluvial deposits passing seaward into sandy beach ridges. Different compaction of these deposits triggered localised changes in the alluvial plain surface, causing the river to develop closely spaced sinuous bends on the muddy alluvial substrate, and mild bends over the sandy beach ridges. Contrasting cohesivity of these two types of substrate contributed to developing tight and mild bends, respectively.

From a sedimentological point of view, point bars of the study belt exhibit a gentle fining upward trend of grain size, although all the upstream parts of the study bars were characterised by a poorly defined vertical grain-size distribution. Scarce vertical changes in grain-size values are associated with limited grain-size variations along the study point bars, making these bars highly homogeneous sedimentary bodies. A limited grain-size variability has been also observed from the upstream toward the downstream reach of the belt. Although the lack of a classical seaward decrease of grain size could be due to observation on a limited belt segment, the dominance of riverine processes on marine ones (e.g., tides) within the fluvio-tidal transition zone could have contributed to preventing mud storage within the channel. Results from this work call for further studies on the dynamics of rivers crossing alluvial and coastal plains with heterogeneous substrates, since these heterogeneities can trigger subtle morphological modifications having a different impact on riverine morpho-sedimentary processes.

Acknowledgments

This work was economically supported in part by the “HYDROSEM: Fluvial and tidal meanders of the Venetian-Po plain: from hydrodynamics to stratigraphy” project (Progetto di Eccellenza CARIPARO 2017- M. Ghinassi) and in part by the University of Padova (SID2016 project, “From channels to rock record: morphodynamic evolution of tidal meanders and related sedimentary products”

– M. Ghinassi). Authors are grateful with L. Ronchi and P. Mozzi for literature support on the study area.

References

Allen, J.R.L., 1965, A review of the origin and characteristics of recent alluvial sediments: Sedimentology, v. 5, p. 89–191, doi:10.1111/j.1365-3091.1965.tb01561.x.

Amorosi, A., Bruno, L., Campo, B., Morelli, A., Rossi, V., Scarponi, D., Hong, W., Bohacs, K.M., and Drexler, T.M., 2017, Global sea-level control on local parasequence architecture from the Holocene record of the Po Plain, Italy: Marine and Petroleum Geology, v. 87, p. 99–111, doi:10.1016/j.marpetgeo.2017.01.020.

Amorosi, A., Colalongo, M.L., and Fusco, F., 1999, Glacio-eustatic Control of Continental–Shallow Marine Cyclicity from Late Quaternary Deposits of the Southeastern Po Plain, Northern Italy: Quaternary Research, v. 52, p. 1–13.

Aslan, A., and Blum, M.D., 1999, Contrasting styles of Holocene avulsion, Texas Gulf coastal plain, USA, *in* Smith, N.D. and Rogers, J. eds., Fluvial sedimentology VI: International Association of Sedimentologists Special Publication, Wiley Online Library, v. 28, p. 193–209, doi:10.1002/9781444304213.ch15.

Bellizia, E., Boaga, J., Fontana, A., D'Alpaos, A., Cassiani, G., and Ghinassi, M., 2021, Impact of genesis and abandonment processes of a fluvial meander on geometry and grain-size distribution of the associated point bar (Venetian Plain, Italy): Marine and Petroleum Geology, v. 127, p. 104951, doi:10.1016/j.marpetgeo.2021.104951.

Bellizia, E., Tognin, D., Boaga, J., Cassiani, G., Finotello, A., D'Alpaos, A., and Ghinassi, M., 2022, From electromagnetic to sediment textural maps: an integrated approach to unravel the intra-point-bar variability of sediment properties: Journal of the Geological Society, doi:10.1144/jgs2021-156.

Bhattacharyya, P., Bhattacharya, J.P., and Khan, S.D., 2015, Paleo-channel reconstruction and grain size variability in fluvial deposits, Ferron Sandstone, Notom Delta, Hanksville, Utah: Sedimentary Geology, v. 325, p. 17–25, doi:10.1016/j.sedgeo.2015.05.001.

Bianchi, V., Ghinassi, M., Aldinucci, M., Boaga, J., Brogi, A., and Deiana, R., 2015, Tectonically driven deposition and landscape evolution within upland incised valleys: Ambra Valley fill, Pliocene-Pleistocene, Tuscany, Italy: Sedimentology, v. 62, p. 897–927, doi:10.1111/sed.12165.

Bluck, B.J., 1971, Sedimentation in the meandering river Endrick: Scottish Journal of Geology, v. 7, p. 93–138, doi:10.1144/sjg07020093.

Blum, M., Martin, J., Milliken, K., and Garvin, M., 2013, Paleovalley systems: Insights from Quaternary analogs and experiments: Earth-Science Reviews, v. 116, p. 128–169, doi:10.1016/j.earscirev.2012.09.003.

Bondesan, A., and Meneghel, M., 2004, Geomorfologia della provincia di

Venezia. Note illustrative della carta geomorfologica della Provincia di Venezia: Padova, Italy, Esedra editrice srl, 514 p.

Bondesan, A., Meneghel, M., Rosselli, R., and Vitturi, A., 2004, La carta geomorfologica della Provincia di Venezia, scala 1:50,000: Firenze, LAC, v. 5.

Bondesan, A., Primon, S., Bassan, V., and Vitturi, A., 2008, Le unità geologiche della Provincia di Venezia: Verona, Italy, Cierre Grafica, 51 p.

Brice, J.C., 1975, Airphoto interpretation of the form and behavior of alluvial rivers.:

Bridge, J.S., Alexander, J., Collier, R.E.L., Gawthorpe, R.L., and Jarvis, J., 1995, Ground-penetrating radar and coring used to study the large-scale structure of point-bar deposits in three dimensions: Sedimentology, v. 42, p. 839–852.

Bruno, L., Campo, B., Di Martino, A., Hong, W., and Amorosi, A., 2019, Peat layer accumulation and post-burial deformation during the mid-late Holocene in the Po coastal plain (Northern Italy): Basin Research, v. 31, p. 621–639, doi:10.1111/bre.12339.

Burnett, A.W., and Schumm, S.A., 1983, Alluvial-River response to neotectonic deformation in Louisiana and Mississippi: Science, v. 222, p. 49–50, doi:10.1126/science.222.4619.49.

Burns, C.E., Mountney, N.P., Hodgson, D.M., and Colombera, L., 2017, Anatomy and dimensions of fluvial crevasse-splay deposits: Examples from the Cretaceous Castlegate Sandstone and Neslen Formation, Utah, U.S.A.: Sedimentary Geology, v. 351, p. 21–35, doi:10.1016/j.sedgeo.2017.02.003.

Carter, D.C., 2003, 3-D seismic geomorphology: Insights into fluvial reservoir deposition and performance, Widuri field, Java Sea: American Association of Petroleum Geologists Bulletin, v. 87, p. 909–934, doi:10.1306/01300300183.

Cassiani, G., Bellizia, E., Fontana, A., Boaga, J., D'Alpaos, A., and Ghinassi, M., 2020, Geophysical and Sedimentological Investigations Integrate Remote-Sensing Data to Depict Geometry of Fluvial Sedimentary Bodies: An Example from Holocene Point-Bar Deposits of the Venetian Plain (Italy): Remote Sensing, v. 12, p. 2568, doi:10.3390/rs12162568.

Chow, V.T., 1959, Open-Channel Hydraulics: New York, McGraw-Hill, 680 p.

Clift, P.D., Olson, E.D., Lechnowskyj, A., Moran, M.G., Barbato, A., and Lorenzo, J.M., 2019, Grain-size variability within a mega-scale point-bar system, False River, Louisiana: Sedimentology, v. 66, p. 408–434, doi:10.1111/sed.12528.

Corwin, D.L., and Rhoades, J.D., 1982, An Improved Technique for Determining Soil Electrical Conductivity-Depth Relations from Above-ground Electromagnetic Measurements: Soil Science Society of America Journal, v. 46, p. 517–520, doi:10.2136/sssaj1982.03615995004600030014x.

D'Alpaos, A., Carniello, L., and Rinaldo, A., 2013, Statistical mechanics of wind wave-induced erosion in shallow tidal basins: Inferences from the Venice Lagoon: Geophysical Research Letters, v. 40, p. 3402–3407,

doi:10.1002/grl.50666.

Davies, N.S., and Gibling, M.R., 2010, Cambrian to Devonian evolution of alluvial systems: The sedimentological impact of the earliest land plants: Earth-Science Reviews, v. 98, p. 171–200, doi:10.1016/j.earscirev.2009.11.002.

Dietrich, W.E., and Smith, J.D., 1983, Influence of the point bar on flow through curved channels: Water Resources Research, v. 19, p. 1173–1192, doi:10.1029/WR019i005p01173.

Dietrich, W.E., and Smith, J.D., 1984, Processes controlling the equilibrium bed morphology in river meanders, *in* River Meandering: Proceedings of the Conference Rivers '83, p. 759–769.

Doornkamp, J.C., and Temple, P.H., 1966, Surface, Drainage and Tectonic Instability in Part of Southern Uganda: The Geographical Journal, v. 132, p. 238–252, doi:10.2307/1792339.

Durkin, P.R., Boyd, R.L., Hubbard, S.M., Shultz, A.W., and Blum, M.D., 2017, Three-dimensional reconstruction of meander-belt evolution, Cretaceous McMurray Formation, Alberta foreland basin, Canada: Journal of Sedimentary Research, v. 87, p. 1075–1099, doi:10.2110/jsr.2017.59.

Durkin, P.R., Hubbard, S.M., Smith, D.G., and Leckie, D.A., 2018, Predicting heterogeneity in meandering fluvial and tidal-fluvial deposits: The point bar to counter point bar transition, *in* Ghinassi, M., Colombera, L., Mountney, N.P., and Reesink, J.H. eds., Fluvial Meanders and Their Sedimentary Products in the Rock Record. Int. Assoc. Sedimentol. Spec. Publ., John Wiley & Sons, v. 48, p. 231–250, doi:10.1002/9781119424437.ch9.

Favero, V., and Serandrei-Barbero, R., 1978, La sedimentazione olocenica nella piana costiera tra Brenta ed Adige, *in* Memorie Società Geologica Italiana, v. 19, p. 337–343.

Finotello, A., D'Alpaos, A., Bogoni, M., Ghinassi, M., and Lanzoni, S., 2020, Remotely-sensed planform morphologies reveal fluvial and tidal nature of meandering channels: Scientific Reports, v. 10, p. 1–13, doi:10.1038/s41598-019-56992-w.

Fontana, A., Mozzi, P., and Bondesan, A., 2008, Alluvial megafans in the Venetian-Friulian Plain (north-eastern Italy): Evidence of sedimentary and erosive phases during Late Pleistocene and Holocene: Quaternary International, v. 189, p. 71–90, doi:10.1016/j.quaint.2007.08.044.

Fontana, A., Mozzi, P., and Bondesan, A., 2010, Late Pleistocene evolution of the Venetian-Friulian Plain: Rendiconti Lincei, v. 21, p. 181–196, doi:10.1007/s12210-010-0093-1.

Fornasiero, A., Gambolati, G., Putti, M., Teatini, P., Ferraris, S., Pitacco, A., Rizzetto, F., Tosi, L., Bonardi, M., and Gatti, P., 2002, Subsidence due to peat soil loss in the Zennare basin (Italy): Design and set-up of the field experiment: Scientific Research and Safeguarding of Venice, p. 201–215.

Friend, P.F., and Sinha, R., 1993, Braiding and meandering parameters, *in* Best, J.L. and Bristow, C.S. eds., Braided Rivers, London, Special Publications, Geological Society, v. 75, p. 105–111, doi:10.1144/GSL.SP.1993.075.01.05.

Frings, R.M., 2008, Downstream fining in large sand-bed rivers: Earth-Science Reviews, v. 87, p. 39–60, doi:10.1016/j.earscirev.2007.10.001.

Frothingham, K.M., and Rhoads, B.L., 2003, Three-dimensional flow structure and channel change in an asymmetrical compound meander loop, Embarras River, Illinois: Earth Surface Processes and Landforms: The Journal of the British Geomorphological Research Group, v. 28, p. 625–644, doi:10.1002/esp.471.

Fustic, M., Hubbard, S.M., Spencer, R., Smith, D.G., Leckie, D.A., Bennett, B., and Larter, S., 2012, Recognition of down-valley translation in tidally influenced meandering fluvial deposits, Athabasca Oil Sands (Cretaceous), Alberta, Canada: Marine and Petroleum Geology, v. 29, p. 219–232, doi:10.1016/j.marpetgeo.2011.08.004.

Gambolati, G., Giunta, G., Putti, M., Teatini, P., Tomasi, L., Betti, I., Morelli, M., Berlamont, J., De Backer, K., Decouttere, C., Monbaliu, J., Yu, C. S., Br0ker, I., Christensen, E.D., Elfrink, B., Dante, A., Gonella, M., 1998, Coastal Evolution of the Upper Adriatic Sea due to Sea Level Rise and Natural and Anthropic Land Subsidence, *in* Gambolati, G. ed., CENAS, Coastline Evolution of the Upper Adriatic Sea due to Sea Level Rise and Natural and Anthropic Land Subsidence, Kluwer Academic Publishers, p. 1–34, doi:10.1007/978-94-011-5147-4_1.

Gambolati, G., and Teatini, P., 1998, Numerical analysis of land subsidence due to natural compaction of the Upper Adriatic Sea basin (G. Gambolati, Ed.): CENAS, Coastline Evolution of the Upper Adriatic Sea due to Sea Level Rise and Natural and Anthropic Land Subsidence, p. 103–132, doi:10.1007/978-94-011-5147-4_5.

Ghielmi, M., Minervini, M., Nini, C., Rogledi, S., Rossi, M., and Vignolo, A., 2010, Sedimentary and tectonic evolution in the eastern Po-Plain and northern Adriatic Sea area from Messinian to Middle Pleistocene (Italy): Rendiconti Lincei, v. 21, p. 131–166, doi:10.1007/s12210-010-0101-5.

Gibling, M.R., 2006, Width and Thickness of Fluvial Channel Bodies and Valley Fills in the Geological Record: A Literature Compilation and Classification: Journal of Sedimentary Research, v. 76, p. 731–770, doi:10.2110/jsr.2006.060.

Gouw, M.J.P., 2007, Alluvial architecture of fluvio-deltaic successions: A review with special reference to Holocene settings: Geologie en Mijnbouw/Netherlands Journal of Geosciences, v. 86, p. 211–227, doi:10.1017/s0016774600077817.

Hartley, A.J., Weissmann, G.S., Nichols, G.J., and Warwick, G.L., 2010, Large distributive fluvial systems: Characteristics, distribution, and controls on development: Journal of Sedimentary Research, v. 80, p. 167–183, doi:10.2110/jsr.2010.016.

Holbrook, J., and Schumm, S.A., 1999, Geomorphic and sedimentary response of rivers to tectonic deformation: A brief review and critique of a tool for recognizing subtle epeirogenic deformation in modern and ancient settings: Tectonophysics, v. 305, p. 287–306, doi:10.1016/S0040-

1951(99)00011-6.

Hooke, J.M., 2007, Complexity, self-organisation and variation in behaviour in meandering rivers: Geomorphology, v. 91, p. 236–258, doi:10.1016/j.geomorph.2007.04.021.

Hubbard, S.M., Smith, D.G., Nielsen, H., Leckie, D.A., Fustic, M., Spencer, R.J., and Bloom, L., 2011, Seismic geomorphology and sedimentology of a tidally influenced river deposit, Lower Cretaceous Athabasca oil sands, Alberta, Canada: AAPG Bulletin, v. 95, p. 1123–1145, doi:10.1306/12131010111.

Ielpi, A., and Ghinassi, M., 2014, Planform architecture, stratigraphic signature and morphodynamics of an exhumed Jurassic meander plain (Scalby Formation, Yorkshire, UK): Sedimentology, v. 61, p. 1923–1960, doi:10.1111/sed.12122.

Ielpi, A., Gibling, M.R., Bashforth, A.R., Lally, C., Rygel, M.C., and Al-Silwadi, S., 2014, Role of vegetation in shaping early Pennsylvanian braided rivers: Architecture of the Boss Point Formation, Atlantic Canada: Sedimentology, v. 61, p. 1659–1700, doi:10.1111/sed.12109.

Jackson, R.G., 1976, Depositional model of point bars in the lower Wabash River: Journal of Sedimentary Research, v. 46, p. 579–594, doi:10.1306/212F6FF5-2B24-11D7-8648000102C1865D.

Jin, D., and Schumm, S.A., 1987, A new technique for modeling river morphology, *in* Gardiner, V. ed., International Geomorphology, Part I, Chichester, UK, Wiley, p. 681–690.

Jones, H.L., and Hajek, E.A., 2007, Characterizing avulsion stratigraphy in ancient alluvial deposits: Sedimentary Geology, v. 202, p. 124–137, doi:10.1016/j.sedgeo.2007.02.003.

Jorgensen, D.W., 1990, Adjustment of alluvial river morphology and process to localized active tectonics: Colorado State University, Fort Collins (CO).

Kasvi, E., Vaaja, M., Alho, P., Hyyppä, H., Hyyppä, J., Kaartinen, H., and Kukko, A., 2013, Morphological changes on meander point bars associated with flow structure at different discharges: Earth Surface Processes and Landforms, v. 38, p. 577–590, doi:10.1002/esp.3303.

Kellerhals, R., Church, M., and Bray, D.I., 1976, Classification and analysis of river processes: Journal of the Hydraulics Division, v. 102, p. 813–829.

Kemp, J., 2004, Flood channel morphology of a quiet river, the Lachlan downstream from Cowra, southeastern Australia: Geomorphology, v. 60, p. 171–190, doi:10.1016/j.geomorph.2003.07.007.

Khan, I.A., Bridge, J.S., Kappelman, J., and Wilson, R., 1997, Evolution of Miocene fluvial environments, eastern Potwar plateau, northern Pakistan: Sedimentology, v. 44, p. 221–251, doi:10.1111/j.1365-3091.1997.tb01522.x.

Knighton, A.D., 1999, Downstream variation in stream power: Geomorphology, v. 29, p. 293–306, doi:10.1016/S0169-555X(99)00015-X.

Labrecque, P.A., Jensen, J.L., Hubbard, S.M., and Nielsen, H., 2011, Sedimentology and stratigraphic architecture of a point bar deposit, Lower

Cretaceous McMurray Formation, Alberta, Canada: Bulletin of Canadian Petroleum Geology, v. 59, p. 147–171, doi:10.2113/gscpgbull.59.2.147.

Lazarus, E.D., and Constantine, J.A., 2013, Generic theory for channel sinuosity: Proceedings of the National Academy of Sciences of the United States of America, v. 110, p. 8447–8452, doi:10.1073/pnas.1214074110.

Leopold, L.B., and Wolman, M.G., 1957, River channel patterns: braided, meandering, and straight: US Government Printing Office.

Li, C., Wang, P., Fan, D., and Yang, S., 2006, Characteristics and formation of late Quaternary incised-valley-fill sequences in sediment-rich deltas and estuaries: a case study from Chi, *in* Dalrymple, R.W., Leckie, D.A., and Tillman, R.W. eds., Incised Valleys in Time and Space: SEPM, Special Publication, p. 141–160.

Marple, R.T., and Talwani, P., 1993, Evidence of possible tectonic upwarping along the South Carolina coastal plain from an examination of river morphology and elevation data: Geology, v. 21, p. 651–654, doi:10.1130/0091-7613(1993)021<0651:EOPTUA>2.3.CO;2.

McLachlan, P., Blanchy, G., and Binley, A., 2021, EMagPy: Open-source standalone software for processing, forward modeling and inversion of electromagnetic induction data: Computers and Geosciences, v. 146, p. 104561, doi:10.1016/j.cageo.2020.104561.

Morozova, G.S., and Smith, N.D., 1999, Holocene Avulsion History of the Lower Saskatchewan Fluvial System, Cumberland Marshes, Saskatchewan-Manitoba, Canada, *in* Smith, N.D. and Rogers, J. eds., Fluvial Sedimentology VI: International Association of Sedimentologists Special Publication., v. 28, p. 231–249, doi:10.1002/9781444304213.ch18.

Mozzi, P., Negrelli, C., Abbà, T., Cadamuro, S., Corrò, E., Fontana, A., Moine, C., Ninfo, A., Primon, S., and Sabbionesi, S., 2013, Paesaggi antichi e potenziale archeologico, *in* Archeologia del paesaggio nell'area costiera veneta: conoscenza, partecipazione e valorizzazione/Arheologija in krajina na obalnem območju Veneta: spoznati, podeliti in ovrednotiti, Cittadella, Padova, Italy, Biblos srl, p. 19–85.

Mozzi, P., Piovan, S., and Corrò, E., 2020, Long-term drivers and impacts of abrupt river changes in managed lowlands of the Adige River and northern Po delta (Northern Italy): Quaternary International, v. 538, p. 80–93, doi:10.1016/j.quaint.2018.10.024.

Nanson, G.C., 1980, Point bar and floodplain formation of the meandering Beatton River, northeastern British Columbia, Canada: Sedimentology, v. 27, p. 3–29, doi:10.1111/j.1365-3091.1980.tb01155.x.

Nanson, G.C., and Page, K., 1983, Lateral accretion of fine-grained concave benches on meandering rivers, *in* Collinson, J.D. and Lewin, J. eds., Modern and ancient fluvial systems. Int. Assoc. Sedimentol. Spec. Publ., Wiley-Blackwell, v. 6, p. 133–143, doi:/10.1002/9781444303773.ch10.

Nardin, T., Feldman, H.R., and Carter, B.J., 2013, Stratigraphic architecture of a large-scale point-bar complex in the McMurray Formation: Syncrude's Mildred Lake Mine, Alberta, Canada: Heavy-oil and oil-sand petroleum

systems in Alberta and beyond: AAPG Studies in Geology, v. 64, p. 273–311, doi:10.1306/13371583St643555.

Nittrouer, J.A., Shaw, J., Lamb, M.P., and Mohrig, D., 2012, Spatial and temporal trends for water-flow velocity and bed-material sediment transport in the lower Mississippi River: Bulletin of the Geological Society of America, v. 124, p. 400–414, doi:10.1130/B30497.1.

Ouchi, S., 1985, Response of alluvial rivers to slow active tectonic movement.: Geological Society of America Bulletin, v. 96, p. 504–515, doi:10.1130/0016-7606(1985)96<504:ROARTS>2.0.CO;2.

Paine, J.G., 2003, Determining salinization extent, identifying salinity sources, and estimating chloride mass using surface, borehole, and airborne electromagnetic induction methods: Water Resources Research, v. 39, p. 1–10, doi:10.1029/2001WR000710.

Paola, C., and Mohrig, D., 1996, Palaeohydraulics revisited: Palaeoslope estimation in coarse-grained braided rivers: Basin Research, v. 8, p. 243–254, doi:10.1046/j.1365-2117.1996.00253.x.

Posamentier, H.W., 2001, Lowstand alluvial bypass systems: incised vs. unincised: AAPG Bulletin, v. 85, p. 1771–1793, doi:10.1306/8626D06D-173B-11D7-8645000102C1865D.

Räsänen, M.E., Salo, J.S., and Kalliola, R.J., 1987, Fluvial Perturbance in the Western Amazon Basin: Regulation by Long-Term Sub- Andean Tectonics: American Association for the Advancement of Science, v. 238, p. 1398–1401, doi:10.1126/science.238.4832.1398.

Rice, S.P., and Church, M., 2001, Longitudinal profiles in simple alluvial systems: Water Resources Research, v. 37, p. 417–426, doi:10.1029/2000WR900266.

Rizzetto, F., Tosi, L., Bonardi, M., Gatti, P., Fornasiero, A., Gambolati, G., Putti, M., and Teatini, P., 2002, Geomorphological Evolution of the Southern Catchment of the Venice Lagoon (Italy): the Zennare Basin: Scientific Research and Safeguarding of Venice, Trends in global change processes, p. 217–228.

Russell, R.J., 1954, Alluvial Morphology of Anatolian Rivers: Annals of the Association of American Geographers, v. 44, p. 363–391.

Schumm, S.A., 1985, Patterns of alluvial rivers: Annual review of Earth and planetary sciences, v. 13, p. 5–27, doi:10.1146/annurev.earth.13.1.5.

Schumm, S.A., 1960, The shape of alluvial channels in relation to sediment type: US Geol. Survey Prof. Pap., v. 352, p. 17–30.

Schumm, S.A., Dumont, J.F., and Holbrook, J.M., 2000, Active tectonics and alluvial rivers: Cambridge, UK, Cambridge University Press, 276 p.

Seminara, G., 2006, Meanders: Journal of Fluid Mechanics, v. 554, p. 271–297, doi:10.1017/S0022112006008925.

Shiers, M.N., Mountney, N.P., Hodgson, D.M., and Cobain, S.L., 2014, Depositional controls on tidally influenced fluvial successions, Neslen Formation, Utah, USA: Sedimentary Geology, v. 311, p. 1–16, doi:10.1016/j.sedgeo.2014.06.005.

Shiers, M.N., Mountney, N.P., Hodgson, D.M., and Colombera, L., 2018, Controls on the depositional architecture of fluvial point-bar elements in a coastal-plain succession, *in* Ghinassi, M., Colombera, L., Mountney, N.P., and Reesink, A.J.H. eds., Fluvial Meanders and Their Sedimentary Products in the Rock Record, John Wiley & Sons, Ltd Chichester, UK, p. 15–46, doi:10.1002/9781119424437.ch2.

Slingerland, R., and Smith, N.D., 2004, River Avulsions and Their Deposits: Annual Review of Earth and Planetary Sciences, v. 32, p. 257–285, doi:10.1146/annurev.earth.32.101802.120201.

Smith, N.D., Cross, T.A., Dufficy, J.P., and Clough, S.R., 1989, Anatomy of an avulsion: Sedimentology, v. 36, p. 1–23, doi:10.1111/j.1365-3091.1989.tb00817.x.

Swan, A., Hartley, A.J., Owen, A., and Howell, J., 2018, Reconstruction of a sandy point-bar deposit: implications for fluvial facies analysis, *in* Ghinassi, M., Colombera, L., Mountney, N.P., Reesink, A.J., and Betaman, M. eds., Fluvial Meanders and Their Sedimentary Products in the Rock Record. Int. Assoc. Sedimentol. Spec. Publ. 48, Ltd, John Wiley & Sons, v. 48, p. 445–474, doi:10.1002/9781119424437.ch17.

Teatini, P., Tosi, L., and Strozzi, T., 2011, Quantitative evidence that compaction of Holocene sediments drives the present land subsidence of the Po Delta, Italy: Journal of Geophysical Research: Earth Surface, v. 116, p. 1–10, doi:10.1029/2010JB008122.

Tosi, L., Rizzetto, F., Bonardi, M., Donnici, S., Serandrei-Barbero, R., and Toffoletto, F., 2007, Note Illustrative della Carta Geologica d'Italia alla scala 1:50.000. foglio 148-149, Chioggia-Malamocco: , p. 164.

Um, E.S., and Alumbaugh, D.L., 2007, On the physics of the marine controlled-source electromagnetic method: Geophysics, v. 72, p. WA13–WA26, doi:10.1190/1.2432482.

Vacchi, M., Marriner, N., Morhange, C., Spada, G., Fontana, A., and Rovere, A., 2016, Multiproxy assessment of Holocene relative sea-level changes in the western Mediterranean: Sea-level variability and improvements in the definition of the isostatic signal: Earth-Science Reviews, v. 155, p. 172–197, doi:10.1016/j.earscirev.2016.02.002.

Willis, B.J., 1989, Palaeochannel reconstructions from point bar deposits: a three-dimensional perspective: Sedimentology, v. 36, p. 757–766, doi:10.1111/j.1365-3091.1989.tb01744.x.

Willis, B.J., and Tang, H., 2010, Three-Dimensional Connectivity of Point-Bar Deposits: Journal of Sedimentary Research, v. 80, p. 440–454, doi:10.2110/jsr.2010.046.

Wood, J.M., 1989, Alluvial architecture of the Upper Cretaceous Judith River Formation, Dinosaur Provincial Park, Alberta, Canada: Bulletin of Canadian Petroleum Geology, v. 37, p. 169–181.

7

CONCLUSIONS

Through a multidisciplinary and integrated approach that combines remote sensing analysis, recovery of sedimentary cores, geophysical investigations, laboratory techniques, literature review and statistical analyses, the present study analyses how sediment properties vary within fluvio-and-tidal-meandering-channel deposits of the late Holocene Venetian Plain and the Venice Lagoon (Italy). In particular, the integrated approach allows to study and characterise point-bar bodies in a 3D perspective, providing qualitative and quantitative data that can be crucial for understanding fluvial deposits, and provide insights to numerical modelling of groundwater flow in surficial aquifers. The main results stemmed out from this research can be summarised by answering the questions posed in Section 1.5 as follows:

1. *What do morphologies and deposits of purely fluvial and purely tidal meandering channels of the Venetian Plain look like? How can they be compared with classical models?*
   Sedimentological and geophysical investigations have allowed to analyse the deposits of fluvial and tidal meander bends by looking at their genesis and evolution mechanisms. Overall, results related to fluvial meander-bend deposits can enrich the panorama of knowledge on the subject, showing that the meanders of the study area can follow classical facies models, although they detach from them in few aspects. Similarly, results from the tidal realm contribute to enriching the knowledge on deposits accumulated from tidal meandering channels in a microtidal regime, and those developed in a subtidal environment.

The analysis of fluvial bends shows that fluvial meander bends of the Venetian Plain have grown up according to different migration styles, also combining some of them, thus allowing to originate point-bar bodies characterised by different morphologies and sinuosity. These findings are corroborated by the concepts described on common-known facies models of fluvial bends. Results show that most of the meander bends developed from a straight or low-sinuosity channel, as usually described in point-bar depositional models. However, the results also highlighted the possibility of meander bends to accrete point-bar deposits from already sinuous channels. This peculiar sinuous shape may have originated following a post-avulsion relocation of the channel, which defined its new track connecting adjacent topographic lows developed within the floodplain that probably resulted from differential compaction of different primary lithologies.

In terms of sedimentary facies, fluvial point bars of the Venetian Plain slightly differ from what is commonly expected from facies models. Indeed, they are homogeneous sand bodies without the commonly described muddy intercalations. Even concerning grain-size trends, point bars in the Venetian Plain do not present the classic well-expressed upward fining, but rather exhibit a blocky vertical grain-size trend, which is especially expressed in the upstream-bar section. The along-bend downstream fining trend of grain size is poorly expressed too, and this is observed regardless of the shape of the bend. Muddy layers are found only at the top of the bar, and mud-clasts commonly occur in the channel-lag deposit. These peculiar grain-size trends/distributions contribute to differentiating point-bar deposits of the study area from classical examples described in the literature, where the downstream and upward increase in mud content is considered as a diagnostic feature of point-bar deposits. This overall lack could be related to the low influence of tidal currents on the fluvial sedimentation, due to the limited tidal excursion occurring in the Mediterranean basin.

By analysing the morphometry of abandoned channel deposits, it emerged that due to gradual deactivation processes, they tend to appear disproportionally narrow compared to the associated point bars, which is good for connectivity, as it decreases compartmentalization. This evidence provides insights to predict connectivity between bar

deposits based on geometrical relationships between channel width and size of the related bars.

Investigations of tidal meanders revealed that related point bars can also originate from already sinuous channel morphologies. This peculiarity can be explained considering the high network density of the microtidal environment analysed, which can cause piracy and connection events between adjacent tidal branches; therefore, these mechanisms can originate new circulation patterns for the main flow, over a pre-existing network, defining channel morphologies that are not necessarily straight.

In the tidal realm, results highlight the importance of the tidal-flow asymmetry in controlling planform evolution and tidal point-bar deposits, corroborating current knowledge on tidal systems. Dealing with the planform evolution, despite the scroll-bar pattern of tidal point bars can be hardly identified, results highlight how the detailed interpretation of high-resolution acoustic profiles can provide a valuable tool for the identification of bedsets, thus allowing for planform-evolution reconstructions. Therefore, results from this study are in line with current knowledge on tidal systems, showing that tidal point-bar bodies of the study area can grow following a complex alternation of different migration phases of the related bends, which are possibly related to the effect of variation in the tidal asymmetry. They can also experience migration when flood and ebb currents are balanced (i.e., no tidal asymmetry). The results also highlighted the possibility of tidal point-bar deposits to accrete following both patterns of lateral migration and vertical aggradation, thus allowing the preservation of ancient deposits instead of eroding them.

From a sedimentological point of view, tidal point-bar deposits of the study area slightly differ from the depositional facies models described for tidal systems. Indeed, although developed in a subtidal setting, tidal point-bar deposits are homogeneous mud bodies, lacking the classical Inclined Heterolithic Stratification. This could be related to the microtidal regime of the area, which can play a fundamental role in determining a narrow range of grain sizes available to be transported by tidal currents. Furthermore, as in the fluvial case studies of the Venetian Plain, the deposits of tidal point bars present a poorly expressed upward fining trend of grain size, although this would be expected following

classical facies models. However, dealing with the along-bend grain-size distribution, results from this study highlight the role of the tidal alternation in defining an overall uniform distribution of grain sizes along the bar, confirming observation from previous works on the study area.

2. *How can we effectively and quantitatively investigate the spatial variability of sediment textural properties within FTMC deposits?*
   Results from this study propose a new integrated and multidisciplinary approach to study the variability of sedimentary properties in point-bar deposits. Specifically, the proposed approach statistically integrates core data and electrical conductivity data to provide information about the spatial variability of sediment grain size and sorting. Results from the application of this methodology provide precise information on the subsurface deposits hosting surficial aquifers, thus providing insights for modelling subsurface permeability patterns.
   The novel aspect of integrating methodologies with a multivariate statistical analysis allows overcoming the limitations provided by the individual application of sedimentary cores or geophysical investigations. Geophysical investigations with FDEM surveys allow to map the electrical conductivity of a volume of deposits, but results are commonly assumed to describe the variability of sediment grain size only. Sedimentary characterisation of deposits through sedimentary cores, however, provides only local information.
   The proposed statistical analysis integrates geophysical and sedimentological data and allows characterising extensively the sediment properties of the sedimentary deposit, identifying the contribution of the sediment grain size and sediment sorting. Moreover, the results allow to go beyond the descriptive assumption that commonly links the variability of the electric conductivity to that of the sediment grain-size, by demonstrating that the electric conductivity is mainly influenced by the sediment sorting.

3. *How do sedimentary and morphological features of meandering channels vary at the channel-belt scale?*

To answer this question a fluvial paleochannel belt from the Venetian Plain, 14 km long and almost 5 km away from the present coastline, has been analysed.

Results show how the fluvial dynamics of a channel belt can be affected by changes in the substrate sedimentological properties. The study case shows how differential compaction and erodibility triggered by different substrates induced relevant changes in the morphometry of meander bends. Results show that at the transition from a subsiding, cohesive substrate (i.e., flood basin mud), to a poorly subsiding, cohesionless one (beach ridge sand), bends of the study belt accreted laterally developing greater sinuosity and smaller radius of curvature compared to the bends flowing before the substrate change. Bends developed on the poorly-subsiding, cohesionless sandy substrate evolved defining wider and less-sinuous bends.

From the sedimentological point of view, the results reveal that point-bars of the study belt are composed of homogeneous sand deposits with poorly expressed internal heterogeneities and along-bar grain-size changes. Differently from classical depositional models, results from this work show that the study channel belt, although placed close to the shoreline, does not seem to show a downstream fining of the grain size, as mud is barely observed in point-bar deposits. This peculiarity could be probably related to the dominance of fluvial processes on tidal ones, because of the reduced tidal regime of the coast (i.e., microtidal), which does not allow an effective tidal modulation of fluvial flows and related mud sedimentation within the channel.

Overall, by analysing the sedimentary deposits of FTMC of the Venetian Plain and in the Venice Lagoon (Italy), results from this thesis contribute to enlarge the current knowledge on the internal structure of the deposits originated from the evolution of FTMC and highlight the relevance of a multidisciplinary approach to study them in a 3D perspective. The results obtained in this work can be crucial for better understanding and modelling the subsurface flow in the study area and similar settings worldwide. In the appendix, an example is given of the application of the results obtained from this work, in which the sedimentological parameters of a case study were used to feed numerical models to simulate the groundwater flow and the pollutant propagation in the

subsurface. This work highlights the importance of a complete understanding of depositional geometries to properly model subsurface permeability patterns.

Insights from the present work improve current knowledge about fluvial and tidal meandering channels and related deposits; however, they also raise new research questions to be investigated in the frame of forthcoming studies, including 1) what dynamic or depositional process may lead to the scarcity of mud deposits in fluvial point-bar deposits? 2) Could these reasons also be responsible for the overall lack of seaward fining of grain sizes at the belt scale? 3) How and how much do tidal currents influence morphodynamic and deposition of fluvial meandering channels in the fluvio-tidal transition zone where coasts are affected by microtidal regimes?

Appendix A

This chapter is a manuscript published in *Remote Sensing* (2020, v. 16, p. 2568, doi: 10.3390/rs12162568) under the title "Geophysical and sedimentological investigations integrate remote-sensing data to depict geometry of fluvial sedimentary bodies: an example from Holocene point-bar deposits of the Venetian Plain (Italy)".

G.C., E.B. and M.G. designed the study. G.C., J.B. and M.G. developed the methodology. E.B., A.F., J.B. and M.G. collected the data. E.B. annotated and maintained the research data. G.C. and E.B. were responsible for data creation and presentation. E.B. and M.G. were the project administrator. J.B and G.C. applied computational techniques to analyse study data. J.B, G.C. and M.G. provided the instrumentation and analysis tools. A.D. verified the reproducibility of the results. All the authors discussed the data and agreed on their interpretation. G.C., E.B., J.B. and A.F. wrote the original draft. A.D. and M.G. provided comments and suggestions to improve the original draft. All the co-authors contributed to the final polishing of the manuscript.

Geophysical and sedimentological investigations integrate remote-sensing data to depict geometry of fluvial sedimentary bodies: an example from Holocene point-bar deposits of the Venetian Plain (Italy)

Giorgio Cassiani[1], Elena Bellizia[1], Alessandro Fontana[1], Jacopo Boaga[1], Andrea D'Alpaos[1], Massimiliano Ghinassi[1]

[1] Department of Geosciences, University of Padova, Via G. Gradenigo 6, IT-35131 Padova, Italy

ABSTRACT

Over the past few millennia, meandering fluvial channels drained coastal landscapes accumulating sedimentary successions that today are permeable pathways. Propagation of pollutants, agricultural exploitation and sand liquefaction are the main processes of environmental interest affecting these sedimentary bodies. The characterization of these bodies is thus of utmost general interest. In this study we particularly highlight the contribution of non-invasive (remote and ground-based) investigation techniques, and the case study focuses on a late Holocene meander bend of the southern Venetian Plain (Northeast Italy). Electromagnetic Induction (EMI) investigations, conducted with great care in terms of sonde stability and positioning, allowed the reconstruction of the electrical conductivity 3D structure of the shallow subsurface, revealing that the paleochannel ranges in depth between 0.8 and 5.4 m and defines an almost 260 m-wide point bar. The electrical conductivity maps derived from EMI at different depths define an arcuate morphology indicating that bar accretion started from an already sinuous channel. Sedimentary cores ensure local ground-truth and help define the evolution of the channel bend. This paper shows that the combination of well-conceived and carefully performed inverted geophysical surveys, remote sensing and direct investigations provides evidence of the evolution of recent shallow sedimentary structures with unprecedented detail.

Keywords: electromagnetic induction; depth inversion; sedimentary processes.

1. Introduction

Modern coastal landscapes are widely shaped by meandering fluvial, fluvio-tidal and tidal channels, which over the late Holocene accumulated complex and extensive sedimentary bodies. These bodies today often define subsoil permeable systems [1] that are often exploited as water reserves for agricultural, industrial, and civil uses [2], and are extremely sensitive to saltwater intrusion [3,4] as well as to contamination [5,6]. These channelized bodies commonly consist of clean and poorly consolidated sand, which can also be affected by liquefaction processes [7]. The 2012 earthquake that occurred in the northeastern portion of the Po Plain (Italy) was the cause of sand eruptions occurred along Holocene paleochannels and crevasse splay deposits down to an 8 m depth [8,9].

Aerial photographs and satellite images are excellent tools to identify and map late Holocene coastal channel networks since the former provide aerial data from the 1950s to present [10–13] and the latter provide multispectral analysis to highlight surficial paleochannel configurations [14–16].

Excellent examples of Remote Sensing applications for these types of geomorphological studies can be found in the recent literature [17–21]. Despite the advantages particularly in locating the position of these surficial bodies, and possibly distinguishing between tide- and fluvial-generated meanders [22], remote sensing alone is of course not capable of providing information at depth, thus remaining essentially a qualitative tool for the characterization of 3D geological structures. On the other hand, direct field surveys [23,24] and microrelief analysis [10,22,25] can provide further information either locally at depth or extensively at the surface. Regardless, a 3D reconstruction is still difficult with these means only [25], if not as a result of interpolation of scarce scattered data.

Addressing these issues requires that extensive and high-resolution data are available to map large areas and, at the same time, investigate the subsoil to a certain depth. This calls for geophysical methods (as they are designed to collect data informative about the subsoil, unlike Remote Sensing sensu strictu) that can also be deployed rapidly with limited or no ground contact so that large areas can be investigated. The most suitable methods, for these purposes, are those based on electromagnetic processes. In particular, approaches based on electromagnetic induction (EMI) allow for noncontact subsurface investigation, with no intrinsic limitations as posed, for instance, to wave-propagation EM

methods such as ground-penetrating radar GPR that can be strongly limited in their depth propagation by the ground electrical conductivity.

EMI is a well-established technique that dates back nearly one century [26] and is based on Faraday's law of electromagnetic induction. The technique is articulated in a variety of specific instrument designs and investigation strategies [27] ranging in investigation depth from very shallow (the first meter or so) to tens of kilometers. For shallow applications [28,29], EMI has had widespread use in hydrological and hydrogeological characterizations [30–32], hazardous waste characterization studies [33,34], precision-agriculture application locations [35–37], archaeological surveys [38,39], geotechnical investigations [40] and unexploded ordnance (UXO) detection [41]. EMI measurements at the small scale are typically conducted in the frequency domain (Frequency Domain Electromagnetics of FDEM) and the results are classically expressed as apparent electrical conductivities (ECa) [42] using the so-called low-induction number approximation [43]. In addition to ECa mapping, the development of multifrequency and multicoil instruments has recently enabled the possibility of inversion of EMI measurements to provide quantitative models of depth-dependent electrical conductivity (EC), as the different acquisition configurations either in terms of coil geometry or frequency allow for multiple independent data to be acquired in sufficient number to warrant inversion. The majority of inversion algorithms use a 1D forward model based on either the linear cumulative sensitivity (CS) forward model proposed by [43] or nonlinear full solution (FS) forward models based on Maxwell's equations (e.g. [44,45]). As with EMI mapping, applications using inverted EMI data have also been diverse (e.g. [46–51]). Applications typically focus on using an inversion based on either the CS or an FS forward model to produce regularized, smoothly varying, models of EC with fixed depths or sharply varying models of EC where layer depths are also a parameter. In the most advanced cases, a full 3D model of electrical conductivity can be reconstructed over a relatively large area, similar to what can be obtained at a larger scale by using e.g., time-domain airborne EMI systems (e.g. [52]). The use of small FDEM measurement systems, with rapid response and easy integration into mobile platforms, is the key factor in the success of EMI techniques for near-surface investigations in these fields, as they allow dense surveying and real-time conductivity mapping over large areas in a cost-effective manner. However, sufficient control on the acquisition geometry is often needed, as the

instrument response has a strong dependence also on the elevation above ground and the relative height of the primary and secondary coils [46].
The purpose of this paper is to show how the integrated use of remote sensing, EMI and direct stratigraphic investigations can provide an effective and comprehensive 3D view of the geometry of a fluvial sedimentary body. Results from the present study highlight the importance of an integrated approach to understand subsurface deposits.

2. Materials and Methods

2.1. Geological setting and study area

The Venetian Plain is located at the north-eastern end of the Po Plain, the largest Italian alluvial plain, and was generated during Holocene transgression by aggradation of fluvial meandering channels [22,23]. Specifically, the study area is located at the boundary between the Venetian Plain and the Po River Delta, in a zone which is characterised by a dense network of alluvial ridges and sand bodies that are the geomorphological products of the complex interaction between the Adige and Po rivers during the late Holocene (Fig. A.1a) [24,53]. These sedimentary bodies currently host a multi-layered system of phreatic and confined aquifers that are affected by saltwater contamination [4,54] and intensive water exploitation. The fluvial sedimentation occurred in an aggrading setting related to the marine highstand and meander belts often correspond to fluvial ridges slightly elevated over the floodplain (i.e. 2 to 5 m above sea level [asl]) [53]. The present surface is a typical lowland landscape, which developed in the last 5000 years by the avulsions of the Adige and Po Rivers [24].
The investigated site is located near the village of Anguillara Veneta (Fig. A.1b), about 1 km north of the current channel of Adige River, in an area with surface elevations ranging between 0.7 and 2.0 m asl, where traces of abandoned meanders are visible in several aerial images and could be followed for about 7 km, from Stanghella to Anguillara Veneta. These paleo-hydrographic traces run nearly parallel to the present Adige River, even if they are slightly out of the natural levee deposits connected to the fluvial ridge of Adige. The river activated its present direction since the early Middle Age, while before it used to flow along the meander belt running from Este to Monselice to Chioggia (from West to East) [55]. Near Anguillara Veneta the present course of the Adige River cuts the so-called fluvial ridge of Rovigo-Saline-Cona, which was formed by the Po River between 4500- and 3500-years BP [24].

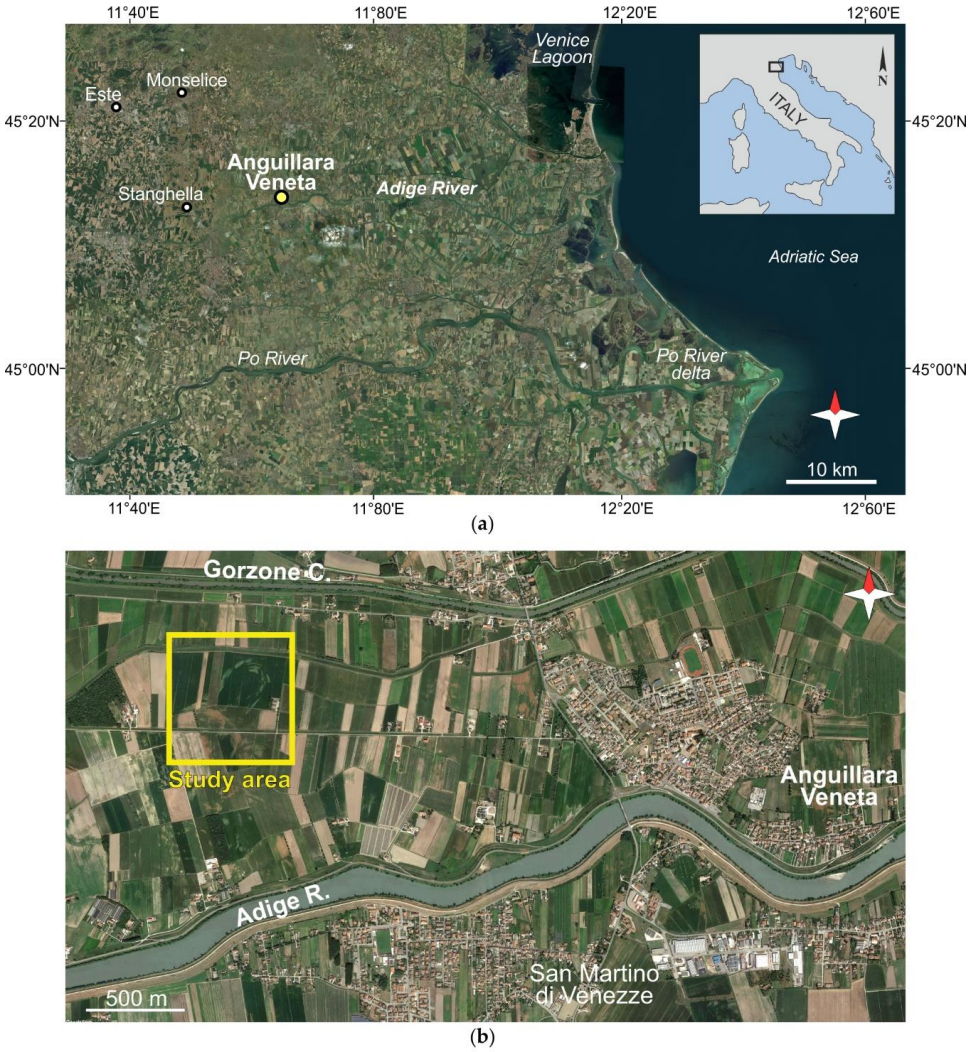

Fig. A.1. The study site: (a) Location of Anguillara Veneta town in the southern Venetian Plain, at the boundary with the Po Plain sensu strictu; (b) Satellite image (2013) of the study area (yellow box) in Anguillara Veneta town, PD (Italy).

The area experienced strong anthropogenic activity since the Roman period, when extensive field systems were settled in the whole Venetian Plain and parts of the Po Delta [24]. A major phase of reclamation started in the 16th century, when the Venetian Republic started the strong management of the river network, leading to the construction of the dense network of dikes, canals and ditches that still characterizes the landscape. During the same period, the Gorzone Canal was also cut, which represents the northern boundary of the study area, to convey the water discharge of the Agno-Guà-Frassine-Santa Caterina river system towards the Adriatic Sea. During the first part of the 20th

century, the reclamation was extended to the coastal plain, where large portions of swamps and lagoon landscapes were drained through the excavation of canals and the use of pumping stations. These interventions made it possible to artificially lower the groundwater table below the surface and to cultivate seasonal crops (e.g., corn, wheat, bit, and soya bean) and vegetables. In the last decades, several strong leveling interventions were carried out to improve the efficiency of the new draining system, as in the field investigated for this study. Besides the positive results, unfortunately, the reclamation also induced fast land subsidence caused by groundwater withdrawal, compaction of the drained soil and degradation of the organic matter formerly present in the marsh sediments [56]. From the downlift rate of the natural subsidence, ranging around 1 mm/y [57], in the last century the velocity strongly increased up to average values of 2 to 5 mm/y with large sectors up to 10 mm/y [58].

A large number of historical photos and maps are available for the Venetian Plain, along with freely-distributed satellite images. Study sites are easily accessible for geophysical investigation and sedimentary cores. For these reasons, this study area represents an ideal site to develop and test the proposed integrated approach.

2.2. Remote sensing

The study site was selected after the identification of the paleo-meanders in the aerial and satellite images. In particular, the first characterization was carried out on some satellite images available from Google Earth, which generally are pansharpened images of true-color composite bands of the Digital Globe company (Westminster, CO, USA) (e.g., Ikonos, QuickBird, WorldView and GeoEye missions). We selected the images with a detailed spatial resolution between 1.0-0.5 m (i.e., images 31/07/2004; 23/06/2007; 06/06/2010; 21/04/2012; 06/08/2013; 16/08/2013; 28/03/2015; 22/06/2017; 18/07/2018), and imported them into the GIS software ArcMap (version 10.7.1) [59] and QGIS 3.10 [60] for image processing and comparison with the images available as basemap reference in ESRI. Moreover, we also considered several zenithal conventional aerial pictures available from the cartographic service of Veneto Region [61], consisting of scanned versions of black/white and color pictures from 1955 to 2008, with scales from 1:33,000 to 1:5000.

To investigate the spectral characteristics of the field surface, we analyzed some images from the satellite Sentinel-2, obtaining the Normalized Difference Vegetation Index (NDVI) and the Normal Difference Moisture Index (NDMI) [62–

64]. These indices have a geometric resolution of 10 m and, being sensitive to plant health and hydraulic stress, respectively [65,66], were used to improve the identification of the traces of paleo-meanders, by linking sedimentology to vegetation health of the area. In particular, we produced the NDVI and NDMI not only from summer scenes, but also from different seasons and years by processing the multispectral bands through the semiautomatic classification plugin (SCP) [67] and Raster Calculator of QGIS 3.10. In fact, in the study area the cultivated plants change with seasons; in addition to the crops growing during summer, winter cultivations such as wheat, barley and different vegetables can be present.

Satellite, aerial and processed images were visualised in a properly georeferenced 3D space provided by the Move 2018.2TM [68] software.

2.3. Geophysical investigations

The EMI surveys at the site were collected using a GF Instruments CMD-Explorer probe [69] that is a six-coil system (three coplanar pairs) operating at a single frequency equal to 10 kHz. The probe can be operated in both horizontal coplanar (HMD) and vertical coplanar (VMD) configurations [70], providing six independent measurements that are generally associated with six different apparent depths of investigation (Table 1). To acquire all six configurations for each geographical location it is, however, necessary to reoccupy with some acceptable degree of approximation the same location twice (once for each coil orientation).

Instrument probe	*Coil inter-distance (m)*	*Frequency*	*Nominal exploration depth (Horizontal mode HMD /Vertical mode VMD)*
1	*1.48*	*10 kHz*	*2.2 / 1.1 m*
2	*2.82*	*10 kHz*	*4.2 / 2.1 m*
3	*4.49*	*10 kHz*	*6.7 / 3.3 m*

Table 1. Technical specifications of the multicoil CMD Explorer FDEM.

The FDEM probe was mounted on a specifically designed wooden carriage and connected to a Trimble 5800 GPS for continuous positioning, collecting data every second [71]. The wooden support was towed by a small tractor (Fig. A.2a). The acquisition apparatus adopted satisfies two fundamental requirements, that proved extremely effective in terms of data quality [72,73]:

(a) Reoccupation of the same location is warranted by the GPS within the required precision (note that the sonde is a few meters long);
(b) The setting of the sonde is the same at all locations, with no changes of either the height above ground or the setting of the sonde that is maintained largely horizontal.

In this manner, we collected about 20,000 EMI data points (Fig. A.2b), each in both HMD and VMD modes, with about one point every 0.5 m along the acquisition lines. The lines have a mutual distance of roughly 10 m (Fig. A.2b).

EMI data were then inverted to retrieve real soil conductivity values. For this purpose, we used the Interpex IX1D inversion software [74], a 1D routine based on smooth depth inversion according to the so-called Occam's approach [75]. The very dense spatial sampling allowed for the reconstruction of the subsoil practically in a 3D fashion by the juxtaposition of the 1D inverted profiles. For all locations, the same number of layers (eight) was used for the inversion thus producing a consistent dataset. The results are presented in terms of 2D horizontal maps at several depths, that were then georeferenced using the Move 2018.2TM [68] software, which also allowed also creation of 3D surfaces, by the linear method, and tetravolumes.

2.4. Sedimentary cores

Six cores were recovered at the study site to analyze sedimentary features of the study deposits and provide ground-truth for geophysical and remote sensing data (Fig. A.2c). The core locations were established based on remote sensing and geophysical data. Cores were collected by using an Eijkelkamp hand auger and a continuous drilling core sampler with rotary technique. Three cores were recovered using an Eijkelkamp hand auger, through a gouge sampler with a length of 1 m and a diameter of 30 mm, which prevented sediment compaction. Depth for these cores spanned from 2.5 to 6 m (Fig. A.2c). Three additional cores were recovered using a continuous drilling core sampler with rotary technique. These latter cores, which were 10 cm in diameter and reached a depth of 10 m, were located in the upstream, central and downstream part of the study bar, respectively (Fig. A.2c). Cores were kept humid in PVC liners and successively cut longitudinally, sampled for grain-size analysis, photographed at high resolution and preserved for making dry peels with epoxy. Each core was characterized following the basic principles of facies analysis highlighting sediment grain size, color, oxidation, sedimentary structures and occurrence of bioturbation, plant debris and shell fragments.

(a)

(b)

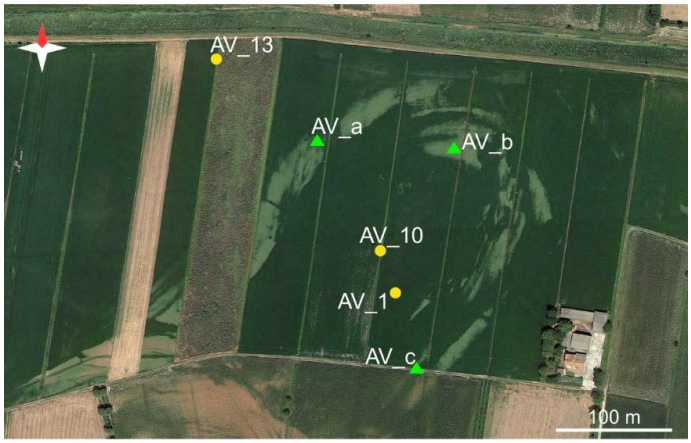

(c)

Fig. A.2. Methodologies: (a - b) Geophysical acquisition: (a) the electromagnetic tool on the wooden sledge dragged by a small tractor on the study field, and (b) the survey path; (c) Position of the recovered cores. Yellow dots and green triangles indicate the hand auger core and the drilled cores with rotary technique, respectively.

The terminology used in this work is graphically summarized in Fig. A.3. The channel thalweg is defined as the deepest part of the active channel, where the coarsest deposits occur. Riffles and pools are situated at bend inflections and bend apexes, respectively, and correspond to the shallower and the deeper portions of the thalweg, respectively. Sinuosity is calculated as the ratio between the along-channel distance between two adjacent riffles and their linear distance (Fig. A.3). Straight channels are characterized by sinuosity close to 1, whereas sinuous channels reach values higher than 2.5.

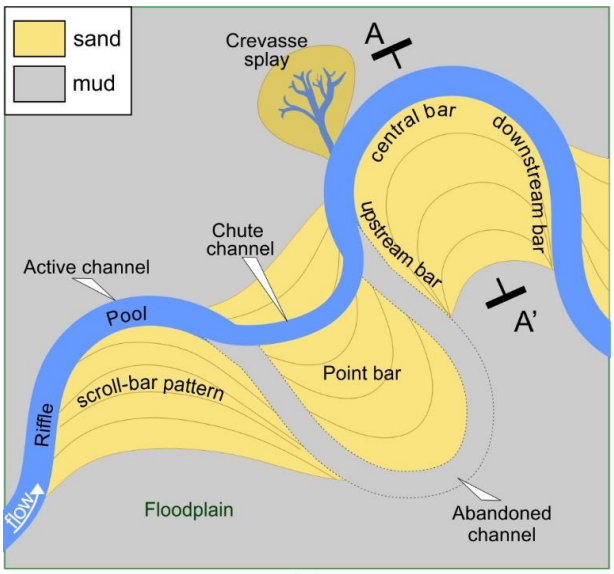

(a)

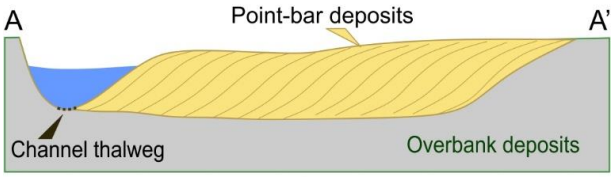

(b)

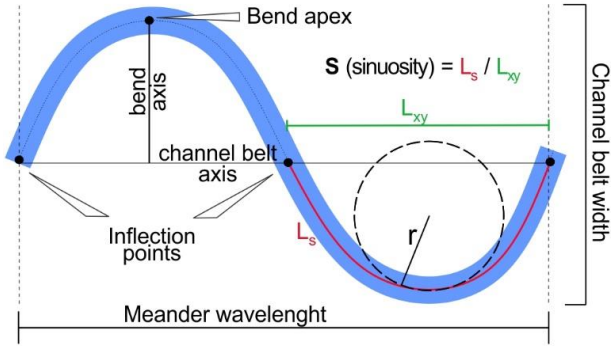

(c)

Fig. A.3. Descriptive terminology for fluvial meanders and related deposits; (a) alluvial plain morphological elements, (b) point-bar deposits and (c) meander-belt morphometry.

3. Results

3.1. Remote sensing

The analyzed satellite images and aerial pictures give a consistent idea of the changes in the land use of the area and the visibility of the paleo-hydrographic traces over the last 60 years. In particular, recent high-resolution true-color composite images allow mapping these features with sub-metric accuracy. The traces mainly consist of cropmarks with vegetation suffering from hydraulic stress during the growing season, and dead patches in July and August. Significant changes can be observed over very short periods (compare e.g., Fig. A.4d, f) during the hot season, while sensitivity is low in spring time (e.g., Fig. A.4e) and is lost in winter, when the fields are covered by scarce vegetation and are bare and plowed, respectively. By comparing satellite images mostly taken during the growing season (i.e., those that best show the traces) differences in vegetation colors allow the identification of buried morphologies of two distinct reaches, hereafter named Reach A and Reach B, and a crevasse splay. Reach A consists of two major bends, called Bend 1 and Bend 2 (Fig. A.4b). The NDVI and NDMI images derived from Sentinel-2 summer images (Fig. A.5c, d) clearly show the differential behavior of the paleo-meanders in comparison to the external floodplain and the inner portion surrounded by Reach A: the vegetation growing on more permeable sandy soil is less healthy than the one living on finer sediments. The paleo-hydrographic traces are much more evidenced by NDVI and NDMI during the summer season and they clearly help in identifying the general pattern of the abandoned channels. However, the rather low resolution of the Sentinel-2 images does not contribute significantly to discriminating in detail the specific morphological and sedimentological features composing the paleo-hydrographic traces.

Bend 1 is an open bend, with an SSW-NNE bend axis, and is characterized by a sinuosity of about 2.2 and a radius of curvature of ca. 140 m. The scroll-bar pattern is particularly clear from cropmarks, in the northern-central portion of the bend (Fig. A.4c, d), showing a different signal compared to the residual channel fill (i.e., light cropmark when the others are dark and vice-versa), testifying the progressive growth of the meander bend. The channel fill displays a width of about 15-20 m and can be better defined where bounded by

opposite-trending scroll bar patterns, like in the upstream side of the bend. The riffle-to-riffle distance on the channel fill is about 260 m.

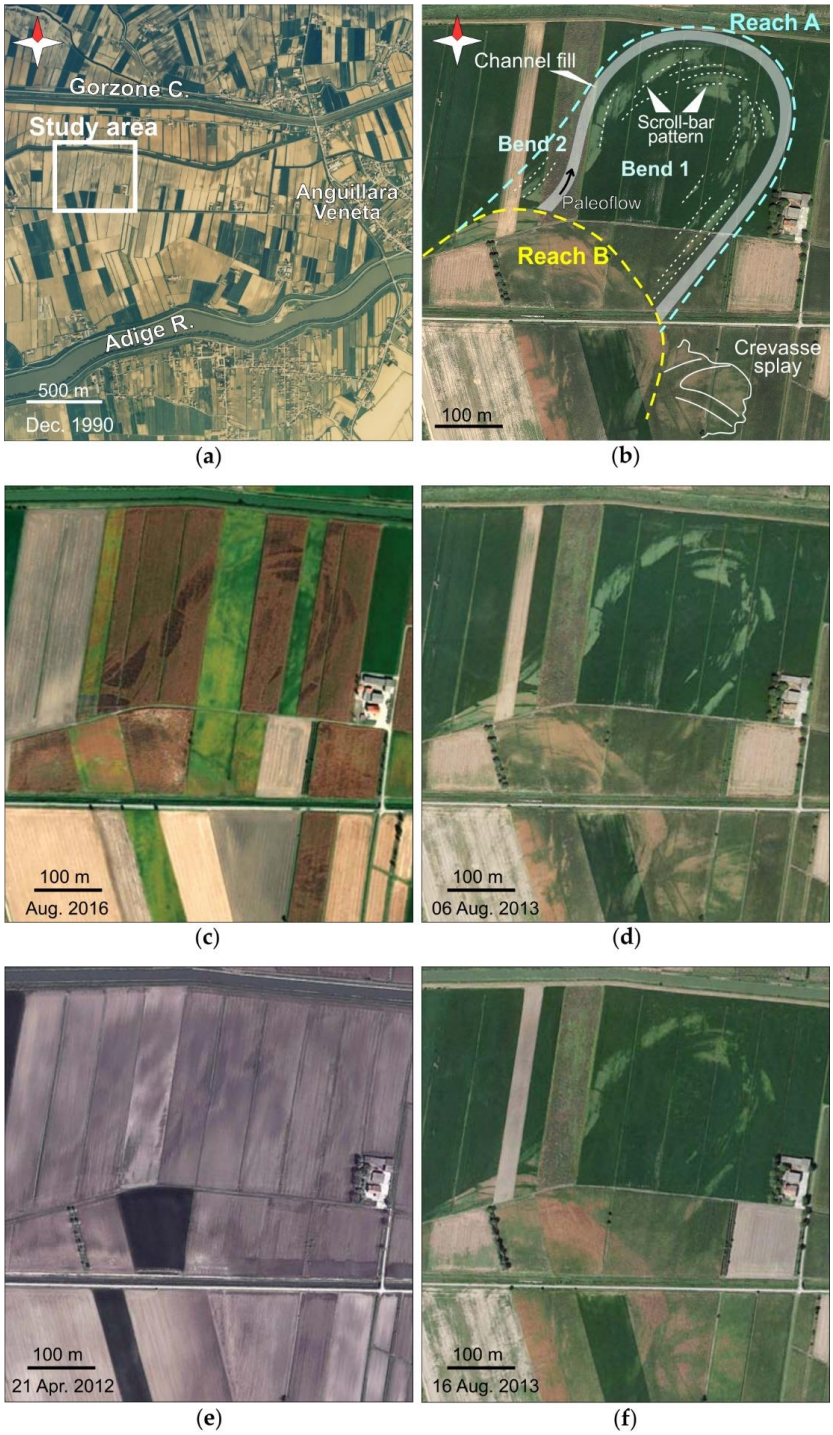

Fig. A.4. Remote sensing results: (a) Aerial photogram of the study area enhancing poorly visible fluvial pattern during winter time; (b) Meander belt reconstruction and fluvial morphology identification in the study area: white dashed lines highlight evidence of scroll-bar morphologies; (c - f) Satellite images (2016, 2013, 2012) providing information about fluvial morphology on the basis of seasons and soil use.

Bend 2 is a low sinuosity bend (i.e., 1.12), with an NW-SE bend axis, characterized by an estimated radius of curvature and riffle-to-riffle distance of 135 and 230 m, respectively. Bend 2 is sited upstream from Bend 1 and shows a scroll-bar pattern that testifies a progressive expansional growth style (sensu [76]) of the bend.

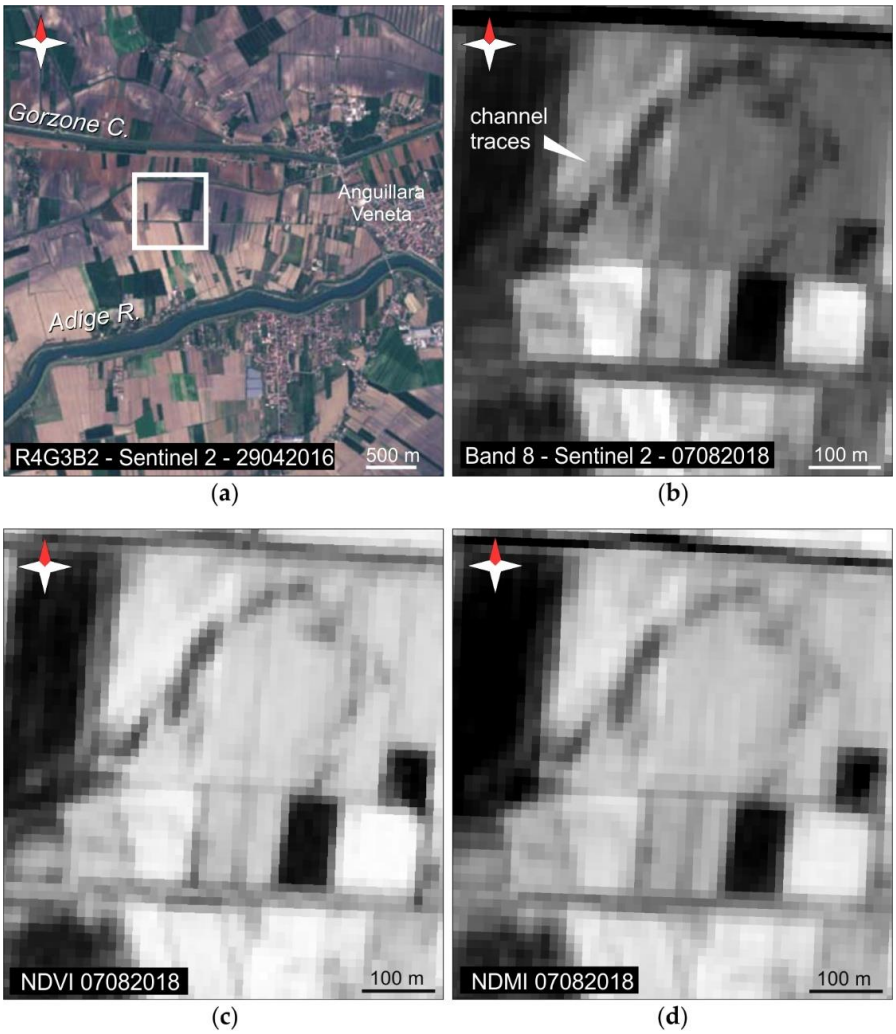

Fig. A.5. Processed satellite images; (a) RGB combination on Sentinel-2 image to highlight petrographic differences in the study area; (b) Band 8, of Sentinel-2 image of the study area, showing paleochannel morphologies; (c – d) NDVI and NDMI indexes calculated on Sentinel 2 images (2018), respectively, enhancing different plant health and hydraulic stress.

Reach B forms a bend occurring south of Reach A, but is less visible from satellite images, and its sinuosity cannot be defined. The radius of curvature is ca. 350 m and the axis of the bend trends ca. SW-NE, although satellite images do not show a clear bar-scroll pattern and the position of the relevant channel fill. Reach B cuts over Reach A suggesting that it developed after a chute channel that cut off Reach A [77], which was later abandoned. Additionally, along the eastern side of Reach B, (Fig. A.4d, f) a divergent pattern of minor channels point to a local development of a crevasse splay sourced from the downstream side of the bend. Several straight dark stripes, with a width of about 1 m, located on Reach B, can be interpreted as traces of abandoned ditches that were associated with a drainage system dating back to Renaissance times and dismissed later on (Fig. A.4d).

3.2. 3D Electrical conductivity model from EMI

The inversion of the EMI data produced a 3D volume of electrical conductivity values. The results are shown in Fig. A.6, where we elected to show the volume sliced horizontally at eight depth levels down to a depth of nearly 8 m below ground, corresponding each to a layer selected in the inversion approach. Note that the inversion as conducted with an Occam approach, but using a limited number of layers compatible with the information contained in the six different acquisition configurations obtainable with the CMD explorer instrument.

An arcuate sedimentary body having low electrical conductivity (i.e., a resistive body) is clearly visible at depth between 1 and 6 m below ground. The internal boundary of this arcuate body (see Slice 5 in Fig. A.6b) is fully visible in the maps, and shows a radius of curvature and a sinuosity of ca. 60 and 2.3, respectively. The external boundary (see Slice 5 in Fig. A.6b) slightly debouches from the maps, but its radius of curvature and sinuosity can be estimated to be ca. 135 and 2.2, respectively (Fig. A.6b) as also confirmed by remote sensing results. Orientation of the outer boundary of this body fits with the orientation of meander Bend 1 of Reach A as depicted by remote sensing analyses, and is also consistent with the associated scroll pattern (Fig. A.4b), suggesting that these low-resistivity deposits represent the point bar body associated with meander Bend 1 of Reach A. Of course, the main contribution of the EMI data is to provide continuous and extensive depth information that is not available from remote sensing. In the shallower layers (slices 1 - 5), the arcuate point-bar body presents low conductivity values with $\sigma < 20$ mS/m, and its conductivity is still close to 40 mS/m at about 5 – 6 m below ground (slices 6 and 7; Fig. A.6b).

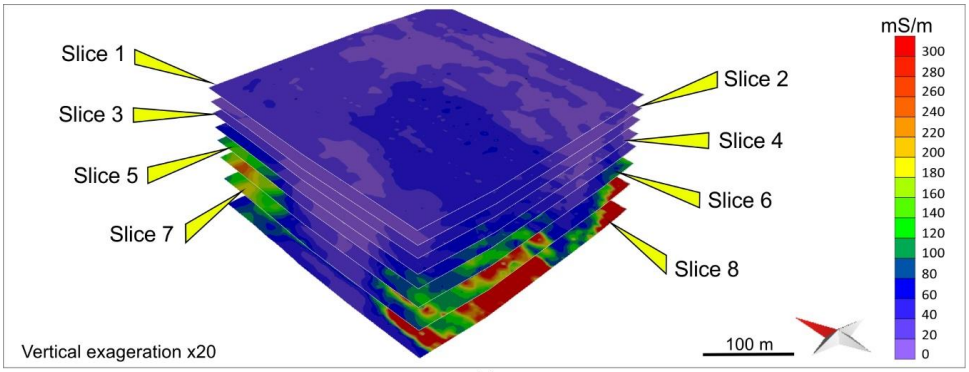

(a)

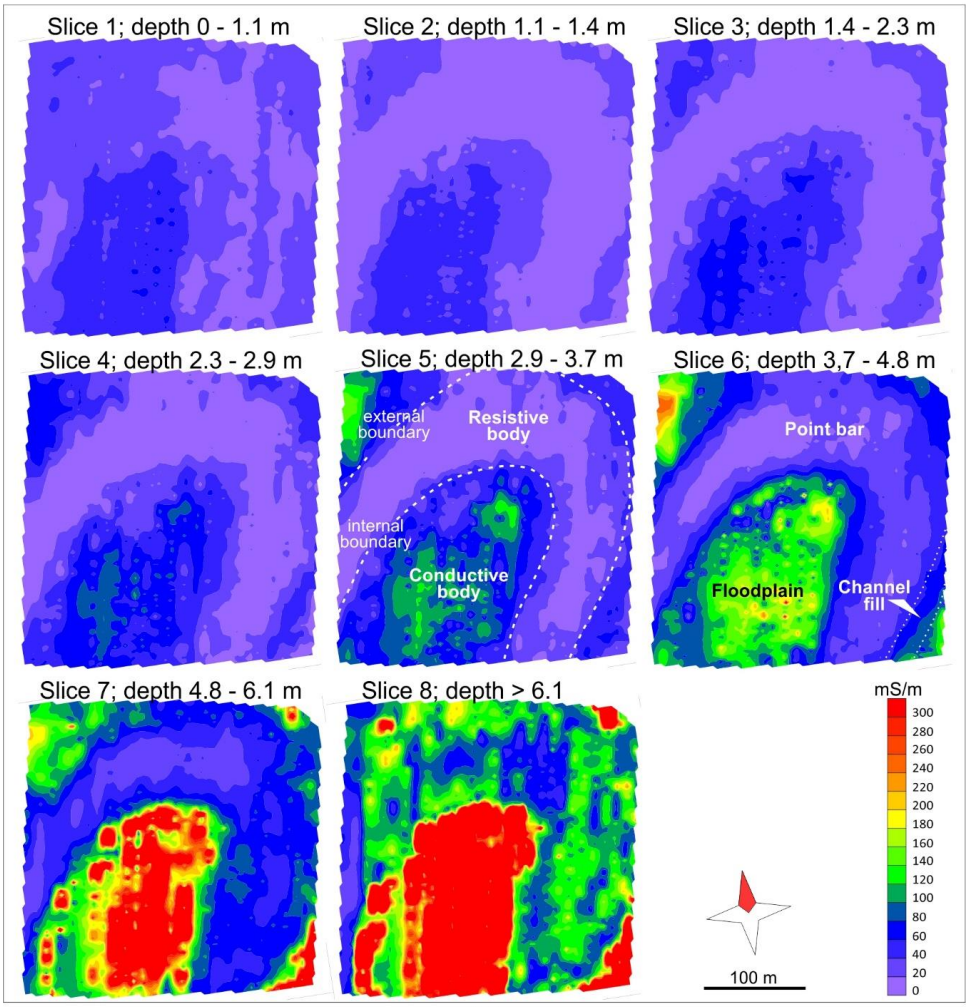

(b)

Fig. A.6. Geophysical results: (a) 3D view of the eight 2D conductivity maps; (b) The eight 2D maps showing difference in conductivity values and highlighting point-bar, channel-fill and floodplain morphologies.

Note that the width of the most resistive part of the bar is clearly shrinking with depth, thus showing the 3D shape of the sand body. At larger depths (slice 8 – below 6.1 m) conductivity increases up to 180 mS/m, delimiting the base of the bar body. It must be noted, however, that the CMD explorer provides, as a rule of thumb, reliable information only down to 6 m below ground and thus slice 8 is effectively an extrapolation due to the need to have an infinite semi-space at the bottom of the electrical conductivity model, and thus should be considered with care. Although the point-bar body shows a fairly homogeneous electrical resistivity, a subtle increase in resistivity values defines a 20 m narrow, NNE-SSW trending belt in the SE corner of slices 2 to 6. The location of this belt fits with that of the abandoned channel forming the meander Bend 1 as apparent in satellite images (Fig. A.4b) and suggests that the higher resistivity values are linked to the coarser material of the deposits filling the abandoned channel. Deposits surrounding the low-resistivity point-bar body show conductivity values spanning from 80 to 250 mS/m, with values close to 100 mS/m down to 3 m below ground, increasing to 250 mS/m below -3 m. Comparison between geophysical data and geomorphic evidence suggests that these electrically conductive sediments represent floodplain deposits in which the Bend 1 meander was cut, thus developing the related point-bar sedimentary body.

3.3. Sedimentology

Core data provide the ground-truth information needed to calibrate/confirm geophysical data with localized information. The cores help define sedimentary features of the electrically resistive point-bar body, related channel-fill deposits and surrounding electrically conductive overbanks. All cores reveal that the deposits were intensely reworked by agricultural activities down to 80 cm below ground. Note that this fact may pose significant limitations to remote sensing interpretation that is forcibly limited to surface images. Reworked deposits are dark brown and consist of very fine sand with a variable amount of mud. Point-bar deposits were completely cored at sites AV_a – c (Fig. A.7). Point-bar deposits occur from 0.8 m to a maximum of 5.4 m below ground and mainly consist of sand with a scarce percentage of mud. Cores AV_a – c reveal that bar deposits cover either organic-rich mud (core AV_b) or sandy deposits (cores AV_a and AV_c). Point-bar deposits are floored by a channel lag that consists of massive medium sand with pebble-sized mudclasts (Fig. A.8a). This basal lag is covered by lower bar deposits, consisting of 1 – 1.5 m of mud-free, well-sorted fine to medium sand, which is commonly massive or crudely plane-parallel

stratified (Fig. A.8b). Upper bar deposits are ca 2.5 – 3 m thick and consist of fine to very fine sand with subordinate mud layers. Sand is plane-parallel to ripple cross-laminated (Fig. A.8c) and contains mud for ca. 12%, 21% and 20% in the upstream, central and downstream zone, respectively. Mud layers (Fig. A.8c) range in thickness between 0.5 and 2 cm, and consist of massive or crudely laminated mud with plant debris. Lower bar deposits are ubiquitously mud free. The overall grain size of the bar deposits does not relevantly change along the bar, which appears as an almost monotonous sandy body from its upstream to downstream reach.

The overbank deposits were cored where geophysical investigations reveal the occurrence of electrically conductive sediments. These deposits mainly consist of silt-rich mud with subordinate sandy layers with horizontal bedding. Mud is massive and can be organic-rich (Fig. A.8d) or slightly oxidized in the lower and upper part of the overbank succession, respectively.

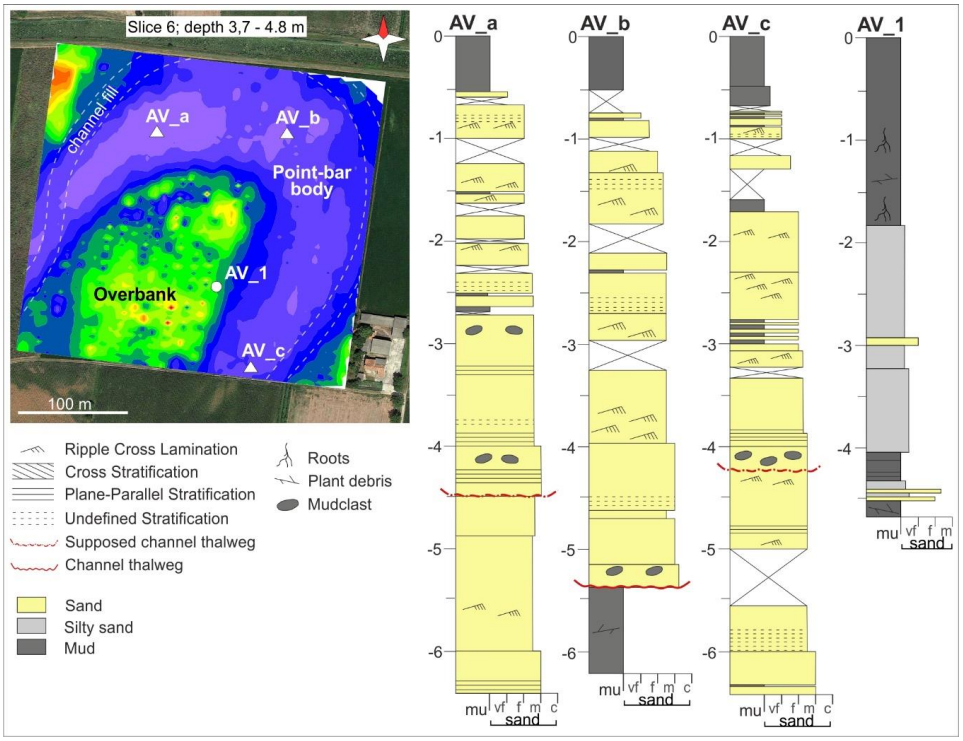

Fig. A.7. Sedimentary features of cores for bar and overbank deposits at the study site. Location of cores conductivity slice 6.

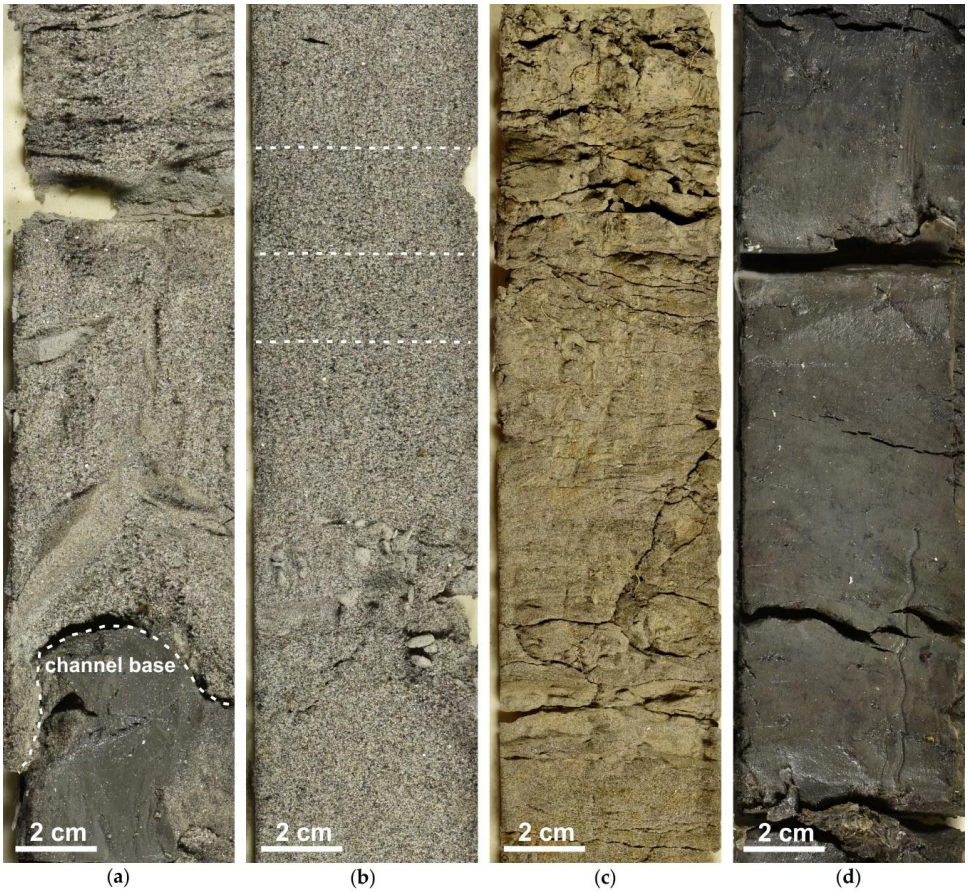

Fig. A.8. Cored deposits; (a) massive medium sand with pebble-sized mudclasts forming the channel lag, (b) fine to medium sands from the lower point bar, and (c) fine to very fine sands, with cross lamination and mud layers from the upper point bar; (d) massive overbank mud with moderate organic content and horizontal bedding.

4. Discussion

4.1. Implications for non-invasive (remote sensing and ground based electromagnetic) investigations

This study shows how remote sensing and ground-based geophysical data represent an ideal combination of non-invasive techniques that can guide direct investigations and, at the same time, can be integrated to provide a 3D reconstruction of the shallow subsoil once supported by the local direct evidence for verification and calibration.

Our results show that in the study area the use of aerial images is very effective in supporting the rapid recognition of geomorphological and sedimentological features with a resolution approaching 0.5 m. However, the aerial pictures

dating back to before the 1980s do not provide useful paleo-hydrographic evidence, probably because (a) conventional zenithal pictures were originally taken for cadastral purposes and, thus, were shot during the winter season when vegetation cover was limited; and (b) widespread leveling of the fields and use of strong plowing machines was common until that time, thus causing severe erosion of the topsoil, especially in the zones where convex landforms were formerly present, with slight accumulation in the depressions. Thus, in correspondence with natural levees and sand ridges related to scroll-bar sequences, the sandy and silty sediments were exhumed, showing a lighter signal in the soilmarks.

Cropmarks appear to be, in general, the most effective indicators of shallow geomorphological features in the considered environment. This is linked to the much higher permeability of the coarser sediments, leading to greater drainage and, in absence of irrigation, water stress to crops especially during the hot season (July and August). As documented in other areas of the Venetian Plain [78], besides the weather condition of the period before the image acquisition, the maximum detail shown by the cropmarks strongly depends on the type of cultivated plants and, in particular, it decreases with the size of the leaves and the plant spacing. The best data are generally found in zones with soya bean or hay meadow crops. Wheat, barley and corn display variable visibility, as the first two are seeded in tight rows and have small leaves, but are harvested before mid-July; in contrast, corn has a larger plant size and larger distance between rows, but is harvested in September or October and thus can (usefully) experience water stress. Note that this study was carried out analyzing freely available high-resolution images, reaching a resolution of about 0.5 m. This suggests that the use of specific images, acquired through latest commercial satellite or drone-borne multispectral scanners, could easily support the recognition of features between 0.1 and 0.5 m with superior results.

Geophysical data play a critical role in our analyses. They bridge the gap between surface extensive information provided by remote sensing (that primarily guided the identification of the study area and the location of the surveys) with the information at depth carried out through traditional drilling and sampling operations. The latter in turn were positioned on the basis of remote sensing and geophysical evidence, thus minimizing the sampling to the locations where this information was needed for verification and calibration. The geophysical data constitute the backbone of the study in that they provide

ultimately the 3D information to fully reconstruct the sedimentary structure of the site. This result, however, is not trivial to achieve.

First, great care must be posed in the acquisition phase. This entails not only the choice of the instrument and the strategy developed for covering a large area – in this case a (non-conductive) sledge towed by a tractor at sufficient distance not to induce current in the metal frame of the tractor itself. In addition, care must be paid when setting the instrument to have a good control of the measurement geometry, which is in turn essential to obtaining reliable inversion results. In this case, the stability of the sledge and the positioning care allowed us to obtain, for all data points, an RMS error of less than 10% between measured and simulated apparent conductivity data at the end of the inversion process. Note that carrying the same sonde by hand, particularly on rugged terrain, can easily unbalance the instrument, with measurements thus taken with some coils much closer to the ground than others. This might induce a very large measurement error that is impossible to correct a posteriori, as the true acquisition geometry is then completely unknown.

Second, obvious outliers must be removed from the dataset. These may include negative or extremely high apparent conductivity values (that are physically implausible for the given acquisition geometry), which may be due to local metallic or magnetic features.

Third, an accurate reconstruction of positioning must be made. The availability of reliable co-located data from HMD and VMD is essential to have the six independent pieces of information necessary for depth inversion. This requires both a guided pace in the field to re-occupy roughly the same locations and proper post-processing to assemble the data that pertain to the same reasonable surrounding of each measurement point, in this case with a radius of 1 m. Noting that the sonde size itself is of a few meters (Fig. A.2a), this accuracy is perfectly acceptable for the purpose at hand.

Fourth, geophysical inversion is an inherently ill-posed problem. In this case, this means that while the general pattern of the electrical conductivity variation with depth is constrained by the data, the subtler details may not be retrieved uniquely. In other words, at each measurement location, a number of different 1D models, which all, however, maintain certain key patterns, can be equivalent in terms of goodness of fit to the measured data within the data uncertainty range. In particular, for example, if conductivity increases with depth, all inverted profiles will display the same general pattern. However, the transition from lower to higher conductivity may happen continuously, or in steps, and

steps may occur at slightly different depths. While this can be viewed as a weakness of geophysical methods (and EMI in this particular case), it is not without remedy. Indeed, geophysics should never be applied without some "ground-truth" coming (as in this case) from drilling investigations (local and not without their uncertainties, but still necessary). Thus, an iterative revision of the inverted vertical profiles was conducted to select, among the plausible electrical conductivity profiles those that also fit reasonably to the direct evidence where this evidence is available. The procedure was simply performed manually, particularly selecting suitable layer interfaces compatible with drilling evidence. This type of procedure should always be applied, and it is in the energy exploration where 3D seismic data are blended, e.g., with well logs coming from deep borings. For the geophysical data used in this study the "ground truth" is given by the local comparison between lithology from sedimentary cores (AV_1, AV_a, AV_b and AV_c) and electrical conductivity derived from EMI inversion at the same locations. A plot showing the resulting correlation, also taking into account the variability of electrical conductivity for the same lithology (shown as standard deviation error bars) is shown in Fig. A.9.

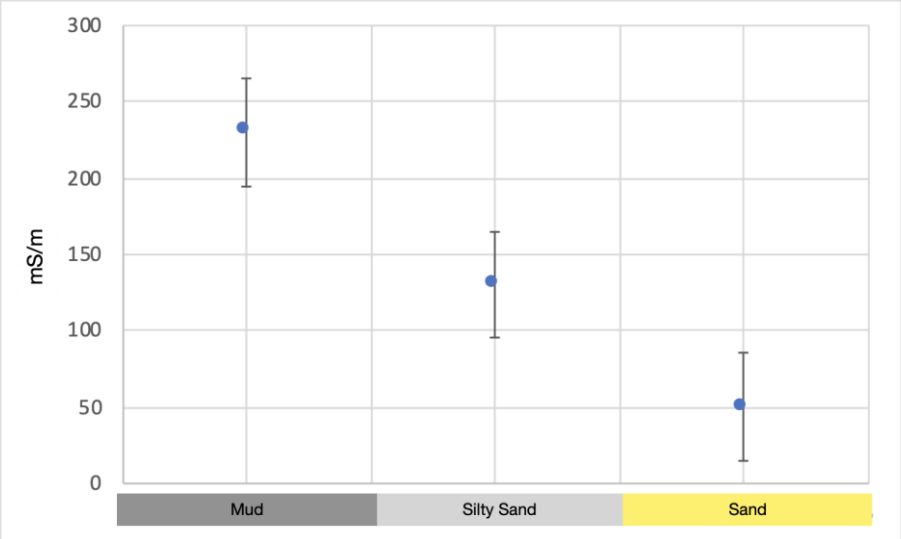

Fig. A.9. Plot of the interpretation of the EMI inverted conductivity intervals after the correlation with the sedimentary cores AV_1, AV_a, AV_b and AV_c.

4.2. Implications for investigation of meandering river deposits

Integrated remote-sensing, geophysical and sedimentological approaches provide insights to discuss key features of investigated point-bar deposits, with specific emphasis on their genesis and internal grain-size variability.

The external boundary of this body is consistent with the morphology of a point bar that originated through lateral migration of a meandering channel [79–81]. Nevertheless, the curved profile of the inner boundary suggests that the bar accretion started from the inner bank of an arcuate channel that showed a sinuosity of ca. 2.3 (Fig. A.6b). This evidence contrasts the common assumption that point bars originate from a progressive increase in channel sinuosity of a relatively straight channel, which gradually migrates laterally until reaching a sinuous configuration [82–85]. The onset of accretion from a sinuous channel allows for storing a reduced volume of bar sediment in comparison with that produced by inception from a straight channel. In the study case, the 3D reconstruction of the bar body from EMI data shows that about 1.8 million m3 of sand are stored in the arcuate point bar body (Fig. A.10a). If one assumes that the accretion of this bar started from a straight channel, as would be suggested by the application of classical sedimentological models to remote-sensing data, the estimated volume of the bar would have been of ca. 3.1 million m3 of sand (Fig. A.10b), leading to a remarkable overestimation of the accumulated sand. The onset of point-bar bar accretion from a sinuous channel was probably driven by pre-existing floodplain morphologies, which, at the early stage of channel development, forced water to drain through the paths defined by adjacent depressed areas [86,87]. The establishment of a curved planform morphology could have been forced by floodplain lithological and morphological heterogeneities [88,89], which are associated with the occurrence of numerous overbank sub-environments, including crevasse-splays, levees, floodplain lakes and floodbasins (cf. [90]). Different deposits and morphologies associated with these sub-environments possibly forced the newly-formed watercourse to connect adjacent depressed areas and assume a sinuous geometry.

The location of the sedimentary cores within the point-bar provides information concerning both vertical and lateral grain-size variability within this sedimentary body, with a particular focus on the comparison between upstream and downstream bar deposits. Although a fining-upward grain size distribution has been broadly considered to be typical of point-bar deposits [84,90,91], a certain variability of vertical grain-size distribution has also been documented [92,93]. Core data show that muddy layers occur in the upper part of the bar, although

mud is visibly subordinate to sand. The grain size of sand varies significantly neither vertically nor downstream, and the bar is, therefore, characterized by widespread weak vertical grain-size trends. Although the lack of a clear vertical fining in the upstream bar zone is consistent with the occurrence of high bed shear stress [94,95], the paucity of muddy deposits in the downstream part of the bar is a peculiar feature, which cannot be ascribed to the overall lack of mud in the system, being that the overbank deposits are entirely made of mud. The open morphology of the bend [96] associated with the study bar could have hindered the formation of a dead zone, which commonly forms in sharp bends [97], preventing the accumulation of mud in the downstream bar zone.

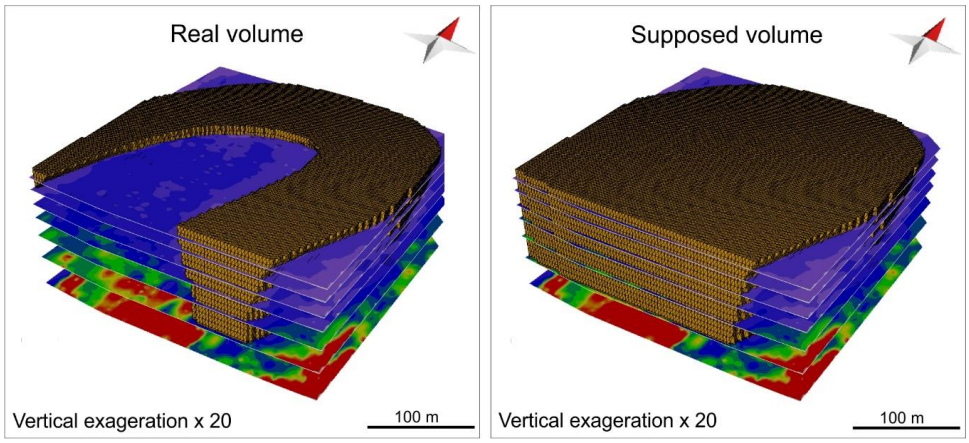

Fig. A.10. Volume of the point-bar body (a) reconstructed through the present study, (b) inferred assuming bar growth from a straight channel, as suggested by classical sedimentological models.

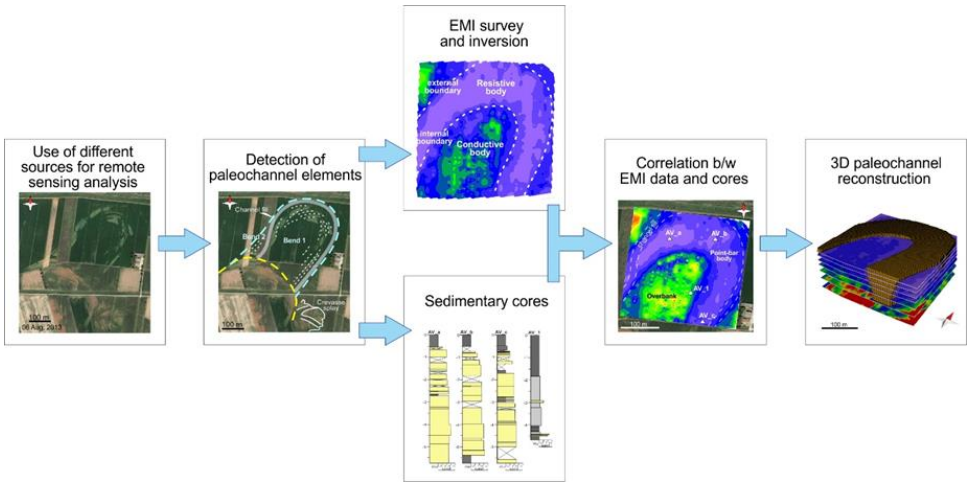

Fig. A.11. Workflow of the overall methodology adopted in this study.

Fig. A.11 shows a summary of the workflow we used to extract the relevant information from each data source and blend the pieces of information towards the final conceptual 3D distributed model of the studied site.

5. Conclusions

This paper presents a successful integrated approach to analyze the distribution of sedimentary facies of a paleo-meander in the Southern Venetian Plain, north-eastern Italy. The approach is based on a combination of remote sensing (aerial and satellite) data, geophysical investigations (electromagnetic surveys), and direct sedimentary coring.

From the methodological point of view, we show that the combined use of non-invasive techniques such as remote sensing and ground-based geophysical data provides an effective method for the purpose at hand. In particular, remote sensing is quite effective for the identification of sites of interest and features at a metric scale, which is potentially linked to different subsoil structures. In the case considered here, cropmarks are the most useful features observed from the satellite images, due specifically to the water stress induced in crops by the higher permeability of sandy bodies with respect to silty sediments. However, remote sensing can only provide information on the ground surface. On the contrary, geophysical methods are specifically designed to reconstruct the subsurface structure on the basis of contrasts of geophysical parameters. In this case, we used electromagnetic induction (EMI) methods, and particularly an FDEM small scale multi-coil system. Well designed, acquired, processed, and inverted EMI data allowed us to extend the surface information provided by remote sensing to a maximum depth exceeding 6 m below ground level, allowing the construction of a 3D model of electrical conductivity of the subsoil. Direct investigations via sedimentary core drilling were positioned on the basis of remote sensing and geophysical data, in order to confirm and calibrate the geophysical investigations, which were also partly re-inverted on the basis of the new evidence. The overall cycle of investigations thus allowed us to set up a 3D stratigraphic model of the site, consistent with all available data. On the other hand, the sequence of investigation activities was designed in such a manner that the information collected at one step optimized the design of the next step, thus reducing the overall effort required to complete the task.

From the sedimentary point of view, the point-bar studied shows an uncommon arcuate morphology, that contrasts the common assumption that point bars

originate from a progressive sinuosity increase of a relatively straight channel that migrates laterally until reaching a sinuous configuration. This can be explained by considering the variety of alluvial sub-environments in the floodplain. These floodplain heterogeneities likely controlled water fluxes over the platform, by facilitating water drainage within traces of depressed areas, defining the sinuous shape of the study channel during the very first phases of channel formation. As far as grain size distribution is concerned, although classical facies models highlight overall trends of upward and downstream fining of grain size within point-bar deposits, the grain-size trends of the study bar do not vary significantly either vertically or laterally. The bar is, indeed, characterized by a widespread weak vertical grain-size trend, and it appears as a homogeneous body of medium to fine sand. The lower mud content in the downstream portion was probably a result of the open morphology of the bend that could have prevented the formation of the dead zone, which is commonly directly linked to mud accumulation in the downstream portion of the sharp bends.

This study provides a solid basis for developing more detailed sedimentological investigations, which could be improved including acquisition of data concerning internal stratal architecture of the alluvial deposits. GPR investigations and recovery of undisturbed sedimentary cores would provide further relevant insights to this approach, with relevant follow up in the frame of subsurface exploration or management of surficial aquifers. Detection of the distinctive morphometric and sedimentological features of Late Holocene paleochannels, would allow a comparison with those of the rivers draining the area currently, and allow quantification of human impact on riverine dynamics [18].

Funding: This work has been supported by project HYDROSEM (Progetti di Eccellenza CARIPARO 2017, Cassa di Risparmio di Padova e Rovigo): Fluvial and tidal meanders of the Venetian-Po plain: From hydrodynamics to stratigraphy" project (PI. M. Ghinassi).

Acknowledgments: Reviewers and Editors are acknowledged. Authors thank M. Cosma for logistic support during field work, and R. Bonato, the land owner of the study area.

References

1. Clement, W.P.; Barrash, W. Crosshole radar tomography in a fluvial aquifer near Boise, Idaho. J. Environ. Eng. Geophys. 2006, 11, 171–184, doi:10.2113/JEEG11.3.171.
2. Galgaro, A.; Finzi, E.; Tosi, L. An experiment on a sand-dune environment in Southern Venetian coast based on GPR, VES and documentary evidence. Ann. Geophys. 2000, 43, 289–295, doi:10.4401/ag-3643.
3. Nofal, E.R.; Amer, M.A.; El-Didy, S.M.; Fekry, A.M. Delineation and modeling of seawater intrusion into the Nile Delta Aquifer: A new perspective. Water Sci. 2015, 29, 156–166, doi:10.1016/j.wsj.2015.11.003.
4. Da Lio, C.; Carol, E.; Kruse, E.; Teatini, P.; Tosi, L. Saltwater contamination in the managed low-lying farmland of the Venice coast, Italy: An assessment of vulnerability. Sci. Total Environ. 2015, 533, 356–369, doi:10.1016/j.scitotenv.2015.07.013.
5. Desbarats, A.J.; Koenig, C.E.M.; Pal, T.; Mukherjee, P.K.; Beckie, R.D. Groundwater flow dynamics and arsenic source characterization in an aquifer system of West Bengal, India. Water Resour. Res. 2014, 50, 4974–5002, doi:10.1002/2013WR014034.
6. Carraro, A.; Fabbri, P.; Giaretta, A.; Peruzzoa, L.; Tateo, F.; Tellini, F. Effects of redox conditions on the control of arsenic mobility in shallow alluvial aquifers on the Venetian Plain (Italy). Sci. Total Environ. 2015, 532, 581–594, doi:10.1016/j.scitotenv.2015.06.003.
7. Romeo, R.W.; Amoroso, S.; Facciorusso, J.; Lenti, L.; Madiai, C.; Martino, S.; Monaco, P.; Rinaldis, D.; Totani, F. Soil liquefaction during the Emilia, 2012 seismic sequence: investigation and analysis. Eng. Geol. Soc. Territ. 2015, 5, 1107–1110, doi:10.1007/978-3-319-09048-1_210.
8. Amorosi, A.; Bruno, L.; Facciorusso, J.; Piccin, A.; Sammartino, I. Stratigraphic control on earthquake-induced liquefaction: a case study from the Central Po Plain (Italy). Sediment. Geol. 2016, 345, 42–53, doi:10.1016/j.sedgeo.2016.09.002.
9. Fontana, D.; Lugli, S.; Marchetti Dori, S.; Caputo, R.; Stefani, M. Sedimentology and composition of sands injected during the seismic crisis of May 2012 (Emilia, Italy): Clues for source layer identification and liquefaction regime. Sediment. Geol. 2015, 325, 158–167, doi:10.1016/j.sedgeo.2015.06.004.
10. Mozzi, P. Alluvial plain formation during the Late Quaternary between the southern Alpine margin and the Lagoon of Venice (Northern Italy). Geogr. Fis. e Din. Quat. 2005, Suppl. 7, 219–229.
11. Ninfo, A.; Ferrarese, F.; Mozzi, P.; Fontana, A. High resolution dems for the analysis of fluvial and ancient anthropogenic landforms in the alluvial plain of Padua (Italy). Geogr. Fis. e Din. Quat. 2011, 34, 95–104, doi:10.4461/GFDQ.2011.34.11.

12. Castiglioni, G.B. Geomorphology of the Po Plain. Earth Surf. Process. Landforms 1999, 24, 1115–1120.
13. Bondesan, A.; Meneghel, M.; Rosselli, R.; Vitturi, A. La carta geomorfologica della Provincia di Venezia, scala 1:50,000; LAC: Firenze, 2004; Vol. 5;.
14. Mehdi, S.M.; Pant, N.C.; Saini, H.S.; Mujtaba, S.A.I.; Pande, P. Identification of palaeochannel configuration in the Saraswati River basin in parts of Haryana and Rajasthan, India, through digital remote sensing and GIS. Episodes 2016, 39, 29–38, doi:10.18814/epiiugs/2016/v39i1/89234.
15. Rossetti, D. de F. Multiple remote sensing techniques as a tool for reconstructing late Quaternary drainage in the Amazon lowland. Earth Surf. Process. Landforms 2010, 35, 1234–1239, doi:10.1002/esp.1996.
16. Wray, R.A.L. Palaeochannels of the Namoi River Floodplain, New South Wales, Australia: The use of multispectral Landsat imagery to highlight a Late Quaternary change in fluvial regime. Aust. Geogr. 2009, 40, 29–49, doi:10.1080/00049180802656952.
17. Demarchi, L.; Bizzi, S.; Piégay, H. Regional hydromorphological characterization with continuous and automated remote sensing analysis based on VHR imagery and low-resolution LiDAR data. Earth Surf. Process. Landforms 2017, 42, 531–551, doi:10.1002/esp.4092.
18. Piégay, H.; Arnaud, F.; Belletti, B.; Bertrand, M.; Bizzi, S.; Carbonneau, P.; Dufour, S.; Liébault, F.; Ruiz-Villanueva, V.; Slater, L. Remotely sensed rivers in the Anthropocene: state of the art and prospects. Earth Surf. Process. Landforms 2020, 45, 157–188, doi:10.1002/esp.4787.
19. Langat, P.K.; Kumar, L.; Koech, R. Monitoring river channel dynamics using remote sensing and GIS techniques. Geomorphology 2019, 325, 92–102, doi:10.1016/j.geomorph.2018.10.007.
20. Finotello, A.; Lanzoni, S.; Ghinassi, M.; Marani, M.; Rinaldo, A.; D'Alpaos, A. Field migration rates of tidal meanders recapitulate fluvial morphodynamics. Proc. Natl. Acad. Sci. 2018, 115, 1463–1468, doi:10.1073/pnas.1711330115.
21. Righini, M.; Surian, N. Remote sensing as a tool for analysing channel dynamics and geomorphic effects of floods. In Flood monitoring through remote sensing; Springer, 2018; pp. 27–59.
22. Fontana, A.; Mozzi, P.; Bondesan, A. Alluvial megafans in the Venetian-Friulian Plain (north-eastern Italy): Evidence of sedimentary and erosive phases during Late Pleistocene and Holocene. Quat. Int. 2008, 189, 71–90, doi:10.1016/j.quaint.2007.08.044.
23. Fontana, A.; Mozzi, P.; Bondesan, A. Late Pleistocene evolution of the Venetian-Friulian Plain. Rend. Lincei 2010, 21, 181–196, doi:10.1007/s12210-010-0093-1.
24. Piovan, S.; Mozzi, P.; Stefani, C. Bronze age paleohydrography of the southern Venetian Plain. Geoarchaeology 2010, 25, 6–35, doi:10.1002/gea.20300.

25. Brivio, L.; Ghinassi, M.; D'Alpaos, A.; Finotello, A.; Fontana, A.; Roner, M.; Howes, N. Aggradation and lateral migration shaping geometry of a tidal point bar: An example from salt marshes of the Northern Venice Lagoon (Italy). Sediment. Geol. 2016, 343, 141–155, doi:10.1016/j.sedgeo.2016.08.005.
26. Parasnis, D.S. Principles of Applied Geophysics; 5th ed.; Chapman & Hall: London, UK, 1997;
27. Telford, W.M.; Geldart, L.P.; Sheriff, R.E. Applied geophysics; Cambridge University Press: Cambridge, UK, 1990;
28. Everett, M.E.; Meju, M.A. Near-Surface Controlled-Source Electromagnetic Induction: Background and Recent Advances. In Hydrogeophysics; Rubin, Y., Hubbard, S.S., Eds.; Springer: Dordrecht, 2005; Vol. 50, pp. 157–184 ISBN 978-1-4020-3101-4.
29. Boaga, J. The use of FDEM in hydrogeophysics: A review. J. Appl. Geophys. 2017, 139, 36–46, doi:10.1016/j.jappgeo.2017.02.011.
30. Lesch, S.M.; Strauss, D.J.; Rhoades, J.D. Spatial Prediction of Soil Salinity Using Electromagnetic Induction Techniques: 1. Statistical prediction models: A comparison of multiple linear regression and cokriging Identification and Estimation. Water Resour. Res. 1995, 31, 373–386, doi:10.1029/94WR02179.
31. Paine, J.G. Determining salinization extent, identifying salinity sources, and estimating chloride mass using surface, borehole, and airborne electromagnetic induction methods. Water Resour. Res. 2003, 39, 1–10, doi:10.1029/2001WR000710.
32. Sambuelli, L.; Leggieri, S.; Calzoni, C.; Porporato, C. Study of riverine deposits using electromagnetic methods at a low induction number. Geophysics 2007, 72, B113–B120, doi:10.1190/1.2754249.
33. Greenhouse, J.P.; Slaine, D.D. The use of reconnaissance electromagnetic methods to map contaminant migration: these nine case studies can help determine which geophysical techniques are applicable to a given problem. Groundw. Monit. Remediat. 1983, 3, 47–59, doi:10.1111/j.1745-6592.1983.tb01199.x.
34. Martinelli, P.; Duplaá, M.C. Laterally filtered 1D inversions of small-loop, frequency-domain EMI data from a chemical waste site. Geophysics 2008, 73, F143–F149, doi:10.1190/1.2917197.
35. Cassiani, G.; Ursino, N.; Deiana, R.; Vignoli, G.; Boaga, J.; Rossi, M.; Perri, M.T.; Blaschek, M.; Duttmann, R.; Meyer, S.; et al. Noninvasive Monitoring of Soil Static Characteristics and Dynamic States: A Case Study Highlighting Vegetation Effects on Agricultural Land. Vadose Zo. J. 2012, 11, doi:10.2136/vzj2011.0195.
36. Gebbers, R.; Lück, E.; Heil, K. Depth sounding with the EM38-detection of soil layering by inversion of apparent electrical conductivity measurements. In Precision Agricolture '07; Stafford, J. V., Ed.; Wageningen Academic Publisher: Skiathos, Greece, 2007; pp. 95–102 ISBN 978-90-8686-024-1).

37. Yao, R.; Yang, J. Quantitative evaluation of soil salinity and its spatial distribution using electromagnetic induction method. Agric. Water Manag. 2010, 97, 1961–1970, doi:10.1016/j.agwat.2010.02.001.
38. Osella, A.; De la Vega, M.; Lascano, E. 3D electrical imaging of an archaeological site using electrical and electromagnetic methods. Geophysics 2005, 70, G101–G107, doi:10.1190/1.1993727.
39. Thiesson, J.; Dabas, M.; Flageul, S. Detection of resistive features using towed Slingram electromagnetic induction instruments. Archaeol. Prospect. 2009, 16, 103–109, doi:10.1002/arp.350.
40. Perri, M.T.; Boaga, J.; Bersan, S.; Cassiani, G.; Cola, S.; Deiana, R.; Simonini, P.; Patti, S. River embankment characterization: the joint use of geophysical and geotechnical techniques. J. Appl. Geophys. 2014, 110, 5–22, doi:10.1016/j.jappgeo.2014.08.012.
41. Huang, H.; SanFilipo, B.; Oren, A.; Won, I.J. Coaxial coil towed EMI sensor array for UXO detection and characterization. J. Appl. Geophys. 2007, 61, 217–226, doi:10.1016/j.jappgeo.2006.06.005.
42. Corwin, D.L.; Rhoades, J.D. An Improved Technique for Determining Soil Electrical Conductivity-Depth Relations from Above-ground Electromagnetic Measurements. Soil Sci. Soc. Am. J. 1982, 46, 517–520, doi:10.2136/sssaj1982.03615995004600030014x.
43. McNeill, J.D. Electromagnetic Terrain Conductivity Measurement at Low Induction Numbers. Tech. note TN6 1980, 15, doi:http://www.geonics.com/pdfs/technicalnotes/tn6.pdf.
44. Wait, J.R. Geo-Electromagnetism; Academic Press: New York, 1982;
45. Frischknecht, F.C.; Labson, V.F.; Spies, B.R.; Anderson, W.L. Profiling methods using small sources. In Electromagnetic Methods in Applied Geophysics, vol. 2; Nabighian, M.N., Ed.; Society of Exploration Geophysicists: Tulsa, 1991; pp. 105–270.
46. Deidda, G.P.; Fenu, C.; Rodriguez, G. Regularized solution of a nonlinear problem in electromagnetic sounding. Inverse Probl. 2014, 30, 1–19, doi:10.1088/0266-5611/30/12/125014.
47. von Hebel, C.; Rudolph, S.; Mester, A.; Huisman, J.A.; Kumbhar, P.; Vereecken, H.; van der Kruk, J. Three-dimensional imaging of subsurface structural patterns using quantitative large-scale multiconfiguration electromagnetic induction data. Water Resour. Res. Res. 2014, 50, 2732–2748, doi:10.1002/2013WR014864.
48. Saey, T.; De Smedt, P.; Delefortrie, S.; Van De Vijver, E.; Van Meirvenne, M. Comparing one- and two-dimensional EMI conductivity inverse modeling procedures for characterizing a two-layered soil. Geoderma 2015, 241–242, 12–23, doi:10.1016/j.geoderma.2014.10.020.
49. Shanahan, P.W.; Binley, A.; Whalley, W.R.; Watts, C.W. The Use of Electromagnetic Induction to Monitor Changes in Soil Moisture Profiles beneath Different Wheat Genotypes. Soil Sci. Soc. Am. J. 2015, 79, 459–466, doi:10.2136/sssaj2014.09.0360.

50. Frederiksen, R.R.; Christiansen, A.V.; Christensen, S.; Rasmussen, K.R. A direct comparison of EMI data and borehole data on a 1000 ha data set. Geoderma 2017, 303, 188–195, doi:10.1016/j.geoderma.2017.04.028.
51. Boaga, J.; Ghinassi, M.; D'Alpaos, A.; Deidda, G.P.; Rodriguez, G.; Cassiani, G. Geophysical investigations unravel the vestiges of ancient meandering channels and their dynamics in tidal landscapes. Sci. Rep. 2018, 8, 1–8, doi:10.1038/s41598-018-20061-5.
52. Viezzoli, A.; Christensen, A.. V.; Auken, E.; Sørensen, K. Quasi-3D modeling of airborne TEM data by spatially constrained inversion. Geophysics 2008, 73, F105–F113, doi:10.1190/1.2895521.
53. Piovan, S.; Mozzi, P.; Zecchin, M. The interplay between adjacent Adige and Po alluvial systems and deltas in the late Holocene (Northern Italy). Géomorphologie Reli. Process. Environ. 2012, 18, 427–440, doi:10.4000/geomorphologie.10034.
54. De Franco, R.; Biella, G.; Tosi, L.; Teatini, P.; Lozej, A.; Chiozzotto, B.; Giada, M.; Rizzetto, F.; Claude, C.; Mayer, A.; et al. Monitoring the saltwater intrusion by time lapse electrical resistivity tomography: The Chioggia test site (Venice Lagoon, Italy). J. Appl. Geophys. 2009, 69, 117–130, doi:10.1016/j.jappgeo.2009.08.004.
55. Mozzi, P.; Piovan, S.; Corrò, E. Long-term drivers and impacts of abrupt river changes in managed lowlands of the Adige River and northern Po delta (Northern Italy). Quat. Int. 2020, 538, 80–93, doi:10.1016/j.quaint.2018.10.024.
56. Teatini, P.; Tosi, L.; Strozzi, T.; Carbognin, L.; Wegmüller, U.; Rizzetto, F. Mapping regional land displacement in the Venice coastland by an integrated monitoring system. Remote Sens. Environ. 2005, 98, 403–413, doi:10.1016/j.rse.2005.08.002.
57. Carminati, E.; Martinelli, G.; Severi, P. Influence of glacial cycles and tectonics on natural subsidence in the Po Plain (Northern Italy): Insights from 14C ages. Geochemistry, Geophys. Geosystems 2003, 4, doi:10.1029/2002GC000481.
58. Teatini, P.; Tosi, L.; Strozzi, T. Quantitative evidence that compaction of Holocene sediments drives the present land subsidence of the Po Delta, Italy. J. Geophys. Res. Earth Surf. 2011, 116, 1–10, doi:10.1029/2010JB008122.
59. ArcGIS Available online: https://www.esri.com/en-us/arcgis/about-arcgis/overview (accessed on Mar 20, 2020).
60. QGIS Available online: https://www.qgis.org/it/site/ (accessed on Mar 25, 2020).
61. Il Geoportale della Regione del Veneto Available online: https://idt2.regione.veneto.it/ (accessed on Apr 3, 2020).
62. Recanatesi, F.; Giuliani, C.; Ripa, M.N. Monitoring mediterranean oak decline in a peri-urban protected area using the NDVI and sentinel-2 images: The Case Study of Castelporziano state natural reserve. Sustainability 2018, 10, doi:10.3390/su10093308.

63. Bannari, A.; Morin, D.; Bonn, F.; Huete, A.R. A review of vegetation indices. Remote Sens. Rev. 1995, 13, 95–120, doi:10.1080/02757259509532298.
64. Piedelobo, L.; Taramelli, A.; Schiavon, E.; Valentini, E.; Molina, J.L.; Xuan, A.N.; González-Aguilera, D. Assessment of green infrastructure in Riparian zones using copernicus programme. Remote Sens. 2019, 11, doi:10.3390/rs11242967.
65. Goodwin, N.R.; Coops, N.C.; Wulder, M.A.; Gillanders, S.; Schroeder, T.A.; Nelson, T. Estimation of insect infestation dynamics using a temporal sequence of Landsat data. Remote Sens. Environ. 2008, 112, 3680–3689, doi:10.1016/j.rse.2008.05.005.
66. Mather, P.M.; Koch, M. Computer Processing of Remotely-Sensed Images: An Introduction; Fourth edi.; John Wiley & Sons: Chichester, UK, 2011; ISBN 9780470742396.
67. Congedo, L. Semi-Automatic Classification Plugin Documentation. 2016, doi:10.13140/RG.2.2.29474.02242/1.
68. MOVE Suite - Petroleum Experts Available online: https://www.petex.com/products/move-suite/ (accessed on May 11, 2020).
69. GF Instruments s.r.o. Available online: www.gfinstruments.cz (accessed on Feb 10, 2020).
70. Um, E.S.; Alumbaugh, D.L. On the physics of the marine controlled-source electromagnetic method. Geophysics 2007, 72, WA13–WA26, doi:10.1190/1.2432482.
71. Trimble - Transforming the Way the World Works Available online: www.trimble.com (accessed on Feb 10, 2020).
72. Allred, B.; Daniels, J.J.; Reza Ehsani, M. Handbook of Agricultural Geophysics; CRC Press: USA, 2008; ISBN 9780849337284.
73. Delefortrie, S.; De Smedt, P.; Saey, T.; Van De Vijver, E.; Van Meirvenne, M. An efficient calibration procedure for correction of drift in EMI survey data. J. Appl. Geophys. 2014, 110, 115–125, doi:10.1016/j.jappgeo.2014.09.004.
74. Interpex Limited - Specialists in PC Based Geophysical Software Available online: www.interpex.com (accessed on Feb 3, 2020).
75. Constable, S.C.; Parker, R.L.; Constable, C.G. Occam's inversion: A practical algorithm for generating smooth models from electromagnetic sounding data. Geophysics 1987, 52, 289–300, doi:10.1190/1.1442303.
76. Ghinassi, M.; Ielpi, A.; Aldinucci, M.; Fustic, M. Downstream-migrating fluvial point bars in the rock record. Sediment. Geol. 2016, 334, 66–96, doi:10.1016/j.sedgeo.2016.01.005.
77. Ghinassi, M. Chute channels in the Holocene high-sinuosity river deposits of the Firenze plain, Tuscany, Italy. Sedimentology 2011, 58, 618–642, doi:10.1111/j.1365-3091.2010.01176.x.

78. Ninfo, A.; Fontana, A.; Mozzi, P.; Ferrarese, F. The Map of Altinum, Ancestor of Venice. Science (80-.). 2009, 325, 577, doi:10.1126/science.1174206.
79. Bhattacharyya, P.; Bhattacharya, J.P.; Khan, S.D. Paleo-channel reconstruction and grain size variability in fluvial deposits, Ferron Sandstone, Notom Delta, Hanksville, Utah. Sediment. Geol. 2015, 325, 17–25, doi:10.1016/j.sedgeo.2015.05.001.
80. Ghinassi, M.; Nemec, W.; Aldinucci, M.; Nehyba, S.; Özaksoy, V.; Fidolini, F. Plan-form evolution of ancient meandering rivers reconstructed from longitudinal outcrop sections. Sedimentology 2014, 61, 952–977, doi:10.1111/sed.12081.
81. Durkin, P.R.; Hubbard, S.M.; Smith, D.G.; Leckie, D.A. Predicting heterogeneity in meandering fluvial and tidal-fluvial deposits: The point bar to counter point bar transition. In Fluvial Meanders and Their Sedimentary Products in the Rock Record. Int. Assoc. Sedimentol. Spec. Publ.; Ghinassi, M., Colombera, L., Mountney, N.P., Reesink, J.H., Eds.; John Wiley & Sons, 2018; Vol. 48, pp. 231–250.
82. Brice, J.C. Evolution of meander loops. Geol. Soc. Am. Bull. 1974, 85, 581–586, doi:10.1130/0016-7606(1974)85<581:EOML>2.0.CO;2.
83. Lewin, J. Initiation of bed forms and meanders in coarse-grained sediment. Bull. Geol. Soc. Am. 1976, 87, 281–285, doi:10.1130/0016-7606(1976)87<281:IOBFAM>2.0.CO;2.
84. Nanson, G.C.; Page, K. Lateral accretion of fine-grained concave benches on meandering rivers. In Modern and ancient fluvial systems. Int. Assoc. Sedimentol. Spec. Publ.; Collinson, J.D., Lewin, J., Eds.; Wiley-Blackwell, 1983; Vol. 6, pp. 133–143 ISBN 0632009977.
85. Wu, C.; Bhattacharya, J.P.; Ullah, M.S. Paleohydrology and 3D facies architecture of ancient point bars, Ferron Sandstone, Notom Delta, south-central Utah, USA. J. Sediment. Res. 2015, 85, 399–418, doi:10.2110/jsr.2015.29.
86. Jones, H.L.; Hajek, E.A. Characterizing avulsion stratigraphy in ancient alluvial deposits. Sediment. Geol. 2007, 202, 124–137, doi:10.1016/j.sedgeo.2007.02.003.
87. Taylor, C.F.H. The role of overbank flow in governing the form of an anabranching river: the Fitzroy River, northwestern Australia. In Fluvial Sedimentology VI. Special Publication of the International Association of Sedimentologists; Smith, N.D., Rogers, J., Eds.; Wiley Online Library, 1999; Vol. 28, pp. 77–91.
88. Motta, D.; Abad, J.D.; Langendoen, E.J.; García, M.H. The effects of floodplain soil heterogeneity on meander planform shape. Water Resour. Res. 2012, 48, 1–17, doi:10.1029/2011WR011601.
89. Bogoni, M.; Putti, M.; Lanzoni, S. Modeling meander morphodynamics over self-formed heterogeneous floodplains. Water Resour. Res. 2017, 53, 5137–5157, doi:10.1002/2017WR020726.

90. Fidolini, F.; Ghinassi, M.; Aldinucci, M.; Billi, P.; Boaga, J.; Deiana, R.; Brivio, L. Fault-sourced alluvial fans and their interaction with axial fluvial drainage: An example from the Plio-Pleistocene Upper Valdarno Basin (Tuscany, Italy). Sediment. Geol. 2013, 289, 19–39, doi:10.1016/j.sedgeo.2013.02.004.
91. Nanson, G.C. Point bar and floodplain formation of the meandering Beatton River, northeastern British Columbia, Canada. Sedimentology 1980, 27, 3–29, doi:10.1111/j.1365-3091.1980.tb01155.x.
92. Ielpi, A.; Ghinassi, M. Planform architecture, stratigraphic signature and morphodynamics of an exhumed Jurassic meander plain (Scalby Formation, Yorkshire, UK). Sedimentology 2014, 61, 1923–1960, doi:10.1111/sed.12122.
93. Swan, A.; Hartley, A.J.; Owen, A.; Howell, J. Reconstruction of a sandy point-bar deposit: implications for fluvial facies analysis. In Fluvial Meanders and Their Sedimentary Products in the Rock Record. Int. Assoc. Sedimentol. Spec. Publ. 48; Ghinassi, M., Colombera, L., Mountney, N.P., Reesink, A.J., Betaman, M., Eds.; John Wiley & Sons: Ltd, 2018; Vol. 48, pp. 445–474.
94. Frothingham, K.M.; Rhoads, B.L. Three-dimensional flow structure and channel change in an asymmetrical compound meander loop, Embarras River, Illinois. Earth Surf. Process. Landforms J. Br. Geomorphol. Res. Gr. 2003, 28, 625–644, doi:10.1002/esp.471.
95. Kasvi, E.; Vaaja, M.; Alho, P.; Hyyppä, H.; Hyyppä, J.; Kaartinen, H.; Kukko, A. Morphological changes on meander point bars associated with flow structure at different discharges. Earth Surf. Process. Landforms 2013, 38, 577–590, doi:10.1002/esp.3303.
96. Finotello, A.; D'Alpaos, A.; Bogoni, M.; Ghinassi, M.; Lanzoni, S. Remotely-sensed planform morphologies reveal fluvial and tidal nature of meandering channels. Sci. Rep. 2020, 10, 1–13, doi:10.1038/s41598-019-56992-w.
97. Ferguson, R.I.; Parsons, D.R.; Lane, S.N.; Hardy, R.J. Flow in meander bends with recirculation at the inner bank. Water Resour. Res. 2003, 39, 1322, doi:10.1029/2003WR001965.

Appendix B

This chapter is a manuscript under review in *Environmental Modelling and Software*, which is titled "Two-dimensional model of flow and transport in porous media: linking heterogeneous anisotropy with stratal patterns in meandering tidal channel deposits of the Venice Lagoon (Italy)".

E.Ba., E.Be. M.P. and M.G. designed the study. M.P., A.D. and M.G. developed the methodology. E.Be. and M.G. collected the data. E.Be. and E.Ba. annotated and maintained the research data. E.Be. and E.Ba. were responsible for data creation and presentation. M.P. and M.G. were the project administrator. E.Ba. and M.P. developed and applied computational techniques to analyse study data. M.P. and M.G. provided the instrumentation and analysis tools. A.D. verified the reproducibility of the results. All the authors discussed the data and agreed on their interpretation. E.Ba. and E.Be. wrote the original draft. A.D., M.P. and M.G. provided comments and suggestions to improve the original draft. All the co-authors contributed to the final polishing of the manuscript.

Two-dimensional model of flow and transport in porous media: linking heterogeneous anisotropy with stratal patterns in meandering tidal channel deposits of the Venice Lagoon (Italy)

Elena Bachini[1], Elena Bellizia[2], Mario Putti [3], Andrea D'Alpaos[2], Massimiliano Ghinassi[2]

[1]Institute of Scientific Computing, TU Dresden, Germany
[2]Department of Geosciences, University of Padua, Italy
[3]Department of Mathematics "Tullio Levi-Civita", University of Padua, Italy

ABSTRACT

Understanding the internal structure of permeable and impermeable sediments (e.g., point-bars and tidal-flat deposits) generated by the evolution of meandering tidal channels is essential for accurate modelling of groundwater flow and contaminant transport in coastal areas. The detailed reconstruction of stratal geometry and hydraulic properties from measurements must be accompanied by depositional history information. In this work, we use high-resolution reconstructions of ancient tidal channels of the Venice Lagoon (Italy) to drive 2D simulations of groundwater flow and transport, showing the importance of incorporating information on the sediment accumulation processes into the hydraulic characteristics and how horizontal anisotropy emerging from these processes significantly influences transport. Effective hydraulic conductivity is modelled with a heterogeneous 2D anisotropic tensor with principal directions aligned with observed sedimentation sequences. Comparison of flow and solute dynamics simulated using reconstructed and theoretical hydraulic properties show drastically different pathways of solute propagation.

Keywords: Meandering tidal channel deposits; Heterogeneous anisotropic conductivity; Groundwater flow and transport.

1. Introduction

Coastal plains are delicate environments where continental and marine processes have intertwined during the past millennia. Holocene fluvial and tidal channels mainly contributed to shaping actual landscapes through the accumulation of complex sedimentary sand bodies (Allen 1965; Bridge 2003;

Khan et al., 1997). The overall flat topography and the availability of freshwater from surficial aquifers make coastal areas suitable for urbanization, agricultural and industrial activities (Amorosi et al., 2013; Boyer et al., 2006; Delagnes et al., 2012). On the other hand, agriculture has to interface with saltwater intrusion, which endangers soil productivity (Da Lio et al., 2015; Nofal et al., 2015), and industrial activities are often responsible for pollutant dispersion in the groundwater (Carraro et al., 2015; Desbarats et al., 2014). Pollutant propagation (e.g., fuel dispersion, herbicides, chemical contamination) is a crucial environmental problem that has been investigated under multidisciplinary approaches (Benner et al., 2008; Carraro et al., 2015, 2013; Christensen and Hatfield, 1994; Desbarats et al., 2014; Harvey et al., 2006; Hatfield and Christensen, 1994; Şimşek et al., 2008; Yang et al., 2001). In coastal areas, the groundwater flow is driven by preferential pathways within permeable deposits accumulated by ancient fluvial and tidal channels. For these reasons, understanding the internal structure of these deposits (i.e., porous media) and flow motion within them is essential to manage unwanted and threatening phenomena such as saltwater intrusion and pollutant propagation. In lagoonal environments, the sedimentary elements associated with the evolution of meandering tidal channels include in-channel and overbank deposits. In-channel elements are sand-prone bars (i.e., point bars) and mud-rich channel fills, which are accumulated during channel migration and deactivation, respectively. Overbank deposits (e.g., tidal flats) are mainly muddy, and along with channel fill units, are the less permeable elements forming coastal sedimentary successions (Cosma et al., 2020a).

Flow and transport processes in porous media can be quantitatively estimated by means of numerical models approximating the solution of the relevant partial differential equations. Solute transport is driven by the fluid velocity as calculated from the solution of the flow equation. A three-step procedure is used: i) solve the flow equation and determine the distribution of the hydraulic head; ii) calculate the discrete velocity vector field from the gradient of the hydraulic potential; and, iii) solve the solute transport equation. The velocity field, which is governed by Darcy law, depends crucially on the hydraulic conductivity coefficient, the mathematical object encoding the internal structure of the geologic formation. This coefficient is typically defined at a spatial scale that is sufficiently large for proper homogenization but small enough to distinguish different geologic formations. The hydraulic conductivity, a property of the porous medium, becomes a tensor when the flow is neither

parallel nor orthogonal to the small-scale heterogeneities. In theory, the arithmetic and harmonic averages should be used as scalar conductivity values along the parallel and orthogonal directions, thus leading to anisotropy (Renard and de Marsily, 1997). The nature of groundwater flow and transport is such that the structure and spatial variability of the conductivity tensor affect the hydraulic head and its gradient at different scales. Indeed, while the hydraulic head is characterized by a global scale of variability (geometric dimension of the geologic formation), its gradient varies at a scale of the order of the scale at which the hydraulic conductivity has been characterized. Solute transport is determined by the flow velocity and direction, and thus acts at the latter scale. The accuracy with which solute fate is predicted is intrinsically determined by the accuracy of Darcy velocity **q**. The detailed reconstruction of both the order of magnitude of the elements of the hydraulic conductivity tensor and the principal directions of anisotropy is crucial for precise quantitative estimates of solute transport (Pauloo et al., 2021). It is well known that, in complex and vertically expanded sedimentary successions (e.g., Ghinassi et al., 2013), anisotropy originates from the averaging of mostly vertical heterogeneities (Renard and de Marsily, 1997) caused by the prevalently one-dimensional sedimentation process. On the other hand, horizontal anisotropy is negligible in groundwater simulations, and it is embodied by the structural heterogeneity attributed to hydraulic conductivity (Fogg, et al., 1998; Fogg, et al., 2000; Weissmann et al., 2004). However, there are many instances when horizontal anisotropy can play a role, but these are only seldom investigated and mostly in non-sedimentary formations (Purkis and Vlaswinkel, 2012). One of the contributions of this paper is to show how an accurate characterization of horizontal anisotropy based on interpretation of the depositional processes can lead to drastically different effects with respect to the case where simplistic depositional models are considered. The presence of strong anisotropies in the horizontal plane add to the difficulties arising from the classical vertical anisotropy and require accurate and anisotropy-robust numerical solvers. In summary, a reliable geologic model should consider detailed reconstructions of stratal geometries and sediment properties. The former can be obtained by coupling geophysical techniques with local drilling. Information from samples obtained from drilling can be used to estimate the order of magnitude of the conductivity coefficients. However, this information does not provide clues on the direction of anisotropy, which must be determined by studying the depositional history of the sediments.

The present work investigates modes of 2D flow within deposits of an ancient tidal channel of the Venice Lagoon (Italy) using numerical models of flow and transport accompanied by a high-resolution characterization of stratal geometries (Bellizia et al., 2022), the spatial distribution of sediment properties, and reconstruction of anisotropy directions. A detailed geological description is less important in areas filled with fine sediments where no flow of practical interest occurs, and so our focus is mainly concentrated on the tidal channel. The objective of this study is to show via numerical experiments the importance of the characterization described above and of the robustness of the numerical discretization used to resolve the inherent spatial variability of the coefficients. To this aim, we use the linear finite element method for spatial discretization because of its robustness against mesh locking when strong anisotropy ratios are present (Manzini and Putti, 2007; Mazzia et al., 2011) together with an efficient conjugate gradient method with ad-hoc preconditioning. We recall here that mesh locking is a numerical phenomenon by which the numerical solver becomes inaccurate if the mesh is not fine enough (Manzini and Putti, 2007). The aim is to highlight a prototypical test case that can be used as a starting point for larger-scale studies, addressing for example management of aquifers in coastal areas in terms of propagation of pollutants or saltwater intrusion.

Results from this work can be applied to worldwide studies of flow motion within surficial permeable bodies originated by the evolution of tidal meandering channels, especially for those developed in coastal areas affected by a microtidal regime.

2. The prototype case: buried meandering tidal channel deposits of the Venice Lagoon

The prototype case deposits are placed in the northern sector of the Venice Lagoon (NE Italy) (Fig. B.1A), which is the largest brackish water body of the Mediterranean basin, developed over the last 6000 years during Holocene transgression, and currently covers an area of about 550 km^2 (Zecchin et al., 2009, 2008). The Venice Lagoon is affected by a semi-diurnal micro-tidal regime, with an average tidal range of ca. 1 m (D'Alpaos et al., 2013) and is dissected by a dense network of tidal channels, which cut through both tidal flats and salt marshes (Finotello et al., 2019, 2020; Ghinassi, et al. 2018a, b).

The prototype case deposits are buried below 1 m of tidal-flat deposits located close to the S. Francesco del Deserto Island, where water depth is ca. 1 m. These deposits were formed in the late Holocene by a 35 m-wide paleochannel (Madricardo et al., 2007) and consist of three adjacent point-bar bodies, named PB1, PB2 and PB3 which are on average 2.5 m thick (Bellizia et al., 2022). The channel belt axis of the paleo-channel system is WNW-ESE oriented (Fig. B.1B). A minor channel, ca. 20 m wide and trending WNW-ESE, crossed bar PB2 developing two bank-attached bars, named B1 and B2. Sedimentary cores show that bar deposits mainly consist of laminated silt and very fine sand with 0.5 - 1 mm-thick muddy laminae. Channel fill and over-bank deposits are made of homogeneous mud (Madricardo et al., 2007; Bellizia et al., 2022). A detailed 3D model based on seismic data (Bellizia et al., 2022) allowed us to depict the effective geometry of bar bodies and identify four major evolutive stages of the study channel. The reconstructed geometry of bars shows that they started to accrete from a sinuous channel, as clearly shown by the arcuate shape of bar PB1, which encloses homogeneous over-bank mud (Fig. B.1C). During the major evolutive stages, bars PB1-3 grew in different directions accumulating silty layers on their slope. These layers strike and dip in different directions, creating anisotropies within the bar sedimentary bodies (Fig. B.1E).

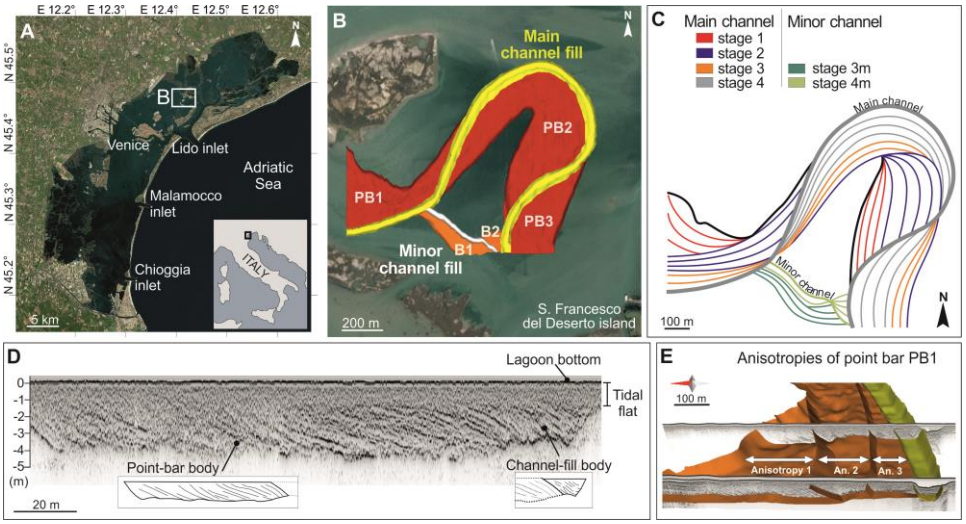

Fig. B.1. The prototype case. (A) The geographic position of the study area in the Venice Lagoon. (B) Position of the buried meandering channel in the study area: the main channel fill (in yellow) with associated point bars (in red), and the minor channel fill (in white) with the bank-attached bars (in orange). (C) The four morphodynamic stages of the study channel. (D) Example of a seismic section of the area, showing morphologies of the lagoon bottom, tidal flat and paleo-channel bodies. (E) Partial 3D view of point bar PB1 with accretionary boundaries defining the internal anisotropies.

3. Methods

The main aim of this work is to show that anisotropy in the hydraulic conductivity tensor plays a major role in the movement of contaminants, such as nutrients and other substances infiltrated from the surface and saltwater intruding from the sea. To drive our experiments, we use a detailed reconstruction of the complex formation described above together with an in-depth understanding of the sedimentary processes that formed it. Another objective is to highlight the challenging issues emerging from the numerical simulations under strong anisotropic flows. To this aim, we design different boundary conditions that trigger numerical ill-conditioning while maintaining the realistic behavior of the test case. The design of our numerical experiments is geared towards these objectives.

3.1. From geological reconstruction to model input data

Typical models of groundwater flow and transport at the regional scale consider a two-dimensional vertically averaged framework (de Ghislain, 1986). This assumption is grounded on the consideration that the vertical flux is small with respect to its horizontal component. The 2D approach is warranted when infiltration from the surface can be neglected. Within this framework, paleo-river beds act as preferential pathways for the movement of contaminants, since they tend to form permeable, elongated sedimentary bodies which are laterally and vertically confined (Gibling, 2006). In Holocene sedimentary bodies, which are not deformed and show a spatial distribution that reflects the present-day orographic configuration, the morphology, and hydraulic characteristics of these formations as well as the regional gradient forcing the flow are the main drivers that need to be taken into account in the design of our test cases. The 2D model for the proposed simulation has been obtained from a detailed 3D reconstruction arising from the integration of seismic data and sedimentary core data. This process allows one to define the boundaries between different types of deposits (e.g., bar, channel fill and overbank deposits). Laminated silt and very fine sand forming bar deposits show a different spatial orientation, which arises from the lateral shifting of the study channel during the four main stages of bar evolution (Fig. B.1C). Silty levels represent the major permeability barriers within bar deposits, and their orientation is consistent with that of the layers generated during the four growth stages.

A total of 201 high resolution (decimeter-scale) seismic sections were used to correlate surfaces bounding the major depositional units in a 3D space. Sedimentary cores were used to integrate such a reconstruction and to define the spatial distribution of different types of deposits. Starting from this three-dimensional reconstruction, we define the average planar position of the morphological features forming our tidal deposits, namely the channels (i.e., main channel and minor channel), the bars (i.e., PB1, PB2, PB3 of the main channel, and B1, B2 of the minor one), and the surrounding subtidal platform. This is obtained by intersecting the mesh surfaces forming the 3D model with a horizontal plane that cuts the reconstructed bar at half of the thickness (Fig. B.2A). The resulting intersection lines are used to define polygons, which define the boundaries of different types of deposits (i.e., overbank, bar and channel fill) in a 2D horizontal domain (Fig. B.2B).

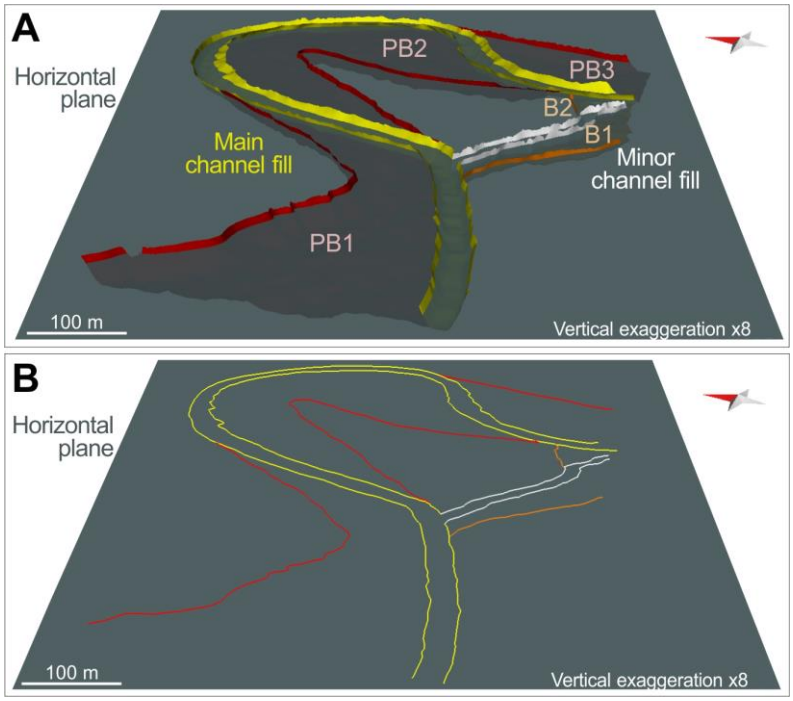

Fig. B.2. 3D basal surfaces of the studied depositional elements (i.e., channel fills and channel bars) intersected with a horizontal plane (A), to obtain the 2D intersection lines (B) that have been used to define the 2D polygons for flow and transport simulations.

Within bar deposits, the same approach has been used to detect boundaries between deposits accreted during the four depositional phases (Fig. B.1C). Additionally, seismic data indicate the orientation of layers within these deposits, pointing out also the alignment of the major permeability barriers.

Specifically, in the obtained 2D model, conductivity is considered to reach its maximum and minimum in directions parallel and orthogonal to the muddy laminae, respectively. The muddy nature of overbank and channel-fill deposits allows one to ascribe them an isotropic conductivity of 10^{-8} m/s. In bar deposits, a conductivity of 10^{-6} m/s and 10^{-8} m/s is assigned in the directions parallel and orthogonal to muddy laminae, respectively.

3.2. Mathematical models of flow and transport

The mathematical model considers a flow equation, to determine the flux vectors of the flow in the porous media, and successively a transport equation to simulate the transport of contaminants due to the computed fluxes. The flow equation is characterized by the presence of spatially varying anisotropy. The idea is to relate the spatial distributions of the anisotropy to the sediment forming depositional environment and test the possible influence of heterogeneous anisotropy on the groundwater flow and transport.

Flow equation. The flow equation in a confined aquifer in R^3 reads:

$$S_s \frac{\partial h}{\partial t} - \nabla \cdot \left(\mathbb{K}_s \nabla h \right) = f \,, \qquad (1)$$

where S_s [1/L] is the elastic storage coefficient, K_s [L/T] is the hydraulic conductivity tensor, and f [1/T] is the (external) source term. The scalar function h [L] is the unknown variable and represents the hydraulic head. We couple this equation with Dirichlet boundary conditions. Darcy flux is then computed by $\mathbf{q}$=-$K_s \nabla h$ [L/T]. We will use equivalently the words Darcy flux or Darcy velocity or simply velocity to mean specific discharge (see (Haitjema and Anderson, 2016) for a discussion on the difference between Darcy velocity and pore velocity). In our simplified two-dimensional framework, we assume that the confined aquifer has a unitary thickness b [L]. Thus, the above equation can be written in a two-dimensional domain Ω, coinciding with a planar shape of the geologic formation, with the hydraulic conductivity replaced by the hydraulic transmissivity $\mathbf{T}$= K_s b [L^2/T] and the elastic storage coefficient replaced by the storativity coefficient S=S_s b [-]. These simplistic assumptions are dictated by the lack of data in the fully three-dimensional distribution of hydraulic properties. We realize that a fully 3D framework would be much more appropriate, and it will be tackled as soon as enough data are collected. However, a 3D approach would need to solve first the formidable task of assessing permeability anisotropy as it relates to the complex sedimentary process in a meandering morphometry.

Since we are interested in a steady-state flow (δh/δt = 0) with f = 0 in the presence of anisotropy, the equation simplifies to:

$$\nabla \cdot (-\mathbf{T} \nabla h) = 0 \qquad \text{in } \Omega \tag{2}$$

$$h = h_D \qquad \text{on } \partial\Omega \tag{3}$$

where K_s is the 2×2 symmetric tensor varying in space that embodies the anisotropic behavior, and h_D is a prescribed value of the solution at the boundary. If the diffusion process is isotropic the conductivity tensor is defined by $K_s = {}_K\mathrm{I}$, where ${}_K$ is a scalar value and I the identity matrix. In the anisotropic case, the tensor is no longer diagonal. We have to define the two vectors **v**, **w** that provide the principal directions of anisotropy (i.e., the eigenvectors of K_s), together with two compatible conductivity values (i.e., the corresponding eigenvalues). Then, the final anisotropic tensor is defined by:

$$\mathbb{K}_s = U \Lambda U^T = \begin{bmatrix} v_1 & w_1 \\ v_2 & w_2 \end{bmatrix} \begin{bmatrix} \kappa_1 & 0 \\ 0 & \kappa_2 \end{bmatrix} \begin{bmatrix} v_1 & v_2 \\ w_1 & w_2 \end{bmatrix}$$

In practice, we set the first eigenvalue ${}_{K1}$ as the coefficient ${}_K$ given by the material with the corresponding eigenvector **v**, the preferential direction of the process. Then, the vector **w** is defined to be orthogonal to **v** and the second eigenvalue ${}_{K2}$ is set to be ${}_{K2} = {}_{K1} * r_a$, where r_a is the chosen anisotropy ratio.

Transport equation. The transport of contaminants in a certain domain Ω is governed by the following equation:

$$n\frac{\partial c}{\partial t} = \nabla \cdot (\mathbb{D} \nabla c) - \nabla \cdot (\mathbf{q}\, c)\,, \tag{4}$$

where n [-] is the porosity and we consider in the first order term the velocity field given by Darcy flux **q** [L/T] as computed by the flow equation. In this case c [-] is the normalized (mass/mass) concentration of the contaminant, and $\mathbb{D}$ [L^2/T] is the dispersion tensor (Bear 1979), defined as:

$$\mathbb{D} = \alpha_L |\mathbf{q}| \mathbb{I} + |\alpha_L - \alpha_T| \frac{\mathbf{q}\mathbf{q}^{\mathrm{T}}}{|\mathbf{q}|} + n D_m \mathbb{I}\,, \tag{5}$$

where α_L [L] is the longitudinal dispersivity, α_T [L] is the transversal dispersivity and D_m [L^2/T] is the molecular diffusion. The equation can be formed by multiple components if multiple contaminants need to be studied. The mathematical model is completed by Dirichlet/Neumann/Cauchy boundary conditions and by initial conditions.

Numerical solution. The above equations are solved using the CATHY solver (Camporese et al., 2010; Weill et al., 2011), a hydrological model based on linear finite elements with stabilization and preconditioned conjugate gradient (PCG) linear solver. This code has been extensively used in several projects (see for example (Passadore et al., 2012; Scudeler et al., 2016)) and has been benchmarked against other similar solvers in (Maxwell et al., 2014; Kollet

et al., 2017). The presence of strong anisotropic diffusion may cause numerical difficulties depending on the method used in the discretization (Manzini and Putti, 2007). The CATHY solver is capable of tackling demanding applications and also the most extreme anisotropic behavior (Mazzia et al., 2011). The PCG scheme of CATHY has been complemented with ad-hoc preconditioners to handle the severe ill-conditioning arising from the anisotropy ratios.

4. Numerical simulations

We consider a square domain given by Ω= [-15,900] × [-205,550] m×m, which contains the specific site of our experimental studies. Different simulations are run considering the variability of three main drivers: i) the regional piezometric gradient; ii) the conductivity tensor; iii) the geometry and anisotropies of the bar bodies. The main terminology related to sedimentary bodies is shown in Fig. B.3C and follows sedimentological studies carried out on tidal meanders and related deposits (Cosma et al., 2019; 2020b).

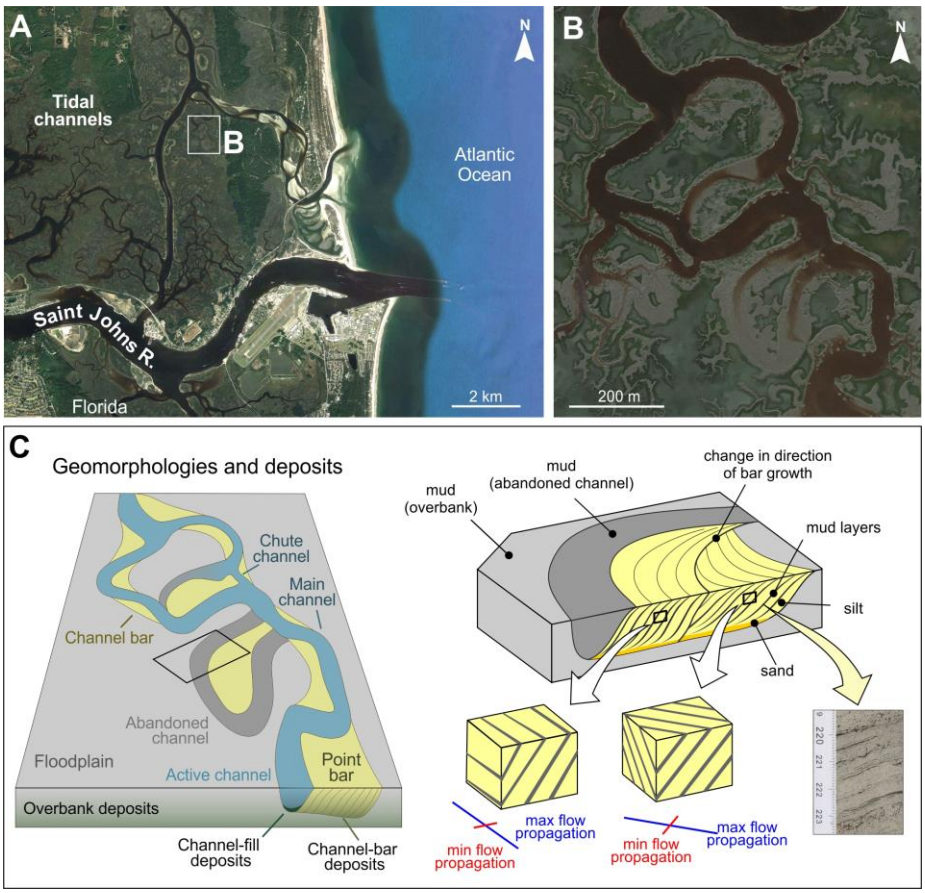

Fig. B.3. (A) Examples from the Florida coast of tidal and fluvial channels flowing orthogonally into the Sea. (B) Zoom in into the tidal network, (C) to recognize the main tidal elements. The abandoned channel cuts through the muddy overbank and is commonly composed of a muddy channel fill and a silty point bar. The channel can experience different transformation styles while accreting the point bar, which can be recognized in bar deposits thanks to changes in the dip direction of strata. Each package of the same inclined strata shows precise 3D orientations of maximum and minimum flow, which are parallel and orthogonal to strata orientation, respectively.

The direction of the regional piezometric gradient is assumed to be parallel to the mean channel belt axis, with an average magnitude of 8×10^{-4}. This assumption aims at simulating a groundwater flow occurring in coastal plains where late Holocene buried channel belts are commonly transverse to the actual coastline. These buried formations have been generated in a paleo-landscape configuration that is fully comparable to the present-day one and can be the main pathways for pollutant propagation to the sea, as well as suffer saltwater intrusion from the sea (Fig. B.3A, B). Accordingly, landward (i.e., south-east towards north-west) and seaward (i.e., north-west towards south-east) regional piezometric gradients are simulated to account for meanders migrating in different directions. In practice, linearly varying Dirichlet boundary conditions are set to simulate the two different scenarios.

Different hydraulic conductivity values are attributed to different deposits. Being uniformly made of clay-rich mud, overbank deposits show a small conductivity, estimated at $K = 10^{-9}$ m/s. The actual value is not important since essentially no flow occurs in these formations. Observed channel-fill mud is assumed to have a conductivity of $K = 10^{-8}$ m/s. Some simulations are also carried out with a conductivity of $K = 10^{-7}$ m/s in order to model cases where a progressive channel abandonment has caused infill of the channel with coarser deposits (Allen, 1965; Fisk, 1947; Toonen et al., 2012). Bar deposits are more permeable, being made of silt and very fine sand. Since bar deposits are considered homogeneous bodies, we associate the same conductivity values for all the bar bodies, estimated at $K = 10^{-6}$ m/s. The presence of muddy laminae affects the flow mobility within the bar deposits, with maximum and minimum values occurring along the strike and dip directions, respectively. We simulate this behavior by assuming a spatially varying effective conductivity tensor K_s with principal directions of anisotropy that follow the strike and dip directions. We consider a constant anisotropy ratio equal to $r_a = 10^{-2}$ in the bars, while an isotropic behavior (i.e., $r_a = 1$) is imposed in the channels and external fills. Sensitivity to this ratio has been verified by using $r_a = 10^{-3}$ with negligible differences in the relative simulations.

Contrasting bar geometries are also considered. In one set of simulations, we reconstruct the bar bodies by dividing the formations into different subregions that take into consideration the bar evolution from a sinuous channel as revealed by seismic data. The resulting subdivision is shown in Fig. B.4A, C. Correspondingly, principal directions of anisotropy follow in each subregion the reconstructed strike and dip orientations (red lines in Fig. B.4). The laminae-following distribution has been implemented in the simulation model by a subdivision of the bar deposits into further subzones where constant anisotropy directions are specified.

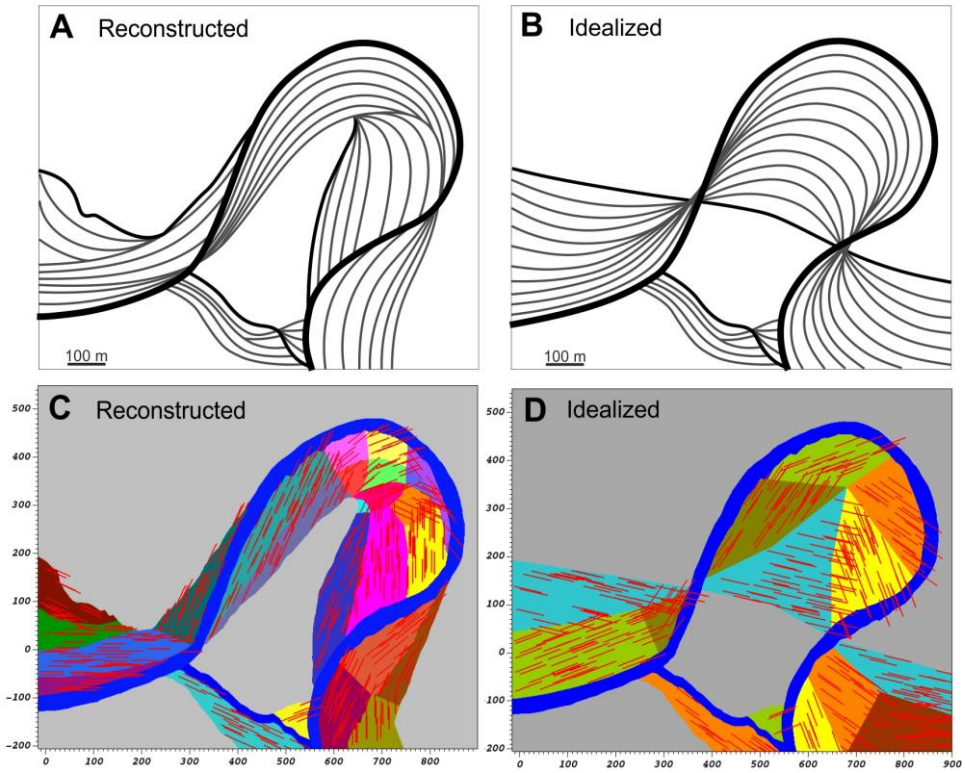

Fig. B.4. Model domain with reconstructed bar bodies (A, C) and idealized geometry (B, D). The corresponding preferential direction of the flow is shown by the red segments. Areas, where no segments are displayed, are assumed to be isotropic.

In the second set of simulations, fluid flow is modelled using an idealized bar geometry (shown in Fig. B.4B, D), established considering a uniform bar accretion from a straight channel, as commonly suggested by classical facies models (Brice, 1974; Finotello et al., 2018; Nanson and Page, 1983). Within the channel-bar bodies, both in the reconstructed and in the idealized case, anisotropies represent areas characterized by almost the same depositional

orientation of the strata composing the porous media, so they are architectural. In the case of the prototype area, anisotropies are related to the different accretion packages that the channel originated during its morphodynamic evolution. Anisotropies strongly define the preferential direction of groundwater flows (Fig. B.4). For the accompanying transport simulations, we have a field estimate of n=0.2 [-], and we have chosen typical values for dispersion coefficients found in the literature by setting α_L=1 [m], α_T=0.1 [m] and a molecular diffusion equal to D_m=10^{-10} [m^2/s] (LaBolle and Fogg, 2001). These values yield a mesh Peclet number slightly larger than two, thus requiring stabilization. We use SUPG with optimal parameters (Bachini et al., 2021). The boundary conditions impose unit normalized concentration in the West and South portions of the boundary where the bars and the channels intersect, and zero concentration in the remaining portions, independently of the direction of the regional gradient. Note that, for an NW to SE regional gradient inflow and outflow occur at the west and south boundaries, respectively, while in the other case they occur in the south and west boundaries. No inflow would ever occur at the north and east boundaries because of extremely low conductivity values. We recall that the transport simulations are intended to highlight the effects of the different distributions of conductivity tensors within the reconstructed bars. The employed boundary conditions force the entrance of contaminants from the principal bar deposits. Different boundary conditions could have been employed depending on the geological reconstruction, but sensitivity to these effects is not of interest to this study.

4.1. Results

Figures B.5 to B.9 show the results of our simulations and are organized as follows. The top panels report the steady-state piezometric head distribution and the velocity vectors as calculated from the flow model. In these figures, the scale of the piezometric head measured in meters is the same for all figures. On the other hand, the scale for Darcy flux changes for each test case to ease the visualization of the vectors. The remaining four panels show the normalized concentration distributions at four different times as driven by the velocity field, using a color scale from red (c=1) to blue (c=0). We would like to note that the times at which we show the results are unrealistically long, but the local effects due to the anisotropy that we want to show depend on the distance of the contaminant source. In our tests, the location of the contaminant source is arbitrarily chosen to highlight the importance of horizontal anisotropy. Hence,

we regard our time as arbitrary. Along the same line, the use of a pure advection equation is mainly dictated by our goal of showing the importance of horizontal anisotropy in general, even though neglection of diffusion may not be warranted in this specific case of very low conductivity.

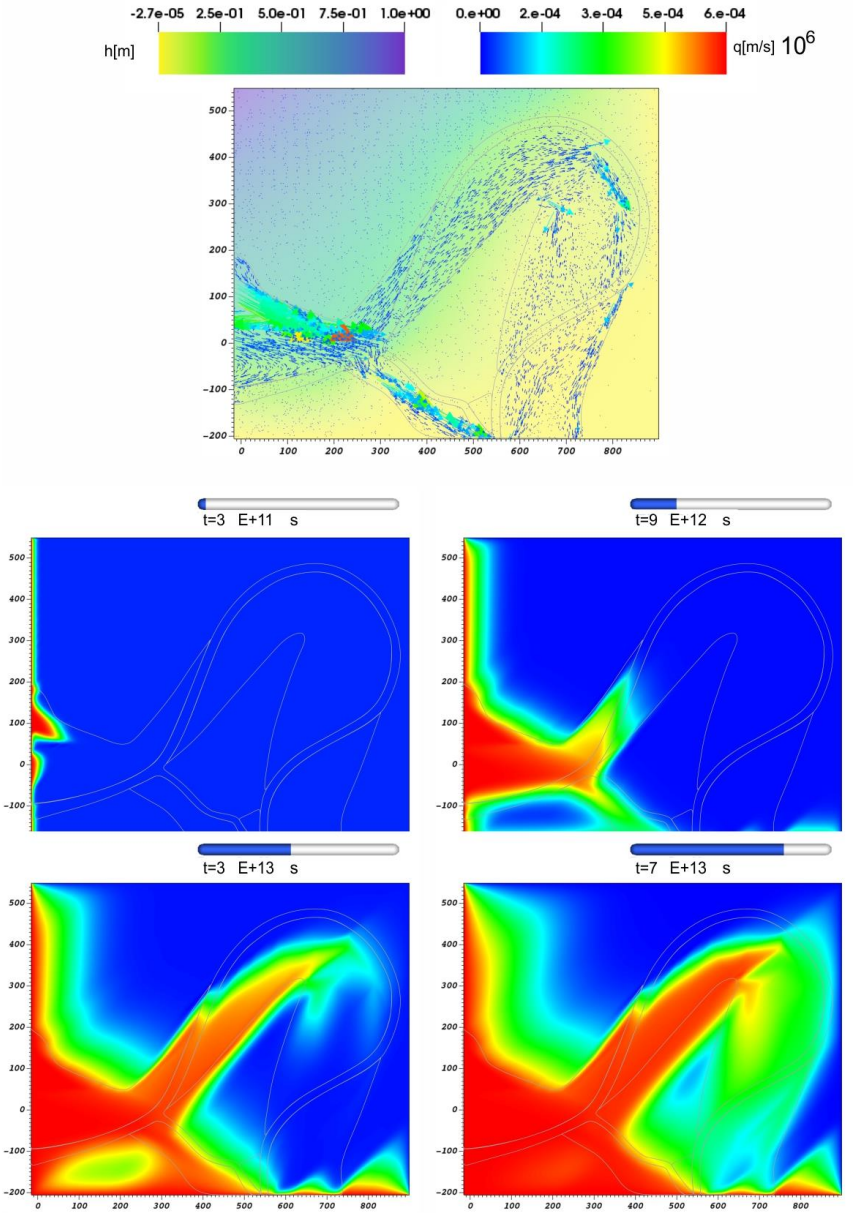

Fig. B.5. Reconstructed bodies and anisotropies: anisotropy r_a=10^{-2}, channel fill K_1 = 10^{-8} m/s, K_2 = r_aK_1, NW to SE gradient. Top panel: steady-state piezometric head distribution and Darcy velocities. Central and bottom panels: normalized concentration (red: c=1, blue: c=0) at four different times (s). The last time corresponds roughly to steady-state.

The first figure in the series (Fig. B.5) shows our results in the case of reconstructed geometry with $_{K}1 = 10^{-8}$ m/s and $_{K}2 = r_{a\ K}1 = 10^{-10}$ m/s. Looking at the top panel, we see that most of the flow occurs in the southern bar of the minor channel fill (B1) and the western bar of the main channel fill (PB1). The recirculation patterns visible in the vicinity of the southern-west boundary are caused by the specific boundary conditions and the fact that bar PB1 is essentially closed by the main channel fill. A secondary flow path follows the geometry of the bars surrounding the main channel fill, the latter acting as a partial barrier between PB1 and PB2, and PB2 and PB3. The Darcy velocity vectors are approximately aligned with the directions of anisotropy, except in the channel fill crossing PB1 and PB2, where an isotropic conductivity tensor is employed. The velocities in the region external to the bars and channel fills are clearly negligible. Not so in the channel fills, although they are at least one order of magnitude smaller than in the bars, in accordance with the value of the hydraulic conductivity. We would like to remark that the linear finite element approach may yield velocity vectors that point in the wrong nonphysical direction in the presence of strong and abrupt heterogeneities. This well-known result, highlighted by Putti and Cordes (1998), can be overcome by the employment of appropriate mass-conservative reconstructions (Scudeler et al., 2016). These effects can be seen in some parts of the domain but are highly localized and typically have no influence on both flow and transport processes. This phenomenon cannot be confused with the recirculation patterns that form where jumps in conductivity values or anisotropy directions are imposed. This can be seen in the lower-left part in PB1 and in the upper-right portion in PB2.

The time sequence in the transport simulation shows a plume entering from the western boundary and progressing towards the meandering bars. Once it reaches the channel fill between PB1 and PB2 the plume drastically decreases its speed (see panel at t = 9E + 6s) while crossing it, as evidenced by the time differences in the solute front position in the main bars before and after the complete crossing of the channel fill. After this, the plume gains speed and progresses following the flow velocities, as dictated by the reconstructed geometry. It is interesting to note that molecular diffusion intervenes mainly at later times in the regions where the velocities are small. Superimposed on molecular diffusion we can clearly discern the effect of variable anisotropy directions, in particular in the upper portion of the meander bar PB2.

Figure B.6 shows the same results in the case of $_{K}1$ = 10^{-7} m/s in the channel fill. The dynamics of the process is essentially the same with a globally faster speed of propagation due to a faster crossing of the channel fill. Here the effect of the changing anisotropy directions is much more pronounced as indicated by the more distinct preferential paths in the solute movement, which causes a quicker filling of the bars.

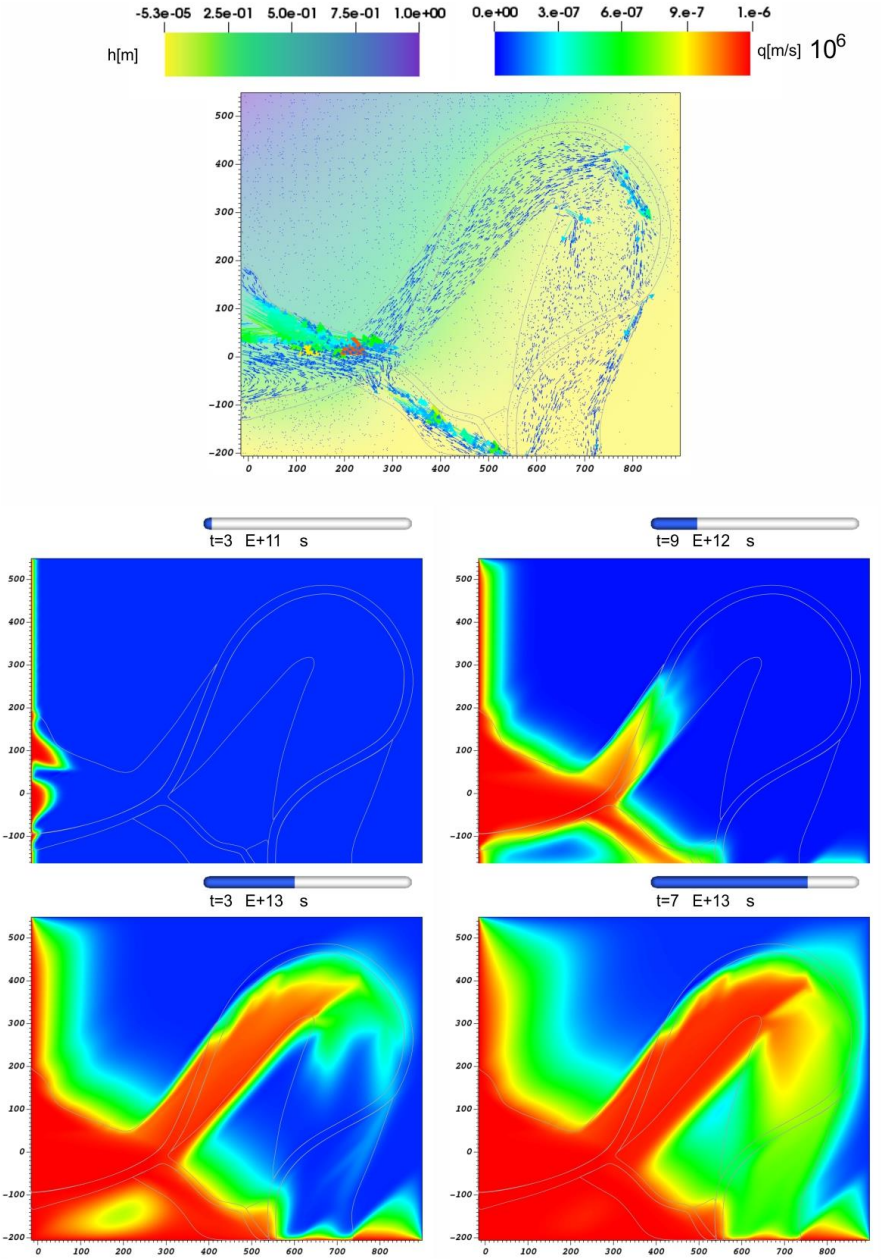

Fig. B.6. Reconstructed bodies and anisotropies: anisotropy ratio r_a=10^{-2}, channel fill K_1 = 10^{-7} m/s, K_2 = $r_a K_1$, NW to SE gradient. Top panel: steady-state piezometric head distribution and Darcy velocities. Central and bottom panels: normalized concentration (red: c = 1, blue: c = 0) at four different times (s). The last time corresponds roughly to steady-state.

When the direction of the gradient is exchanged from NW-SE to SE-NW (Fig. B.7) contaminant intrusion is more prominent because the channel fill is farther from the inflow boundary than in the previous simulations.

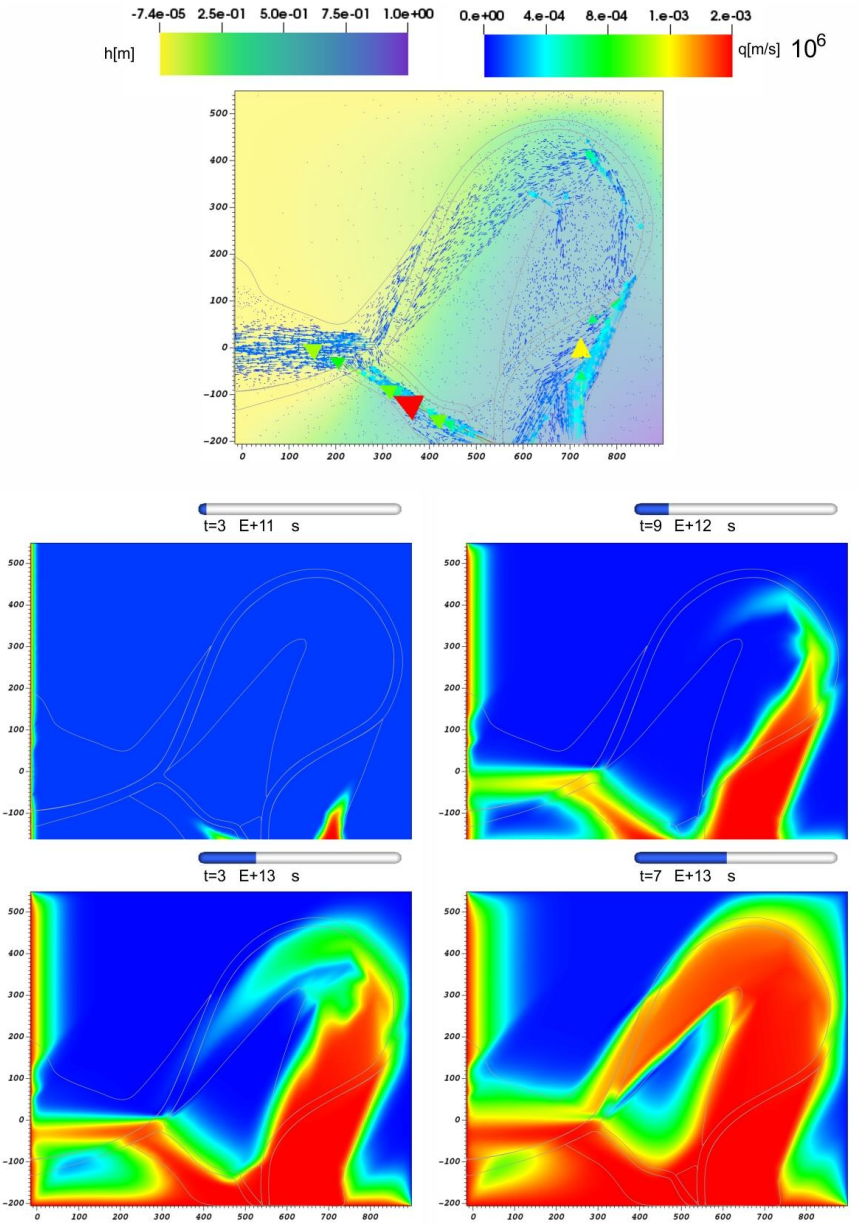

Fig. B.7. Reconstructed bodies and anisotropies: anisotropy ratio r_a=10^{-2}, channel fill K_1 = 10^{-8} m/s, K_2 = r_{aK1}, SE to NW gradient. Top panel: steady-state piezometric head distribution and Darcy velocities. Central and bottom panels: normalized concentration (red: c = 1, blue: c = 0) at four different times (s). The last time corresponds roughly to steady-state.

All the flow and transport details remain essentially the same as described before. The scenario changes completely when we use the idealized bar geometry (see Fig. B.4B, D). Indeed, Fig. B.8 and Fig. B.9, which represent the results of the simulation in the case of the NW-SE and SE-NW imposed regional gradients, respectively, clearly show that the contaminant does not enter the meander bar PB2 and PB3. Since the magnitude of the hydraulic conductivity is the same in both reconstructed and idealized geometries, the difference must be ascribed entirely to the effects of anisotropy. This shows the importance of an accurate reconstruction not only of the geological formations but also their hydraulic characteristics.

4.2. Discussion

Several studies report the importance of having interconnected permeable channelized bodies to guarantee fluid flow in the subsurface (Donselaar and Overeem, 2008; Willems et al., 2017; Willis and Tang, 2010; Yan et al., 2019). The sedimentary record of meandering tidal channels comprises sand-prone in-channel elements (e.g., channel-bar deposits) and muddy over-bank deposits. Channel bars, which accumulated during the lateral migration of a channel, are the most permeable bodies developed by tidal networks and the emerging flow patterns are directly related to their intra- and inter-connectivity (Pranter et al., 2007; Willis and Sech, 2018a). Channel-fill deposits, which accumulated within the channel during its deactivation, are less permeable since they commonly exhibit a basal sandy layer covered by a plug fill (Allen, 1965; Brivio et al., 2016; Donselaar and Overeem, 2008; Jackson et al., 2005; Toonen et al., 2012; D'Alpaos et al., 2017). Over-bank deposits (e.g., tidal flats) are considered almost impermeable as they are composed of mostly fine sediments (mud and peat layers). Subsurface deposits of reclaimed coastal areas were commonly generated in tidal networks, and fluid flow within these sediments is governed by their sedimentary features and stratal patterns, which originated during the morphodynamic evolution of tidal channels (Brivio et al., 2016; Choi and Jo, 2015; Dashtgard et al., 2012; Dashtgard and La Croix, 2015; Ghinassi et al., 2018b; La Croix and Dashtgard, 2015). The variability of growth styles shown by the prototype bars is at the origin of the emerging complex internal architecture (Willis and Sech, 2018a, 2018b; Yan et al., 2019).

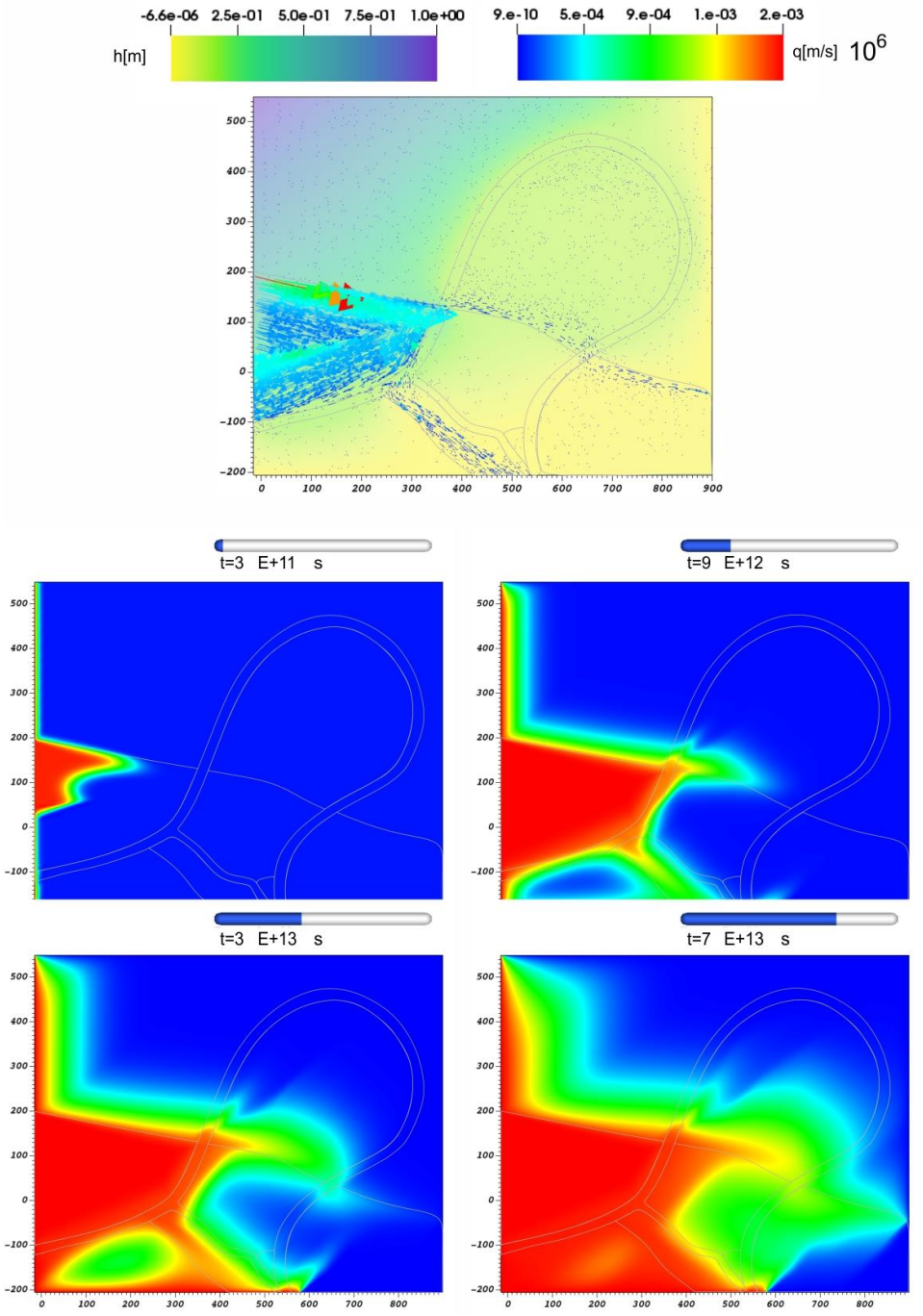

Fig. B.8. Idealized geometry and anisotropies: anisotropy ratio r_a=10^{-2}, channel fill K_1 = 10^{-8} m/s, K_2 = $r_a K_1$, NW to SE gradient. Top panel: steady-state piezometric head distribution and Darcy velocities. Central and bottom panels: normalized concentration (red: c=1, blue: c=0) at four different times (s). The last time corresponds roughly to steady-state.

The associated accumulation of mud layers with a variable spatial orientation has a strong impact on flow motion within the bar. Numerical results clearly show that flow develops within the bar in directions parallel to the strike of muddy layers, where conductivity is higher. Over a local scale (i.e., the bar scale), this configuration causes flow paths that can strongly disagree with the regional groundwater gradient (Willis and Tang, 2010). Additionally, the lateral pinching out of accretionary packages causes internal compartmentalization of the bar with further local reduction of flux magnitudes. The simulation of this variability has been effectively achieved by modeling the flow behavior using a planar anisotropic conductivity tensor adapted to the sedimentation history. Following this framework, our numerical test with opposing piezometric gradients does not provide significantly different flow patterns but highlights the important role of intra-bar anisotropies in seaward or landward fluids.

The choice to compare simulation results based on reconstructed and idealized bar complexes highlights the importance of accurate 3D geometric modelling of the subsurface deposits to properly predict groundwater flows. The use of simplistic models (Brice, 1974; Finotello et al., 2018; Lewin, 1976; Nanson and Page, 1983; Wu et al., 2015) can underestimate the effective permeable volume in the subsoil, as shown by Bellizia et al., (2021) and Cassiani et al., (2020), thus limiting the accuracy of the prediction of the effective propagation styles (see Fig. B.10). Specifically, in the numerical simulations of the idealized case, subsurface flow in the point bar opposite to the inflow boundary (i.e., within PB2 and PB3, in simulations with the NW-SE oriented gradient, and PB2 and PB1 in simulations with the SE-NW oriented gradient) is negligible, as shown in Fig. B.8 and Fig. B.9. Indeed, in the idealized belt contaminant propagation is hindered where adjacent bars connect only at the channel inflection point. On the other hand, in the reconstructed case, the flow is constrained by the channel fill, but hydraulic gradients propagate across giving rise to non-negligible Darcy velocities in the neighboring bars. For this reason, contaminants propagate in the bar following the directions of anisotropy if given enough time to cross the channel fill.

Since the accretion mechanisms of the different structures are responsible for the architectural anisotropies of the permeable bodies, the study case highlights how performing a thorough stratal evolution reconstruction of a channelized system is crucial to correctly predict groundwater flows. Especially within PB2, anisotropies play a key role in the fluid motion.

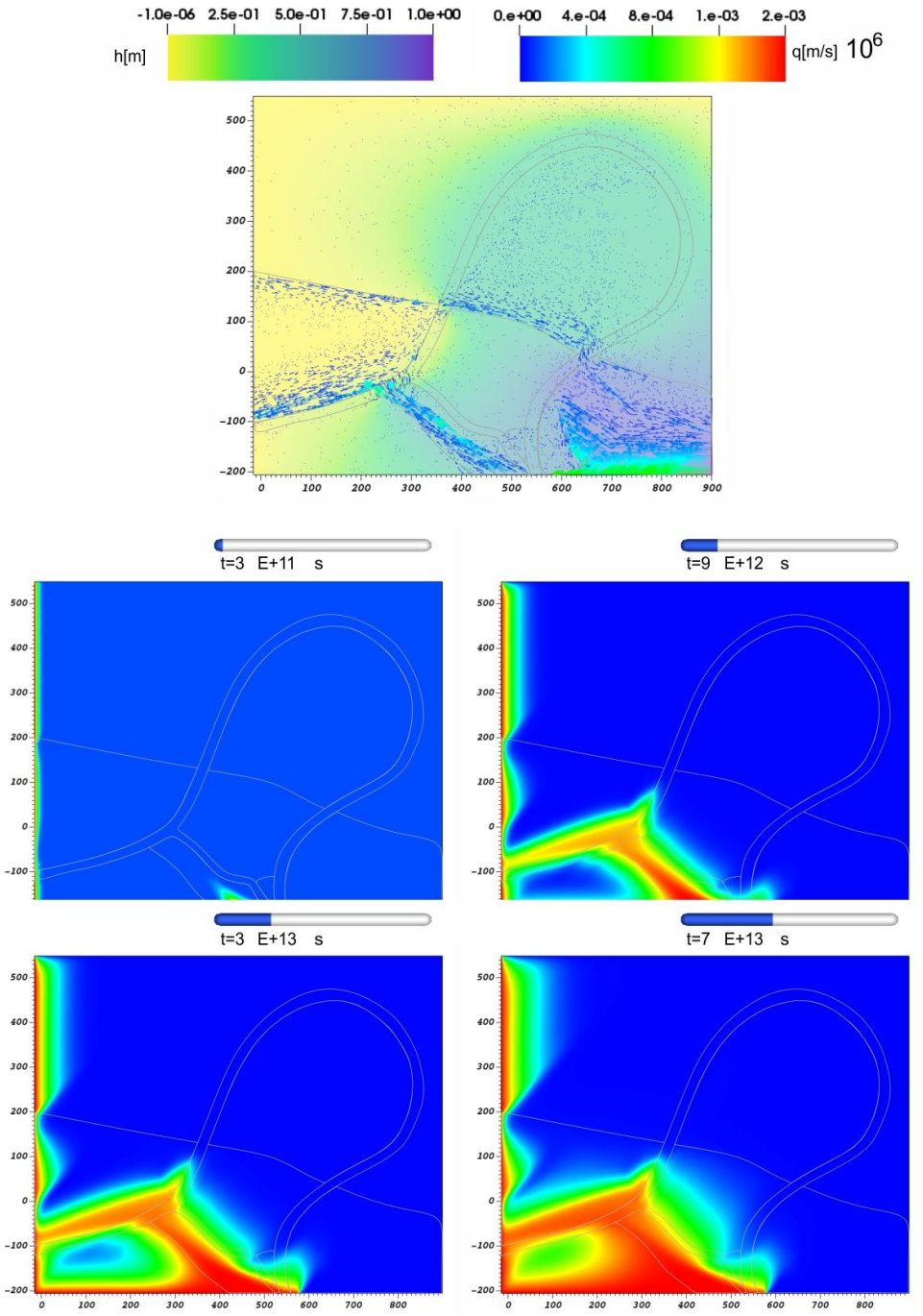

Fig. B.9. Idealized geometry and anisotropies: anisotropy ratio r_a = 10^{-2}, channel fill K_1 = 10^{-8} m/s, K_2 = $r_a K_1$, SE to NW gradient. Top panel: steady-state piezometric head distribution and Darcy velocities. Central and bottom panels: normalized concentration (red: c = 1, blue: c = 0) at four different times (s). The last time corresponds roughly to steady-state.

Darcy velocities show marked changes in their orientation close to the apex zone according to the principal directions of anisotropy, thus remaining confined within the bar body. On the other hand, anisotropies in the idealized belt have gentler boundaries, allowing the formation of smoother trajectories (Fig. B.4). However, our results show that the cross-bar channels control fluid motion. Indeed, chute channels are associated with cut-off mechanisms as they cut through a meander bend shortening the channel length (Constantine et al., 2010; Ghinassi, 2011; McGowen and Garner, 1970). In our simulations, the entire minor channel system acts as a preferential pathway connecting PB1 and PB3 in both landward and seaward regional flow, effectively disconnecting in the idealized case PB2 from the active flow region. In the simulations with the two gradient orientations, the highest Darcy velocities are observed in the B1 body, which is the more extended bar of the minor channel system, whereas B2 is practically isolated from the overall permeable system due to its position with respect to the main and minor channel fills. Overall, these simulations highlight that minor channel systems strongly act as preferential pathways when they are almost parallel to the main channel belt axis.

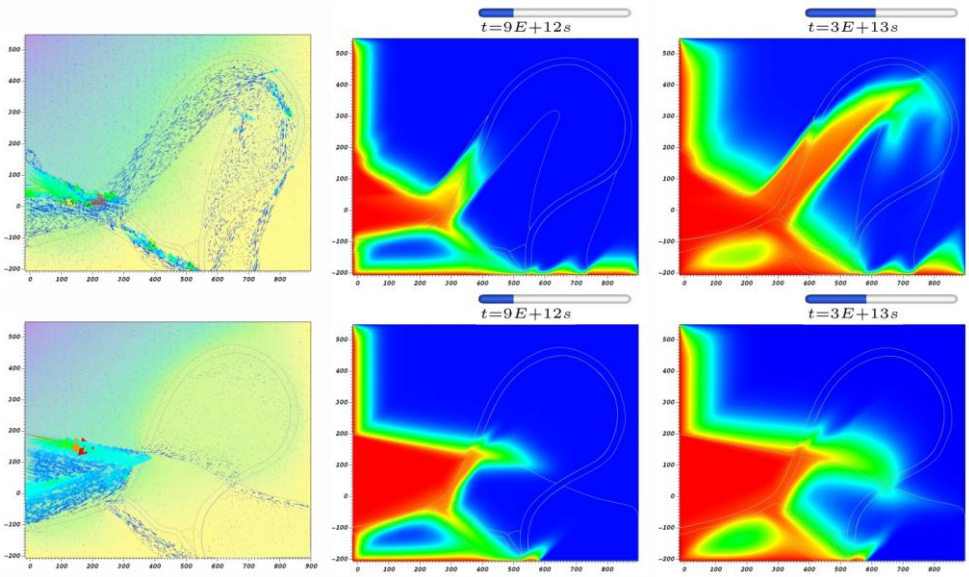

Fig. B.10. Comparison of flow velocities and concentration distributions in the cases of reconstructed (top panels) and idealized (bottom panels) geometries and anisotropies: anisotropy ratio r_a= 10^{-2}, channel fill $_{K1}$= 10^{-8} m/s, $_{K1}$ = r_{aK1}, NW to SE gradient.

Simulations in the study case reveal that the grain-size composition of the channel fill strongly affects the connectivity between adjacent bar bodies by its influence on the hydraulic properties of the formation, as highlighted by several

studies (Ambrose et al., 1991; Donselaar and Overeem, 2008; Pranter et al., 2007; Willis and Tang, 2010). Channel fills with sedimentary facies similar to those of the related bar deposits allow a better interconnection between adjacent bars than channel fills characterized by lower conductivity values. Simulations with the two different K*s* for the channel fills remark this feature. Note that, contrary to our prototype case of tidal origin, fluvial paleochannels may exhibit higher differences between the conductivity of the channel fill and the bar bodies.

Acknowledgments

This work was sponsored by "HYDROSEM: Fluvial and tidal meanders of the Venetian-Po plain: from hydrodynamics to stratigraphy" project (Progetto di Eccellenza CARIPARO 2017, PI Massimiliano Ghinassi) and University of Padova (SID2016 project, titled "From channels to rock record: morphodynamic evolution of tidal meanders and related sedimentary products", PI Massimiliano Ghinassi). Authors are thankful to S. Donnici (IGG, CNR Padova) and F. Madricardo (ISMAR, CNR Venezia) for providing geophysical and core data obtained in the frame of "ECHOS" project (Ministero delle Infrastrutture e dei Trasporti- Provveditorato Interregionale per le Opere Pubbliche del Veneto - Trentino Alto Adige - Friuli Venezia Giulia, Consorzio Venezia Nuova).

Data Availability

Datasets related to this article can be found at https://data.mendeley.com/datasets/drp7gj7mbb/draft?a=6eb3ddf0-3bd2-4ecf-9f49-75ba4ae499f3, an open-source online data repository hosted at Mendeley Data (Bellizia et al., 2021).

References

Allen, J.R.L. 1965. "A Review of the Origin and Characteristics of Recent Alluvial Sediments." Sedimentology 5: 89–191. https://doi.org/10.1111/j.1365-3091.1965.tb01561.x.

Ambrose, W.A., N. Tyler, and M.J. Parsley. 1991. "Facies Heterogeneity, Pay Continuity, and Infill Potential in Barrier-Island, Fluvial, and Submarine-Fan Reservoirs: Examples from the Texas Gulf Coast and Midland Basin." In The Three-Dimensional Facies Architecture of Terrigenous Clastic Sediments, and Its Implications for Hydrocarbon Discovery and

Recovery: SEPM Concepts in Sedimentology and Paleontology, edited by A.D. Miall and N. Tyler, 3:13–21. Cambridge University Press. https://doi.org/10.2110/csp.91.03.

Amorosi, A., M. Bini, M. Giacomelli S.and Pappalardo, C. Ribecai, V. Rossi, I. Sammartino, and G. Sarti. 2013. "Middle to Late Holocene Environmental Evolution of the Pisa Coastal Plain (Tuscany, Italy) and Early Human Settlements." Quat. Int 303: 93–106. https://doi.org/10.1016/j.quaint.2013.03.030.

Bachini, E., M. W. Farthing, and M. Putti. 2021. "Intrinsic Finite Element Method For Advection-Diffusion-Reaction Equations on Surfaces." Jcp 424. https://doi.org/10.1016/j.jcp.2020.109827.

Bear, J. 1979. Hydraulics of Groundwater. McGraw-Hill.

Bellizia, E., J. Boaga, A. Fontana, A. D'Alpaos, G. Cassiani, and M. Ghinassi. 2021. "Impact of Genesis and Abandonment Processes of a Fluvial Meander on Geometry and Grain-Size Distribution of the Associated Point Bar (Venetian Plain, Italy)." Mar. Pet. Geol. 127: 104951. https://doi.org/10.1016/j.marpetgeo.2021.104951.

Bellizia, E., S. Donnici, F. Madricardo, A. Finotello, A. D'Alpaos, and M. Ghinassi. 2022. "Ontogeny of a Subtidal Point Bar in the Microtidal Venice Lagoon (Italy) Revealed by Three-Dimensional Architectural Analyses." Sedimentology 69: 1399-1423. https://doi.org/https://doi.org/10.1111/sed.12956.

Benner, S. G., M.L. Polizzotto, B.D. Kocar, S. Ganguly, K. Phan, K. Ouch, M. Sampson, and S. Fendorf. 2008. "Groundwater Flow in an Arsenic-Contaminated Aquifer, Mekong Delta, Cambodia." Appl. Geochemistry 23: 3072–87. https://doi.org/10.1016/j.apgeochem.2008.06.013.

Boyer, P., N. Roberts, and D. Baird. 2006. "Holocene Environment and settlement on the Çarşamba Alluvial Fan, South-central Turkey: Integrating Geoarchaeology and Archaeological Field Survey." Geoarchaeology 21: 675–98. https://doi.org/10.1002/gea.20133.

Brice, J. C. 1974. "Evolution of Meander Loops." Geol. Soc. Am. Bull. 85: 581–86. https://doi.org/10.1130/0016-7606(1974)85<581:EOML>2.0.CO;2.

Bridge, J. S. 2003. Rivers and Floodplains. Forms, Processes and Sedimentary Record. Blackwell Science, Ltd.

Brivio, L., M. Ghinassi, A. D'Alpaos, A. Finotello, A. Fontana, M. Roner, and N. Howes. 2016. "Aggradation and Lateral Migration Shaping Geometry of a Tidal Point Bar: An Example from Salt Marshes of the Northern Venice Lagoon (Italy)." Sediment. Geol. 343: 141–55. https://doi.org/10.1016/j.sedgeo.2016.08.005.

Camporese, M., C. Paniconi, M. Putti, and S. Orlandini. 2010. "Surface-Subsurface Flow Modeling with Path-Based Runoff Routing, Boundary Condition-Based Coupling, and Assimilation of Multisource Observation Data." Wrr 46: W02512. https://doi.org/10.1029/2008WR007536.

Carraro, A., P. Fabbri, A. Giaretta, L. Peruzzo, F. Tateo, and F. Tellini. 2013.

"Arsenic Anomalies in Shallow Venetian Plain (Northeast Italy) Groundwater." Environ. Earth Sci. 70: 3067–84. https://doi.org/10.1007/s12665-013-2367-2.

Carraro, A., P. Fabbri, A. Giaretta, L. Peruzzo, F. Tateo, F. Tellini. 2015. "Effects of Redox Conditions on the Control of Arsenic Mobility in Shallow Alluvial Aquifers on the Venetian Plain (Italy)." Sci. Total Environ. 532: 581–94. https://doi.org/10.1016/j.scitotenv.2015.06.003.

Cassiani, G., E. Bellizia, A. Fontana, J. Boaga, A. D'Alpaos, and M. Ghinassi. 2020. Geophysical and Sedimentological Investigations Integrate Remote-Sensing Data to Depict Geometry of Fluvial Sedimentary Bodies: An Example from Holocene Point-Bar Deposits of the Venetian Plain (Italy)." Remote Sens. 12: 2568. https://doi.org/10.3390/rs1216256.

Choi, K. S., and J. H. Jo. 2015. "Morphodynamics of Tidal Channels in the Open Coast Macrotidal Flat, Southern Ganghwa Island in Gyeonggi Bay, West Coast of Korea." J. Sediment. Res. 85: 582–95. https://doi.org/10.2110/jsr.2015.44.

Christensen, B. A., and K. Hatfield. 1994. "In Situ Restoration of Contaminated Surficial Aquifers. Part I: The Flow Process." In: IAHS Publications - Series of Proceedings and Reports-Intern. Assoc. Hydrological Sciences, 313–22.

Constantine, J.A., S.R. McLean, and T. Dunne. 2010. "A Mechanism of Chute Cutoff Along Large Meandering Rivers with Uniform Floodplain Topography." Geol. Soc. Am. Bull. 122: 855–69. https://doi.org/10.1130/B26560.1.

Cosma, M., A. Finotello, A. Ielpi, D. Ventra, O. Oms, A. D'Alpaos, and M. Ghinassi. 2020a. "Piracy-Controlled Geometry of Tide-Dominated Point Bars: Combined Evidence from Ancient Sedimentary Successions and Modern Channel Networks." Geomorphology 370: 107402. https://doi.org/https://doi.org/10.1016/j.geomorph.2020.107402.

Cosma, M., M. Ghinassi, A. D'Alpaos, M. Roner, A. Finotello, L. Tommasini, and R. Gatto. 2019. "Point-Bar Brink and Channel Thalweg Trajectories Depicting Interaction Between Vertical and Lateral Shifts of Microtidal Channels in the Venice Lagoon (Italy)." Geomorphology 342: 37–50. https://doi.org/10.1016/j.geomorph.2019.06.009.

Cosma, M., N. Yan, L. Colombera, N. P. Mountney, A. D'Alpaos, and M. Ghinassi. 2020b. "An Integrated Approach to Determine Three-dimensional Accretion Geometries of Tidal Point Bars: Examples from the Venice Lagoon (Italy)." Sedimentology. https://doi.org/10.1111/sed.12787.

D'Alpaos, A., M. Ghinassi, A. Finotello, L. Brivio, L. G. Bellucci, and M. Marani. 2017. "Tidal Meander Migration and Dynamics: A Case Study from the Venice Lagoon." Mar. Pet. Geol. 87: 80–90. https://doi.org/10.1016/j.marpetgeo.2017.04.012.

Dashtgard, S.E., and A.D. La Croix. 2015. "Sedimentological Trends Across the Tidal–Fluvial Transition, Fraser River, Canada: A Review and Some Broader Implications." In Fluvial -Tidal Sedimentology, edited by P.J.

Ashworth, J.L. Best, and D.R. Parsons, 111–26. Developments in Sedimentology. Elsevier. https://doi.org/10.1016/B978-0-444-63529-7.00005-5.

Dashtgard, S.E., J.G. Venditti, P.R. Hill, S.M. Johnson, and A.D. La Croix. 2012. "Sedimentation Across the Tidal-Fluvial Transition in the Lower Fraser River, Canada." Sediment. Rec. 10: 4–9. https://doi.org/10.2110/sedred.2012.4.4.

Delagnes, A., C. Tribolo, P. Bertran, M. Brenet, R. Crassard, J. Jaubert, L. Khalidi, et al. 2012. "Inland Human Settlement in Southern Arabia 55,000 Years Ago. New Evidence from the Wadi Surdud Middle Paleolithic Site Complex, Western Yemen." J. Hum. Evol. 63: 452–74. https://doi.org/10.1016/j.jhevol.2012.03.008.

De Ghislain, M. 1986. Quantitative Hydrogeology. Groundwater Hydrology for Engineers. New York: Academic Press.

Desbarats, A.J., C.E.M. Koenig, T. Pal, P.K. Mukherjee, and R.D. Beckie. 2014. "Groundwater Flow Dynamics and Arsenic Source Characterization in an Aquifer System of West Bengal, India." Water Resour. Res. 50: 4974–5002. https://doi.org/10.1002/2013WR014034.

Donselaar, M.E., and I. Overeem. 2008. "Connectivity of Fluvial Point-Bar Deposit: An Example from the Miocene Huesca Fluvial Fan, Ebro Basin, Spain." Am. Assoc. Pet. Geol. Bull. 92: 1109–29. https://doi.org/10.1306/04180807079.

Finotello, A., A. Canestrelli, L. Carniello, M. Ghinassi, and A. D'Alpaos. 2019. "Tidal Flow Asymmetry and Discharge of Lateral Tributaries Drive the Evolution of a Microtidal Meander in the Venice Lagoon (Italy)." J. Geophys. Res. Earth Surf. 124 (12): 3043–66. https://doi.org/10.1029/2019JF005193.

Finotello, A., M. Ghinassi, L. Carniello, E. Belluco, M. Pivato, L. Tommasini, and A. D'Alpaos. 2020. "Three-Dimensional Flow Structures and Morphodynamic Evolution of Microtidal Meandering Channels." Water Resour. Res. 56 (7). https://doi.org/10.1029/2020WR027822.

Finotello, A., S. Lanzoni, M. Ghinassi, M. Marani, A. Rinaldo, and A. D'Alpaos. 2018. "Field Migration Rates of Tidal Meanders Recapitulate Fluvial Morphodynamics." Proc. Natl. Acad. Sci. U.S.A. 115: 1468. https://doi.org/10.1073/pnas.1711330115.

Fisk, H.N. 1947. Fine-Grained Alluvial Deposits and Their Effects on Mississippi River Activity. Vols 1-2. Mississippi River Commission, Vicksburg, MS.

Fogg, G. E., S. F. Carle, and C. Green. 2000. "Connected-Network Paradigm for the Alluvial Aquifer System." Special Paper-Geological Society of America, no. 348: 25–42.

Fogg, G. E, C. D. Noyes, and S. F. Carle. 1998. "Geologically Based Model of Heterogeneous Hydraulic Conductivity in an Alluvial Setting." Hydrogeology Journal 6 (1): 131–43.

Ghinassi, M. 2011. "Chute Channels in the Holocene High-Sinuosity River

Deposits of the Firenze Plain, Tuscany, Italy." Sedimentology 58: 618–42. https://doi.org/0.1111/j.1365-3091.2010.01176.x.

Ghinassi, M., F. Fidolini, M. Magi, and M. Sagri. 2013. "Depositional Environments of the Plio-Pleistocene Upper Valdarno Basin (Tuscany, Italy)." Italian Journal of Geosciences 132: 33–53.

Ghinassi, M., L. Brivio, A. D'Alpaos, A. Finotello, L. Carniello, M. Marani, and A. Cantelli. 2018a. "Morphodynamic Evolution and Sedimentology of a Microtidal Meander Bend of the Venice Lagoon (Italy)." Mar. Pet. Geol. 96: 391–404. https://doi.org/10.1016/j.marpetgeo.2018.06.011.

Ghinassi, M., A. D'alpaos, A. Gasparotto, L. Carniello, L. Brivio, A. Finotello, M. Roner, et al. 2018b. "Morphodynamic Evolution and Stratal Architecture of Translating Tidal Point Bars: Inferences from the Northern Venice Lagoon (Italy)." Sedimentology 65: 1354–77. https://doi.org/10.1111/sed.12425.

Gibling, M. R. 2006. "Width and Thickness of Fluvial Channel Bodies and Valley Fills in the Geological Record: A Literature Compilation and Classification." J. Sediment. Res. 76 (5): 731–70. https://doi.org/10.2110/jsr.2006.060.

Haitjema, H. M., and M. P. Anderson. 2016. "Darcy Velocity Is Not a Velocity." Groundwater 54 (1): 1–1.

Harvey, C.F., K.N. Ashfaque, W. Yu, A.B.M. Badruzzaman, M.A. Ali, P.M. Oates, H.A. Michael, et al. 2006. "Groundwater Dynamics and Arsenic Contamination in Bangladesh." Chem. Geol. 228: 112–36. https://doi.org/10.1016/j.chemgeo.2005.11.025.

Hatfield, K., and B.A. Christensen. 1994. "In Situ Restoration of Contaminated Surficial Aquifers. Part II: The Chemical Process." In: IAHS Publications - Series of Proceedings and Reports-Intern. Assoc. Hydrological Sciences, 323–32.

Jackson, M.D., S. Yoshida, A.H. Muggeridge, and H.D. Johnson. 2005. "Three-Dimensional Reservoir Characterization and Flow Simulation of Heterolithic Tidal Sandstones." Am. Assoc. Pet. Geol. Bull. 89: 507–28. https://doi.org/10.1306/11230404036.

Khan, I.A., J.S. Bridge, J. Kappelman, and R. Wilson. 1997. "Evolution of Miocene Fluvial Environments, Eastern Potwar Plateau, Northern Pakistan." Sedimentology 44: 221–51. https://doi.org/10.1111/j.1365-3091.1997.tb01522.x.

Kollet, S., M. Sulis, R. M. Maxwell, C. Paniconi, M. Putti, G. Bertoldi, E. T. Coon, et al. 2017. "The Integrated Hydrologic Model Intercomparison Project, IH-MIP2: A Second Set of Benchmark Results to Diagnose Integrated Hydrology and Feedbacks." Wrr 53: 867–90. https://doi.org/10.1002/2016WR019191.

LaBolle, E. M., and G. E. Fogg. 2001. "Role of Molecular Diffusion in Contaminant Migration and Recovery in an Alluvial Aquifer System." Transp. Porous. Med. 42 (1): 155–79. https://doi.org/10.1023/A:1006772716244.

La Croix, A.D., and S.E. Dashtgard. 2015. "A Synthesis of Depositional Trends in

Intertidal and Upper Subtidal Sediments Across the Tidal–Fluvial Transition in the Fraser River, Canada." J. Sediment. Res. 85: 683–98. https://doi.org/10.2110/jsr.2015.47.

Lewin, J. 1976. "Initiation of Bed Forms and Meanders in Coarse-Grained Sediment." Geol. Soc. Am. Bull. 87: 281–85. https://doi.org/10.1130/0016-7606(1976)87<281:IOBFAM>2.0.CO;2.

Madricardo, F., S. Donnici, A. Lezziero, F. De Carli, S. Buogo, P. Calicchia, and E. Boccardi. 2007. "Palaeoenvironment Reconstruction in the Lagoon of Venice Through Wide-Area Acoustic Surveys and Core Sampling." Estuar. Coast. Shelf Sci. 75: 205–13. https://doi.org/10.1016/j.ecss.2007.02.031.

Manzini, G., and M. Putti. 2007. "Mesh locking effects in the finite volume solution of 2-D anisotropic diffusion equations." Jcp 220 (2): 751–71. https://doi.org/10.1016/j.jcp.2006.05.026.

Maxwell, R., M. Putti, S. Meyerhoff, J. d. Delfs, I. e. Ferguson, V. Ivanov, J. Kim, et al. 2014. "Surface-Subsurface Model Intercomparison: A First Set of Benchmark Results to Diagnose Integrated Hydrology and Feedbacks." Wrr 50. https://doi.org/10.1002/2013WR013725.

Mazzia, A., G. Manzini, and M. Putti. 2011. "Bad behavior of Godunov mixed methods for strongly anisotropic advection-dispersion equations." Jcp 230 (2): 8410–26. https://doi.org/10.1016/j.jcp.2011.07.021.

McGowen, J.H., and L.E. Garner. 1970. "Physiographic Features and Stratification Types of Coarse-grained Pointbars: Modern and Ancient Examples." Sedimentology 14: 77–111. https://doi.org/10.1111/j.1365-3091.1970.tb00184.x.

Nanson, G.C., and K. Page. 1983. "Lateral Accretion of Fine-grained Concave Benches on Meandering Rivers." In Modern and Ancient Fluvial Systems, 133–43. John Wiley & Sons, Ltd. https://doi.org/10.1002/9781444303773.ch10.

Nofal, E.R., M.A. Amer, S.M. El-Didy, and A.M. Fekry. 2015. "Delineation and Modeling of Seawater Intrusion into the Nile Delta Aquifer: A New Perspective." Water Sci. 29: 156–66. https://doi.org/10.1016/j.wsj.2015.11.003.

Passadore, G., M. Monego, L. Altissimo, A. Sottani, M. Putti, and A. Rinaldo. 2012. "Alternative Conceptual Models and the Robustness of Groundwater Management Scenarios in the Multi-Aquifer System of the Central Veneto Basin, Italy." Hj 20: 419–33. https://doi.org/10.1007/s10040-011-0818-y.

Pauloo, R. A., G. E. Fogg, Z. Guo, and C. V. Henri. 2021. "Mean Flow Direction Modulates Non-Fickian Transport in a Heterogeneous Alluvial Aquifer-Aquitard System." Water Resources Research 57 (3): e2020WR028655.

Pranter, M.J., A.I. Ellison, R.D. Cole, and P.E. Patterson. 2007. "Analysis and Modeling of Intermediate-Scale Reservoir Heterogeneity Based on a Fluvial Point-Bar Outcrop Analog, Williams Fork Formation, Piceance

Basin, Colorado." Am. Assoc. Pet. Geol. Bull. 91: 1025–51. https://doi.org/10.1306/02010706102.

Purkis, S. J., and B. Vlaswinkel. 2012. "Visualizing lateral anisotropy in modern carbonates." AAPG Bulletin 96 (9): 1665–85. https://doi.org/10.1306/02211211173.

Putti, M., and C. Cordes. 1998. "Finite Element Approximation of the Diffusion Operator on Tetrahedra." SIAM J. Sci. Comput. 19 (4): 1154–68. https://doi.org/10.1137/S1064827595290711.

Renard, P., de Marsily, G. 1997. "Calculating Equivalent Permeability: A Review." Awr 20 (5–6): 253–78.

Scudeler, C., L. Pangle, D. Pasetto, G.-Y. Niu, T. Volkmann, C. Paniconi, M. Putti, and P. Troch. 2016. "Multiresponse Modeling of Variably Saturated Flow and Isotope Tracer Transport for a Hillslope Experiment at the Landscape Evolution Observatory." Hess 20: 4061–78. https://doi.org/10.5194/hess-20-4061-2016.

Scudeler, C., M. Putti, and C. Paniconi. 2016. "Mass-Conservative Reconstruction of Galerkin Velocity Fields for Transport Simulations." Awr 94: 470–85. https://doi.org/10.1016/j.advwatres.2016.06.011.

Şimşek, C., U. Gemici, and S. Filiz. 2008. "An Assessment of Surficial Aquifer Vulnerability and Groundwater Pollution from a Hazardous Landfill Site, Torbali/Turkey." Geosci. J. 12: 69–82. https://doi.org/10.1007/s12303-008-0009-6.

Toonen, W.H.J., M.G. Kleinhans, and K.M. Cohen. 2012. "Sedimentary Architecture of Abandoned Channel Fills." Earth Surf. Process. Landf. 37: 459–72. https://doi.org/10.1002/esp.3189.

Weill, S., A. Mazzia, C. Paniconi, and M. Putti. 2011. "Coupling Water Flow and Solute Transport into a Physically-Based Surface–Subsurface Hydrological Model." Awr 34: 128–36. https://doi.org/10.1016/j.advwatres.2010.10.001.

Weissmann, G. S., Y. Zhang, G. E. Fogg, and J. F. Mount. 2004. "Influence of Incised-Valley-Fill Deposits on Hydrogeology of a Stream-Dominated Alluvial Fan." In Aquifer Characterization. SEPM Society for Sedimentary Geology.

Willems, C.J.L., H.M. Nick, M.E. Donselaar, G.J. Weltje, and D.F. Bruhn. 2017. "On the Connectivity Anisotropy in Fluvial Hot Sedimentary Aquifers and Its Influence on Geothermal Doublet Performance." Geothermics 65: 222–33. https://doi.org/10.1016/j.geothermics.2016.10.002.

Willis, B.J., and R.P. Sech. 2018a. "Emergent Facies Patterns Within Fluvial Channel Belts." In Fluvial Meanders and Their Sedimentary Products in the Rock Record, 509–42. Int. Assoc. Sedimentol. Spec., Publ. 48. John Wiley & Sons. https://doi.org/10.1002/9781119424437.ch19.

Willis, B.J., and R.P. Sech. 2018b. "Quantifying Impacts of Fluvial Intra-Channel-Belt Heterogeneity on Reservoir Behaviour." In Fluvial Meanders and Their Sedimentary Products in the Rock Record, 543–72. Int. Assoc.

Sedimentol. Spec., Publ. 48. John Wiley & Sons. https://doi.org/10.1002/9781119424437.ch20.

Willis, B.J., and H. Tang. 2010. “Three-Dimensional Connectivity of Point-Bar Deposits.” J. Sediment. Res. 80: 440–54. https://doi.org/10.2110/jsr.2010.046.

Wu, C., J.P. Bhattacharya, and M.S. Ullah. 2015. “Paleohydrology and 3D Facies Architecture of Ancient Point Bars, Ferron Sandstone, Notom Delta, South-Central Utah, USA.” J. Sediment. Res. 85: 399–418. https://doi.org/10.2110/jsr.2015.29.

Yan, N., L. Colombera, N.P. Mountney, and R.M. Dorrell. 2019. “Fluvial Point-Bar Architecture and Facies Heterogeneity, and Their Influence on Intra-Bar Static Connectivity in Humid Coastal-Plain and Dryland Fan Systems.” In Fluvial Meanders and Their Sedimentary Products in the Rock Record, 475–508. Int. Assoc. Sedimentol. Spec., Publ. 48. John Wiley & Sons. https://doi.org/10.1002/9781119424437.ch18.

Yang, Y.S., X.Y. Lin, T. Elliot, and R.M. Kalin. 2001. “A Natural-Gradient Field Tracer Test for Evaluation of Pollutant-Transport Parameters in a Porous-Medium Aquifer.” Hydrogeol. J. 9: 313–20. https://doi.org/10.1007/s100400100127.

Zecchin, M., L. Baradello, G. Brancolini, F. Donda, F. Rizzetto, and L. Tosi. 2008. “Sequence Stratigraphy Based on High-Resolution Seismic Profiles in the Late Pleistocene and Holocene Deposits of the Venice Area.” Mar. Geol. 253: 185–98. https://doi.org/10.1016/j.margeo.2008.05.010.

Zecchin, M., G. Brancolini, L. Tosi, F. Rizzetto, M. Caffau, and L. Baradello. 2009. “Anatomy of the Holocene Succession of the Southern Venice Lagoon Revealed by Very High-Resolution Seismic Data.” Cont. Shelf Res. 29: 1343–59. https://doi.org/10.1016/j.csr.2009.03.006